Western Graduate&PostdoctoralStudies

Western University
Scholarship@Western

Electronic Thesis and Dissertation Repository

10-19-2016 12:00 AM

Foundation Effects of Trees Under Wind Loads

Padmavathi Venkata Sagi
The University of Western Ontario

Supervisor
Timothy Newson
The University of Western Ontario

Graduate Program in Civil and Environmental Engineering
A thesis submitted in partial fulfillment of the requirements for the degree in Doctor of Philosophy
© Padmavathi Venkata Sagi 2016

Follow this and additional works at: https://ir.lib.uwo.ca/etd

 Part of the Aerodynamics and Fluid Mechanics Commons, Civil Engineering Commons, and the Geotechnical Engineering Commons

Recommended Citation

Sagi, Padmavathi Venkata, "Foundation Effects of Trees Under Wind Loads" (2016). *Electronic Thesis and Dissertation Repository*. 4352.
https://ir.lib.uwo.ca/etd/4352

This Dissertation/Thesis is brought to you for free and open access by Scholarship@Western. It has been accepted for inclusion in Electronic Thesis and Dissertation Repository by an authorized administrator of Scholarship@Western. For more information, please contact wlswadmin@uwo.ca.

Abstract

Damage due to windthrow can cause extensive loss of property and lives during extreme windstorm events. Current predictive approaches are generally empirical and based on a posteriori surveys of failures. A more rigorous engineering approach to understanding response phenomenon in trees subjected to extreme winds has been attempted. Considering the complexity of windthrow, experiments and tree stability analysis were conducted in different viewpoints. Norway spruce trees were chosen because of their ubiquity in North America and susceptibility to windthrow. Winching tests were conducted on a well-instrumented mature Norway spruce field tree. Tracked tree-root system response to failure winch load and the estimated material properties of the tree-root-soil system were used to examine the applicability of simple engineering principles to tree stability analysis. A Winkler foundation model was used to study the root-soil plate anchorage for the first time. The stiffness estimates of the mature tree roots were found to be higher for the middle of the root structures. To study windthrow phenomenon, a novel wind tunnel experimental technique was used. Instrumented tree saplings with complete structural root systems were placed in a custom-built planter box installed in a boundary layer wind tunnel and were tested to failure with clay or sand soil media. Rigorous analysis of the wind tunnel tests data gave a better understanding on dynamics of tree root soil interaction and soil root anchorage mechanics. Tree sway, damping, natural frequency and admittance estimates of the tree-root system with increase in wind loading were made for the first time. Non-linear variation in damping with increase in wind speed and significant difference in energy transfer to the root system with change in soil media (twice as much in sand compared to clay) was observed. Comparison of geometric, elastic, and stress similitude and dimensionless scaling parameters for the mature tree, and the tree saplings identified the differences in tree responses with scaling. Relatively tree saplings showed higher stiffness in response. Dynamic loading and the resulting tree sapling response were analyzed in detail through the rainflow technique. Static and dynamic load response was compared in detail through secant modulus of elasticity and dynamic load factor. Load transfer to the root system was around 15% higher under dynamic loading conditions. The effect of trenching on tree stability was also studied using the wind tunnel. This study supports the current trenching guidelines of three times the stem diameter distance as the safe distance for both sand and clay

soil media. However, with stronger soil media (clay) load redistribution in the root system was observed with increase in trenching volumes and wind load. Although similar tree response was observed with changes in soil media, the effect of soil strength on tree stability appears to be a vital component of windthrow research.

Keywords: Windthrow, Winkler foundation model, wind tunnel, tree sway, damping, natural frequency, admittance, rainflow, soil mechanics, scaling, stiffness, root modulus of elasticity, dynamic load factor, trenching.

Co-Authorship Statement

All of the work presented in this thesis was performed by Padmavathi Sagi. Chapters 2 to 5 of the thesis will be submitted to scholarly journals as manuscripts co-authored by Padmavathi Sagi, Timothy Newson, Craig Miller and Steve Mitchell.

Acknowledgments

I am forever grateful to my supervisor Dr. Timothy Newson, for giving me this incredible opportunity. His friendly guidance, unwavering support, and persistence made this thesis possible. I cannot thank him enough for spending his valuable time on my experimental work, when the wind tunnel testing was so overwhelming for me. Every single time I needed a meeting, he allotted time for me. He never lost his zest until we reached our goals.

A special thanks to Dr. Craig Miller and Dr. Steve Mitchell (University of British Columbia) for their helpful technical assistance with the experiments and the research. I am also thankful to Dr. David Gatey for his immense support with the experimental setup.

I would like to thank my friends, Dr. Bilal, Dr. Diwakar, and Dr. Sampat, for being there for me in every step of the way. The support they gave me was invaluable. Time spent with my friends made my journey gratifying.

I am indebted to my parents (Prasad Varma Sagi and Uma Sagi) for making my every dream possible, teaching good values, letting me make my decisions and motivating me every step of the way. Lastly but not the least, my caring husband Dr. Suresh Datla who taught me the true meaning of life companionship, gave me unconditional love and support and joy of my life, my beautiful daughter Aditi.

To my daughter, Aditi.

Table of Contents

List of Tables

List of Figures

Nomenclature

$H_R(f)^2$	dimensionless mechanical admittance function
h_t	height (m)
h_{cg}	tree center of gravity height (m)
P_f	probability of failure
c_g	coefficient of gradation
c_l	undrained shear strength at the liquid limit (N/m^2)
c_u	undrained shear strength (N/m^2)
c_{uu}	uniformity coefficient
f_n	natural frequency (Hz)
m_k	kth moment of a random variable (first moment is $m_1 = \mu$)
π_i	dimensionless parameter
σ^2	variance of a random variable
σ_v'	effective vertical stress
ϕ'	friction angle (degrees)
ϕ_p'	peak friction angle (degrees)
A	frontal area (m^2)
c	soil cohesion (kPa)
C_A	crown frontal area (m^2)
C_c	soil coefficient of curvature
C_D	drag coefficient
D	diameter (m)
DBH	diameter at breast height (m)
d_t	stem deflection (m)
E	Young's modulus of elasticity (N/m^2)
F	force (N)
F_d	drag force (N)
g	gravitational coefficient (m/s^2)
h, H	tree height (m)
I	moment of inertia (m^4)

I_L	liquidity index
J	flexural rigidity (N/m^2)
k	stiffness (N/m)
k_θ	rotational stiffness (Nm/degree)
ℓ ,L	length (m)
P_a	atmospheric pressure (kN/m^2)
R_{wm}	mineralogy function
S	gauge factor
S_{st}	stem breakage height (m)
S_v	stem volume (m^3)
U	fluid velocity (m/s)
V_o	response data in Volts
V_s	input voltage (V)
w_L	liquid limit
w_P	plastic limit
x	amplitude (m)
Zo	roughness length (m)
$\Gamma(f)$	aerodynamic admittance function
θ	rotation (rad)
ρ	correlation coefficient/air density (kg/m^3)
φ	dilation angle
Φ	standard normal distribution function
ρ_s	structural density (kg/m^3)
$S(n)$	power spectrum of the random function at the frequency n
f, ω	frequency (Hz)
ε	bandwidth parameter/strain
μ	viscosity (kg/ms)
ξ	damping ratio

Chapter 1

1 Introduction

1.1 Stability of trees under wind loading

In many parts of the world, the stability of trees under wind loading is a matter of growing concern. When wind storms occur, urban and forest areas can suffer from major economic and environmental losses because of tree failure. Major storms like the Canterbury wind storm in New Zealand in 1975 [Zeng et al. 2007], European storms Vivian in 1990, and Lothar and Martin in 1999 [Kerzenmacher and Gardiner 1998, Cucchi et al. 2004], and 1989 Hurricane Hugo in USA are a few examples of economic losses because of tree failure under extreme wind loading. Another growing problem in urban parts of the world is land scarcity. Shortage of land is forcing trees to grow even closer to urban structures [Ow et al. 2010], increasing risk to peoples' safety and the structural damage because of tree failure under extreme wind events. Since 1990, 1.3 million people were reported killed in major storm events all over the world [EM-DAT, 2014]. In last ten years, USA has suffered six major wind storm disasters with an estimated US$119 billion [EM-DAT, 2014] in economic losses. The most recent storm, 2014 cyclone Hudhud in India, which had wind speeds up to 205 km/h [BBC, 2014] lead to some estimated damages of US$11 billion [EM-DAT, 2014] and the loss of more than six lives; significant amounts of damage were due to the tree related failures [Figure 1-1]. Concerns associated with this damage and loss of life have led to an increased interest in tree stability research over the last few decades.

Assuming that tree and root systems are healthy, the key factors that affect the failure bending moment or wind speed, are diameter at breast height (DBH), tree height (H), crown frontal area (A), stem volume (S_v), stem breakage strength (S_{st}), root plate architecture, depth (d), diameter (D), and weight (W), and the strength of the soil and roots. Tree failure can occur either by stem breakage or uprooting. If the tree stem is healthy, the stem taper is not too high (H/DBH <60) [Moore 2000 and Peltola et al. 2000] and the tree has a shallow root plate, the most probable mode of failure under extreme wind events is uprooting. On the other hand, if the site is deeply ripped (the mechanical manipulation of

the soil to break up impermeable subsurface layers that occurs as part of the initial preparation of the soil to establish an agricultural or silvicultural operation) [Rees and Ali 2011] and the width of the root plate is high, the most probable form of tree failure would be the stem breakage [Papesch et al. 1997].

James et al. [2006] examined the influence of tree size and architecture on the mechanical stability under dynamic loading. With increase in tree size, frontal area increases, which in turn increases the drag force and the overturning moment about the base of the tree. However, with increase in branch mass, mass damping increases and reduces energy transfer from the wind to the tree making the tree more stable. This complexity suggests evaluating the trees with different canopy architectures differently. As long as the tree stem is able to resist the overturning moment, the entire load from the upper part of the tree is transferred to the root soil system [Stokes 1999]. Once the load is transferred to below the ground level structure of the tree, it is incumbent on the root-soil plate architecture, individual root strength, and the soil strength to anchor the tree and prevent uprooting [Coutts 1983 & 1986, Crook and Ennos 1996, Moore 2000]. Soil type and strength not only impacts the anchorage strength, but also plays a huge role in forming the root plate architecture [Mergen 1954, Stokes 1999]. Soil strength is also highly dependent on water content. Because of the adaptive nature of trees, both the above and below ground tree structure varies with the environmental loading conditions and the type of soil. This complexity changes the anchorage strength of every tree, depending on the combined effect of type of species, age, soil, precipitation and loading.

The total load acting on the tree not only depends on the frontal area, but also depends on the nature of the wind loading. The nature of the wind loading can be best described from a wind profile, turbulence or gustiness, and the wind spectrum. Wind load varies with wind speed, turbulence intensity, and wind profile [Holmes 2001, DNV 2010]. As wind speed varies with height, direction and time, the wind speed time series is non-linear and non-stationary. Wind conditions can also be transient (gusts, squalls, extreme changes in wind direction, and simultaneous changes in wind speed and direction) in nature. The wind profile is the variation of wind speed with elevation and varies with terrain conditions. Turbulence intensity and gust factor gives us the measure of turbulence or gustiness of the

wind loading. Turbulence intensity is the ratio of standard deviation to the mean wind speed and the gust factor is the ratio of maximum wind speed to the mean wind speed. A wind spectrum is the distribution of turbulence with frequency. Short term stationary wind conditions can be described by a spectrum. Wind spectra can be determined from the measured wind speed data or using available standard expressions, e.g., Davenport, Harris, and Kaimal spectra [Davenport 1967, Harris 1968, and Kaimal 1972].

Windthrow is a very complicated field of study with varying canopy and root architecture, change in soil conditions, which also vary with the water content and density, and the variable nature of wind loading. Fortunately, like any other structure, trees follow the laws of physics. Tree stability analysis has been attempted previously in many ways. Based on the failure type, analysis can be divided into two categories: 1) stem fracture or tree stability estimate based on the above ground dendrometric properties of the tree and, 2) soil-root plate anchorage mechanics or tree stability estimates based on the below ground properties of the root plate and soil. Tree failure statistics indicate that the probability of failure through uprooting are much higher and that uprooting resistance is the most complex property to determine. Even though by definition the soil-root plate anchorage estimate should be based on soil strength parameters, none of the available anchorage models covertly include soil strength as a parameter [e.g. Blackwell et al. 1990, Peltola and Kellomäki 1993]. The research in this thesis concentrates on the uprooting mode of failure, to investigate the role of soil strength parameters on tree anchorage, from an engineering point of view.

1.2 Tree stability analysis

The stability of trees under wind loading has been studied from different perspectives over the last few decades. Tree stability analysis can be split into three major categories based on the study techniques: 1) static analysis, 2) dynamic analysis, and 3) numerical and computer modelling.

Static analysis studies the tree stability under constant loading conditions, rather than under the time varying nature of wind loading conditions. Even though windthrow is the study of tree stability under wind loading, because of the complexity of the subject, wind load is

often simulated with constant pull loads in the field to analyze the response of trees. Static analysis is conducted by pulling trees with a cable attached to the tree stem and a winch. Winching is the most common method of testing to study the windthrow and is used as both a destructive and non-destructive method of testing. Winching tests not only help many researchers to categorize the factors affecting the windthrow, but also help to predict the failure wind load. The main focus of winching studies has been to relate the failure load to various measures of tree and root plate. Fraser [1962], Papesch et al. [1997], Moore [2000] and Peltola et al. [2000] found significant and positive linear correlation between the maximum resistive bending moment to the tree height (H), diameter at breast height (DBH) and stem volume ($H \times DBH^2$). Cremer et al. [1982] and Petty and Swain [1985] proposed the stem taper (H/DBH) as an important index of tree stability with respect to stem failures.

Winching studies have also been used to study the tree stability based on root plate dimensions. In some studies it was the root plate diameter, which controlled the anchorage strength of the trees [Anderson et al. 1989, Papesch et al. 1997] and other studies suggested that the root plate depth and soil-root plate volume also have a significant effect on anchorage [Moore 2000, Crook and Ennos 1996, Mickovski and Ennos 2003]. Winching studies were also used to identify the root anchorage components [Coutts 1983 & 1986, Blackwell et al. 1990], to relate uprooting resistance as a function of stem base rotation or root plate rotation [Neild and Wood 1999, Lundström et al. 2007, Sani et al. 2012 and Szoradova et al. 2013], and to identify the strain distribution during anchorage failure [Crook and Ennos 1996, Crook et al. 1997, Stokes 1999]. Only a few winch studies were focused on linking the anchorage efficiency with change in soil conditions [Fraser 1962, Moore 2000, Cucchi et al. 2004, Ow et al. 2010]. Even though static winching tests helped to understand the basis of tree-root-soil response to lateral pull load, this is far from the reality of wind loading. Oliver and Mayhead [1974], Gardiner et al. [1997], James et al. [2013] reported that the failure wind loads are often much lower than the predictive wind loads obtained from static load tests.

The dynamic response of trees to wind loading can be achieved in two ways, through experimental measurements or numerical modeling. Tree dynamic response to the applied

wind field can be found in two ways: 1) with the aid of tree dynamic properties (i.e., natural frequency and damping) or 2) mechanical and aerodynamic admittance function. Tree dynamic properties can be measured through free (force sway with a pull of an attached rope and release) or forced vibrations (sway under wind loading). Complex tree sway response to dynamic loading is analysed to obtain the dynamic properties under undamped and damped oscillations. The dominant oscillating frequency of the tree response is considered to be the natural frequency and the wind energy dissipated by the tree structure is referred to as tree damping energy. The aerodynamic and mechanical admittance functions couple the tree response to wind loading in the frequency domain [see Figure 1-2].

Hoag et al. [1971], Mayhead [1973], Gardiner [1989], Peltola [1996], James [2003], Moore and Maguire [2004, 2005 & 2008], Spatz et al. [2007], Jonsson et al. [2007], Garcia et al. [2008], Sellier and Fourcaud [2005 & 2009], Kane and James [2011] and many other authors estimated the dynamic properties of the structure to determine the tree dynamic response. Sellier and Fourcaud [2005] observed that the heaviest element (the trunk) is the predominant element governing the free oscillations of a tree. Sugden [1962], Milne [1991], Gardiner [1992], and Moore and Maguire [2005] found increases in natural frequency with complete de-branching of a tree. Under forced vibrations (under wind loading), tree response depends on the excitation frequency of the wind load and the dynamic nature of the tree structure. Holbo et al. [1980], Mayer [1987], Gardiner [1992] and Peltola [1996] noted that trees respond most to the gusts close to their natural sway frequency, which is also called the resonant frequency (first natural frequency). In the case of resonance, large tree oscillations with increase in bending of the stem and higher load on the root plate were observed [Milne 1991, Spatz et al. 2007 and Spatz and Theckes 2013].

Damping of the tree structure under wind events can be categorized into internal and external damping [Hoag et al. 1971]. Internal damping is due to the internal friction of the wood, friction of the root soil plate and the structural damping due to the movement of the branches [Moore and Maguire 2004] and the external damping is due to the aerodynamic drag of the crown and the collision between neighboring trees. Milne [1991] Gardiner

[1992] and Moore and Maguire [2005] noted decreases in damping with crown de-branching. Spatz and Bruechert [2000] noted increases in damping with low modulus of elasticity of branches. Most of the damping estimates were obtained from the forced vibration response. In the case of free vibrations (damped oscillations), most studies [Moore and Maguire 2004, Jonsson et al. 2007] assume velocity proportional to damping (viscous damping), but none of the literature reports the quantitative change in damping with increase in wind speed. Although Jonsson et al. [2007] indicated a low influence of root architecture on the first natural frequency, *the influence of root architecture and soil properties on damping* has still not been explored.

Tree dynamic response to wind loading has been studied by many researchers using dynamic response and the properties of the above ground structure with changing wind loads, but the effect of the soil on tree dynamic response is seldom considered in windthrow studies. Often windthrow studies assume that the below ground structure of the tree is rigid, so the effect of soil medium on the dynamic response of the above ground structure is neglected. In reality, structural response to dynamic loading is not only defined by the dynamic properties of the above ground structure but also by the interaction of the structure with the supporting soil. Measuring techniques of tree dynamic response has come a long way from using stop watch [Sugden 1962], to laser transducers, tilt sensors, strain gauges, accelerometers, prism based systems and laser interferometers [Blackburn et al. 1988, Milne 1991, Roodbaraky et al. 1994, Gardiner 1995, Peltola 1996, Baker 1997, Hassinen et al. 1998, Sellier et al. 2006 & 2008, James and Haritos 2010 and James et al. 2013]. Increased sophistication of instrumentation is now driving changes in analytical approaches. With more opportunities for wide-ranging tree response data, the possibilities of exploring tree dynamic response to wind loading are endless.

Tree stability has also been numerically modelled using finite element method (FEM) based codes. Tree stem and branch interaction response to wind loading was studied by Moore 2002, Moore and Maguire 2008, Sellier et al. 2006 & 2008, Hu et al. 2008 and Sellier and Fourcaud 2009. Using FEM, the authors were able to examine the stem and the branches individually [Moore 2002, Sellier et al. 2006], modes of vibration were identified [Sellier et al. 2006], good representation of mechanical admittance function was made at

the natural frequency [Sellier et al. 2008]. Dupuy et al. 2005 and 2007, Fourcaud et al. 2007, and Yang et al. 2014 examined the variation in anchorage strengh with change in root morphological and soil mechanical parameters using the ABAQUS software. From these studies, number of lateral roots, soil cohesion, modulus of elasticity of roots and soil had the most influence on the root-soil plate anchorage and the formation of root-soil plate during overturning varied with change in soil media.

Even though using the numerical models tree and root-soil plate response with increase in dynamic loading can be examined, some of the key parameters are still missing. More importantly the aerodynamic admittance to calculate the wind load on trees [Spatz and Bruechert 2000], and root-soil interaction parameter to estimate amount of resistance offered by the roots in different soil conditions needs to be determined to improve the model sophistication. Change in tree dynamic response to increase in wind loading also needs to be determined to properly validate the numerical modelling.

1.3 Root anchorage mechanics

The foundation is the most important component of any structure. As long as the structure is built well, it is the foundation that increases the life and stability of the structures. In the case of trees, even the structural development of the tree depends greatly on the roots and the soil surrounding the roots. Considering the importance of the root system and the soil supporting the entire structure, it is surprising that it is the least studied area in the windthrow research.

The stability of trees can be better understood if we know how the combined effect of the entire tree and root system resists the loads acting on them. Following common practice, the stability of trees can be improved by making simple changes to tree form and structure such as pruning. Numerous studies have been conducted to analyze the contribution of tree structural components to tree stability. In the case of the soil-root system it is not possible to improve the root anchorage with simple practical changes and we are still unclear as to how small changes in the soil-root system could affect anchorage [Blackwell et al. 1990].

The very complex and rather difficult nature of root anchorage research gained momentum once Coutts [1983 & 1986] quantified the components of root anchorage [see Figure 1-3]. He observed that the windward roots provide most resistance among the four identified components. Soil–root plate weight plays the second most important role. The leeward side hinge resistance to bending is the third component, and soil resistance plays the most important role in the early stages of loading and offers minimum resistance at maximal loads. Blackwell et al. [1990] added the weight of the stem and crown as the fifth component of anchorage. They also found that the contribution of anchorage components changes during the process of uprooting.

Blackwell et al. [1990] developed a mathematical model for shallowly rooted trees. The entire tree root system was assumed to rotate about a pivot and solved numerically using computer analysis. They presented a parametric sensitivity analysis that showed the change in maximum resistive turning moment with 10% decrease and increase in standard parameter values. It is curious to see that no change in maximum resistive turning moment was reported with ±10% change in overall soil strength. Even though many researchers [Mergen 1954, Fraser 1962, Crook and Ennos 1993, Ennos 1994, Moore 2000, Cucchi et al. 2004] observed consistent change in maximum resistive turning moment with soil shear strength, it is still not clear how much soil shear strength variation could alter the tree stability. Based on the soil type and hydraulic conductivity, the available water content, soil shear strength variation could be marginal or significant. *As consistent changes in tree stability with change in soil have been observed* [Anderson et al. 1989, Moore 2000, Cucchi et al. 2004], as well as water content [Cucchi et al. 2004] and freezing conditions [Peltola et al. 2000], it is apparent from previous studies, that this area needs to be explored further.

Achim and Nicoll [2009] presented a ‘Resistance’ model to predict the anchorage strength of a given tree, soil group and rooting depth, but the soil resistance under the plate and leeward root stiffness were disregarded in this model. Neild and Wood [1999], Lundström et al. [2007], Sani et al. [2012] and Szoradova et al. [2013] used a root-soil plate stiffness parameter to estimate the resistive turning moment based on the winched tree data. The problem with these methods is the need for large data sets. To estimate the tree stability with less damage to trees, tree sapling tests could be used, but the results need to be scaled

properly to infer the mature tree anchorage strength from the tree sapling test results. Ennos [1993] and Stokes [1999] studied the scaling aspects of root anchorage with the tree age. Ennos [1993] presented the isometric and elastic scaling of anchorage components using stem length and Stokes [1999] reported proportional increases in anchorage strength with the third power of the trunk diameter. *To connect the static loading tests to dynamic loading conditions, the change in root anchorage strength due to tree vibration also needs to be addressed to predict the anchorage strength of any tree under wind loading conditions*; any study of dynamic analysis of tree anchorage is also still missing from the literature.

Mergen [1954], Fraser [1962], Anderson et al. [1989], Moore [2000], Cucchi et al. [2004], Ow et al. [2010] observed positive correlation between root plate anchorage and soil shear strength. Trees on clayey soils showed shallow root systems and higher resistance to uprooting, where-as trees on sandy soils showed deep spreading root system and also uprooting was the dominant mode of failure. Winching test results showed that the well-drained soils not only increased the rooting depth, but also improved the anchorage strength significantly. As the quantitative details of the anchorage strength with varying soil shear strength are still not available, *comparative studies on models and real plants in sandy and clayey soils still need to conducted* [Ennos 1994].

In addition to soil strength, it is also important to understand the regions of the root plate which contribute most to the anchorage strength. Crook and Ennos [1996], Crook et al. [1997], Stokes [1999] studied the strain on roots with the applied lateral pull load and Watson [2000] reported the strain on roots through long-term monitoring of tree and root response to wind loading. Strain along the lateral roots, close to the trunk contributed most to tree stability and the windward roots provided more anchorage compared to the leeward lateral roots. As the windthrow is a dynamic process, it is important to know the anchorage response under sub-critical and critical wind load conditions. It is also important to know the dynamic properties of the root anchorage components, to improve the numerical windthrow modelling. As several authors [Coutts 1986, Blackburn et al. 1988, Gardiner et al. 1997, Papesch et al. 1997] reported, root *anchorage weakening and damping are significant factors in the windthrow process* and this area of research still needs to be developed.

1.4 Research motivation

As wind loading is a stochastic process, interaction between wind, tree, and soil-root system is extremely complicated and collecting a mature field tree-root system response to the increase in wind loading and change is soil conditions is impractical, we have considered a new approach in this thesis.

In order to understand the dynamic response of a tree-root-soil system to changing wind speed and soil conditions:

i. We examined a mature field tree and root system in response to the static winch loading;

ii. We tested tree saplings with root systems in clay and sand in a wind tunnel;

iii. We conducted an extensive analysis of field tree response to static pull loads and dynamic response of tree saplings with root systems in the different soil media to increases in wind loading;

iv. We further examined the stability response with changing root architecture and soil media to increases in wind loading, using a novel trenching method in the wind tunnel experiments.

Since the research in this thesis concentrates on the analysis of a mature field tree response to static loading and tree sampling dynamic response to the wind loading, an appropriate tree species was required for study.

We chose the Norway spruce (Picea abies) as a reference species because of the following reasons, i) it is well populated in both native (Europe) and non-native (North America) lands, ii) being an ornamental and Christmas tree, it is widely planted in urban communities as well, and is often damaged in storm events, iii) it is a large, fast growing tree which generally tends to have a plate root system, making it more susceptible to windthrow, and iv) it is already a well-studied species in windthrow research [Brüchert et al. 2000, Peltola et al. 2000, Spatz and Bruechert 2000, Jonsson et al. 2006 & 2007, Lundstrom et al. 2007 and 2008].

1.5 Research objectives

The goals of the four articles presented in this thesis are listed below:

i) To investigate the load response of a mature field tree along with the root system subjected to static loads and to develop a simple model incorporating soil strength parameters that connects the tree bending response to the root plate anchorage strength for static loading.

ii) To study the dynamic response of tree sapling stem and roots, with structural root systems embedded in sand and clay soil media under wind loading.

iii) To compare the field tree response with tree sapling response tested in the wind tunnel, to study tree scaling and the difference between the static and dynamic load responses of trees.

iv) To examine the effect of trenching volumes on tree stability with increases in wind speed and changes in soil properties.

1.6 Thesis organization

This is an Integrated-Article Thesis with Chapter 1 introducing the aims of this thesis, along with the research objectives. Chapters 2-5 are the four manuscripts with self-contained introductions and summary. Even though this is an integrated article format, a number of the chapters are inter-related, Chapter 2 and 3 are the necessary precursor for Chapter 4. Chapter 6 presents the summary and the main conclusions derived from the entire thesis. Further content description for each chapter is given below.

Chapter 2 describes the winching test study conducted on a mature field tree to help understand the tree and root response to lateral static pull loads. The tree, root and soil material properties are studied in detail along with the structural details. The methods and instrumentation of the tree and root structure to collect the response data are discussed. The data analysis using basic engineering principles is discussed. An initial model that can help derive the failure wind load using non-destructive testing is introduced. The key aspect of novelty in this study is, the predictive model that combines the stem deflection with a Winkler foundation model of the root system.

Chapter 3 describes novel wind tunnel testing of tree saplings, with root systems in sand and clay and the stem base on a force-balance apparatus. The tree saplings with root systems were instrumented to collect the response data with increase in wind loading; the new instrumentation techniques used for the study are presented. The response data are used to derive the tree sapling dynamic properties. The dynamic analysis included the tree sapling and root sway response, natural frequency, damping and admittance with increase in wind speed. For the first time, change in tree sapling and root component damping ratios with increase in wind speed are presented and also the root admittance is presented with varying root architecture and soil medium.

Chapter 4 presents the comparison of the tree sapling (model) response from Chapter 3 to the full scale field tree response from Chapter 2. The main aim of this chapter is to help link the field tree response from the model tree response thereby determining scaling and similitude between the two sets of trees. Geometric, elastic and stress similarities of the model and full scale trees are discussed along with the load transfer to the root system. In this chapter the tree sapling response under static and dynamic loading are compared with root systems in both sand and clay medium. Dynamic loading characteristics such as fatigue and ratcheting patterns are examined. The effect of load direction on tree stability under both static and dynamic loading is also presented. Secant modulus of rotation and dynamic load factor are presented with increase in static and dynamic loading.

Chapter 5 presents a novel wind tunnel testing technique used for trenching. The instrumented tree sapling and root response with increase in wind speed and trenching is presented. The effect of trenching and loss of root structure on tree stability is examined in both clay and sand soil media. Tree stem deflection, secant modulus of rotation, sway, admittance, root response and probability of failure are examined with increase in wind speed and incremental trenching and compared with change in soil medium.

1.7 Thesis format

The format of this thesis is an Integrated-Article Thesis. This thesis follows the guidelines specified by the Faculty of Graduate Studies at the University of Western Ontario. Each chapter, except the first and the last are presented in a technical paper format without an abstract, but with its own references. Tables and figures of each chapter are presented at the end of bibliography section of the respective chapters. The list of symbols and abbreviations of the entire thesis is presented in the opening sections of the respective chapters. The SI (System International) unit system is used throughout the thesis.

1.8 References

Achim, A., & Nicoll, B. C. (2009). Modelling the anchorage of shallow-rooted trees, Forestry, 82(3). http://doi.org/10.1093/forestry/cpp004

Anderson, C. J., Campbell, D. J., Ritchie, R. M., & Smith, D. L. O. (1989). Soil hear strength measurements and their relevance to windthrow in Sitka spruce. Soil Use and Management, 5(2), 62–66.

Baker, C. J. (1997). Measurements of the natural frequencies of trees. Journal of Experimental Botany, 48(310), 1125–1132.

BBC (2014). http://www.bbc.com/news/world-asia-india-29581787.

Blackburn, P., & Petty, J. A. (1988). An assessment of the static and dynamic factors involved in wind throw. Forestry, 61(1), 29–43. http://doi.org/10.1093/forestry/61.1.29

Blackwell, P. G., Rennolls, K., & Coutts, M. P. (1990). A Root Anchorage Model for Shallowly Rooted Sitka spruce, Forestry, 63(1).

Brüchert, F., Becker, G., & Speck, T. (2000). The mechanics of Norway spruce [Picea abies (L.) Karst]: Mechanical properties of standing trees from different thinning regimes. Forest Ecology and Management, 135(1–3), 45–62. https://doi.org/10.1016/S0378-1127(00)00297-8

Castro-García, S., Blanco-Roldán, G. L., Gil-Ribes, J. a., & Agüera-Vega, J. (2008). Dynamic analysis of olive trees in intensive orchards under forced vibration. Trees - Structure and Function, 22(6), 795–802. http://doi.org/10.1007/s00468-008-0240-9

Coutts, M. P. (1983). Root architecture and tree stability. Plant and Soil, 71, 171–188. http://doi.org/10.1007/BF02182653

Coutts, M. P. (1986). Components of tree stability in sitka spruce on peaty gley soil. Forestry, 59(2), 173–197. http://doi.org/10.1093/forestry/59.2.173.

Cremer, K.W., Borough, C.J., McKinnell, F.H. and Carter, P.R. 1982 Effects of stocking and thinning on wind damage in plantations. N. Z. J. For. Sci. 12, 224-268.

Crook, M. J., & Ennos, A. R. (1996). The anchorage mechanics of deep rooted larch, Larix europea x L-japonica. Journal of Experimental Botany, 47(303), 1509–1517. http://doi.org/10.1093/jxb/47.10.1509

Crook, M. J., Ennos, A R., & Banks, J. R. (1997). The function of buttress roots: a comparative study of the anchorage systems of buttressed (Aglaia and Nephelium ramboutan species) and non-buttressed (Mallotus wrayi) tropical trees. Journal of Experimental Botany, 48(314), 1703–1716. http://doi.org/10.1093/jxb/48.9.1703

Crook, M.J., and Ennos, A.R., (1993). The mechanics of root lodging in winter wheat, Triticum aestivum L. Journal of Experimental Botany 44, 1219–1224.

Cucchi, V., Meredieu, C., Stokes, A., Berthier, S., Bert, D., Najar, M., Lastennet, R. (2004). Root anchorage of inner and edge trees in stands of Maritime pine (Pinus pinaster Ait.) growing in different podzolic soil conditions. Trees, 18(4), 460–466. http://doi.org/10.1007/s00468-004-0330-2

Davenport, A. G. (1964). The buffeting of large superficial structures by atmospheric turbulence. Annals of the New York Academy of Sciences, 116(1), 135–160.

Davenport, A. G. (1967) Gust Loading Factors. ASCE Journal of the structural division, 93:11-34.

DNV-RP-C205 “Environmental Conditions and Environmental Loads”, Det Norske Veritas, Høvik, Norway, 2010.

EM-DAT: The OFDA/CRED International Disaster Database 2014. http://www.bbc.com/news/world-asia-india-29592243

Ennos, A. R. (1993). The Scaling of Root Anchorage. Journal of Theoretical Biology. http://doi.org/10.1006/jtbi.1993.1040

Fraser, A. I. (1962). The soil and roots as factors in tree stability. Forestry, 34, 117–127. http://doi.org/10.1093/forestry/34.2.117

Gardiner, B. (1989). Mechanical characteristics of Sitka Spruce. Forestry Commission Occasional Paper No. 24.

Gardiner, B. (1992). Mathematical modelling of the static and dynamic characteristics of plantation trees. In: Mathematical Modelling of Forest Ecosystems (Franke, J. & Roeder, A. eds) Frankfurt

Gardiner, B. A, Stacey, G. R., Belcher, R. E., & Wood, C. J. (1997). Field and wind tunnel assessments of the implications of respacing and thinning for tree stability. Forestry, 70(3), 233–252. http://doi.org/10.1093/forestry/70.3.233

Gardiner, B. A. (1995). The interaction of wind and tree movement in forest canopies. In M. P. Coutts and J. Grace [eds.], Wind and trees, 41–59, Cambridge University Press, Cambridge, UK.

Harris, R.I. (1968). On the spectrum and auto-correlation function of gustiness in high winds. Electrical Research Association. Report number 5273.

Hassinen, A., Lemettinen, M., Peltola, H., and Gardiner, B. (1998). A prism-based system for monitoring the swaying of trees under wind loading, Agricultural and Forest Meteorology, 90(3): 187–194.

Hoag, D.L., Fridley, R.B. and Hutchinson, J.R., 1971. Experimental measurement of internal and external damping properties of tree limbs. Transactions of the ASAE: 20-28.

Holbo, H. R., Corbett, T. C., and Horton, P. J. (1980). Aeromechanical behavior of selected Douglas-fir. Agricultural Meteorology, 21(2), 81–91. http://doi.org/10.1016/0002-1571(80)90056-4

Holmes, J. D. (2001). Wind Loading of Structures. Spon Press, New York.

James, K. (2003). Dynamic Loading of Trees. Journal of Arboriculture, 29(3), 1–7.

James, K. R., Haritos, N., & Ades, P. K. (2006). Mechanical stability of trees under dynamic loads. American Journal of Botany, 93(10), 1522–1530. http://doi.org/10.3732/ajb.93.10.1522

James, K., and Haritos, N. (2010). The Role of Branches in the Dynamic Response Characteristics of Trees, Australian Earthquake Engineering Society 2010 Conference, The Institution of Engineers, Australia.

James, K., Hallam, C., and Spencer, C. (2013). Tree stability in winds: Measurements of root plate tilt. Biosystems Engineering, 115(3), 324–331. http://doi.org/10.1016/j.biosystemseng.2013.02.010

Jonsson, M. J., Foetzki, A., Kalberer, M., Lundström, T., Ammann, W., and Stöckli, V. (2007). Natural frequencies and damping ratios of Norway spruce (Picea abies (L.) Karst) growing on subalpine forested slopes. Trees - Structure and Function, 21(5), 541–548. http://doi.org/10.1007/s00468-007-0147-x

Jonsson, M. J., Foetzki, A., Kalberer, M., Lundström, T., Ammann, W., & Stöckli, V. (2006). Root-soil rotation stiffness of Norway spruce (Picea abies (L.) Karst) growing on subalpine forested slopes. Plant and Soil, 285(1–2), 267–277. https://doi.org/10.1007/s11104-006-9013-7

Kaimal, J. C., Wyngaard, J. C., Izumi, Y. and Cote, O. R. (1972). "Spectral characteristics of surface-layer turbulence." Journal of Royal Meteorological Society, 98, 563-589

Kane, B., & James, K. R. (2011). Dynamic properties of open-grown deciduous trees. Canadian Journal of Forest Research, 41(2), 321–330. http://doi.org/10.1139/X10-211

Kerzenmacher T, Gardiner B. A. (1998) A mathematical model to describe the dynamic response of a spruce tree to the wind. Trees 12:385–394

Lundström, T., Heiz, U., Stoffel, M., and Stöckli, V. (2007). Fresh-wood bending: linking the mechanical and growth properties of a Norway spruce stem. Tree Physiology, 27(Siau 1995), 1229–1241.

Lundström, T., Jonas, T., and Volkwein, A. (2008). Analyzing the mechanical performance and growth adaptation of Norway spruce using a non-linear finite-element model and experimental data. Journal of Experimental Botany, 59(9), 2513–2528. http://doi.org/10.1093/jxb/ern116

Mayer, H. (1987). Wind-induced tree sways. Trees, 1, 195–206. http://doi.org/10.1007/BF01816816

Mayhead, G. J. (1973). Sway periods of forest trees. Scottish Forestry, 27, 19–23.

Mergen, F. (1954). Mechanical aspects of wind-breakage and wind firmness. Journal of Forestry, 52: 119-125.

Mickovski, S. B., & Ennos, A. R. (2003). Anchorage and Asymmetry in the Root System of Pinus peuce. Silva Fennica, 37(2), 161–173.

Milne, R. (1991). Dynamics of swaying of Picea sitchensis. Tree Physiology, 9(11976), 383–99. Retrieved from http://www.ncbi.nlm.nih.gov/pubmed/14972849

Moore, J. R. (2000). Differences in maximum resistive bending moments of Pinus radiata trees grown on a range of soil types. Forest Ecology and Management, 135, 63–71. http://doi.org/10.1016/S0378-1127(00)00298-X

Moore, J. R. (2002). Mechanical Behavior of Coniferous Trees Subjected to Wind Loading, 232.

Moore, J. R., and Maguire, D. A. (2004). Natural Sway Frequencies and Damping Ratios of Trees: Concepts, Review and Synthesis of Previous Studies. Trees, 18, 195–203. http://doi.org/10.1007/s00468-004-0387-y

Moore, J. R., and Maguire, D. A. (2005). Natural sway frequencies and damping ratios of trees: influence of crown structure, Trees, 19:363–373. http://doi.org/10.1007/s00468-004-0387-y

Moore, J. R., and Maguire, D. A. (2008). Simulating the dynamic behavior of Douglas-fir trees under applied loads by the finite element method. Tree Physiology, 28(1), 75–83. http://doi.org/10.1093/treephys/28.1.75

Neild, S. A., and Wood, C. J. (1999). Estimating stem and root-anchorage flexibility in trees, Tree Physiology, 19(3):141-151.

Oliver, H.R., and Mayhead, G.J. (1974). Wind measurements in a pine forest during a destructive gale. Forestry, 47(2): 185–194. doi:10.1093/forestry/47.2.185.

Ow, L. F., Harnas, F. R., Indrawan, I. G. B., Sahadewa, A., Sim, E. K., Rahardjo, H., and Tan, P. Y. (2010). Tree-pulling experiment: An analysis into the mechanical stability of rain trees. Trees - Structure and Function, 24(6), 1007–1015. http://doi.org/10.1007/s00468-010-0470-5

Papesch, A. J. G., Moore, J. R., and Hawke, A. E. (1997). Mechanical stability of Pinus radiata trees at Eyrewell forest investigated using static tests. New Zealand Journal of Forestry Science, 27(2), 188–204.

Peltola, H. (1996). Swaying of Trees in Response to Wind and Thinning in A Stand of Scots Pine, Boundary-Layer Meteorol, 77: 285–304.

Peltola, H., and Kellomaki, S. (1993). A mechanistic model for calculating windthrow and stem breakage of Scots pines at stand edge. Silva Fennica.

Peltola, H., Kellomäki, S., Hassinen, A., and Granander, M. (2000). Mechanical stability of Scots pine, Norway spruce and birch: An analysis of tree-pulling experiments in Finland. Forest Ecology and Management, 135, 143–153. http://doi.org/10.1016/S0378-1127(00)00306-6

Petty, J. A. and Worrell, R. (1981) Stability of Coniferous tree stems in relation to damage by snow. Forestry, 54, 115-128.

Petty, J.A., and Swain, C. (1985). Factors influencing stem breakage of conifers in high winds. Forestry, 58: 75–84.

Rees, S. W., and Ali, N. (2012). Tree induced soil suction and slope stability. Geomechanics and Geoengineering, 7(2), 103–113. http://doi.org/10.1080/17486025.2011.631039

Roodbaraky, H., Baker, C., Dawson, A. and Wright, C. (1994). Experimental observations of urban trees. J. Wind Engng Ind. Aerodyn. 52, 171–184

Sani, L., Lisci, R., Moschi, M., Sarri, D., Rimediotti, M., Vieri, M., and Tofanelli, S. (2012). Preliminary experiments and verification of controlled pulling tests for tree stability assessments in Mediterranean urban areas. Biosystems Engineering, 112(3), 218–226. http://doi.org/10.1016/j.biosystemseng.2012.04.004

Sellier, D., & Fourcaud, T. (2009). Crown Structure and Wood Properties: Influence on Tree Sway and Response to High Winds. American Journal of Botany, 96(5), 1–12. https://doi.org/10.3732/ajb.0800226

Sellier, D., and Fourcaud, T. (2005). A mechanical analysis of the relationship between free oscillations of Pinus pinaster Ait. saplings and their aerial architecture. Journal of Experimental Botany, 56(416), 1563–1573. http://doi.org/10.1093/jxb/eri151

Sellier, D., Brunet, Y., and Fourcaud, T. (2008). A numerical model of tree aerodynamic response to a turbulent airflow. Forestry, 81(3), 279–297. http://doi.org/10.1093/forestry/cpn024

Sellier, D., Fourcaud, T., and Lac, P. (2006). A finite element model for investigating effects of aerial architecture on tree oscillations. Tree Physiology, 26(2), 799–806. http://doi.org/10.1093/treephys/26.6.799

Spatz, H. C., and Bruechert, F. (2000). Basic biomechanics of self-supporting plants: Wind loads and gravitational loads on a Norway spruce tree. Forest Ecology and Management, 135, 33–44. http://doi.org/10.1016/S0378-1127(00)00296-6

Spatz, H. C., and Theckes, B. (2013). Oscillation damping in trees. Plant Science, 207, 66–71. http://doi.org/10.1016/j.plantsci.2013.02.015

Spatz, H. C., Brüchert, F., and Pfisterer, J. (2007). Multiple resonance damping or how do trees escape dangerously large oscillations, American Journal of Botany, 94(10), 1603–1611. http://doi.org/10.3732/ajb.94.10.1603

Stokes, A. (1999). Strain distribution during anchorage failure of Pinus pinaster Ait. at different ages and tree growth response to wind-induced root movement. Plant and Soil, 217, 17–27. http://doi.org/10.1023/A:1004613126353

Sugden M. J. (1962). Tree sway period: a possible new parameter for crown classification and stand competition. Forestry Chronical, 38, 336–344.

Szoradova, A., Praus, L., and Kolarik, J. (2013). Evaluation of the root system resistance against failure of urban trees using principal component analysis. Biosystems Engineering, 115(3), 244–249. http://doi.org/10.1016/j.biosystemseng.2013.03.001

Watson, A. (2000). Wind-induced forces in the near-surface lateral roots of radiata pine. Forest Ecology and Management, 135(1-3), 133–142. http://doi.org/10.1016/S0378-1127(00)00305-4

Zeng, H., Pukkala, T. and Peltola, H. (2007). The use of heuristic optimization in risk management of wind damage in forest planning. Forest Ecology and Management, 241: 189-199.

Figure 1-1 Loss of trees and infrastructure after cyclone Hudhud 2014 in Vishakhapatnam, India [www.deccanharold.com]

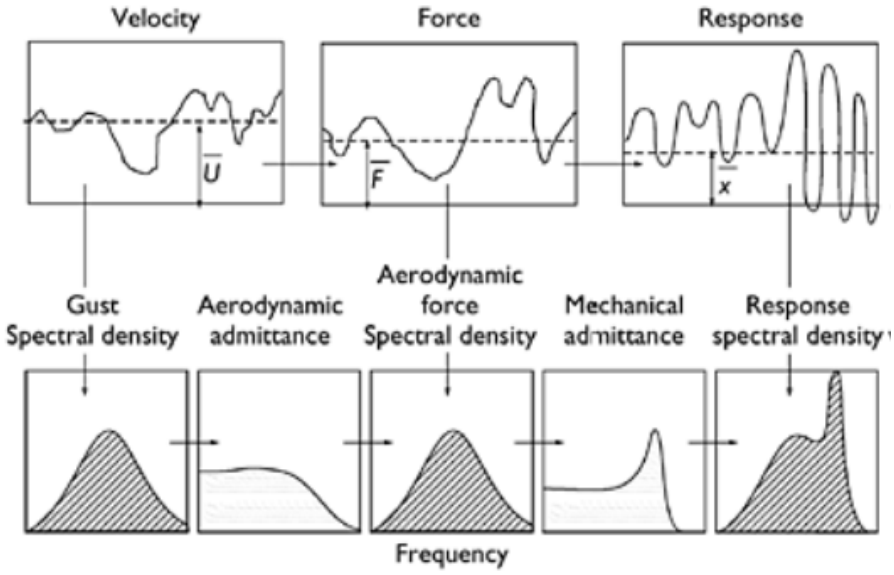

Figure 1-2 The random vibration (frequency domain) approach to resonant dynamic response [Davenport 1964]

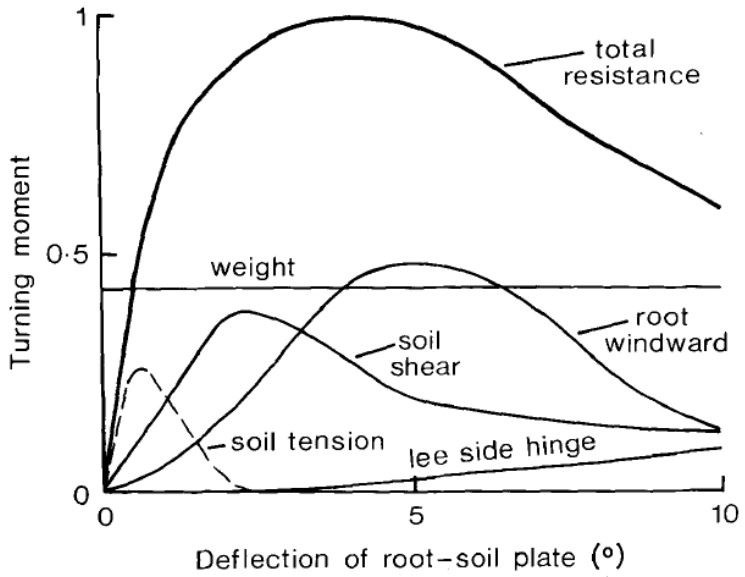

Figure 1-3 Schematic representation of the contribution of components of anchorage to the total turning moment during uprooting [Coutts 1983]

Chapter 2

2 Stem and root system response of a full-scale Norway spruce during static loading

2.1 Introduction

Change in climate patterns are causing storms to be more intense and the occurrence of storms has also begun to increase [IPCC 2007]. Among the various factors causing storm damage to infrastructure, windthrow is responsible for a significant amount of economic loss and more notably loss of many peoples' lives during wind storms. Given the importance of tree stability to the economics and safety of society in both urban and forested environments, it is not surprising that windthrow studies have gained popularity over the last few decades [e.g. Coutts 1983 & 1986, Crook and Ennos 1996, Stokes 1999, Gardiner et al. 2000, Moore 2000, Lundstrom et al. 2007, James and Kane 2008]

Tree failure under wind loading can be either from stem breakage or uprooting. Relative strength of the stem in bending or the anchorage resistance of the root-soil system will decide the form of failure [Pretty and Worrell, 1981]. In general, tree stability is estimated based on the dendrometric characteristics of the tree (usually thorough visual inspection), empirical and/or mechanical models [Kamimura and Shiraishi 2007]. Visual assessment is the least reliable approach and is an over-simplified method because of the absence of root plate information and possible concealment of wood defects. Empirical or regression models are developed from winching test data sets or from wind damage surveys [Hanewinkel et al. 2004]. Even though these statistical models are accurate for particular stands, one problem with these methods is their limited applicability to other types of stand, as these methods are developed based on specific tree and stand attributes [e.g. Valinger and Fridman, 1999; Lanquaye and Mitchell, 2005; Scott and Mitchell, 2005]. Empirical methods only give general information on the windthrow mechanism [Gardiner et al. 2008]. Semi-empirical models such as ForestGALES and HWIND are used successfully in the forestry sector [Peltola and Kellomäki 1993, Gardiner et al. 2000, Elie and Ruel 2005], but tree stability assessment in urban environments is less well developed and

potentially more complex because of thigmomorphogenesis (as urban trees are more likely to be isolated and exposed).

In urban settings, the stability of each tree needs to be estimated with good reliability, which can be complicated since very different resistance can be found from tree to tree. This is partly due to the mechanical characteristics of the available soil medium; such as its compaction, water content, and the attendant irrigation system, and also the availability of space (i.e. limitations because of the urban infrastructure). Nicoll and Ray 1996 noted that the rooting depth of 46-year-old Sitka spruce (*Picea sitchensis (Bong.) Carr.*) was restricted because of water table. Root systems had more structural root mass on the leeward side compared to the windward side because of prevailing wind. Also, trees under greater wind exposure showed stronger anchorage [Nicoll et al. 2008]. Hence root system growth can be very different from one tree to another. Changes in the tree root anchorage can be significantly different because of the adaptable nature of trees and the root systems. Another commonly used method of prediction is the mechanistic approach and this can be the most reliable approach available in such situations. The mechanistic approach is the characterization of the physical process involved in tree uprooting or failure [Gardiner et al. 2008]. The main advantage of the mechanistic method is its adaptability to various situations [Kamimura and Shiraishi 2007], making it the most accurate method available to test the anchorage strength of urban trees. For urban areas, accurate assessment of potentially variable tree stabilities is particularly more important because of the high risk of safety and damage.

The mechanistic approach for tree stability assessment or characterization of tree failure is commonly obtained using static pull (winching) tests [Coutts 1986, Peltola et al. 2000, Stokes et al. 2005, James et al. 2013]. Total over-turning bending moment and stem fracture resistance estimates are fairly accurate physical models; factors affecting estimates such as tree stem properties and tree weight are involved in the model, but it is not the case when it comes to root anchorage estimate. Coutts [1983&1986] and Blackwell et al. [1990] identified the components of anchorage as windward root resistance, soil root plate weight, leeward hinge resistance to bending, soil resistance and the weight of stem and crown; they observed that the soil resistance plays most important role in early stages of loading and

fails when the applied force reaches about 70% of the total anchorage resistance. Even though soil fails in shear long before the occurrence of uprooting, because of the plastic nature of soil it continues to resist displacement [Ennos 1994]. Consistent windthrow stability variation with change in soil shear strength has been observed by many researchers [Mergen 1954, Fraser 1962, Dupey et al. 2005a, Crook and Ennos 1996, Ennos 1994, Moore 2000, Cucchi et al. 2004], soil strength parameters are still not the main contributing parameter in any of the root anchorage models [Blackwell et al. 1990, Peltola and Kellomäki 1993].

Even though soil strength plays an important role in tree stability [Moore 2000], because of the complexity of root anchorage none of the available mechanical anchorage resistance models include soil strength parameters. Among the available root anchorage models, Achim and Nicoll [2009] disregarded the leeward root and soil resistance in the modelling process. Even though Blackwell et al. [1990] considered all of the aspects in their mathematical model, it did not accommodate the soil strength sensitivity (the root anchorage model showed no change in anchorage strength with ±10% change in soil shear strength).

Root movements under wind induced loading or static winching of the tree has also been examined in the field of windthrow research [Ennos 1995, Crook and Ennos 1996, Crook et al. 1997, Stokes 1999, Watson 2000], for better understanding of root anchorage mechanics. All of the studies in this area used strain gauges on the roots to track the load response. These studies suggest that while winching the tree, stresses on the root-soil plate were high and close to the trunk; bending in the leeward laterals was observed, while the windward laterals were pulled out of the ground. The windward roots provided most of the anchorage compared to the leeward lateral roots. As the usage of the finite element methods in tree stability has increased [Fourcaud et al. 2003, 2008, Dupuy et al 2007, Yang et al. 2014], more detailed root-plate system responses to the applied loading has become possible [Lundstrom et al. 2007]. These models showed the significance of soil strength on root-soil plate anchorage strength.

Dupuy et al. 2005 and 2007, Fourcaud et al. 2007, and Yang et al. 2014 examined the variation in anchorage strength with change in root morphological and soil mechanical parameters using the ABAQUS software. Dupuy et al. 2005 examined the influence of root morphology on root anchorage using simple root system arrengements. Single root pull out was found to be a combination of root and soil failure and root-soil interaction resistance. Number of lateral roots and soil cohesion were proven to be significant contributing parameters to root anchorage, in addition to root diameter and number of branches in the rooting arrengement. Dupuy et al. 2007 determined that the soil type influences the failure mode. Even though the numerical model predicted higher resistance than the measured values in the field, relative comparison between cohesive (cohesion, c = 20 kPa; friction angle, $\varphi = 0^o$; Poisson's ratio, $\nu = 0.49$; unit weight, $\gamma = 20$ kN/m^3 and Young's modulus, E = 20MPa) and frictional soils (c = 1.5 kPa; $\varphi = 25^o$; $\nu = 0.3$; $\gamma = 20$ kN/m^3 and E = 20 MPa) with respect to root-soil anchorage strength was made. Simulations with cohesive soil resulted in 70 % increase in anchorage strength compared to the frictional soil resistance measured in field. Fourcaud et al. 2007 examined the relative roles of root anchorage using numerical simulations, superficial laterals, deep roots, tap roots, and soil charecteristics in anchorage were studied. Saturated soft clay (c = 5 kPa; $\varphi = 2^o$; $\nu = 0.45$; $\gamma = 1$ kN/m^3 and E = 5 MPa) and loamy sand (c = 2 kPa; $\varphi = 40^o$; $\nu = 0.25$; $\gamma = 1.5$ kN/m^3 and E = 10 MPa) were chosen in ABAQUS software simulations with 12 different root patterns. In clayey soil, the longest roots influenced the size of the root-soil plate formed during overturning and localized roots had no influence on anchorage strength. In sandy soil, tap and deep roots had more influence on anchorage strength and also removing individual roots influenced the anchorage strength.

Yang et al. 2014 examined the effect of individual root behaviour and soil on the anchorage strength. Successive root breakage effects were linked to the tree overturning response. The initial slope of the root-soil anchorage stiffness varied from -37.5 to 32.1 % positively with ± 50 % varation in root modulus of elasticity. Whereas with ± 50 % variation in soil modulus of elasticity, the initial stiffness of the root-soil anchorage varied -19.2 to 8.3 %. However cohesion and frictional properties of the soil individually did not change the stiffness significantly. The complex root-soil interaction under tree lateral response needs

to be investigated further and soil components should be incorporated in the root anchorage models to improve the accuracy of tree stability estimates.

Another essential method used by many researchers [Neil and Wood 1999, Lundström et al 2007 and Szoradova et al. 2013] was estimating the root-soil plate stiffness parameter using static pulling tests. This study has been done using both destructive and non-destructive methods. The root-soil plate stiffness parameter is the ratio of stem base bending moment to the root plate rotation angle. This is an essential component to understand root anchorage mechanics. From the literature, small trees showed more deformable root-soil plate rotation compared to larger trees making larger trees more vulnerable to wind loading [Lundström et al 2007]. Root-soil plate rotation was observed to be higher under dynamic loading compared to static pull loads [James et al. 2013]. The trend of moment-rotation curves indicates the tree failure load through uprooting and is parameter dependent [Szoradova et al. 2013]. Even though this is a laborious process, its non-destructive features are especially useful in urban settings. Sinn and Wessolly [1989] published the "generalized tipping curve" using the data obtained from destructive tests of 400 trees. This curve gives empirical guidelines of tree failure probability under given loads, and this method gives quantitative information on tree stability through non-destructive methods.

The present work utilizes this approach to provide detailed field data. In this study, we tracked the load response of a full-scale, well instrumented mature Norway spruce tree in the field with a complete root system under controlled winch loading and propose a novel root plate foundation model to aid interpretation of the load-deflection behavior. The strain gauge response of the roots (attached along the root plate length), were used to estimate the load–deflection relation at a number of locations (along the length of the windward and leeward roots) to map the stiffness variation across the spread of the root plate and provide parameters for the model.

The soil supporting the root plate is idealized as a Winkler beam on springs foundation model, which is a widely used predictive tool for soil-structure interaction problems. Traditional Winkler foundation models have a system of closely spaced independent

springs simulating the soil response, aligned along the foundation length and attached to the structural foundation. This load deflection method has been modified by many researchers since Bartlett [1979], to model the complex behavior of various soil-structure interaction problems. The system of Winkler springs can also be combined with dash pot and gap elements to extend the usage of the model to dynamic and uplift loading problems.

Yim and Chopra [1984], Chopra and Yim [1985] investigated the earthquake vibration response of structures with partial uplift on a Winkler foundation. Chen and Lai [2003] proposed an elasto-plastic Winkler foundation model for seismic response of a bridge pier. Allotey and Naggar [2003] provided a complete analytical solution for the static moment–rotation response of a rigid footing resting on a Winkler soil model for different cases: an elastic condition, uplift only condition, soil yield only conditions to soil yield and foundation uplift condition corresponding to moment-rotation curve segments. Houlsby et al. [2005] generalized a Winkler model to capture the response of a rigid foundation subjected to combined vertical, horizontal and moment loading. Raychowdhury and Hutchinson [2009] proposed a nonlinear Winkler-based shallow foundation model for seismic loading.

The model proposed herein builds upon the work of Chopra and Yim [1985], Allotey and Naggar [2003], Houlsby et al. [2005] and Raychowdhury and Hutchinson [2009]. The model response has been limited to static loading for the scope of this work, but it can also be extended to dynamic loading problems in the future. This chapter provides a well-documented static pull test on a full scale tree and the calibration of this model. It is hoped that this will provide the basis for greater understanding of windthrow and a predictive model for use as a tool by various stakeholders.

2.2 Research objectives

The objective of this study was to examine the form of a mature tree and its root-soil plate, estimate the static and dynamic properties of the entire system, understand the response of tree and root plate to static winching loads, and develop a model for determining the critical failure load through stem breakage or uprooting. A key aspect of novelty is the incorporation of the soil strength into the model. A Norway spruce was used in the study

due to their ubiquity in the Ontario landscape, simplicity of form and common damage during windstorms. Data analysis has been performed to determine the following aspects:

i. To study the form and material behavior of a mature tree and its root structure;

ii. To examine the rotation and deflection along the height of the stem under static loads;

iii. To study the bending moment profiles derived from the stem deflection profiles for successive increments of static load;

iv. To study the vertical and lateral stress distribution along the length of leeward and windward roots under static loads;

v. To estimate the stiffness resistance offered by the leeward and windward roots in relation to uprooting;

vi. To develop a predictive model combining the deflection of the stem with a Winkler foundation model of the root system, to estimate the tree anchorage stability based on the root-soil stiffness.

2.3 Chapter organization

This chapter describes the static tree pulling test and the dynamic sway tests that were conducted on a mature field tree. Tree stem taper, crown shape, and mass distribution are detailed. Excavated root plate size and architecture are described. The examined material properties of stem, root and soil are presented. Using sway tests, the natural frequency and damping of the stem and the roots is estimated. The experimental setup is discussed. The data recorded using tilt sensors installed at various heights of the stem is presented and processed. Tree response is studied using engineering principles along with available modeling techniques in tree stability analysis. The tree stem load deflection, curvature and bending moment profiles are discussed with increase in winch load. The root response data recorded using the strain gauge rings attached along the root length with increase in winch load is analyzed. The response data of roots are used to determine strain, bending moment, shear force, and deflection response of the roots with increase in winch load. An elastic

large deflection cantilever model of the tree stem is combined with a Winkler foundation model to provide insight into the root plate behavior. The tree anchorage strength is also estimated using the base bending moment and root-soil plate rotation response to the applied pull load through the tangent intersection method.

2.4 Tree shape and taper

A mature 24-year-old Norway spruce tree was selected in the Davey tree farm, in Shalersville, Ohio, USA, during the Tree Biomechanics Research week in 2010. This tree was selected at the edge of the cultivated tree farm. Although this is not strictly an 'urban' tree this environment is taken as a proxy for this type of tree given the shape of the stand, number, and spacing of the surrounding trees. The ratio of live crown length (22.8 m) to total height (23.1 m) was 0.99. The 23.1 m tall spruce tree was pruned up to the height of 6.45 m above the ground level, to allow easy setup and access of sensors on the stem and also on the root plate. The pruning also helped to shift the overall center of gravity of the stem and crown closer to the pull height.

The tree was pulled to failure with a cable attached at a height of 9.57 m as shown in the Figure 2-1. Once the tree was winched to failure, stem taper, wood density, representative length of the branches, number of branches and the weight of branches along the stem height was measured. The root plate was uncovered with an airspade and excavated from the ground to measure the dimensions and determine the architecture.

2.4.1 Stem

Total height of the tree (H) and the diameter at breast height (DBH) were 23.1 m and 0.458 m respectively, and the stem taper (H/DBH) was 50.4, which is less than the proposed threshold in the literature of 60 (a highly tapered tree) making it potentially less vulnerable to stem breakage, e.g. Papesch et al. 1997, Peltola et al. 2000, Moore 2000, Kamimura and Shiraishi 2007, and more similar to an urban tree.

Diameter of the stem was measured from stump height to 16.5 m height of the tree at 3 m intervals and the remainder of the values from 16.5 m to 23 m height were extrapolated using a linear fit of measured diameters as shown in Figure 2-2. Total stem volume was

estimated assuming a linear taper shape. Stem diameter at stump height (DSH) was 0.547 m and the lowest diameter (D_o) of the stem (estimated from the linear fit) was 0.023 m. The total mass, volume, and mass density of the stem were estimated as 1072 kg, 1.34 m^3, and 800 kg/m^3 respectively. The mass center of gravity was estimated to be 5.83 m above ground level.

2.4.2 Crown

Crown shape and mass distribution of the selected Norway spruce tree was measured. Before the test setup, the tree was pruned up to 6.75 m of the tree height above the ground level. The pruned branch mass was 53% of the foliage mass. The total foliage mass weighed after pruning was 540.5 kg. After the winch pull, the entire tree was divided into 0.3 m long sections. Branches from each section were collected separately. Representative weight and length of the branches from each section was noted and plotted as shown in Figures 2-3 and 2-4. The representative branch length at 1.4 m height was 5.4 m. The Centre of gravity of the crown mass shifted from 8.0 m to 12.3 m above ground level after pruning. The overall center of mass of the upper part of the tree structure was estimated to be 8.3 m above ground level.

2.4.3 Root Plate

The root plate area was cleaned and partially exposed using an air spade, to confirm selection of a tree with symmetric root plate architecture and enable instrumentation to be attached. The top layer of the winched tree root plate consisted of 11 lateral structural roots, which were evenly distributed and were partially exposed. One windward root and a leeward root from the root plate were selected for instrumentation. Taper of the instrumented roots was measured and strain gauges were attached along the length of the roots. The taper and shape of the selected roots is shown in the Figures 2-6 and 2-7. After the winching test, structural roots in the top layer of the root plate were completely exposed using the air spade. After careful examination of the lateral structural roots, the entire root system was pulled out. A top view of the root plate and architecture are as shown in the Figure 2-5. The mid-section of the root plate consisted of around 20 sinker roots distributed more or less evenly and almost all the sinker roots had two sub-branches. The length of the

roots in the mid-section varied from 1.3 to 0.7 m with an average of 0.044 m diameter. The extracted root plate system is shown in Figure 2-5. The average depth of the root plate was about 0.9 m. The diameter of the root plate varied from 3.1 to 3.4 m. The base area and the volume of the root plate were measured using root plate pictures Figure 2-8 using the ImageJ software. The plate base area and the volume were measured and found to be 3.9 m^2 and 1.16 m^3.

2.5 Material properties

2.5.1 Static

The stem and root material strength properties were examined. Three-point bending tests and the moisture content tests were conducted on wood samples collected from the stem. Test setup for the three-point bending tests was as shown in the Figure 2-9. ASTM D198-09 method of testing was used to test the modulus of elasticity with a beam shaped sample taken from various points in the stem. The span between the two supports was adjusted to five times the thickness of the tested sample [Figure 2-9]. Even though span to depth ratio should be 15:1, because of the size of the available sample from the tested tree stem the span was taken five times the sample thickness. Table 2-1 shows the values vary between 0.8 and 1.2 GPa. The estimated value of the E was five to seven times lower than a typical spruce tree E. As this is the only available estimate from the tested tree [USDA Wood Handbook], E=1.2 GPa is considered for further calculations. Brüchert et al. [2000] examined the E of Norway spruce tree stem structural wood and found it to vary from 3 to 8 GPa. They also found that the E of a dominant tree is 1.9 to 3.6 GPa lower than the average structural E value. In this site, the selected tree was dominant, therefore the E of 1.2GPa is presumed to be reasonable (but on the low side).

ASTM D4442-07 method was also used to measure the moisture content of the collected samples. The moisture content tests were conducted a number of months after the winching test was done. The moisture content of the trunk was observed to be quite low (<10%) which might be because of the dry state of the sample when tested (see Table 2-1). The root sample had 56.8% moisture when tested. The modulus of elasticity of the root was also estimated using the average sonic wave velocity of 2645 m/sec measured by Göcke L.

[2011] (Personal communication) using sonic sensors on the windward root during the pull tests. Using the ASTM C1419-99a method, Modulus of elasticity of the root was estimated as 3.57 GPa based on the measured sonic wave velocity. The discrepancy between the measurements may be accounted for by the low moisture content. The sonic value is therefore taken as more representative and will be used in further calculations.

2.5.2 Dynamic

Response data of the free swaying tree and root system was recorded using sensors installed on the stem and a windward and a leeward root. The tree was pulled and released manually with a cable latched at 9.57 m height on the stem. Natural frequency and damping of the stem and root were calculated using tilt sensor response data on the stem and response data of the strain gauges on the roots. As the pull was manual, only the sensors at 9.31 m height and a strain gauge recording the vertical response of the root on the leeward side located at 0.6 m from the tree center logged enough data to carry out a dynamic analysis. Natural frequency was determined using the raw data plots and also from the spectral analysis. Natural frequency of the stem and the root are calculated as 0.35 Hz and 0.39 Hz respectively. It is important to note that, the data sampling rate of the sensors on the roots was ten times higher than the stem sensor sampling rate.

Damping ratio was estimated using three different methods: Autocorrelation, half power band width and using the motion decay response plots. An average damping ratio of the stem at 9.31 m height and the leeward root were measured as 0.023 and 0.05; natural frequencies and damping ratios of Norway spruce trees growing on subalpine forested slopes varied from 0.14 to 0.3 Hz and 0.027 to 0.055 respectively [Jonsson et al. 2007].

2.5.3 Soil

Soil samples were collected from a 1x1m trench dug 30 m from the tree. Six soil samples were collected from the trench at intermediate depths. Geotechnical properties of the soil in the site were studied using particle size distribution, consistency limits and the fall cone tests on the samples collected from the trench. The soil is categorized based on the particle size distribution of the tested samples. The soil was sieved manually using 5 sieves (4.75mm, 1.0mm, 0.25mm, 0.075mm and 0.01mm sieve openings). Hydrometer tests were

not conducted because of time constraints. All of the samples collected were around 75% finer than the 1.0mm sieve size and around 25% finer than the 0.075 mm sieve size. The soil can therefore be classified as silty sand (SM). With uniformity coefficient varying from 20-30 (Cu >6) and coefficient of gradation at around 1 in most cases and below 3 in all cases, it can be classified as well graded sand (SW). Liquid limit and the plastic limit of the sampled soil passing the sieve number 60, with an opening size of 0.250 mm were as listed in Table 2-2. Liquid limit and plasticity indices (liquid limit-plastic limit) calculated using the concept of Atterberg limits [ASTM-D4318], shows that the soil can be classified as sandy organic clay (OL) based on the plasticity chart. The Davey tree company classified this location as silty loam.

Water content of the samples varied from 25 to 13% with depth as shown in the Figure 2-11. Undrained shear strength of the sampled soil was also estimated using the Geonor Fall cone apparatus. The soil properties measured from the soil samples collected from the trench are also listed in Table 2-2. Soil shear strength was also tested insitu using a Pilcon Hand Vane tester. The in-situ soil shear strength in the trench, both in vertical and horizontal direction showed comparable strength. Soil strength under the tree in the root-soil plate was found to be twice as high compared to the soil collected from the trench as shown in the Figure 2-10 showing the potential sink effects of the roots.

2.6 Instrument setup

In order to examine the load response of an entire tree and root system to both static and dynamic loading, the tree stem and the root system were instrumented with tilt sensors and strain gauges respectively. The tree was swayed and winched to failure and the resultant dynamic and static load response was recorded.

The selected Norway spruce tree for the experimental study was pruned up to the height of 6.75 m. The stem was instrumented with 6 tilt sensors and a strain gauge at the base. Tilt sensors (N4 inclinometers with $\pm 70^{o}$ range; 3 from Seika and 3 from Reiker with 3.65 $mV/^{o}$ sensitivity) were placed at three different heights (0.3 m, 5.8 m and 9.31 m above the stem base) on the stem. At each location, 2 tilt sensors were attached, one sensor to track the stem deflection in the winch pull direction and the other sensor to track the response in

transverse direction (90^{o} from the winch pull direction). A strain gauge was placed at a height of 0.8 m on the stem in the leeward direction of the stem to track the response in the winch pull direction.

Two roots were selected for instrumentation, one root on the leeward (winch pull) direction and the other one on the windward (counter to the winch pull) direction. KFG-30-120-C1-11L1M2R type strain gauges were used to track the root response; these strain gauges are two wire lead gauges with 30 mm gauge length and 120-ohm resistance. To attach the strain gauges, bark was removed carefully without damaging the root wood fibers. Strain gauges were glued to the roots using Cyanoacrylate adhesive (CC-35X5), which is best suited for porous materials with operating temperature range of -30 to 120^{o}C. Strain gauges were attached at three locations along the length of each root in regular intervals, to track the lateral and vertical strain with increase in winch load as shown in Figure 2-13. A ring of four gauges were attached at each location; two were located opposite one another to track the vertical strain and the other two placed 90 degrees from the previous ones to track the lateral response. Each set of two gauges were placed diametrically opposed to one other so that one gauge would track the tension and the other would track compression response. They were connected to the logger in a basic Wheatstone bridge configuration using half bridge arrangement.

The winching test methodology used was very similar to the tests conducted by Byrne and Mitchell [2007] as shown in Figure 2-12. The cable attachment height was 9.57 m. A manual Tirfor winch with 3200 kg capacity was used for the final pull to tree failure. For the sway tests, the cable was manually pulled and released. The applied winching force was recorded using a load cell attached inline to the pull cable. Data from stem, roots and load cell were recorded using three different loggers and analyzed using the respective calibrations.

2.7 Response of tree to loading to failure

Stem response data during winching was collected from the calibrated tilt sensors attached at three different heights (0.3 m, 5.8 m and 9.31 m) on the stem [Figure 2-12]. The winch cable attachment height and the calculated center of mass of the pruned tree superstructure

above the ground level were 9.57 m and 8.3 m respectively. Stem rotation at each height is taken as the angle of deflection of that particular stem location from stem base obtained from the tilt sensor response [Figure 2-14]. At each load increment, stem rotation data of the three tilt sensors was used to estimate the stem deflection. Stem deflection (d_t) from each data point was calculated using the following equation:

$$d_t = h_t \tan\theta \qquad [2\text{-}1]$$

Where d_t and h_t are the respective deflection and height (meters), and θ is the rotation (degrees), at each tilt sensor location on the stem.

Total overturning bending moment [M_c] due to the static pull load and the self-weight was estimated using the following equation [after Urata et al. 2011]:

$$M_c = M_w + M_s = (hF\cos\varphi + \delta F\sin\varphi) + \delta_G W_T g \qquad [2\text{-}2]$$

Where M_w is the moment of pulling load [Nm], h is the pull height [m], F is the pulling load [N], φ and δ are the angle of pull and the horizontal displacement of the stem at pull height respectively and M_s, δ_G, W_T, and g are the self-loading moment, horizontal stem displacement at the center of gravity of the above ground part, above ground mass and gravity [9.8m/s^2], respectively.

Base bending moment due to the winch load and self-weight of the tree superstructure was estimated as shown in Figure 2-14 using Equation [2-1] and [2-2]. The deflection at pull height (9.57 m) was taken as the deflection at the Tilt sensor 1 (at 9.31 m height) and the deflection at the center of mass height (8.3 m) was estimated using linear interpolation between Tilt sensor1 (at 9.31 m height) and Tilt sensor 2 (at 5.8 m height). This data was used to calculate the base bending moment for each load increment.

Stem rotation at the tilt sensor locations with increase in base bending moment was as shown in the Figure 2-15. Stem rotational response to the base bending moment with increase in winch load was used to understand the variation in rotational stiffness of the stem with increase in tree height. The peak stem rotation was approximately 4 degrees at 0.4H above the stem base and caused a basal bending moment of 10^5 Nm. The slope of the

base bending moment vs rotation curve is taken as the rotational stiffness of the stem. Clear decrease in rotational stiffness with stem height can be observed [Figure 2-15], at the stem base (0.3m above the ground level) the rotational stiffness was 8.3 MN.m/rad, at 5.8 m the rotational stiffness was 1.9 MN.m/rad and at 9.31 m height above the ground level the stem rotational stiffness was 1.4 MN.m/rad. High rotational stiffness at stem base shows the significant component of root-soil stiffness in the base bending moment response.

Figure 2-16 shows deflection of the stem at three different heights (9.31 m, 5.8 m and 0.3 m) with increase in winch load. The stem horizontal deflection to the increase in winch load gives an indication of stem stiffness variation with height. The highest observed rotations were about 0.7 m at approximately 25 kN winch load. The linear part of the load vs deflection curve indicates the elastic nature of the stem deflection. At the stem base (0.3 m height above the ground level), stem showed linear deflection up to the failure load; at 5.8 m above the ground level, stem showed linear deflection up to 73% of the failure load; and at 9.31 m above the ground level, the stem showed linear deflection up to 85% of the failure load as shown in the Figure 2-16.

For easier understanding of the tree response with increasing winch load, four successive load increments were chosen and the stem rotations at three different locations along the stem height were collected from the load response data of the tilt sensors. Tree deflection at each load increment along the stem height (at three tilt sensor locations) was fitted to a second degree polynomial function [$y = ax^2 + bx + c$] and extrapolated to get the deflection profile of the tree along the entire tree height with increase in winch load. Figure 2-17 shows the deflection profile of the tree for each load increment. The tree stem failed at 26.5 kN winch load, proportional increase in stem deflection up to 80% of the failure load can be observed from Figure 2-17. It needs to be noted that only at three stem locations the deflections were recorded at only 3 stem locations and the remainder were extrapolated; these deflection profiles were only plotted to visualize the stem response to increase in winch load.

The bending moment profile of the stem was estimated using the deflection profile of the tree. The deflection profile, i.e. the transverse displacement (y) of the stem along the stem

location (x) at each load increment was differentiated once and twice with respect to tree height (x) to estimate the bending moment profile of the stem at each load increment. The curvature and bending moment relationship using Euler-Bernoulli beam theory [Thomson 1993] as shown below:

$$\text{curvature} = \frac{1}{R} = \frac{\frac{d^2y}{dx^2}}{\left[1 + \left(\frac{dy}{dx}\right)^2\right]^{\frac{3}{2}}} = \frac{M(x)}{EI(x)} \qquad [2\text{-}3]$$

where M(x) is the bending moment along the tree stem height(x); E is the Young's modulus of elasticity, which is taken constant (1.2 GPa is obtained from three point bending tests) throughout the stem height; $I(x) = \frac{\pi d_x^4}{64}$ is the moment of inertia of the tree cross-section along the tree height (cross-section is assumed as circular), and dx is the diameter of the tree stem varying along the tree height; In order to accommodate the large scale deflections of the stem, the curvature of the stem was not simplified to $\frac{d^2y}{dx^2}$.

The curvature and bending moment profile M(x) of the tree were calculated using Equation [2-3] at each load increment and are shown in the Figures 2-18 and 2-19 respectively. The maximum curvature value was found to be 0.55. From Figure 2-18, it is interesting to note that at failure load the highest curvature point was the stem fracture point. This proves the suitability of this approach for this study.

The bending moment profiles of the tree stem at five load increments are presented in Figure 2-19. The pull height of the winch was 9.57 m above the ground level and the crown was pruned up to 6.57 m height above the ground level. The overall tree center of mass (stem + crown) was estimated to be 8.3 m above the ground level. The maximum bending moment at the stem base, sudden shift in profile at the crown height and pull height can be observed from the bending moment profiles. It is interesting to note, proportional increase in bending moment with increase in winch load up to the failure load. The bending moment reduced by 4-5 orders of magnitude up the tree from approximately 1.0 MNm at the base to 10 Nm at 20 m height. At failure the bending moment below the winch pull height and

the overall tree center of mass height was very high, showing the tree weight contribution to the failure load.

The stem fracture resistance is commonly estimated using the following equation [after Pretty and Worrell, 1981], Maximum resistive bending moment [M_b] at breast height [1.4 m] is estimated as

$$M_b = \frac{\pi \times MOR \times DBH^3}{32} \quad [2\text{-}4]$$

Where MOR is the modulus of rupture [MPa], MOR can be estimated based on the density relationship developed by Walford [1993]; this estimate is based on tree family and maturity.

Base bending moment at failure load was used to estimate the fracture strength (MOR) of the stem [2-4]. Maximum base bending moment at the fracture load was estimated using Equation [2-2] to be 118 kNm and modulus of rupture was estimated as 12.5 MPa. Maximum resistive bending moment of pine trees on different soils tested by Moore [2000] varied from 79 kNm to 122 kNm and the modulus of rupture of 15 m tall Norway spruce trees was estimated as 36.26 MPa with a 6.99 MPa standard deviation by Peltola [2000]. In this study, the tree was 23.1 m in height, and showed higher resistive bending moment and lower modulus of rupture.

2.8 Response of roots to loading to failure

A major aim of this study has been to model the anchorage strength of the root system. Since the anchorage strength (rooting) of the tested tree was higher than expected, the tree unfortunately failed due to stem fracture. The root response data collected during sub-failure winching has therefore been used to try to estimate the anchorage strength. Even though the selected tree root anchorage strength was much higher than expected and the movement of the root plate was not visible to the naked eye or the video (used to identify the root plate movement), the attached instrumentation on the roots can be used to study the root response to increases in winch load. To help understand the root plate response with increase in winch load, the same load increments as those used to study the stem

response were chosen to study the anchorage strength. Therefore, the response data of the three strain gauges located on both the windward and leeward roots were used to determine the strain acting at each gauge location with increase in winch load.

For the study, the strain gauged root on the winching side of the tree is considered to be the leeward root and the strain gauged root on the counter-winch side of the tree as the windward root. The three sampling locations on each root enabled a fit to a second degree polynomial equation [$y = ax^2 + bx + c$] to determine the strain response along the root length at each load increment. Strain response plots at each load increment were used to calculate the bending moment response plots. Shear force distribution and the deflection profiles of the windward and leeward roots were estimated using the bending moment profiles of the root response in both vertical and horizontal direction at each load increment.

The strain (ε) on the roots from the response data was estimated using the relationship shown below:

$$\varepsilon = 2\frac{V_o}{V_s}\frac{1}{S} \qquad [2\text{-}5]$$

Where V_o is the response data in Volts, V_s is the input voltage used (5V), (the constant 2 is used as the gauges were connected using a half bridge mode) and S is the gauge factor given by the manufacturer (for the gauges used, S is 2.08).

For easier understanding of the root plate response with increasing winch load, four successive load increments and the failure load were chosen as per the study of the stem response. Root strain gauge responses at each load increment were plotted and were used to visualize the root response. The strain response of the roots in the horizontal and vertical directions relative to the ground level plane were plotted in Figures 2-20 and 2-21 respectively.

In Figure 2-20, horizontal or lateral strain responses of both windward and leeward roots for the incremental winch loads are presented. Leeward root horizontal strain response was higher compared to the windward root response and also the pattern of strain response is similar with increase in winch loads. The highest strain response on the leeward side was

350 μstrain compared to 150-250 μstrain on the windward side. For the case of the vertical strain response of the roots [Figure 2-21], the strain close to the trunk was much higher and the windward root vertical response was a little higher for the failure winch loads. Vertical strain close to the trunk exceeded 600 μstrain, whereas the highest strain at the ends of the root plate was -100 μstrain on the leeward side and 200 μstrain on the windward side. Proportional response of roots to the applied winch load indicates that the anchorage strength was much higher than the stem failure strength. A similar root strain response was also observed by Stokes [1999].

Bending moment (BM) response of the roots was calculated using the following equation.

$$BM = \varepsilon EZ \qquad [2\text{-}6]$$

Where E is the modulus of elasticity of the roots and is taken as 3.7 GPa (estimated using the sonic wave speed recorded on the windward root). The same value was used for both the roots and all of the gauge locations. Z is the second moment of inertia calculated using the measured diameters at each gauge location $\left[Z(x) = \frac{\pi R_x^3}{32}\right]$, where R_x is the diameter of the root at the strain gauge location.

Bending moment response of both the windward and the leeward root in both vertical and transverse directions was fitted to a second degree polynomial, using the data logged from the three strain gauge locations of each case. In the second degree polynomial, bending moment is represented by y and x is the location of the strain gauge along the root length. At the stump (i.e. the full diameter of the base of the stem), x is taken as zero varying up to the full root length.

$$\text{Bending Moment (BM)} = y = ax^2 + bx + c \qquad [2\text{-}7]$$

Lateral and vertical bending moment responses of roots with increase in winch loads are presented in Figure 2-22 and 2-23 respectively. Bending moment response of the leeward root was much higher compared to windward root response; both lateral and vertical bending moment response of the roots were very similar. The maximum bending moment response of the leeward root was 1.3 kNm in the horizontal direction and close to the stem,

whereas the bending moment response on the windward root was 0.1 kNm in the opposing direction (close to the stem). In the vertical direction, maximum bending moment response was 2.4 kNm on the leeward root and the windward root showed 0.4 kNm of maximum bending response in the opposing direction. Root bending moment response close to the stem was much higher, for both leeward and windward roots. Opposing bending moments can be observed on windward and leeward roots because of the applied pull load. A similar bending response pattern to that observed in this study was also found by Niklas [2000].

Differentiating the bending moment profile in Equation [2-7] with respect to the root length gave the shear force profile:

$$\text{Shear Force} = \frac{dy}{dx} = 2ax + b \qquad [2\text{-}8]$$

Note: x varies from 0 (at the stump end) to the root length at the root tip.

Lateral and vertical shear force distribution along the root length are as shown in Figures 2-24 to 2-25 respectively. Shear force on the leeward root was about 7 to 11 times higher than the shear force on the windward root. Dominant compressive load on the leeward root and the tensile load on the windward root can be clearly observed. Maximum shear force in the horizontal direction, close to the stem on the leeward root was 7.8 kPa and on the windward root it was 0.8 kPa in the opposing direction. Maximum shear force in the vertical direction close to the stem on the leeward root was 12.2 kPa, whereas on the windward root it was around 0.8 kPa close to the stem and also at the end of the root plate. The windward root response was in the opposite direction to the maximum response of the leeward root. Similar shear force patterns were also found by Niklas [1999].

Load per unit length acting on the windward and the leeward root at each load increment is obtained by differentiating the shear force along the root length.

$$\text{Load per unit length (Load intensity)} = \frac{d^2y}{dx^2} = 2a \qquad [2\text{-}9]$$

For the ease of this analysis, each root is assumed to act as a cantilever beam with a fixed end at the stump. Based on this assumption, rotation and deflection are taken as zero at x=0

(the stump end). Integrating the bending moment profile once and twice gave rotation and deflection profiles respectively along the root length as shown below:

$$\text{Rotation} = \int \frac{BM}{EI} = \int a_1x^2 + b_1x + c_1 = \frac{a_1x^3}{3} + \frac{b_1x^2}{2} + c_1x + d_1 \quad [2\text{-}10]$$

$$\text{Deflection} = \iint \frac{BM}{EI} = \frac{a_1x^4}{12} + \frac{b_1x^3}{6} + \frac{c_1x^2}{2} + d_1x + e_1 \quad [2\text{-}11]$$

The integration constants d and e were derived as zeros using the cantilever beam boundary conditions (fixed at the stem). The horizontal and vertical deflection profiles along the root length are as shown in the Figures 2-26 and 2-27 respectively. Lateral deflection of the leeward root was around 20 times higher compared to the windward root lateral deflection. Vertical deflection of the leeward root was half as much compared to the windward root vertical deflection. The maximum horizontal deflection of the leeward root was 28 mm away from the stem and the maximum deflection of the windward root was close to the stem and was around 2 mm in the opposite direction. Maximum vertical deflection of the windward root was 12.2 mm close to the stem compared to the leeward root 4 mm deflection away from the stem in the opposite direction. The data suggests that when the stem was tilted (while winching towards the leeward side), the leeward root slides horizontally and compressive load on the root pushed the root vertically into the ground. Whereas the windward root was pulled out of the ground slightly in the vertical direction with little lateral displacement.

To calculate the root-soil stiffness at each strain gauge location, each load per unit length parameter was estimated using Equation [2-9] and plotted with the respective deflection profiles estimated using Equation [2-11] as shown in the Figure 2-28. These load-deflection curves are generally used in geotechnical engineering to analyze buried pipeline and lateral loaded pile responses. Structurally the concept is the same for the root-soil plate structure; the root plate can be represented as a pile and the supporting soil medium can be represented as a series of non-linear springs as would be used for a laterally loaded pile in soil. Stiffness is the slope of the load-deflection curve; the linear part of the load deflection curve gives the elastic stiffness of the root-soil structure at that particular location. Stiffness

values estimated from the load-deflection curves [Figure 2-28] are also presented in Table 2-3.

The windward root lateral stiffness (k_h) values were not determined because of a lack of response (i.e. insufficiently high loads); the windward root barely moved in the horizontal direction up to the failure load. As the leeward root showed around twice the stiffness values for the vertical response compared to the vertical stiffness values of the windward root and the leeward root lateral stiffness values were also relatively low, the windward root lateral stiffness (k_h) values were therefore taken based on the leeward root lateral stiffness values. As shown in Table 2-3, the horizontal stiffness of the windward root was therefore taken as half of the leeward root lateral stiffness values at the respective locations on the windward root. Vertical stiffness (k_v) values of the two roots varied from 1.6 to 12.3 N/mm^2 and the lateral stiffness (k_v) values of the roots varied from 0.026 to 0.114 N/mm^2.

The overall stiffness of each spring at a single location (i.e. 1, 2 or 3) is the equivalent stiffness of the vertical and horizontal spring combination. As the horizontal and vertical springs are assumed to be in series at each location, the spring stiffness can therefore be estimated with:

$$k_{eq\ (local)} = \frac{1}{\frac{1}{k_v} + \frac{1}{k_h}} \qquad [2\text{-}12]$$

Since the three springs on each root are side by side, the load response of the spring affects the response of the other springs and deflection by different amounts, so the equivalent spring stiffness of each root needs to be calculated assuming the springs are parallel to each other. The three springs on both windward and the leeward direction were therefore assumed to be in parallel as shown in Table 2-3. The equivalent spring stiffness of the windward and the leeward root soil stiffness were estimated using Equation [2-13] :

$$\mathrm{k_{eq\ (root)}} = k_1 + k_2 + k_3 \qquad [2\text{-}13]$$

The equivalent stiffness of the windward and the leeward root was estimated as 0.115 N/mm^2 and 0.229 N/mm^2 respectively. As the load from the stem base is transferred to the

attached roots from the same stem base point to both sides, the equivalent stiffness values of windward (ww) and leeward (lw) roots are assumed to be in series. Therefore, the equivalent stiffness of the entire root plate is estimated to be 0.076 N/mm^2 [Table 2-3].

What also needs to be determined is whether the minimal windward lateral response of the root was limited to this particular root structure or this is the general nature of root plate response? In general, the stiffness was much higher closer to the stem [Table 2-3], as is also described in the literature [e.g. Coutts 1983, Crook and Ennos 1996, Niklas 2000, Stokes 1999, Lundstrom 2007].

The load intensity and deflection curves obtained at different root locations [Figure 2-28] are not straight lines for the tree tested in this study; elastic-plastic deformation of the root-soil response can therefore be clearly observed. Since the system has nonlinear stiffness that varies with width (foundation length) and position (vertical and horizontal response), this comparison allows us to find the relative stiffness of the windward and the leeward root to the root plate anchorage and also helps us to identify the key locations of the root plate, that offer the maximum resistance to uprooting. Blackwell et al. [1990] used a similar approach in their mathematical root anchorage modelling and also represented the root-soil resistance by an array of springs. Even though the model of Blackwell et al. [1990] did not show any change in anchorage resistance with ±10% change in soil shear strength, the importance of soil strength on root anchorage was noted. In this study, the root-soil stiffness is explicitly included using the experimental data obtained from the full scale experiment.

Non-linear load-deflection analysis of laterally loaded piles which structurally behave as tree roots can be analyzed using p-y curves [Matlock 1970, Reese et al., 1975]. Once the equivalent p-y relationship (subgrade reaction modulus) for a given combination of pile size (root size) and soil type is established, it is a simple and relatively straight forward approach to estimate the load-deflection behavior of roots for different soil media. Whilst there are a range of equations available to *a priori* estimate the subgrade reaction modulus for foundations, due to the novel nature of root plate mechanics, this approach requires further work. Even though these techniques need to be explored further and more tests and

analysis need to be conducted to validate the method, this appears to be a valuable approach to explore the effect of soil strength on tree stability.

2.9 Estimating the anchorage strength using the tangent intersection method

The capacity of the soil to support loads from a building foundation with no shear failure can be determined based on its bearing capacity (bearing pressure at which the supporting ground fails in shear [Whitlow 2001]). In geotechnical engineering, one of the methods used to estimate the bearing capacity of a foundation from load-displacement curves is the tangent intersection method [Mansur and Kaufman, 1956]. In this method, two tangent lines are plotted along the initial and later part of the load-displacement curve as shown in Figure 2-31, the intersection point of the two tangent lines is taken as the 'bearing capacity'. The same approach was therefore used to estimate the maximum contact pressure between the root plate and soil with no shear failure, due to the absence of this type of failure in the field testing, thereby allowing an estimate of anchorage strength.

In many studies, stem base moment is considered to be the root stiffness [Jonsson et al. 2006, Ghani et al. 2009, and Szoradova et al. 2013]. To compare the stem base stiffness to the root plate stiffness, in this chapter the stem base bending moment with the base bending moment rotation from the strain gauge data is plotted as shown in Figure 2-29. The stem base stiffness (for small rotations) was estimated to be 146.69 kNm/degree or 8258 kNm/rad; similar stiffness results were also obtained by Jonsson et al. 2006 for Norway Spruce.

In addition to the instrumentation used for this experimental study [Section 2.6], PiCUS: TreeQinetic® inclinometers were also used by other researchers on the roots as shown in the Figure 2-30. The data of the root response to the applied pull load was obtained through personal communication [Wassenaer and Detter, 2011]. The TreeQinetic® inclinometers have 0.005^{o} accuracy, 0.005^{o} resolution and $\pm 15^{o}$ measuring range. The root rotational response from the TreeQinetic® inclinometers, to the base bending moment (estimated using Equation [2-2]) is shown in the Figure 2-30.

As the tree failed through stem fracture, the maximum vertical rotational response of the root plate is only 1.2^{o} in Figure 2-30, and the stem base rotation from the strain gauge readings was only 0.6^{o} [Figure 2-29]. As uprooting failure usually occurs at a root zone tilt of 2.5 to 4^{o} [Coutts 1986, Lundstrom et al. 2007a, Wessolly and Erb 1998, Brudi and Van Wassenaer 2002], the response data from Figure 2-30 was extrapolated using a second order polynomial. The root response which recorded higher rotational response is used for further calculations. The extrapolated response is shown in Figure 2-31; using the tangent intersection method, the uprooting of this tree would have occurred at 4.8^{o} tilt and 345 kNm base bending moment. These values fall under the norms of failure load presented in the literature; Lundstrom et al. [2007a] reported an anchorage strength of 200 to 400 kNm for 70 Norway spruce tree tested with similar properites as this study.

This method could be another simple and useful approach to estimate tree stability through non-destructive testing; a major problem in root research has been to assess the root anchorage strength with no damage [Smit et al. 2000, Szoradova et al. 2013]. It also needs to be noted that the limit loads estimated using this method tend to vary by 2%-5% based on drawing the deviation of the tangent lines [Hung and Kim 2014].

2.10 Winkler foundation model for the root plate response

Using the findings of Sections 2.8 & 2.9, a modified Winkler foundation model is proposed to describe shallow root plate response to wind loading on trees. Using this force-resultant model, the entire behavior of the root-soil plate can be captured in terms of the applied resultant force and the corresponding displacements. A Winkler foundation model is chosen not only because of its relative simplicity but also because of its versatility. This model can incorporate nonlinear aspects of foundation response with minimum computational efforts.

Even though Blackwell et al. [1990] represented the soil with a number of springs spread under the root plate area, this model was not explored fully by incorporating soil-root stiffness parameters. The soil spring failure was estimated based on an assumption that the proportion of spring failure is a function of transformed deflection, making the model non-variable with respect to soil strength (anchorage strength did not vary with ±10% change

in soil shear strength). As has been observed by various researchers, the soil strength has a significant effect on the anchorage strength of trees [Anderson et al. 1989, Moore 2000, Cucchi et al. 2004, Ow et al. 2010]. Therefore, it is advantageous to have a root-soil anchorage model which varies with the soil strength. However, the precise relation between the root plate anchorage strength and the root-plate soil shear strength is still unknown.

As shown in Figure 2-32, the foundation (root-soil plate) is assumed to have a diameter of 2b. A series of springs with stiffness, k_w represents the soil-structure interaction. The structural response of the slender column with mass (m) at the top is governed by a stiffness, k_b. Rotations of the foundation (θ) and the cantilever base are assumed to be the same. It is assumed in the analysis of the earthquake response of structures that rotational stiffness is constant until one edge of the foundation uplifts. The same assumption can be used for a soil-root anchorage model. The relation between the static moment (M) applied at the center of gravity of a structure and the resulting foundation-mat rotation (θ) for both unbonded and bonded conditions is as shown in the Figure 2-33 [Yim and Chopra 1984]. It is also noted by Yim and Chopra [1984], that the rotational stiffness is constant as long as the foundation mat is bonded to the supporting elements. Hence using this idealization, the slope of the elastic region or the rotational stiffness can be taken as $k_\theta = \frac{2k_w b^3}{3}$.

The ultimate and critical moment can be estimated in this study by assuming the moment-rotation relation shown in the Figure 2-33. Also using this idealization, the uplift moment and the uplift root plate rotation is reached at the point where the moment rotation curve shown in Figure 2-33 transitions from the elastic region to the plastic region (point A). The uplift rotation is defined as:

$$\theta_u = \frac{p}{2k_w b^2} \qquad [2\text{-}14]$$

Where the structural weight, p= mg and the total vertical load acting on the foundation is p. From the model it can be observed that the uplift is initiated when $\theta_u = \frac{p}{2k_w b^2}$, corresponding to the uplift moment m_u= pb/3. Beyond these values the response in non-linear and at the critical load (M_c) the tree fails. The foundation rotational stiffness (k_θ) is

based on the beam stiffness ($k=k_b$) and this is taken as $k_\theta = k_b h^2$ (h is the beam height [Figure 2-32] and the Winkler foundation stiffness (by rearranging) is calculated using:

$$k_w = \frac{3k_\theta}{2b^3} \quad [2\text{-}15]$$

Once the equivalent stiffness (k_w) of the Winkler foundation is obtained (from experimental data), the next step is to estimate the failure load.

When a tree structure is subjected to wind loading the load transferred to the root plate is a combination of vertical, horizontal and moment loading. Considering the complexity of the problem and the scope of this work, the wind load for this study was replicated by a static winch load and the root plate by a point-wise Winkler model [Houlsby et al. 2005] as shown in Figure 2-32. The tree stem and crown was idealized as a flexible cantilever structure with a lumped mass (m) on top and the lateral stiffness (k_b). The root plate is taken as the foundation mat on the soil and the soil as a Winkler foundation with spring elements distributed over the width of the foundation. For this case three springs on each side were chosen; spring stiffness was estimated from the load deflection curves at each location as described in Section 2.6.5.

However, it should be noted that there is a difference between a structural foundation and root-soil plate due to the anchorage strength. Hence this Winkler foundation theory may need to be modified to incorporate the additional anchorage strength potentially offered by the root-soil plate. To quantify the effect of root anchorage strength and estimate the ultimate failure loads, this idea is further explored in the calculations below.

2.10.1 Winkler foundation stiffness estimates

The following represents a first estimate of the behavior based on this model. Four different estimates of k_w can be made from the assembled dataset.

1) *Winkler foundation stiffness estimate using equivalent spring stiffness* [Figure 2-28]:

As $k_{eq}=k_w$, from the spring calculations, if the vertical and lateral springs are assumed to be in series, k_w= 76 kN/m^2;

2) Winkler foundation stiffness estimate using stem base rotational stiffness* [Figure 2-29]*:

Root plate rotational stiffness from the strain gauge at the stem base = k_θ= 147.8 kNm/degree.

From the Winkler foundation approach, $k_\theta = 2k_w b^3/3$

[In this case k_b, is already estimated in terms of k_θ (kNm/degree), so k_θ is directly taken from the calculations.]

Using Equation [2-15], k_w= 51.2 kN/m^2;

3) Winkler foundation stiffness estimate using the tree natural frequency:

Total mass of the tree above ground was=m= 1613 kg [Section 2.4.1 & 2.4.2]

Natural frequency=ω=0.35 s^{-1} [Section 2.5.2]

Hence, the tree stem stiffness; $k_b = m\omega^2$

∴ k_b=197.6 N/m

foundation rotational stiffness based on the beam stiffness using $k_\theta = k_b h^2$ is

k_θ=105.4 kNm/degree

and using the Winkler foundation approach, $[k_\theta = 2k_w b^3/3]$

k_w= 36.5 kN/m^2;

4) Winkler foundation stiffness estimate using root plate rotational stiffness* [Figure 2-30]*:

Root plate rotational stiffness from the strain gauge at the stem base = k_θ= 89 kNm/degree

Using Equation [2-15], k_w= 51.2 kN/m^2.

Having estimated k_w from the various tree response properties, the uplift rotation and loads can be estimated using, $\theta_u = \frac{p}{2k_w b^2}$ and $M_u=\theta_u * k_\theta$. To conduct these calculations, the tree 'weight' (p) needs to be considered. A pertinent question to ask for this model idealization, does the weight of the root-soil plate need to be included in the total tree weight (p)? The initial Winkler foundation stiffness estimates conducted here address the anchorage responses of the root plate to the above ground failure load, thus p is initially taken as the tree weight above ground only = 15.8 kN [Section 2.4.1 & 2.4.2].

The ultimate rotation and the failure bending moment estimates are as shown in Table 2-4. From the literature [e.g. Coutts 1986, Lundstrom et al. 2007a, Wessolly and Erb 1998, Brudi and Van Wassenaer 2002], the uprooting failure occurs for a root zone tilt of 2.5 to 4^o. The estimated failure rotation from these estimates varied from 2.2^o to 5.6^o [Table 2-4] and the failure moment from 491-499 kNm. Even though some of the estimated results are slightly on the high side, given the high anchorage strength of the examined tree, these results seem plausible. The results obtained using Winkler foundation theory are plotted as shown in Figure 2-34. It is interesting to note, the ultimate failure moment obtained from various parameters is approximately the same. If this is the case for many trees, the ultimate failure load from ultimate bending moment can be obtained using a simple parameter like tree natural frequency. The failure envelope obtained in this study [Figure 2-34] could also be obtained with less invasive methods.

2.10.2 Modification of the Winkler foundation model for the root plate structure:

Another approach to the modelling could be to include the mass of the root plate in the total tree structure weight (p).

If only the geometry and unit weight of the tree are available, it is informative to predict the failure values of the tree. From the Winkler model [Figure 2-33], uplift failure bending moment is Mu= pb/3,

Where, p=total weight of the structure and b=radius of the foundation= 1.63 m.

To estimate the total weight of the tree including the root-soil plate (p), the following calculations are conducted:

Tree mass above ground = 1613 kg [Section 2.4.1 & 2.4.2];

Root-soil plate volume measured using ImageJ software (a hemispherical shape is assumed for further calculations with 0.9 m depth) = 1.16 m^3 [Section 2.4.3];

$1/4^{th}$ of the stem volume is taken as the root volume and the rest of the root-soil plate volume as the soil volume [Danjon et al. 2005];

Stem volume = 1.34 m^3; root density= 1000 kg/m^3 (green weight) [Dupuy et al 2005]; and soil density=20 kN/m^3 [Section 2.5.3];

Therefore, the above ground tree weight+ root-soil plate weight =32 kN;

With p=32kN and b=1.63 [Section 2.4.3], therefore M_u= pb/3=17.4 kNm.

It is clear from this analysis that the ultimate bending moment from the Winkler foundation calculations (M_u= pb/3) is now still very low compared to the tangent intersection method (385 kNm) [Figure 2-31] and the previous Winkler foundation stiffness estimates (490 to 500 kNm) [Table 2-4]. It can be postulated that for a tree root structure that the equivalent stiffness (k_{eq}=k_w) of the Winkler foundation is the combination of tree-root-soil weight and the anchorage strength of the root soil plate. Coutts [1983 & 1986] and Blackwell et al. [1990] identified the components of tree anchorage as windward root resistance, soil root plate weight, leeward hinge resistance to bending, soil resistance and the weight of stem and crown. So some of the additional 'missing' capacity should be due to the rotational bending stiffness of the roots at one end of the root plate (k_r) and the tensile (or pullout) capacity of the roots at the other end of the root plate (k_t). Root reinforced soil shear

strength along the root plate and the total weight of the entire tree and root-soil plate are the remaining components of anchorage.

2.10.2.1 Components of tree-root anchorage:

Further calculations are presented below to investigate this hypothesis and to include the aspects of tree anchorage shown in Figure 2-35. It is assumed five windward and five leeward roots of an average diameter of 0.044 m and 1.0 m length contribute to tensile and compressive strength respectively. The major anchorage components are i) tree weight (w_t) and root plate weight (w_r), ii) tensile resistance of the windward root, iii) soil shear strength along the base of the root plate and iv) bending strength of the leeward roots, and are explored further as shown below:

1) Anchorage resistance from tree and root plate weight:

The total tree and root-soil plate weight = 32 kN;

Anchorage resistance component from the structural weight=P_w = 32 kN;

The corresponding resisting moment of the weight component, $M_w=P_wb/3$=17.4 kNm.

2) Tensile (or pull-out resistance) of the windward roots:

(a) Bischetti et al. [2005] suggested the mean tensile strength of Norway spruce tree roots was 38.94 MPa.

In this study, the Norway spruce tree had around 10 structural roots evenly distributed with an average diameter of 0.044 m.

Cross sectional area of 5 roots =5X $\frac{\pi d^2}{4}$ = 0.0076 m^2

Giving an overall tensile strength= P_t =38.94(0.0076) = 0.296 MN =296 kN

∴ total resisting moment from root tensile strength component = M_t =160.83 kNm;

(OR)

(b) Abe & Ziemer [1991] provided an empirical equation of tree root pull-out resistance as:

Pull-out resistance (in pounds of force) =278.7X (root diameter in inches) ^1.03

As almost all the roots were subdivided each with an average diameter of 0.044 m, so 5 roots were taken as the roots resisting the pull-out

P_r= 490.8X5 lbf = 10.92 kN

∴ total resisting moment from root pull-out resistance component = M_r = 5.8 kNm.

(c) Soil shear strength:

Shear strength of the root reinforced soil from vane shear field test = 120 kPa [Figure 2-10].

As 70% of the total root volume contributes to tree stability [Lundstrom et al. 2008],

hence 70% of the root soil plate surface area is considered to contribute to the shear strength [Figure 2-35]

=0.7[$\pi r\sqrt{(r^2 + h^2)}$] = 6.68 m^2

Overall shear force estimated from the vane shear tests =P_s=120X6.68= 800.4 kN

Resisting moment component from soil shear strength = M_s =435 kNm.

(d) Root compressive bending strength:

Stokes and Mattheck [1996] reported the root compression strength of Norway spruce varied from 29.3(±1.6) to 24.5(±1.9) MPa, (± standard error).

Average compressive strength of root = 27 MPa (Stokes and Mattheck 1996), is taken to estimate the root compressive strength.

Compressive strength=P_c= 27(0.0076) = 0.21 MN =210 kN

∴ total resisting moment from compressive strength component = M_c= 114.1 kNm.

Therefore, the total anchorage strength/capacity is approximately 730 kNm. Root-soil weight appears to account for only 2 to 3% of the capacity and the compressive and tensile strength of roots appears to account for 38% of the capacity. The soil shear strength component seems to provide a much higher resistance for the tree root-plate to failure along the surface area of the root-soil plate base. However, the later component will reduce as the soil fractures and the plate uplifts, losing contact with the soil below.

A new predictive method can to be generated along the lines of the Yim and Chopra [1984] model for tree stability analysis, and some of the possible ways of estimating the equivalent stiffness and moment and rotational response are explained in this section. With the availability of large numbers of tree response data sets, one of these simple methods could be quite useful to estimate tree root anchorage strength.

2.11 Discussion

The main aim of this study was to understand the tree-root-soil response to lateral pull loads; to examine the applicability of simple engineering principles to the tree-root-soil response and to introduce soil component to the tree stability analysis. Even though the winched tree failed through stem breakage instead of uprooting, the recorded response of stem and roots to static pull loads up to the tree failure is used for analysis. The static pull load was applied at an angle of 14.7^{o} as shown in Figure 2-12. The stem breakage height was 2 m above the ground and the tree stem failed through stem breakage at a 26.5 kN winch load.

THE STEM RESPONSE

The stem response recorded by the tilt sensors at three different heights (0.3m, 5.8m, and 9.31m; two sensors at each height tracked the response in transverse directions) was used to derive the deflection and bending moment profile of the stem at four selected load increments as explained in Section 2.7.

- Winch pull height was chosen close to the tree center of gravity to see the stem response to wind loading; only 0.8 m deflection was observed at the tree center of gravity height, before the failure load was reached.

- Assuming the tree stem response to be similar to a cantilever beam response seems to be a reasonable assumption. With three sensors along the length of the stem, proportional increase in stem response up to 90% of the failure load was found. This could be a simple analytical and experimental technique to estimate various tree stem responses.

- Bending moment response to winch load was 4-5 orders higher at the stem base, compared to the bending moment response of the stem above 90% of the tree height. The stem base deflection increased up to 0.6^{o} before failure.

- The curvature profile at failure load obtained from the calculations was a maximum at the actual stem breakage height [Figure 2-18], proving this analytical technique to be a

useful means to estimate the stem breakage height. In this study, the tree stem broke at <10% of the stem height.

The conducted winch test on the instrumented tree helped to understand the deflection and bending response of the tree with increase in lateral winch load. Further testing needs to be conducted to prove the applicability of this technique. Because of the simplicity of this approach, it is worth exploring further. It is also important to note that in this case, the root plate was extremely stable and might have helped the stem to act as a true cantilever.

THE ROOT PLATE RESPONSE

A root on the windward side and one on the leeward side were selected and instrumented using strain gauges. The tree was winched to failure and the data was collected from strain gauges during winching. Using the data obtained from strain gauges on the roots, strain, bending moment, shear force and deflection profiles of windward and leeward roots with increase in winch load were calculated, plotted and discussed [Figures 2-20 to 2-27]. Using load deflection profiles on roots [Figure 2-28], stiffness constants, k_v, k_h & k_{eq} were calculated [Table 2-3].

Three sensors along each root helped to quantify the load response of the roots at each load increment. Bending moment and shear force responses were qualitatively same as presumed by Niklas [1999], strain and deflection profiles were same as observed by Crook and Ennos [1996] and Stokes [1999]. This suggests that the analytical and experimental techniques presented in this chapter can be extremely useful to obtain the quantitative information of root-soil plate response under various conditions.

If the tree had uprooted, it would have been very useful to understand root response up to the failure load. But the root plate barely moved, the response presented in this study can only be considered as the initial load response. Similar studies with Norway spruce under different soil conditions would be extremely valuable for comparison and finite element modelling.

The root plate was modeled as a Winkler foundation model supporting the tree structure. The tree structure was modeled as a flexible cantilever with a lumped mass at the top. A relation between structural deformations of the tree associated with base shear was proposed. An important feature of this study is to integrate soil strength parameters in the critical failure load model. In this study a new simple methodology was proposed to estimate the critical failure load (tangent intersection method) [Figure 2-31].

The tangent intersection method explained in this chapter could be a simple and extremely useful method to estimate the anchorage strength of an individual tree. Even though the use of the "generalized tipping curve" helps to identify the safety factor for tree stability, the boundary conditions were not well defined and is only from the data of 400 trees tested. It is more reliable to estimate the anchorage strength of a tree from its own bending and rotational response [Szoradova et al. 2013]. Through this technique (if proven reliable), the stem bending response of up to 0.5° base inclination would be enough to estimate root anchorage strength.

The Winkler foundation model proposed in this chapter could be a feasible way to examine the effect of soil on tree anchorage strength. If proven useful, this method can also be extended to wind loading problems. The stiffness estimates of the roots were higher for the middle of the root structure [Niklas 1999]. Even though quantitatively comparable, the stiffness estimates in this study were higher close to the stem and much lower away from the stem. An explanation could be the effect of soil on the root structure, the stiffness estimates of Niklas [1999] were estimated using the wood sample. In this study the stiffness estimates along the root length were from the combined stiffness of the root-soil plate. The Winkler foundation stiffness estimates could be a new and easier way to estimate the tree anchorage strength.

2.12 Conclusions

This study shows that the stem response can be assumed to give a cantilever beam response to estimate the stem breakage point. Strain gauge placements on three locations on each

root allowed tracking of the stress and strain response of roots with increase in winch loading. From this analysis, as only three strain gauge locations on each root were used, an assumption of zero rotation and zero deflection under the tree stem was made to calculate the root response. In future experiments, an extra strain gauge grid near the tree stem would improve the accuracy of estimates.

This experimental technique helped to examine the root-soil stiffness (subgrade soil modulus) at three different locations on both windward and leeward side of the root system. Once the equivalent modulus of subgrade reaction (k_w) is established (using the strain gauges response) depending on the soil and the root type, a Winkler foundation model could be used in a wide array of situations (with change in both soil and tree species). To estimate the modulus of reaction, static load tests based on ASTM-D1196 standards were used. Using the Winkler foundation model principles, the failure loads of the winched tree were estimated based on four different characteristics of the tree; root soil plate anchorage stiffness (estimated based on root-soil interaction), stem base rotational stiffness, tree natural frequency and root-soil plate rotational stiffness. The estimated failure turning moments were approximately the same from these four characteristics of the tree, showing this could be a feasible method in windthrow research. Also, a more practical tangent intersection method is introduced in this study; using this method tree root-soil plate failure load can be estimated with a stem bending response as little as 0.5^o.

2.13 References

Abe, K., & Ziemer, R. R. (1991). Effect of tree roots on a shear zone: modeling reinforced shear stress. *Canadian Journal of Forest Research*, 21(7), 1012–1019. http://doi.org/10.1139/x91-139

Achim, A., & Nicoll, B. C. (2009). Modelling the anchorage of shallow-rooted trees, *Forestry*, 82(3). http://doi.org/10.1093/forestry/cpp004

Allotey, N., & Hesham El Naggar, M. (2003). Analytical moment–rotation curves for rigid foundations based on a Winkler model. *Soil Dynamics and Earthquake Engineering*, 23(5), 367–381. http://doi.org/10.1016/S0267-7261(03)00034-4

Anderson, C. J., Campbell, D. J., Ritchie, R. M., & Smith, D. L. O. (1989). Soil hear

strength measurements and their relevance to windthrow in Sitka spruce. *Soil Use and Management*, 5(2), 62–66.

ASTM C1419-99a, Standard Test Method for Sonic Velocity in Refractory Materials at Room Temperature and Its Use in Obtaining an Approximate Young's Modulus, *ASTM International*, West Conshohocken, PA, 1999, www.astm.org.

ASTM D198-09, Standard Test Methods of Static Tests of Lumber in Structural Sizes, *ASTM International*, West Conshohocken, PA, 2009, www.astm.org.

ASTM D4442-07, Standard Test Methods for Direct Moisture Content Measurement of Wood and Wood-Base Materials, *ASTM International*, West Conshohocken, PA, 2007, www.astm.org.

Bartlett, P. (1979). *Foundation rocking on a clay soil*. M.E. Thesis, University of Auckland, New Zealand.

Bischetti, G. B., Chiaradia, E. A., Simonato, T., Speziali, B., Vitali, B., Vullo, P., & Zocco, A. (2005). Root strength and root area ratio of forest species in Lombardy, *Plant and Soil*, 278:11–22. http://doi.org/10.1007/s11104-005-0605-4

Blackwell, P. G., Rennolls, K., & Coutts, M. P. (1990). A Root Anchorage Model for Shallowly Rooted Sitka spruce, *Forestry*, 63(1): 73-91.

Brüchert, F., Becker, G., & Speck, T. (2000). The mechanics of Norway spruce [Picea abies (L.) Karst]: Mechanical properties of standing trees from different thinning regimes. *Forest Ecology and Management*, 135(1-3), 45–62. http://doi.org/10.1016/S0378-1127(00)00297-8

Brudi, E., & Wassenaer, P. Van. (2001). Trees and Statics: Non-Destructive Failure Analysis, In: E. Thomas Smiley and K. Coder (Eds.). 2001. *Tree Structure and Mechanics Conference Proceedings: How Trees Stand Up and Fall Down*. Savannah, Georgia, U.S. pp. 53–69..

Byrne, K. E., & Mitchell, S. J. (2007). Overturning resistance of western redcedar and western hemlock in mixed-species stands in coastal British Columbia. *Canadian Journal of Forest Research*, 37(5), 931–939. http://doi.org/10.1139/X06-291

Chen, X.-C., & Lai, Y.-M. (2003). Seismic response of bridge piers on elasto-plastic Winkler foundation allowed to uplift. *Journal of Sound and Vibration*, 266(5), 957–965. http://doi.org/10.1016/S0022-460X(02)01382-2

Chopra, A. K., & Yim, C. S. (1985). Simplified earthquake analysis of structures with foundation uplift. *J.Strct. Eng*., 111(4), 906–930.

Coutts, M. P. (1983). Root architecture and tree stability. *Plant and Soil*, 71, 171–188. http://doi.org/10.1007/BF02182653

Coutts, M. P. (1986). Components of tree stability in sitka spruce on peaty gley soil. *Forestry*, 59(2), 173–197. http://doi.org/10.1093/forestry/59.2.173

Crook, M. J., & Ennos, A. R. (1996). The anchorage mechanics of deep rooted larch, Larix europea x L-japonica. *Journal of Experimental Botany*, 47(303), 1509–1517. http://doi.org/10.1093/jxb/47.10.1509

Crook, M. J., Ennos, A. R., & Banks, J. R. (1997). The function of buttress roots: a comparative study of the anchorage systems of buttressed (Aglaia and Nephelium ramboutan species) and non-buttressed (Mallotus wrayi) tropical trees. *Journal of Experimental Botany*, 48(314), 1703–1716. http://doi.org/10.1093/jxb/48.9.1703

Cucchi, V., Meredieu, C., Stokes, A., Berthier, S., Bert, D., Najar, M., Lastennet, R. (2004). Root anchorage of inner and edge trees in stands of Maritime pine (Pinus pinaster Ait.) growing in different podzolic soil conditions. Trees, 18(4), 460–466. http://doi.org/10.1007/s00468-004-0330-2

Danjon, F., Fourcaud, T., & Bert, D. (2005). Root architecture and wind- firmness of mature Pinus pinaster. *New Phytologist*, 168(1), 387–400. http://doi.org/10.1111/j.1469-8137.2005.01497.x

Dupuy, L. X., Fourcaud, T., Lac, P., & Stokes, A. (2007). a Generic 3D Finite Element Model of Tree Anchorage Integrating Soil Mechanics and Real Root System Architecture. *American Journal of Botany*, 94(9), 1506–1514. http://doi.org/10.3732/ajb.94.9.1506

Dupuy, L., Fourcaud, T., & Stokes, A. (2005). A numerical investigation into the influence of soil type and root architecture on tree anchorage. *Plant and Soil*, 278(1-2), 119–134. http://doi.org/10.1007/s11104-005-7577-2

Elie, J., & Ruel, J. (2005). Windthrow hazard modelling in boreal forests of black spruce and jack pine. *Canadian Journal of Forest Research*, 35, 2655–2663. http://doi.org/10.1139/X05-189

Ennos, A. R. (1993). The Scaling of Root Anchorage. *Journal of Theoretical Biology*. http://doi.org/10.1006/jtbi.1993.1040

Ennos, A. R. (1995). *Development of buttresses in rainforest trees: the influence of mechanical stress*. In: Coutts MP, Grace J Eds. Wind and trees. Cambridge University Press, 293-301.

Fourcaud, T., Blaise, F., Lac, P., Castéra, P., & De Reffye, P. (2003). Numerical modelling of shape regulation and growth stresses in trees: II. Implementation in the AMAPpara software and simulation of tree growth. *Trees - Structure and Function*, 17(1), 31–39. http://doi.org/10.1007/s00468-002-0203-5

Fraser, A. I. (1962). The soil and roots as factors in tree stability. *Forestry*, 34, 117–127. http://doi.org/10.1093/forestry/34.2.117

Gardiner, B., Byrne, K., Hale, S., Kamimura, K., Mitchell, S. J., Peltola, H., & Ruel, J. C. (2008). A review of mechanistic modelling of wind damage risk to forests. *Forestry*, 81(3), 447–463. http://doi.org/10.1093/forestry/cpn022

Gardiner, B., Peltola, H., & Kellomäki, S. (2000). Comparison of two models for predicting the critical wind speeds required to damage coniferous trees. *Ecological Modelling*, 129(1), 1–23. http://doi.org/10.1016/S0304-3800(00)00220-9

Ghani, M. A., Stokes, A., & Fourcaud, T. (2009). The effect of root architecture and root loss through trenching on the anchorage of tropical urban trees (Eugenia grandis Wight). *Trees - Structure and Function*, 23(2), 197–209. http://doi.org/10.1007/s00468-008-0269-9

Hanewinkel, M., Zhou, W., & Schill, C. (2004). A neural network approach to identify forest stands susceptible to wind damage, *Forest Ecology and Management*, 196, 227–243. http://doi.org/10.1016/j.foreco.2004.02.056

Houlsby, G. T., Cassidy, M. J., & Einav, I. (2005). A generalised Winkler model for the behaviour of shallow foundations. *Géotechnique*, 55(6), 449–460. http://doi.org/10.1680/geot.2005.55.6.449

Hung, L. C., & Kim, S. R. (2014). Evaluation of Undrained Bearing Capacities of Bucket Foundations Under Combined Loads. *Marine Georesources and Geotechnology*, 32(1), 76–92. http://doi.org/10.1080/1064119X.2012.735346

James, K. R., & Kane, B. (2008). Precision digital instruments to measure dynamic wind loads on trees during storms, *Agricultural and Forest Meteorology*, 148, 1055–1061. http://doi.org/10.1016/j.agrformet.2008.02.003

James, K., Hallam, C., & Spencer, C. (2013). Measuring tilt of tree structural root zones under static and wind loading. *Agricultural and Forest Meteorology*, 168, 160–167. http://doi.org/10.1016/j.agrformet.2012.09.009

Jonsson, M. J., Foetzki, A., Kalberer, M., Lundström, T., Ammann, W., and Stöckli, V. (2007). Natural frequencies and damping ratios of Norway spruce (Picea abies (L.) Karst) growing on subalpine forested slopes. Trees - Structure and Function, 21(5), 541–548. http://doi.org/10.1007/s00468-007-0147-x

Jonsson, M. J., Foetzki, A., Kalberer, M., Lundström, T., Ammann, W., & Stöckli, V. (2006). Root-soil rotation stiffness of Norway spruce (Picea abies (L.) Karst) growing on subalpine forested slopes. Plant and Soil, 285(1–2), 267–277. https://doi.org/10.1007/s11104-006-9013-7

Kamimura, K., & Shiraishi, N. (2007). A review of strategies for wind damage assessment in Japanese forests. *Journal of Forest Research*, 12(3), 162–176. http://doi.org/10.1007/s10310-007-0005-0

Lanquaye-opoku, N., & Mitchell, S. J. (2005). Portability of stand-level empirical

windthrow risk models, *Forest Ecology and Management*, 0378, 134–148. http://doi.org/10.1016/j.foreco.2005.05.032

Lundström, T., Jonsson, M. J., & Kalberer, M. (2007). The root–soil system of Norway spruce subjected to turning moment: resistance as a function of rotation. *Plant and Soil*, 300(1-2), 35–49. http://doi.org/10.1007/s11104-007-9386-2

Mergen, F. (1954). Mechanical aspects of wind-breakage and wind firmness. *Journal of Forestry*, 52: 119-125.

Moore, J. R. (2000). Differences in maximum resistive bending moments of Pinus radiata trees grown on a range of soil types. *Forest Ecology and Management*, 135, 63–71. http://doi.org/10.1016/S0378-1127(00)00298-X

Neild, S. A., & Wood, C. J. (1999). Estimating stem and root-anchorage flexibility in trees, *Tree Physiology*, 19(3):141-151.

Niklas, K.J. 1999. Variations of the mechanical properties of Acer saccharum roots. *J. Experim. Bot.* 50 (331): 193–200.

Niklas, K. J. (2000). Computing factors of safety against wind-induced tree stem damage. *Journal of Experimental Botany*, 51(345), 797–806. http://doi.org/10.1093/jexbot/51.345.797

Ow, L. F., Harnas, F. R., Indrawan, I. G. B., Sahadewa, A., Sim, E. K., Rahardjo, H., Tan, P. Y. (2010). Tree-pulling experiment: An analysis into the mechanical stability of rain trees. *Trees - Structure and Function*, 24(6), 1007–1015. http://doi.org/10.1007/s00468-010-0470-5

Papesch, A. J. G., Moore, J. R., & Hawke, A. E. (1997). Mechanical stability of Pinus radiata trees at Eyrewell forest investigated using static tests. *New Zealand Journal of Forestry Science*, 27(2), 188–204.

Peltola, H., & Kellomaki, S. (1993). A mechanistic model for calculating windthrow and stem breakage of Scots pines at stand edge. *Silva Fennica*, 27(2).

Peltola, H., Kellomäki, S., Hassinen, A., & Granander, M. (2000). Mechanical stability of Scots pine, Norway spruce and birch: An analysis of tree-pulling experiments in Finland. *Forest Ecology and Management*, 135, 143–153. http://doi.org/10.1016/S0378-1127(00)00306-6

Petty, J. A. and Worrell, R. 1981 Stability of Coniferous tree stems in relation to damage by snow. *Forestry* 54, 115-128.

Raychowdhury, P., & Hutchinson, T. C. (2009). Analysis of the sources of uncertainty for portfolio level earthquake loss estimation. *Earthquake Engineering & Structural Dynamics*, 38, 679–698. http://doi.org/10.1002/eqe

Scott, R. E., & Mitchell, S. J. (2005). Empirical modelling of windthrow risk in partially harvested stands using tree, neighborhood, and stand attributes, *Forest Ecology and Management*, 218, 193–209. http://doi.org/10.1016/j.foreco.2005.07.012

Sinn, G., & Wessolly, L. (1989). a Contribution to the Proper Assessment of the Strength and Stability of Trees. *Arboricultural Journal*. http://doi.org/10.1080/03071375.1989.9756400

Stokes, A, & Mattheck, C. (1996). Variation of wood strength in tree roots. *Journal of Experimental Botany*, 47(298), 693–699. http://doi.org/10.1093/jxb/47.5.693

Stokes, A. (1999). Strain distribution during anchorage failure of Pinus pinaster Ait. at different ages and tree growth response to wind-induced root movement. *Plant and Soil*, 217, 17–27. http://doi.org/10.1023/A:1004613126353

Stokes, A., Salin, F., Kokutse, A. D., Mochan, S., Dorren, L., Kokutse, N., & Ghani, M. A. (2005). Mechanical resistance of different tree species to rockfall in the French Alps, *Plant and Soil*, 278: 107–117. http://doi.org/10.1007/s11104-005-3899-3

Szoradova, A., Praus, L., & Kolarik, J. (2013). Evaluation of the root system resistance against failure of urban trees using principal component analysis. *Biosystems Engineering*, 115(3), 244–249. http://doi.org/10.1016/j.biosystemseng.2013.03.001

Thomson, W. (1993). *Theory of Vibration with Applications*, Englewood Cliffs, NJ: Prentice Hall, Inc., fourth edition.

Urata, T., Shibuya, M., Koizumi, A., Torita, H., & Cha, J. Y. (2012). Both stem and crown mass affect tree resistance to uprooting. *Journal of Forest Research*, 17, 65–71. http://doi.org/10.1007/s10310-011-0249-6

Valinger, E. and Fridman, J. (1999). Models to Assess the Risk of Snow and Wind Damage in Pine, Spruce, and Birch Forests in Sweden, *Environ Manage*, 24(2), 209–217.

Walford, G.B., (1993). *Strength of New Zealand grown softwood poles*. Proceedings IPENZ Annual conference, Hamilton, New Zealand.

Watson, A. (2000). Wind-induced forces in the near-surface lateral roots of radiata pine. *Forest Ecology and Management*, 135(1-3), 133–142. http://doi.org/10.1016/S0378-1127(00)00305-4

Yang, M., Defossez, P., Danjon, F., & Fourcaud, T. (2014). Tree stability under wind: simulating uprooting with root breakage using a finite element method. *Annals of Botany*, 114, 695–709. http://doi.org/10.1093/aob/mcu122

Yim, C., & Chopra, A. K. (1984). Earthquake response of structures with partial uplift on Winkler foundation. *Earthquake Engineering & Structural Dynamics*. Retrieved from http://onlinelibrary.wiley.com/doi/10.1002/eqe.4290120209/abstract

Table 2-1 Moisture content and modulus of elasticity (E) of tree samples

SAMPLE	Height (m)	E in GPa (ASTM D198-09)	Moisture Content, % $\frac{W1-W2}{W2}\times 100$ (ASTM D4442-07)	E=**Modulus of elasticity** W1=**initial sample weight** W2=**dried sample weight**
Root sample (d)	-	-	56.78	
Disk A of trunk	0.72	0.8	8.3	
Disk B of trunk	3.28	1.2	7.34	
Disk C of trunk	5.86	0.87	7.87	
Disk D of trunk	10.85	1.2	8.62	

Table 2-2 Soil properties

Sample	**Diameters corresponding to percent finer**			**Uniformity coefficient (C_u)** $C_u=\frac{D_{60}}{D_{10}}$	**Coefficient of gradation (C_c)** $C_c=\frac{D_{30}^2}{D_{60}\times D_{10}}$	**Water content %**	**Liquid limit %**	**Plastic limit %**
	D_{10} (mm)	D_{30} (mm)	D_{60} (mm)					
 **SA1**	0.02	0.05	0.4	20	0.3125	38.04	42.18	25.42
SA2	0.02	0.1	0.5	25	1	34.87	36.56	22.78
SA3	0.02	0.1	0.5	25	1	33.78	37.14	25.57
SA4	0.02	0.1	0.6	30	0.833	26.99	29.69	14.66
SA5	0.025	0.15	0.55	22	1.63	27.03	29.33	23.73
SA6	0.022	0.1	0.5	22.7	0.91	27.49	28.82	14.49

Table 2-3 Stiffness estimates from load deflection curves

Strain gauge location	Distance from trunk center (m)	Vertical response stiffness (k_v) (N/mm^2)	Lateral response stiffness (k_h) (N/mm^2)	Equivalent stiffness (K_{eq}) (N/mm^2)		
		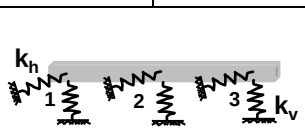		$k_{eq(local)} = \frac{1}{\frac{1}{k_v}+\frac{1}{k_h}}$	$\boldsymbol{k_{eq(root)} = k_1 + k_2 + k_3}$	$\boldsymbol{k_{eq(root\ plate)} = \frac{1}{1/k_{ww} + 1/k_{lw}}}$
W1	1.4	1.62	(0.026)*	0.025	**0.114**	**0.076**
W2	0.9	2.96	(0.033)*	0.033		
W3	0.4	11.77	(0.057)*	0.057		
L1	0.6	12.27	0.114	0.113	**0.229**	
L2	0.9	6.32	0.066	0.065		
L3	1.13	4.56	0.051	0.050		

Note: * approximated values of stiffness

Table 2-4 Failure load estimates using the modified Winkler foundation theory

Winkler foundation stiffness estimate using:	**k_w (kN/m^2)**	**k_θ (kNm/^{o})**	**$\theta_u = \frac{p}{2k_w b^2}$ (^{o})**	**$M_u = k_\theta * \theta_u$ (kNm)**
1) Load deflection response of root plates (equivalent stiffness)	76	219.0	2.2	491.7
2) Stem base strain gauge response	51	147.8	3.3	494.4
3) Natural frequency of the tree	36	105.4	4.7	499.5
4) Root plate rotational response	31	89.0	5.6	498.4

Figure 2-1 Norway spruce tree, before and during winch testing

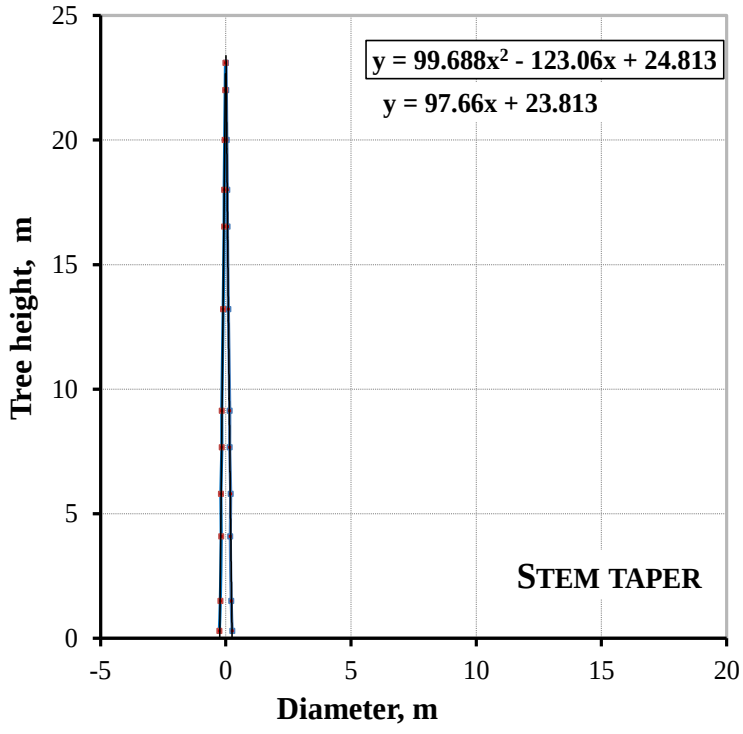

Figure 2-2 Stem Taper

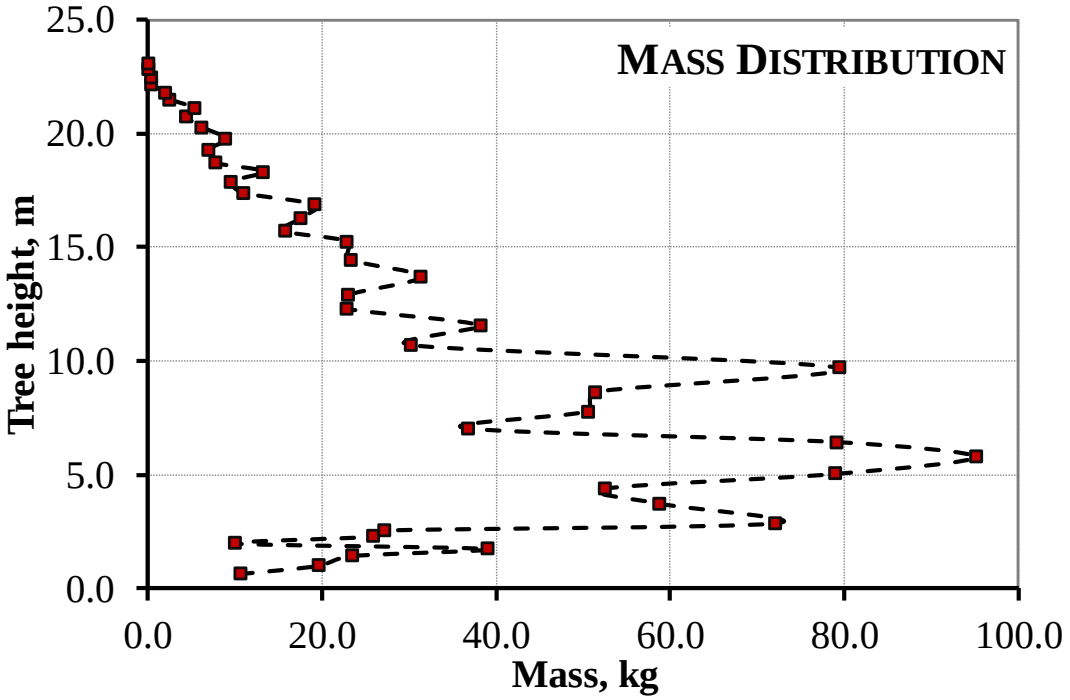

Figure 2-3 Branch mass distribution varying with tree height (prior to pruning)

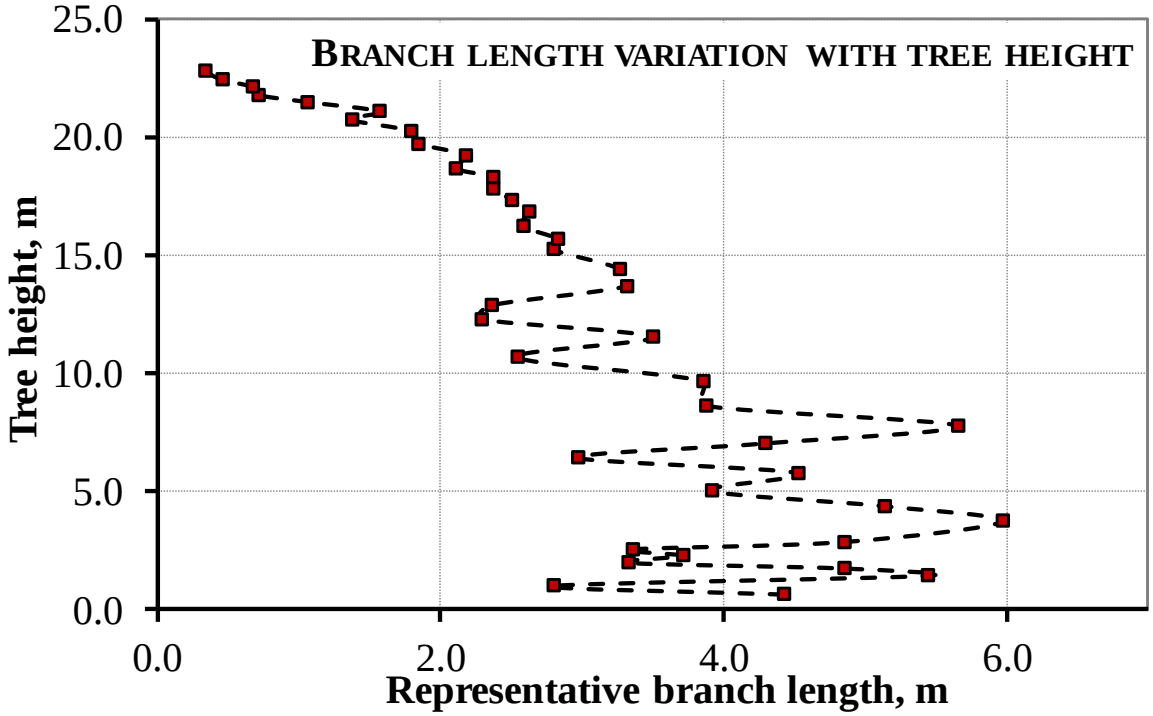

Figure 2-4 Representative branch length varying with tree height (prior to pruning)

Figure 2-5 Root plate images and architecture

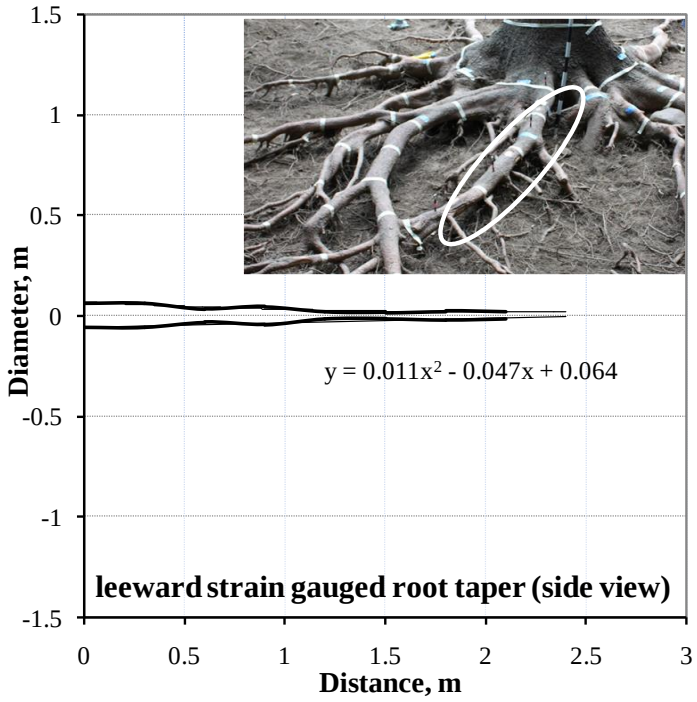

Figure 2-6 Leeward root taper

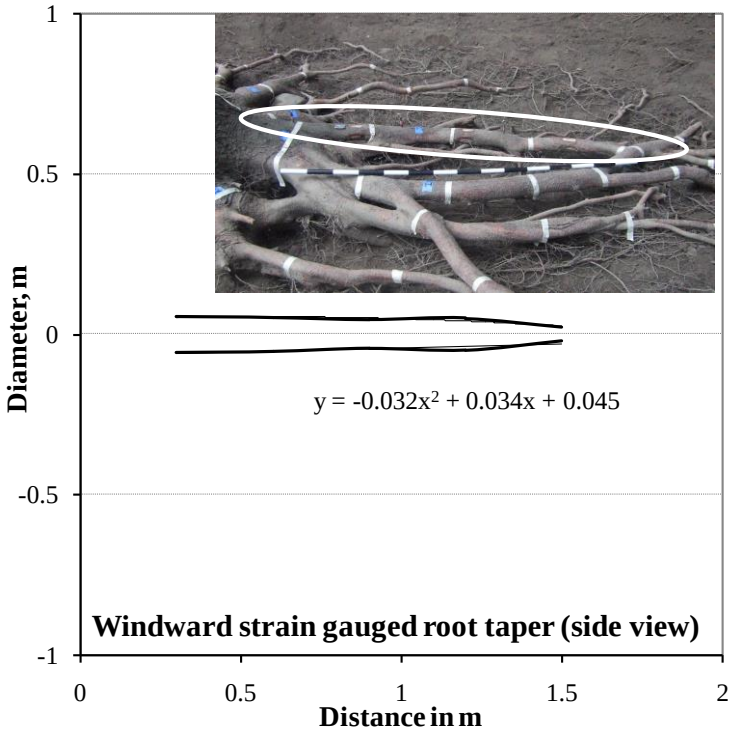

Figure 2-7 Windward root taper

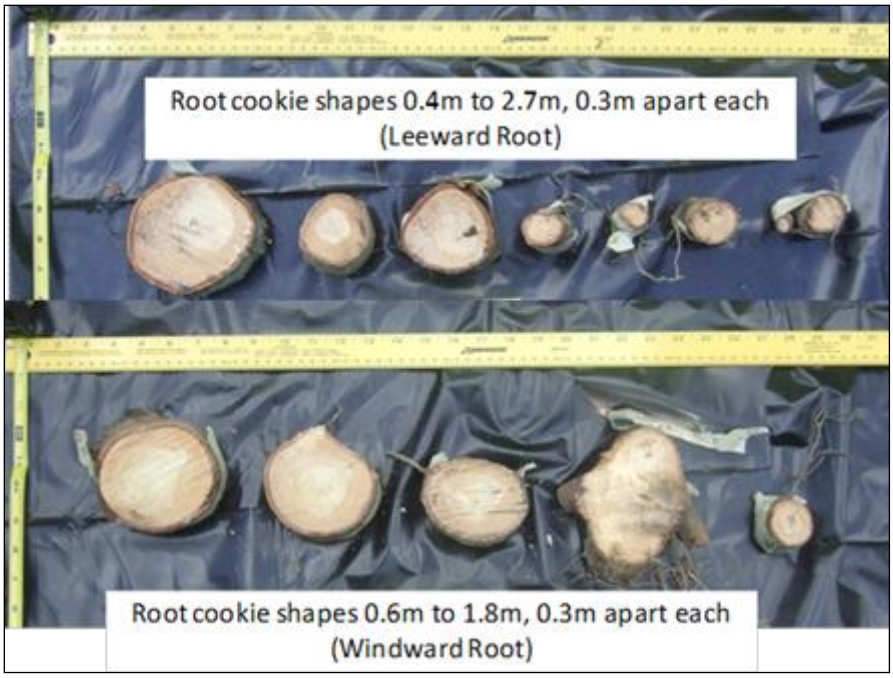

Figure 2-8 Root cookie shapes

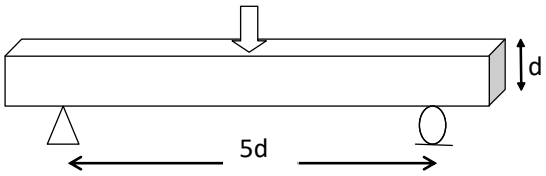

Sample collected from trunk	Height (m)	E in GPa (ASTM D198-09)
Disk A	0.72	0.8
Disk B	3.28	1.2
Disk C	5.86	0.87
Disk D	10.85	1.2

Figure 2-9 Three-point bending test setup and calculated Young's modulus (E) of tree samples from beams cut from disks

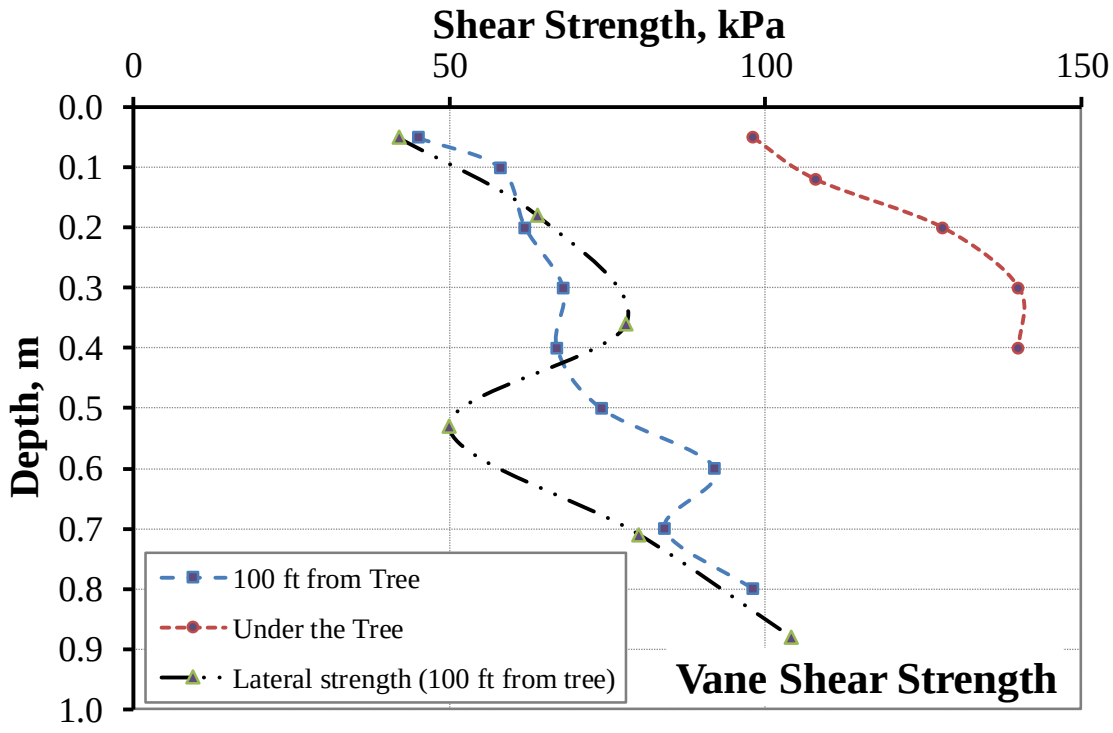

Figure 2-10 Vane shear strength with depth

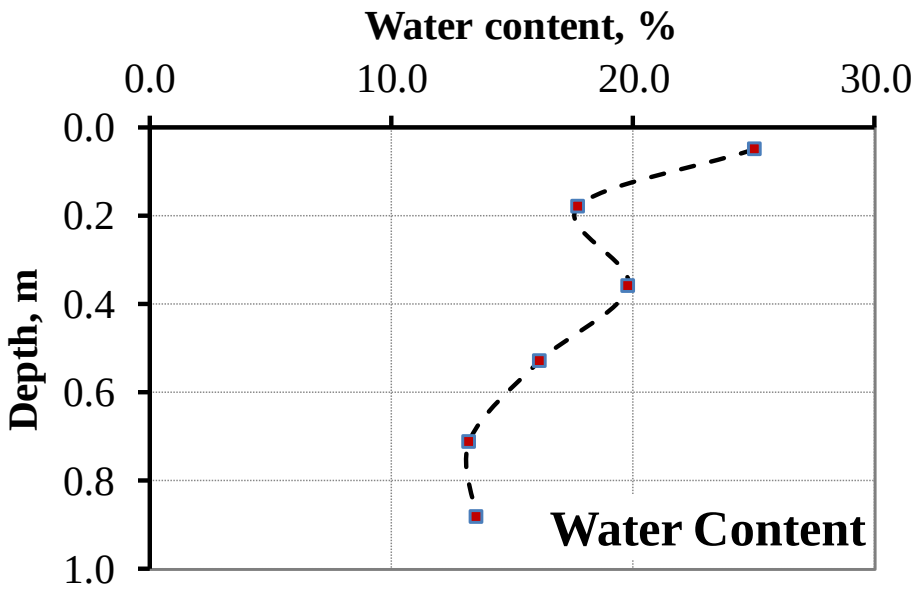

Figure 2-11 Water content in the soil with depth

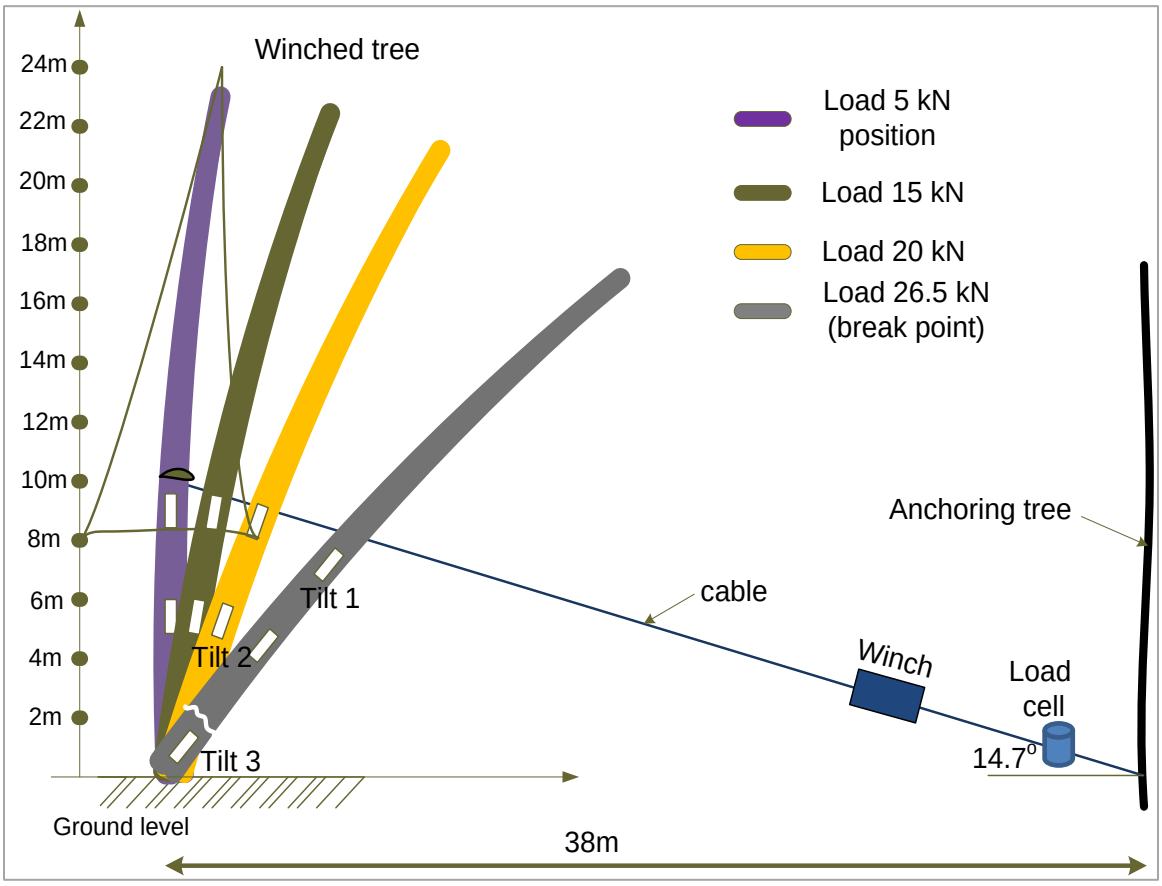

Figure 2-12 Stem deflection with increase in winch load

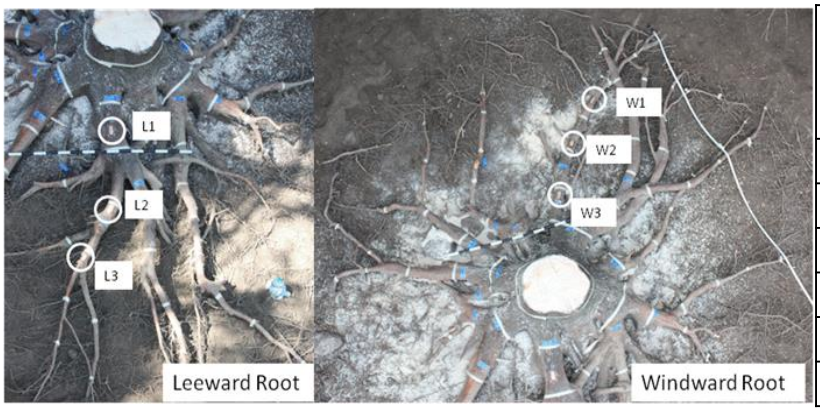

Strain gauge location	Distance from trunk centre (m)
W1	1.4
W2	0.9
W3	0.4
L1	0.6
L2	0.9
L3	1.13

Figure 2-13 Strain gauge locations on the roots

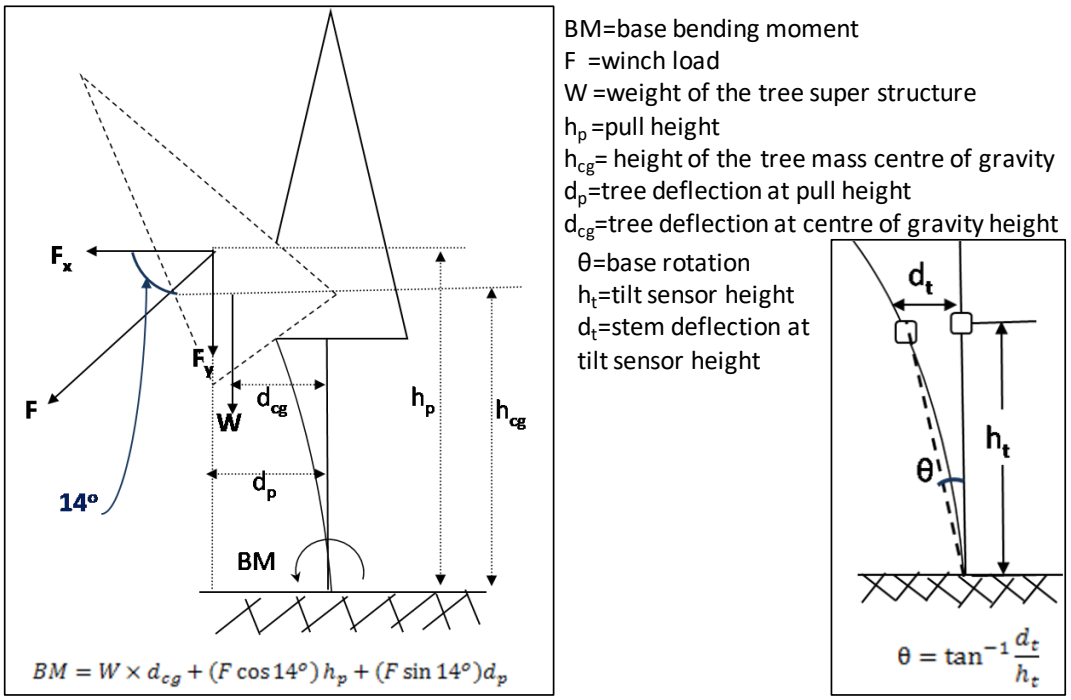

Figure 2-14 Base bending moment and rotation estimate

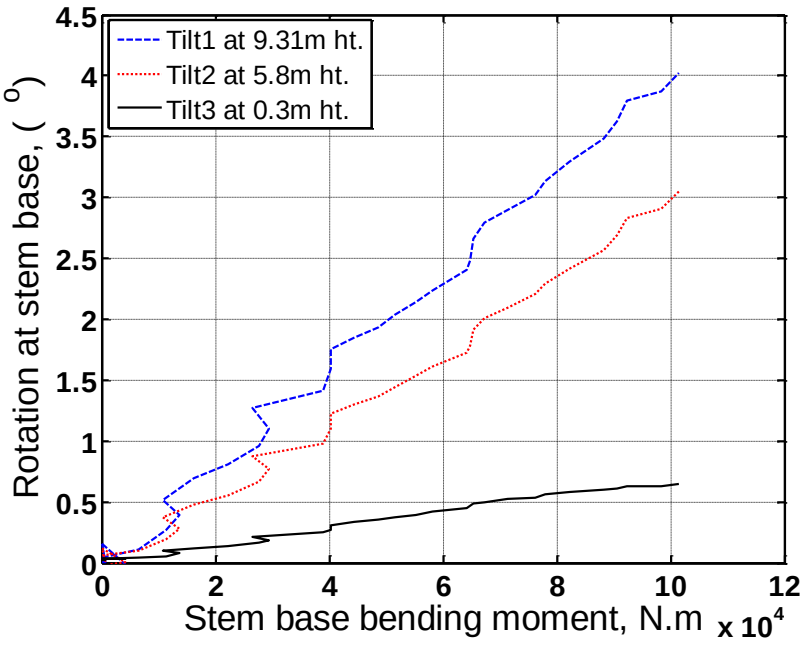

Figure 2-15 Rotation of the stem at various heights from base, with increase in base bending moment

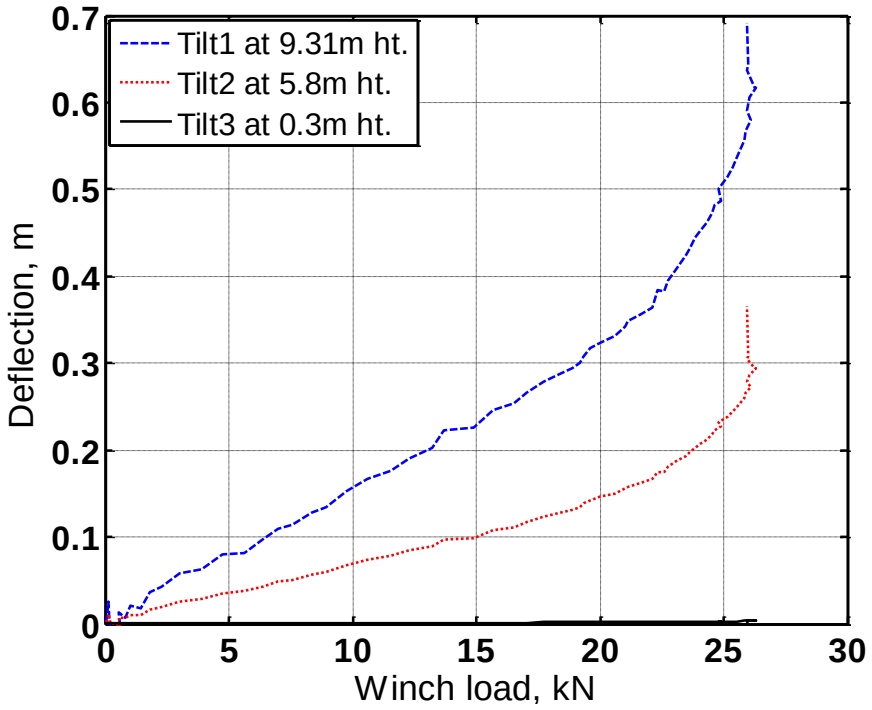

Figure 2-16 Stem deflection recorded using tilt sensors at various heights with increase in winch load

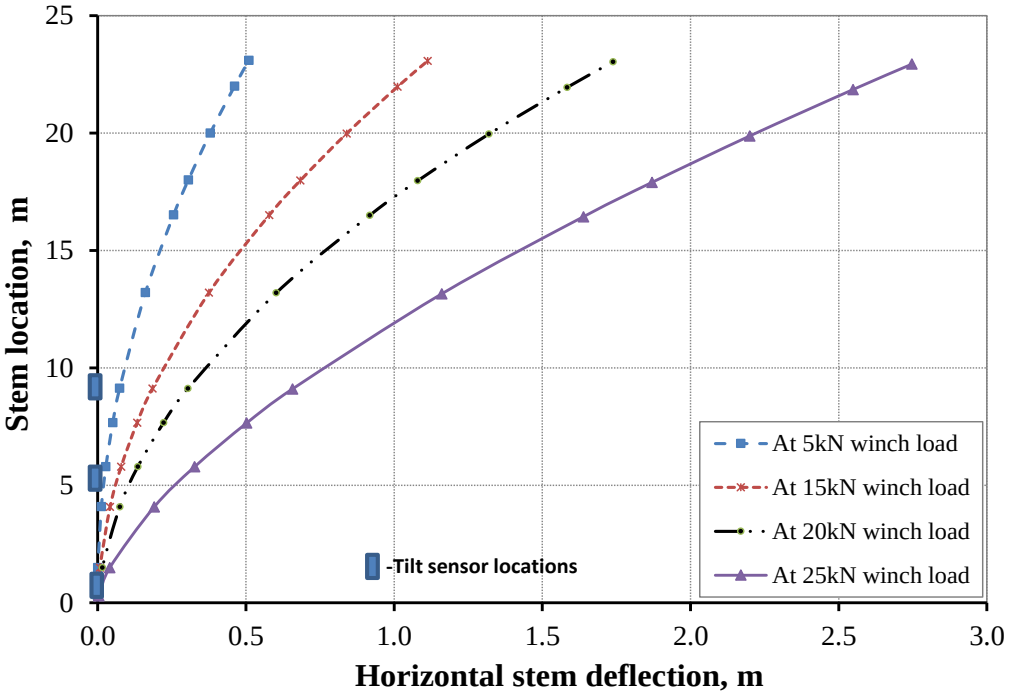

Figure 2-17 Deflection profile of the tree stem with increase in winch load

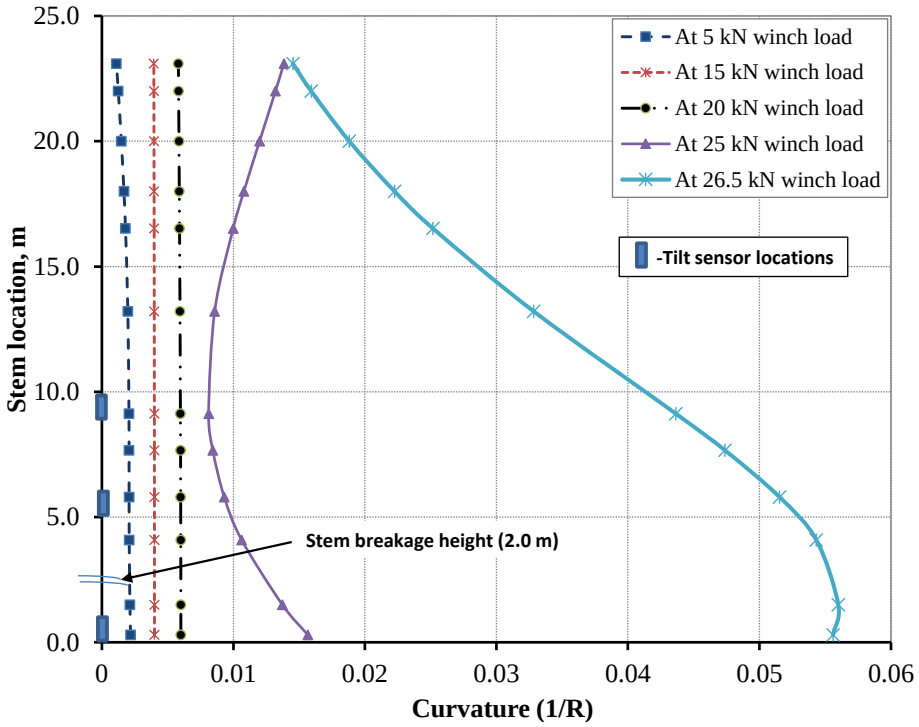

Figure 2-18 Curvature along the length of the tree stem with increase in winch load

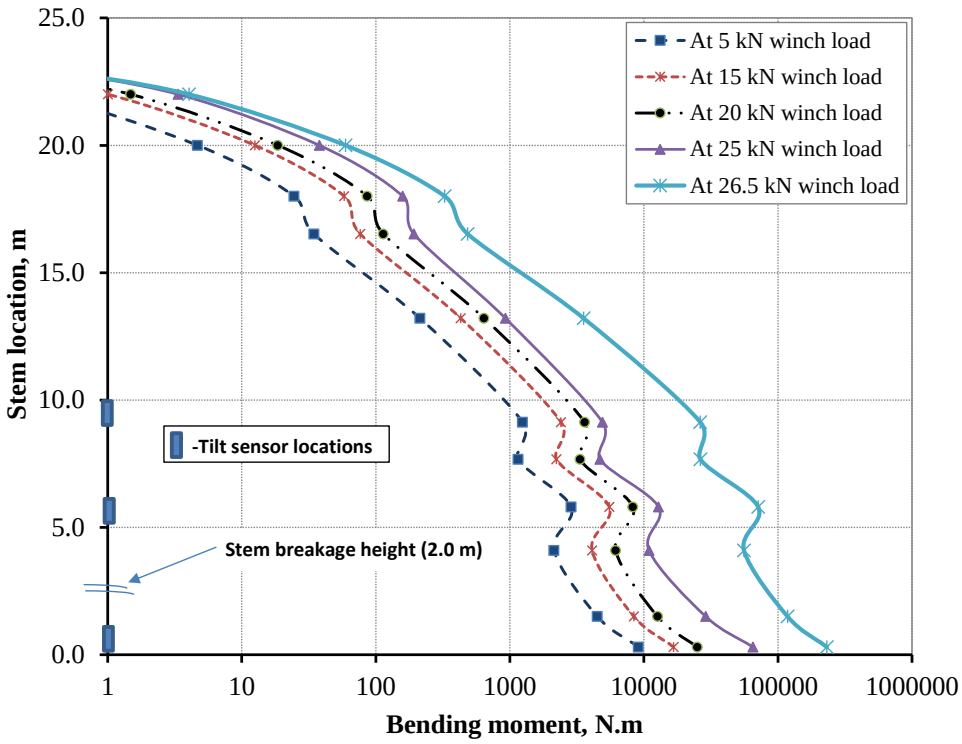

Figure 2-19 Bending moment profile of the tree stem with increase in winch load

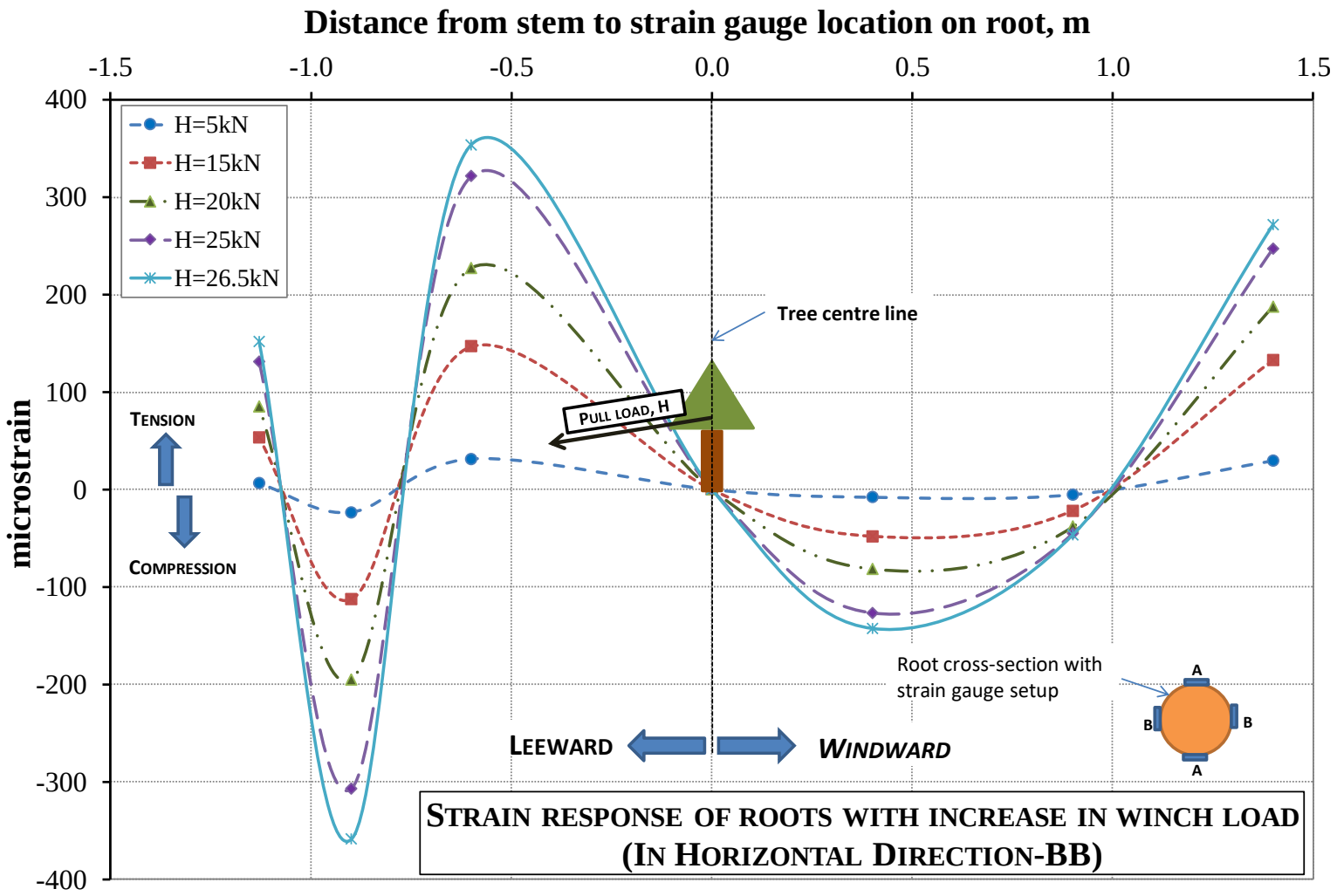

Figure 2-20 Lateral strain response of roots with increase in winch load

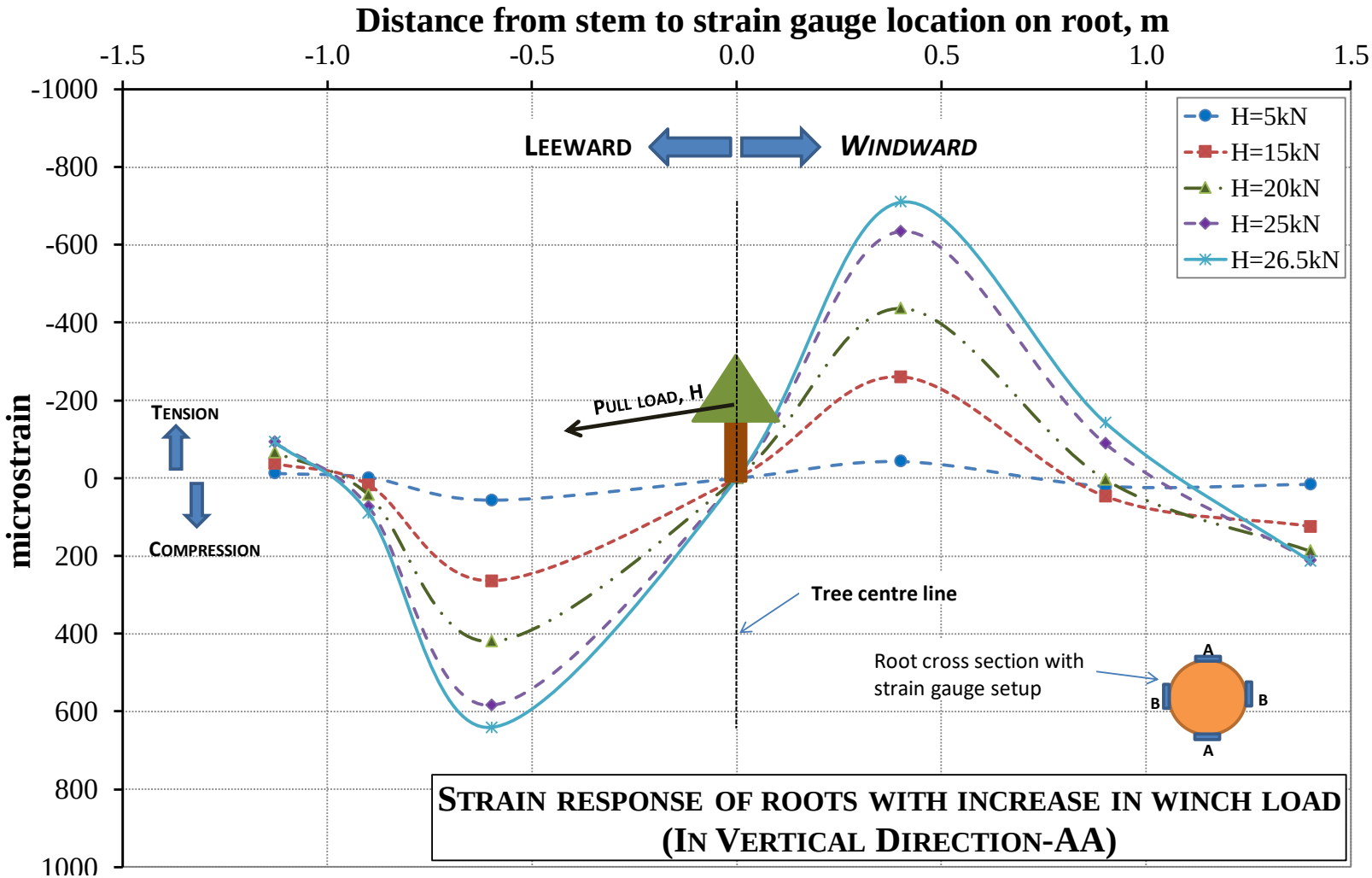

Figure 2-21 Vertical strain response of roots with increase in winch load

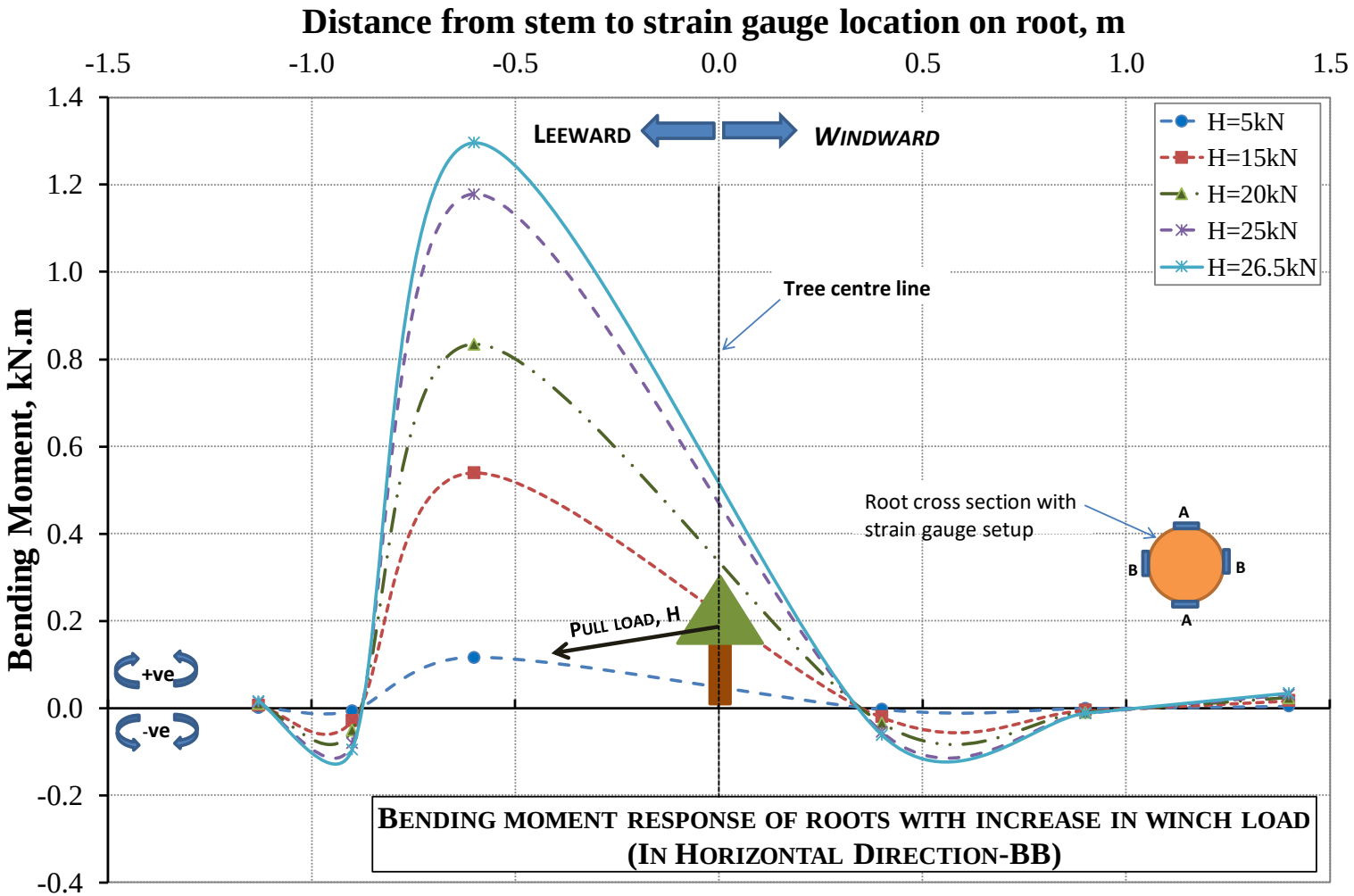

Figure 2-22 Lateral bending moment response of roots with increase in winch load

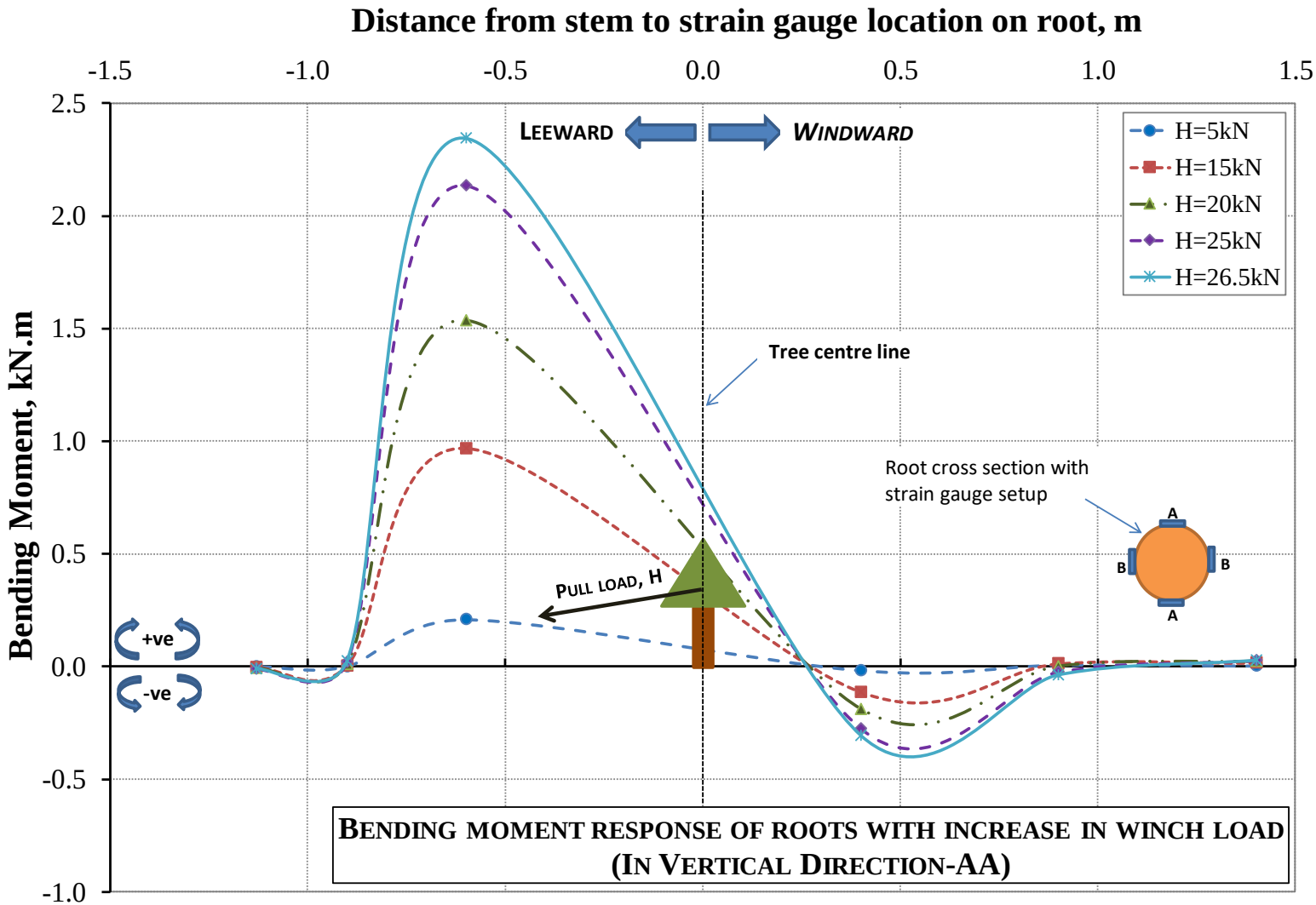

Figure 2-23 Vertical bending moment response of roots with increase in winch load

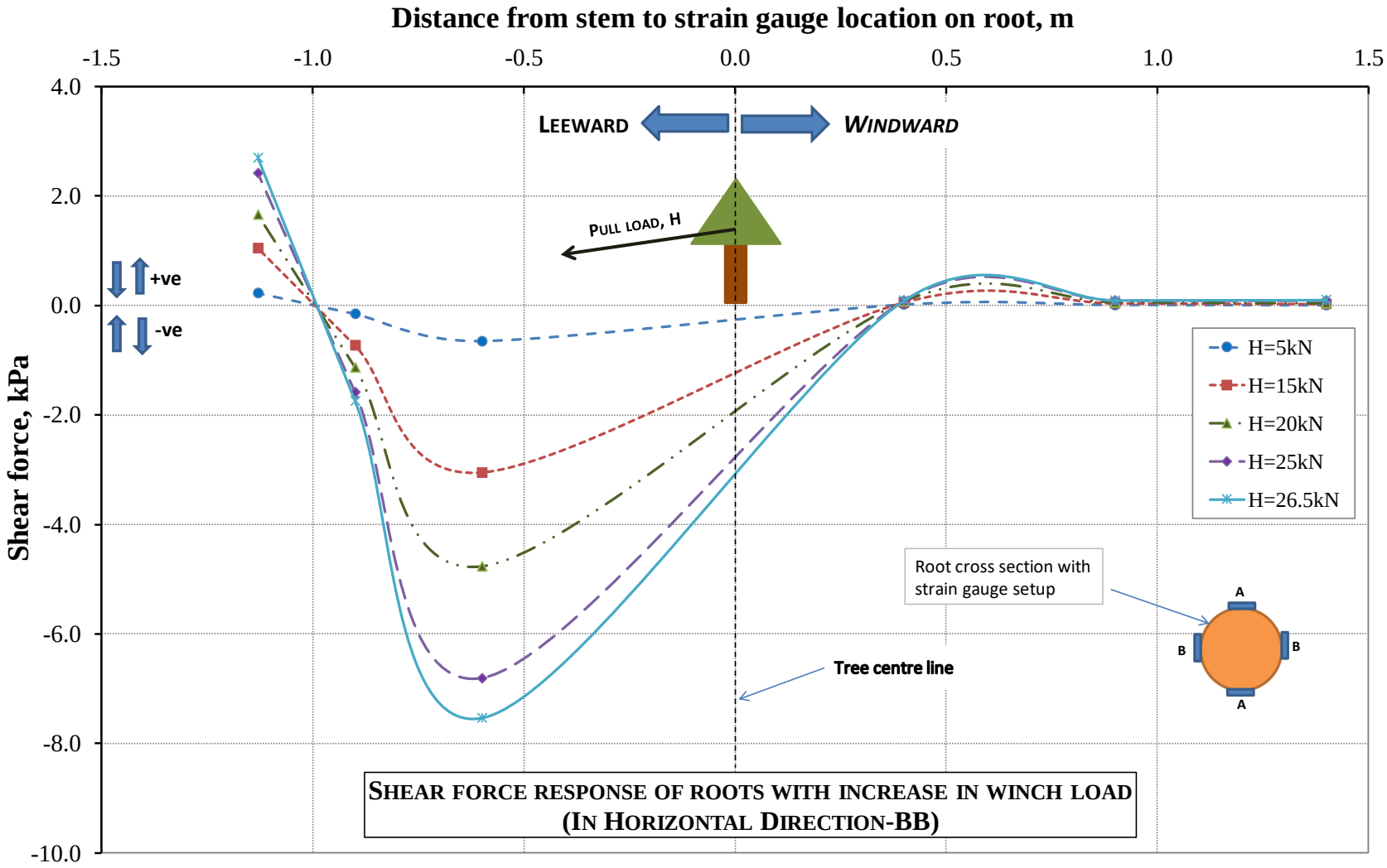

Figure 2-24 Lateral shear response of roots with increase in winch load

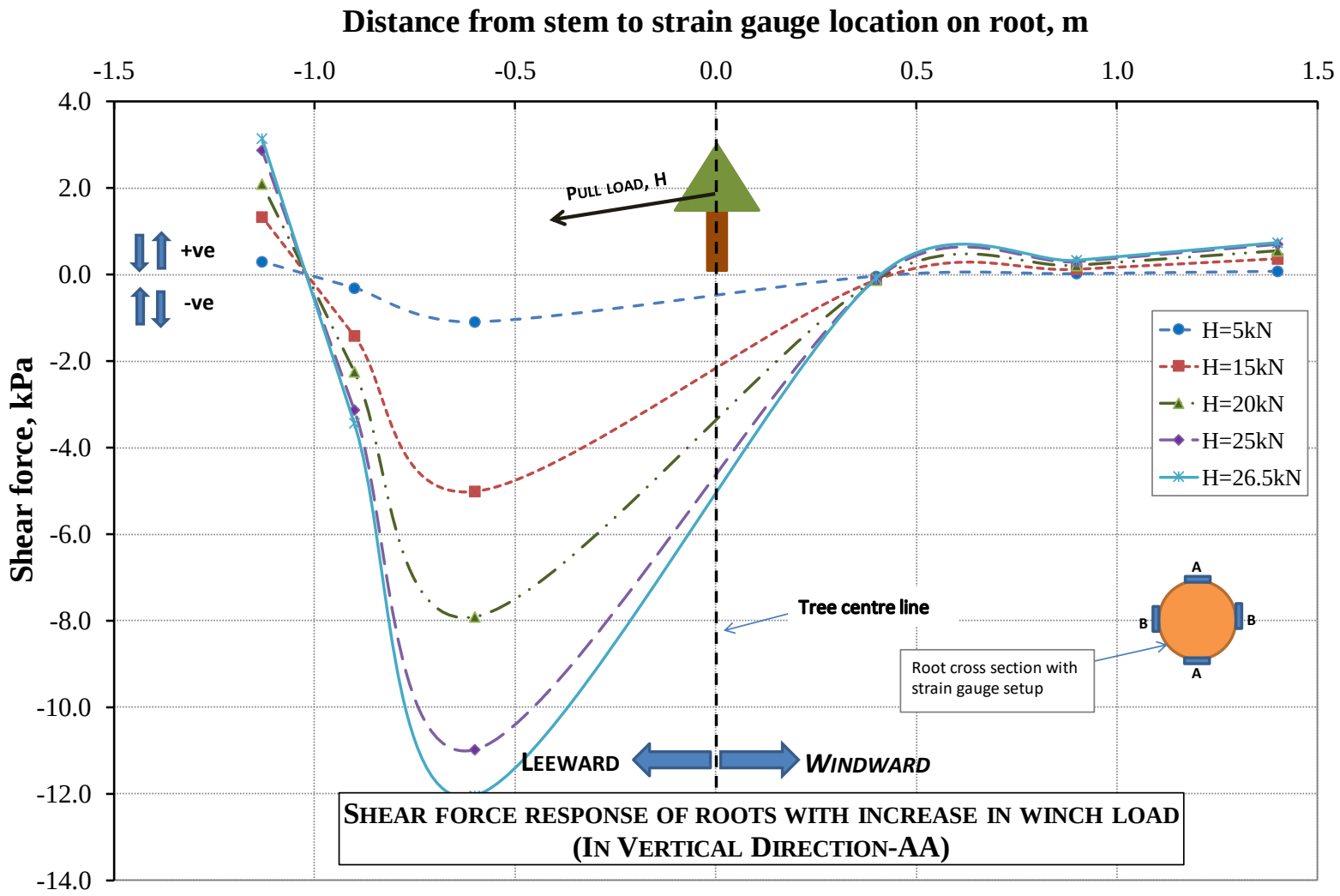

Figure 2-25 Vertical shear response of roots with increase in winch load

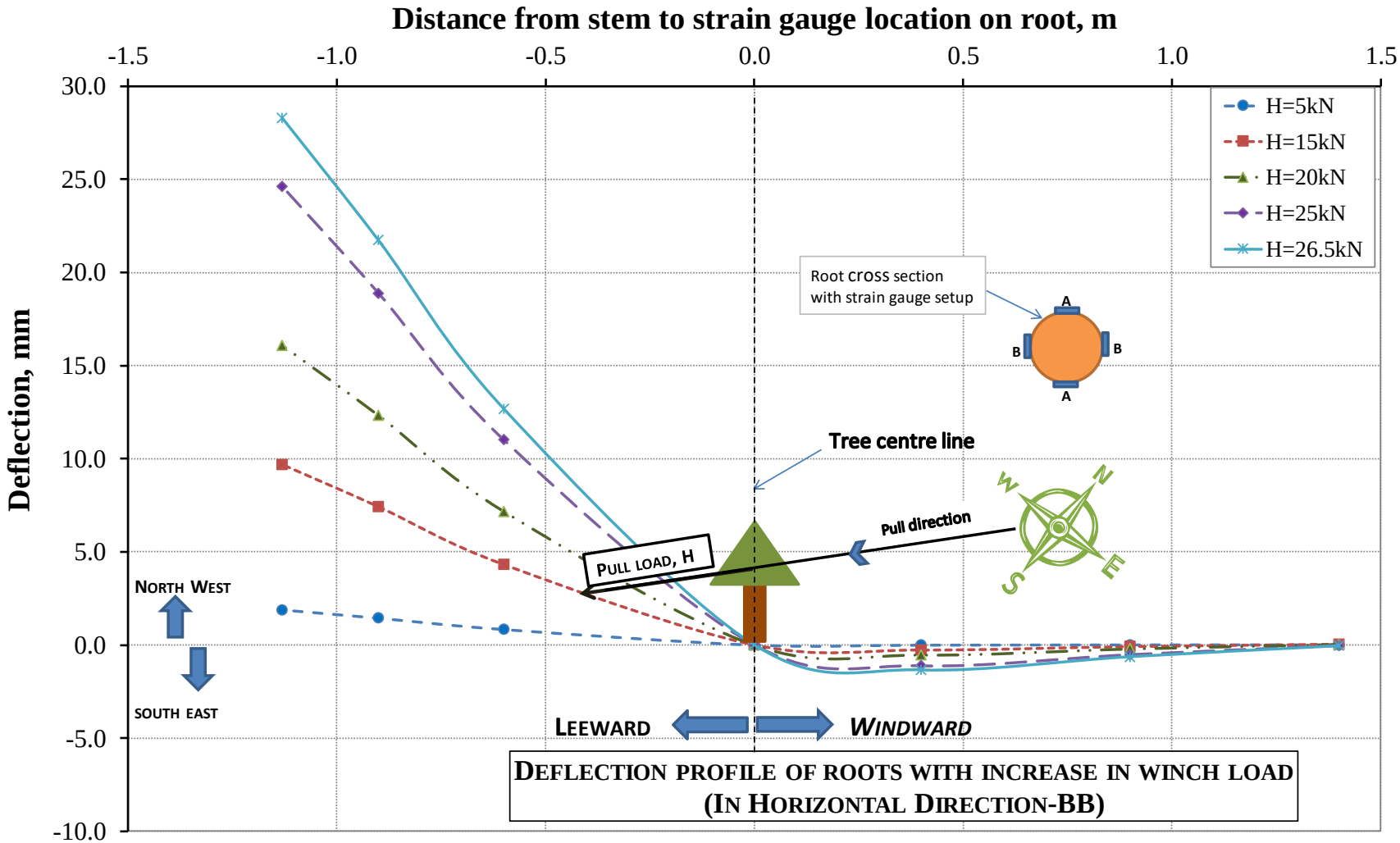

Figure 2-26 Lateral deflection of roots with increase in winch load

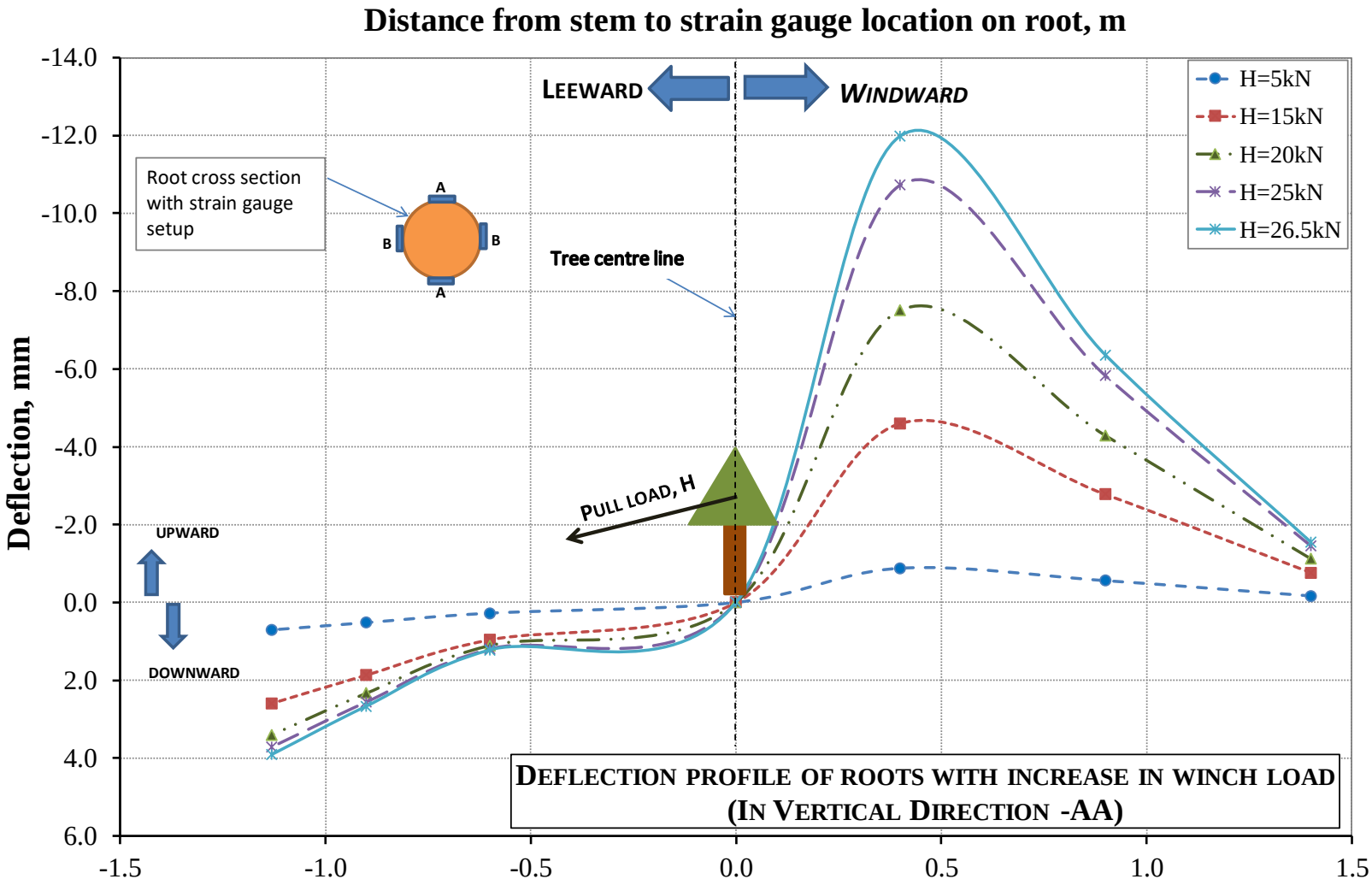

Figure 2-27 Vertical deflection of roots with increase in winch load

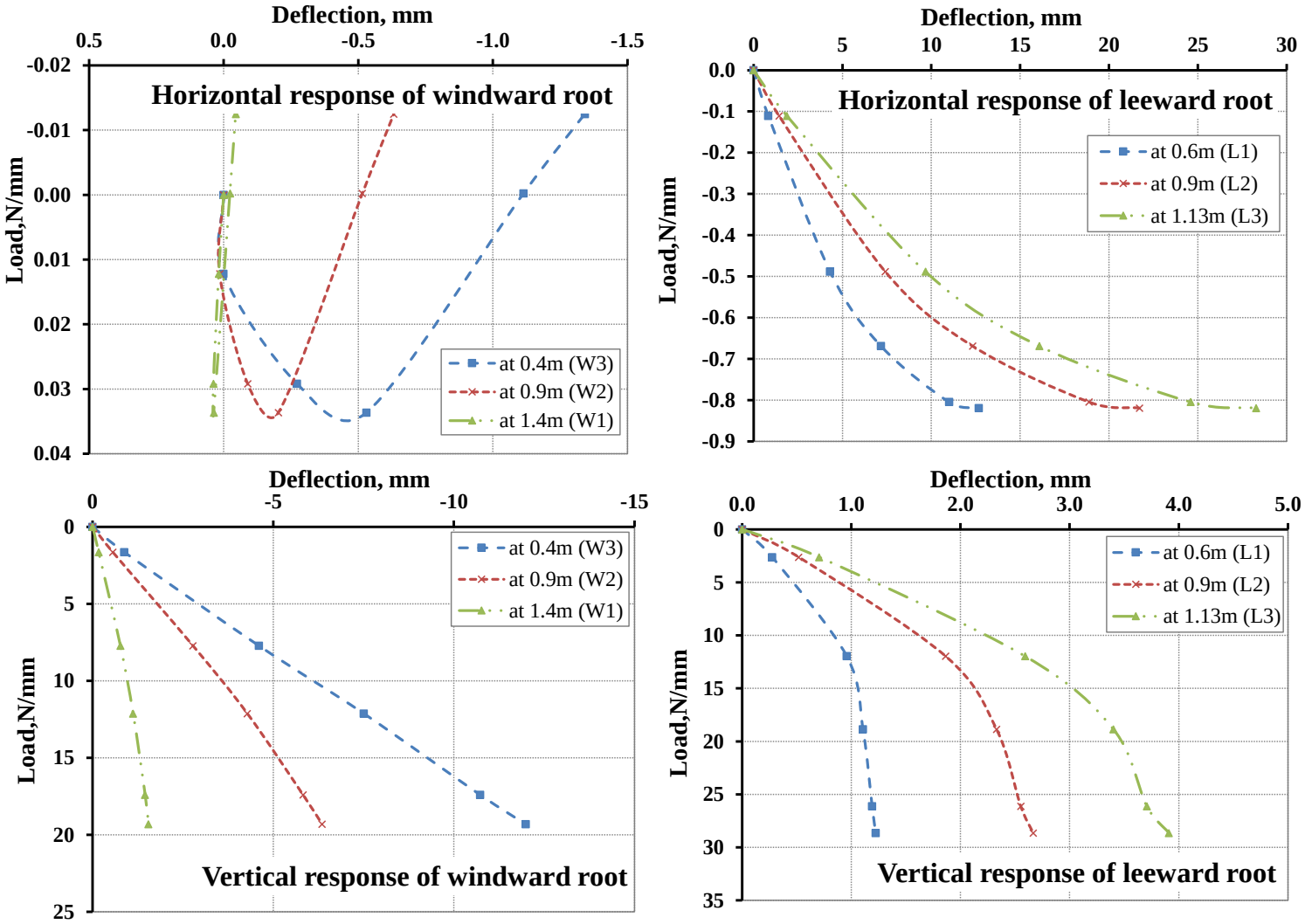

Figure 2-28 Load-deflection response of roots with increase in winch load

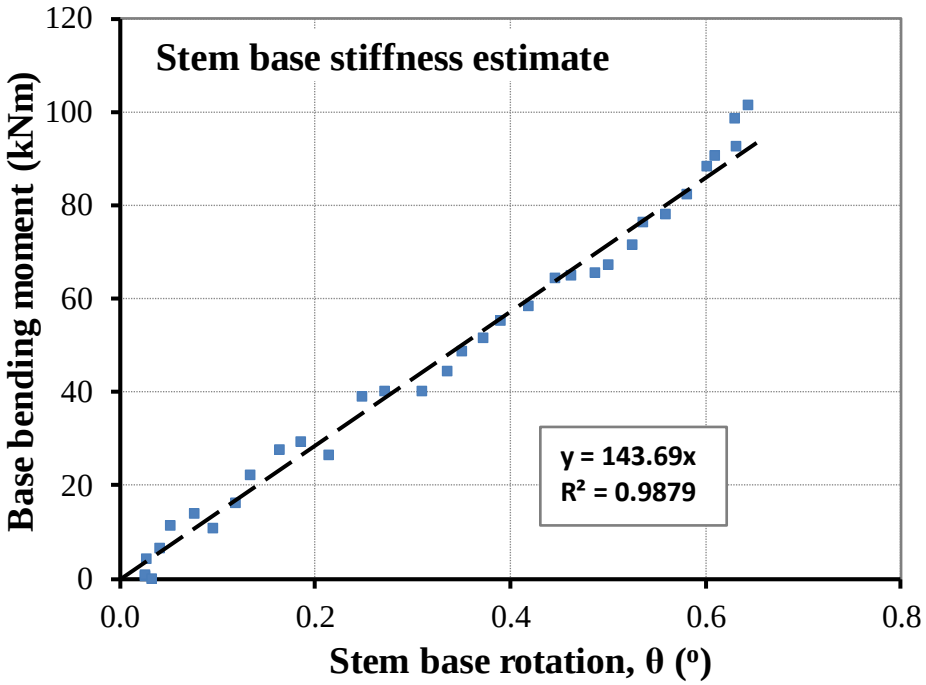

Figure 2-29 Stem base rotational response (0.8 m above ground level) with increase in base bending moment

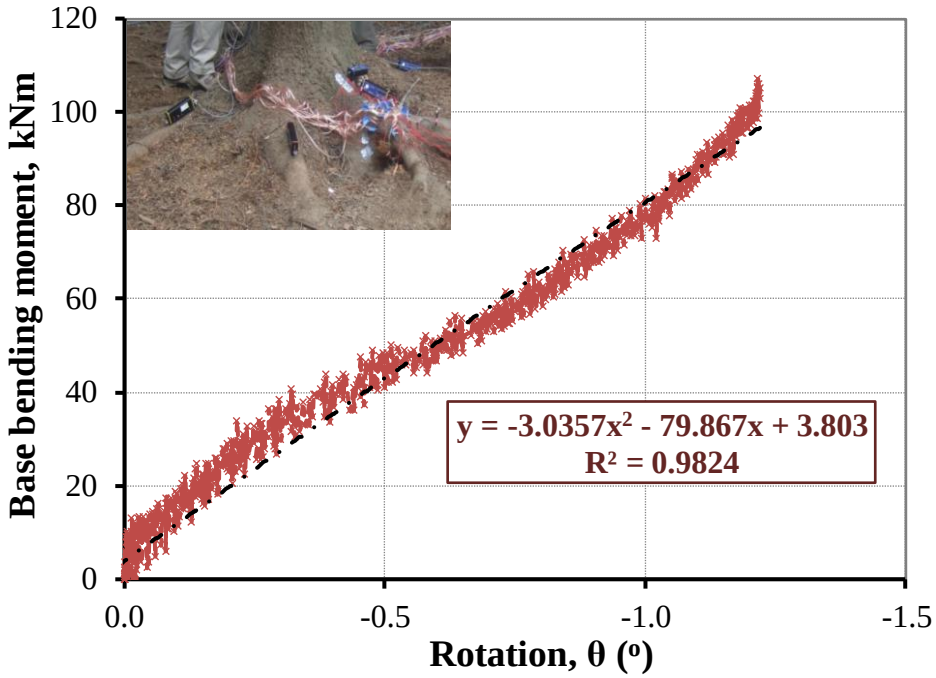

Figure 2-30 Root plate rotational response obtained from the TreeQinetic System

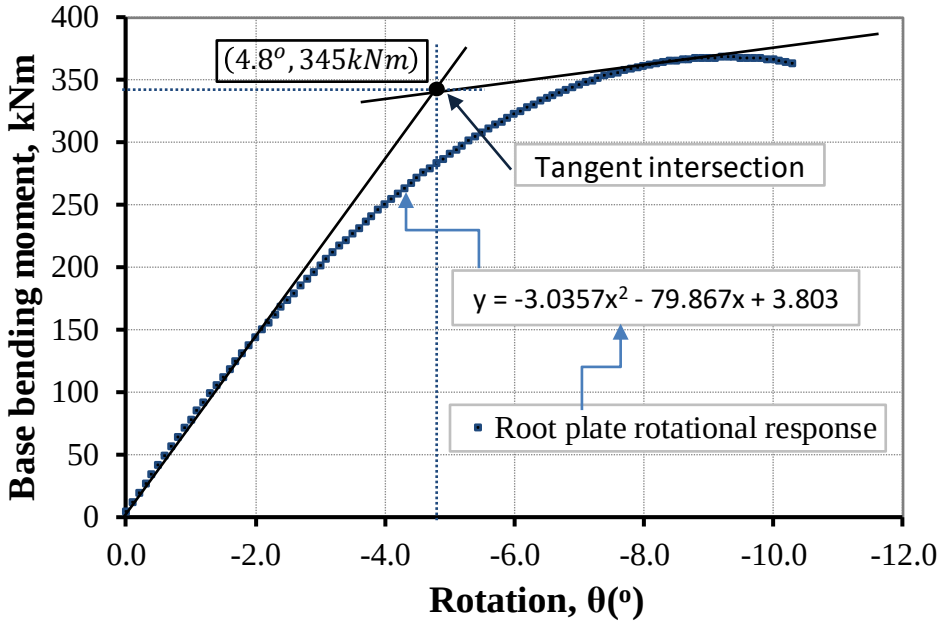

Figure 2-31 Tree anchorage strength estimate from tangent intersection method

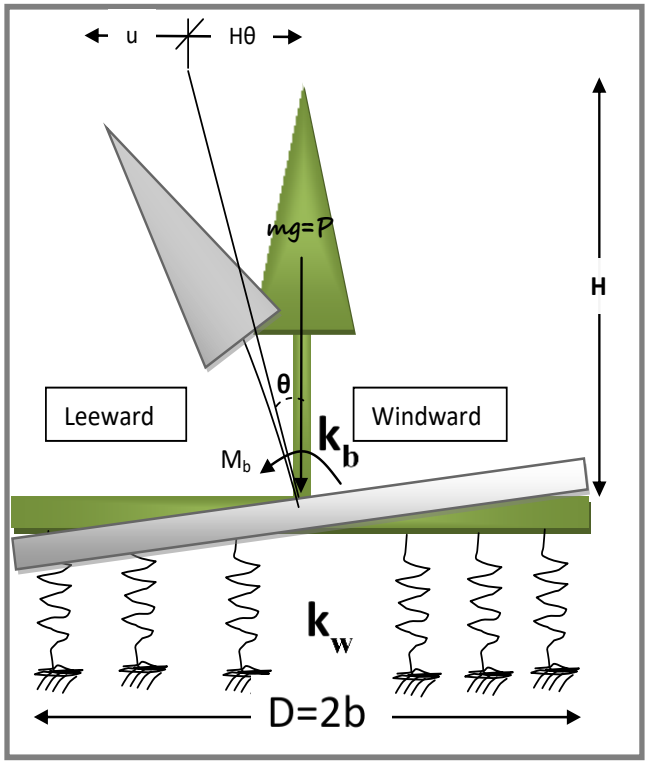

Figure 2-32 Modified Winkler foundation model of the tree root system

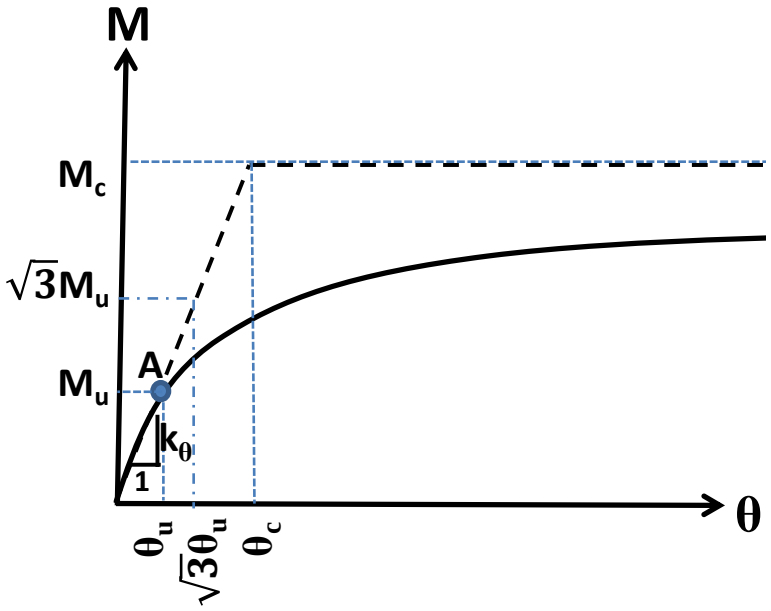

Figure 2-33 Properties of Winkler foundation, moment-rotation relation for foundation mat (after Chopra and Yim 1985)

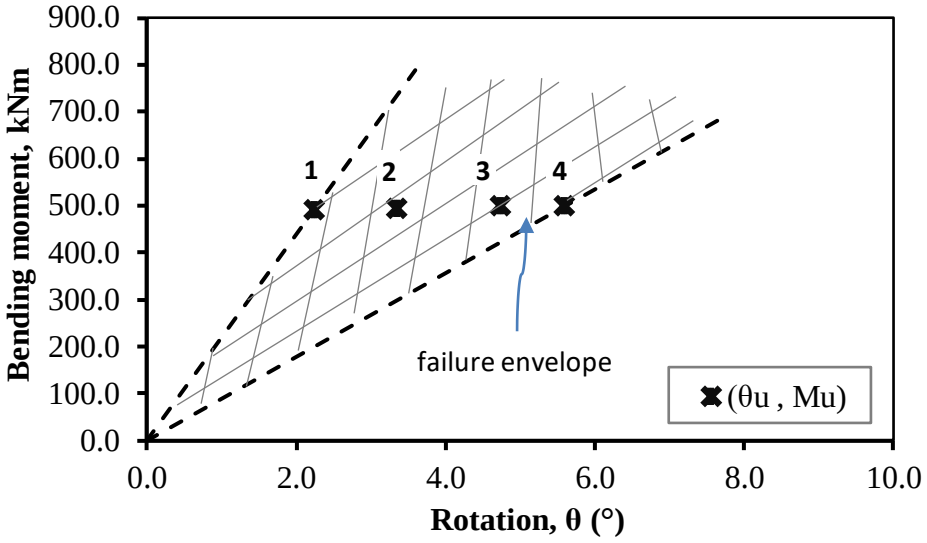

Figure 2-34 Failure envelope from Winkler foundation theory

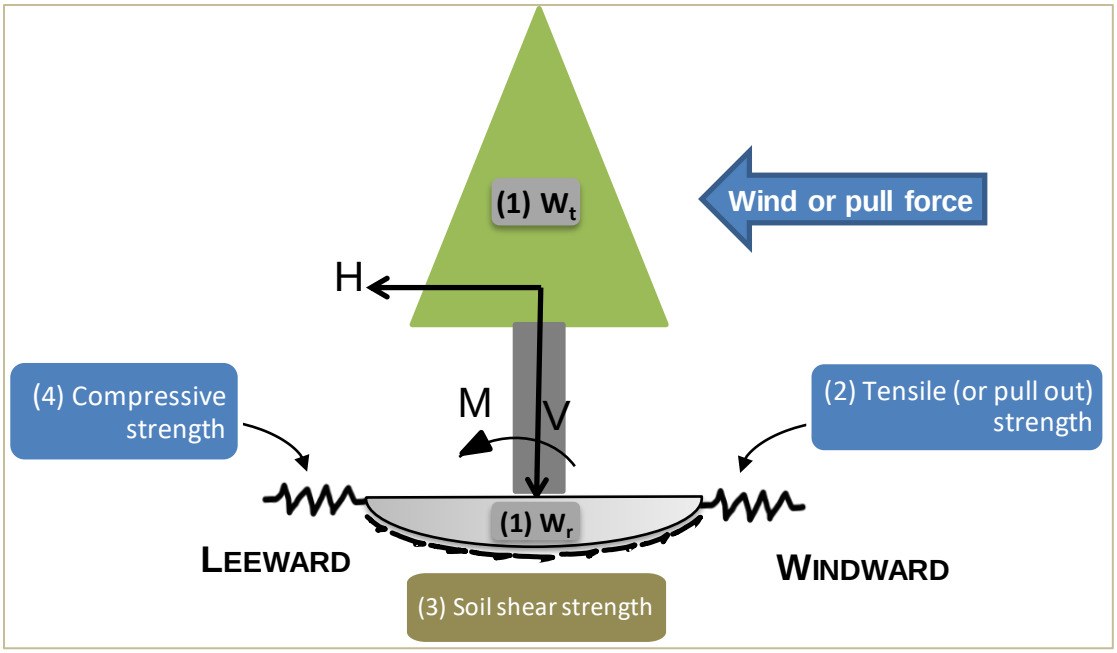

Figure 2-35 Component of root-soil plate anchorage

Chapter 3

3 Understanding the dynamics of tree-root-soil interaction using a wind tunnel

3.1 Introduction

This chapter describes novel experimental wind tunnel testing techniques used to enable a thorough dynamic analysis of the tree saplings. The instrumentation for the tree saplings and the wind tunnel experimental setup and techniques will be discussed. The collected response data and the applied wind speed data, calibration and analysis are presented. Statistical analysis of the tree and root sway response will be discussed along with sway plots of each tree sapling with increases in wind speed. Detailed dynamic analysis of the response data will be shown. The collected response data is used to estimate the natural frequency of tree sapling components. The internal and external damping of the tree saplings will also be presented with increases in wind speed and change in soil medium. The tree response data from force balance tests will be used to measure the aerodynamic admittance and estimate the components of drag force. Using the collected response data, the mechanical admittance of the above and below ground tree structure will be examined and discussed with changes in soil medium and increases in wind speed. All of these dynamic characteristics of the tree and root behavior are used to better understand the response of the tree-root-soil system to random dynamic loading from the wind field of a wind tunnel.

3.2 Background

Three of the major components influencing the uprooting of trees are tree structure, wind load and the soil-root system anchorage. For sub-failure wind events, a tree undergoes a complex sway motion in response to wind loads. The kinetic energy transferred from the wind loading is stored in the tree and is dissipated through damping of the tree and its branches; the remaining energy is transferred to the soil-root plate. If the tree root plate efficiently transfers the wind energy to the ground, the tree survives the wind event. The uprooting resistance of any tree structure depends on its efficiency to dissipate the wind

energy. In order to understand tree stability, we need to consider three important aspects for wind events: 1) how much energy is transferred to the tree from the wind, 2) how much transferred energy is dissipated by the tree components above ground, and 3) how efficiently the root plate and soil dissipate the remaining wind energy.

Part of the survival strategy of a tree is the sway response [Mayhead, 1973]. Oscillatory tree movements due to wind gusts lead to a characteristic sway motion. The tree sway response is determined by the dynamic properties of the structure and the wind load. Complex tree sway responses to wind loading have been studied previously using various methodologies [e.g. Mayer, 1987 and 1989; Hassinen et al., 1998; James, 2006; James and Kane, 2008; Sellier et al., 2008; James et al., 2013 and Kane et al., 2014]. The sway plots from these studies were used to identify the representative difference between types of dynamic response, i.e. between experimental and modelled data [Sellier et al., 2008]; different canopy architecture [James et al., 2006]; soil moisture conditions [Mayer, 1987 and Mayer et al. 1989] and the stem location from the edge to within the stand [Peltola, 1996]. Sway plots have also been used to gain information to determine sway frequency, damping and to correlate the direction of sway with the wind loading direction.

The energy transferred to the tree from the wind field can be determined based on the type of wind loading, canopy architecture and the frontal area. Even though a tree absorbs energy at all of its natural frequencies, the maximum energy is generally absorbed for the first natural frequency [Holbo et al. 1980, Mayer et al. 1989 and Peltola 1996]. As trees are dynamic systems, the wind response is conditioned by the dynamic properties of the tree structure and the load applied. Dynamic response of any structure can be studied under free and forced vibrations. The natural frequency of a tree is commonly measured using free vibrations (undamped oscillations), i.e. the tree stem is pulled from its rest position and released; the dominant oscillating frequency of the tree response is considered to be the natural frequency. Sellier and Fourcaud [2005] observed that the heaviest element (the trunk) is the predominant element governing free oscillations of a tree. Sugden [1962], Milne [1991], Gardiner [1992], and Moore and Maguire [2005] found increases in natural frequency with complete de-branching of trees and Jonsson et al. [2007] found a limited influence of root architecture on the first natural frequency. Under forced vibrations (under

wind loading), tree response depends on the excitation frequency of the wind load and the dynamic nature of the tree structure. Holbo et al. [1980], Mayer [1987], Gardiner [1992] and Peltola [1996] noted that trees respond most to gusts close to their natural sway frequency, which is also known as the resonant frequency. For resonance, large tree oscillations have been observed with increase in bending of the stem and higher loads on the root plate [Milne, 1991; Spatz et al., 2007 and Spatz and Theckes, 2013].

The wind energy dissipated by a tree structure is referred to as the tree damping energy. It depends on the dynamic properties of the tree structure and the type of wind event. Hoag et al. [1971], Mayhead et al. [1973], Gardiner [1989], Peltola [1996], James [2003], Moore and Maguire [2004, 2005 and 2008], Spatz et al. [2007], Jonsson et al. [2007], Garcia et al. [2008], Sellier and Fourcaud [2009], Kane and James [2011] and many other authors have estimated the dynamic properties of the structure to determine the tree dynamic response. Damping of the tree structure under wind events can be categorized into internal and external damping [Hoag et al. 1971]. Internal damping is due to the internal friction of the wood, friction of the root soil plate and the structural damping due to the movement of the branches [Moore and Maguire 2004]. The external damping is due to the aerodynamic drag of the crown and crown collisions between neighboring trees. Milne [1991], Gardiner [1992] and Moore and Maguire [2005] found a decrease in damping with crown de-branching. Spatz and Bruechert [2000] noted an increase in damping with low modulus of elasticity of the branches. Structural damping is measured using the free vibration response of the tree. Under forced vibrations, the mode of vibration with the lowest natural frequency dissipates the most energy, thus the damping ratio of the first mode of vibration has the greatest importance [Mayer 1987 and Peltola 1996]. The effect of the root-soil plate on the damping needs to be studied in greater detail [Jonsson et al., 2007 & Moore and Maguire 2008].

Two important approaches for quantifying tree response to wind loading are: 1) information on the dynamic properties of the tree to model the dynamic response or 2) the wind force and tree response spectra to develop mechanical transfer functions. Mechanical transfer functions can be determined by dividing the tree response spectrum by the wind spectrum. Holbo et al. [1980], Mayer [1987], Mayer et al. [1989], Saunderson et al. [1999],

Gardiner [1992 & 1998], Baker [1995], Peltola [1996], Miller [2005], Moore and Maguire [2008], Sellier et al. [2008] and Ciftci et al. [2013] were among the few researchers to use a mechanical admittance function [H(f)] as a measure of tree response to wind loading. The admittance function is used to analyze the transfer of energy from the wind field to the tree. The resonant response of any structure can also be best captured through an admittance function.

The dynamic response of trees to wind loading has been studied by many researchers using the dynamic properties of the above ground structure with changing wind loads, but the effect of soil on the tree dynamic response is seldom considered in wind studies. Often wind studies assume that the below ground structure of the tree is rigid, so the effect of the soil medium on the dynamic response of the above ground structure is neglected. In reality, structural response to dynamic loading is not only defined by the dynamic properties of the above ground structure, but also by the interaction of the structure with the supporting soil. Mergen [1954] reported that 92% of trees on non-cohesive soils failed by uprooting and only 11% on clayey soils failed by this mode. It is clear that the cohesive strength of soil has a huge impact on the uprooting resistance, but how it is influencing the sway response and hence the dynamic behavior is also important to understand tree stability.

In this chapter the dynamic behavior of Norway spruce tree saplings in sand and clay soils with increasing wind load is studied using three approaches:

1) Statistical analysis of sway plots.

The dynamic behavior of tree saplings was examined through tracked sway plots. Tree saplings with symmetric and asymmetric root systems were investigated with root plates in sand and clay soil media. The sway response of the roots was also tracked to understand the root plate dynamics based on the root plate architecture and soil support.

2) Dynamic properties of the tree structure (i.e. natural frequency and damping).

The natural frequency of tree saplings was examined under undamped oscillations and under increases in wind loading. The root natural frequency was also investigated for the

first time and furthermore the dominant frequency of the roots under forced vibrations was studied for both sand and clay.

The structural and aerodynamic damping measurements of the tree saplings and root systems were presented. The effect of the root architecture and soil on tree damping with increases in wind load was examined. The results of three commonly used methodologies for evaluating damping, were also compared to help select the most suitable technique for future damping estimates of trees.

3) Dimensionless mechanical transfer function

The mechanical admittance of the tree stem base bending moment was examined. For the first time in windthrow research, the root admittance in different soil media with increases in wind speed is examined. The theoretical aerodynamic admittance to the tree sapling experimental aerodynamic admittance is also compared.

In this chapter the dynamic response of the tree and root plate is also examined in greater detail. Since the shear strength of any soil is the combination of internal friction and cohesion, two soil media with contrasting properties have been used. The silica sand used in this study possesses purely frictional behavior and the clay has a purely cohesive nature. The root plate sway response, dynamic properties and the admittance function with increases in wind speed and change in root plate architecture and soil conditions were analyzed for the first time.

3.2.1 Research aims and objectives

The aim of this chapter is to understand the dynamic behavior of tree-root structure under incremental wind loading conditions for different soil media. The dynamic behavior of the tree-root structure helps to understand the energy transfer and hence the tree stability. To achieve this aim, three aspects were considered: sway response, dynamic properties and mechanical admittance.

The extensive data collected on the response of the instrumented tree saplings in the wind tunnel was used:

i. To investigate the tree stem and root sway response with increases in wind speed, change in soil medium and root plate architecture;

ii. To estimate the dynamic properties of the tree components with increases in wind speed and change in soil conditions and root asymmetry;

iii. To investigate the drag coefficient and center of gravity of the tree saplings with increases in wind speed using data from force balance tests and to validate the drag force equation and aerodynamic admittance theories;

iv. To investigate the mechanical admittance of a tree sapling with changes in soil medium, root asymmetry, and wind speed;

v. To investigate the energy transfer to the roots and the root admittance with changes in architecture, soil medium and wind speed.

3.3 Experimental setup

3.3.1 Introduction

To study and understand the dynamic response of trees to wind loading, wind tunnel tests were conducted with tree saplings in a custom built sunken planter box. The experiments were conducted in the Boundary Layer Wind Tunnel (BLWT) laboratory at the Western University, Ontario, Canada. The tree sapling test setup in the wind tunnel is as shown in the Figure 3-1. The high speed test section of the BLWT II is capable of wind speeds up to 100 km/h or 27 m/s and was used for the testing. The BLWT II high speed test section measures 3.4 m in width, 2.5 m in height and 39 m in length. The inside of the wind tunnel has automated floor roughness elements as shown in the Figure 3-3. The floor exposure used was “open country”, i.e. the floor roughness of the wind tunnel is set to reproduce a boundary layer wind profile with velocity gradient equivalent to an open country terrain.

This flow was achieved by adjusting the floor roughness, the height of the roughness elements varied from 0.01 m at the downstream panel to 0.08 m at the upstream panel.

3.3.2 Instrumentation

Wind velocity during the tests was recorded using five pitot tubes and a hot wire anemometer. Three pitot tubes at ceiling height (2 m above wind tunnel floor) recorded the reference wind speed. Two pitot tubes were used to record the wind speed at two different heights of the tree structure as shown in Figure 3-1. The recordings were made in m/s with 0.1 mm/s precision. A hot-wire anemometer was placed at a height close to the center of gravity of the tree, to measure the turbulence of the wind field. The hotwire anemometers were pre-calibrated to record 1 volt for 3.048 m/s (10 ft/s) wind speed. The data was recorded to 4 decimal places.

KFG-30-120-C1-11L1M2R type strain gauges were used to track the stem and root response, these strain gauges are two wire lead gauges with 30 mm gauge length and 120 ohm resistance. The maximum permitted bridge energizing voltage was 25 V rms (root-mean-square Voltage).

The other instrumentation used were laser transducers and accelerometers. Three laser transducers were used to measure the deflection of the stem at three different levels as shown in Figure 3-1. LB series, Keyence laser displacement transducers were used with ± 10 cm measuring range and 180 µm resolution. Depending on the tests, five to eight accelerometers were installed on the stem and roots for each test to measure the acceleration response of tree and root structure to wind loading and also to verify the strain gauge responses. The accelerometers used were Entran EGA miniature accelerometers with 15 mV/g sensitivity.

3.3.3 Tree sapling instrumentation

The tree saplings selected were 1.4 m and 1.2 m tall Norway spruce (Picea abies [L.] H.Karst.) trees (known hereafter as T1 & T2) and were utilized as a reference species, since it is ubiquitous in urban and rural Ontario. T1 had a symmetrical root system and T2 had a more asymmetrical root system; the root systems are as shown in Figures 3-4 and 3-5. Both

the tree saplings (T1 & T2) were pruned up to the height of 0.5 m and 0.4 m respectively above the ground level. The DSH (diameter at stump height) of the tree saplings T1 and T2 were 44 mm and 48 mm respectively. The structural root system of the saplings was generally kept intact. To ensure a simple root architecture, all of the fine roots were pruned leaving just the structural roots (> 0.4 mm diameter) in place, as shown in Figures 3-4 and 3-5. Generally fine roots occur in clusters, but help reinforce soil more homogenously [Reubens et al. 2007]. Makarova et al. [1997] noted incremental plastic strains decreased with increase in root diameter under cyclic loading conditions. Schwarz et al. [2010] observed that the fine roots contribute more during the initial stages of pull out compared to the coarser roots. As fine roots have low bending stiffness [Bischetti et al. 2005] they tend to break before coarse roots but they stay in position relative to the adjacent soil particles, while coarse roots can slip out of the soil [Ennos 1990]. Even though removal of fine roots might significantly alter the root-soil plate anchorage strength, in this experimental study the fine roots were removed for simplicity purposes.

To attach the strain gauges, bark was removed carefully without damaging the stem and root wood fibers; strain gauges were glued to the stem and roots as shown in Figures 3-2, 3-4 and 3-5 using Cyanoacrylate adhesive (CC-35X5). This is best suited to porous materials with an operating temperature range of -30 to 120^{o}C. Strain gauges were attached at two locations along the stem length of each tree sapling to track the lateral and windward strain response with increase in wind load as shown in Figure 3-2. A ring of four gauges were attached at each location; two located opposite one another to track the windward strain for the stem and vertical in the case of the roots. The other two were placed 90 degrees from the previous ones, to track the lateral responses. Each set of two gauges were placed diametrically opposite one other, so that one gauge would track the tension response and the other would track the compression response. These were connected to the logger in a basic Wheatstone bridge configuration using a half bridge arrangement. A similar ring of four gauges was attached at two locations on the T1 root system; one on the windward root and the other on the leeward root as shown in Figure 3-4. These were used to track the vertical and lateral response of the roots during wind loading. Each ring of four gauges was attached at three locations on the T2 root system as shown in Figure 3-5, to track the vertical

and lateral response of roots in the soil. A set of two strain gauges were used on Root1a of tree sapling T2 to track the lateral response.

The moisture content and specific gravity of the tree and root samples was estimated based on ASTM D2395-07a (Standard Test Methods for Specific Gravity of Wood and Wood-Based Materials). The moisture content of tree stem samples varied from 60 to 80% and root samples varied from 40 to 50 %. The average specific gravity of the tree stem and root samples at the given moisture content were 0.44 and 0.55 g/cm^3. Three-point bending tests were conducted on stem and root samples collected from the saplings. Tree saplings stems were cut into 300 mm long specimens and the roots into specimens of 220 mm to 280 mm in length. ASTM D198-09 method of testing was used to estimate the modulus of elasticity. The span between the two supports was adjusted to five times the thickness of the tested specimen. The tree sampling stem was cut into three pieces prior to three point bending tests, to minimize the taper effect. Even though span to depth ratio should be 15:1, because of the size of the available sample from the tested tree stem the span was taken five times the sample thickness. The stem modulus of elasticity varied from 0.6 to 0.7 GPa, with the variation in stem center diameter from 20 mm to 30 mm. The estimated value of the E was five to seven times lower than the standard spruce tree E [USDA Wood Handbook]. Modulus of elasticity of the root samples varied from 0.15 to 0.5 GPa with the specimen center diameter varying from 7 to 13 mm. As this is the only available estimate from the tested tree, E=0.6 GPa is considered for further calculations.

3.3.4 Soil preparation and rooting medium

A custom built octagonal sunken planter box, with sides measuring 0.36 m and depth of 1.2 m was built to fit the turntable in the downwind section of the wind tunnel. The planter box was filled with soil leaving 0.1 m depth unfilled. The tree sapling with root plate was placed in the middle of the planter box and the root plate was carefully buried in soil by filling the remaining soil box without causing any significant strain to the root plate and the attached instrumentation as shown in the Figure 3-1.

Trees growing in different soils have different advantages and limitations. Clay retains the moisture well, provides anchorage but unlocking the nutrients is a problem. Silty soil has

better drainage but has a risk of compaction. Sandy soils have free drainage, poor fertility and low anchorage. The loams (combination of clay, silt and sand) is the best soil for trees to grow. In this study, two soil media with contrasting states and properties were chosen to gain insight into the effect that soil has on tree response to wind loading to examine the change in root anchorage mechanics.

Sand tests were conducted with Barco #32 silica sand (Barco, 2015) in a dry state, to test the root response to wind loading in a purely frictional soil. The silica sand specifications are as shown in the Figure 3-6. The particle size distribution curve (ASTM D6913) is shown in Figure 3-6. The grading characteristics obtained from the particle size distribution curve are D_{10}=0.3 mm; D_{30}=0.395 mm and D_{60}=0.52 mm. The uniformity coefficient, $c_u = \frac{D_{60}}{D_{10}}$ =1.73 and the coefficient of gradation, $c_g = \frac{(D_{30})^2}{D_{60} \times D_{10}}$ =1.0, indicate a well-graded uniform sand. The maximum and minimum void ratio of the silica sand estimated by Varshoi [2012] in accordance with ASTM 4254 were 0.63 and 0.47 respectively. The maximum and minimum dry density of the silica sand based on void ratio estimates and specific gravity are 17.7 kN/m^3 and 15.9 kN/m^3. Peak friction angle (ϕ_p') and dilation angle (φ) of the silica sand were estimated by Deljoui [2012]. Peak friction angle (ϕ_p') in accordance with ASTM D3080 varied from 42° to 47° at very low normal pressures and dilation angle (φ). The dilation angle (φ) estimated based on Bolton [1986] varied from 14° to 20°. For the wind tunnel tests, preparation of the dry silica sand was achieved with air pluviation through a # 10 sieve from constant height (0.63 m) to achieve uniform density in the planter box. The top 0.2 m was filled in three layer and compacted by hand using 0.08×0.08×0.39 m wooden block. Density of the top 0.2 m deep silica sand in the sand box was measured as 16.4 kN/m^3 giving a relative density D_r=0.28.

The clay soil was prepared using Bentonite (sodium form). For every 25 % of Bentonite, 75 % of water was added and blended in a laboratory mixer; care was taken to ensure that the clay was blended effectively. The percentage of Bentonite or water in the clay mix is calculated as (weight of Bentonite or weight of water/total weight of the mix) ×100. The clay was sealed after preparing the mix to ensure consistent soil states. The moisture content, w (mass of water/dry soil particles) of the clay samples collected during the wind

tunnel testing period varied from 265 % to 250 %. Atterberg limits are widely used by geotechnical engineers to define the plastic properties of clay. Two important characteristics: liquid limit (moisture content at which soil just begins to flow) and plastic limit (lowest moisture content at which soil can rolled into 3 mm threads by hand without crumbling) of clay can be estimated based on B.S. 1377:1967. The Bentonite used was highly plastic in nature. The liquid limit (w_L) and plastic limit (w_P) of typical sodium Bentonites were found by Feng [2000] to be 280 % and 37 % and by Zentar et al. [2009] to be 305 % and 52 %. In this study an average of the standard error (SE) values were taken as 45 % and 290 %. The liquidity index, I_L [$(w\text{-}w_P/w_L\text{-}w_P)\times100$] at 255 % of water content was 85.7 % and the plasticity index, I_P (w_L-w_P) was 245 %. To estimate the undrained shear strength of clay, Wood (1990) proposed an equation relating liquidity index and remoulded undrained shear strength as shown in Equation [3-1] below.

$$c_u = c_l R_{MW}^{(1-I_L)} \qquad kPa \tag{3-1}$$

From Equation [3-1], c_L=1.7 kPa (meaning c_u=1.7 kPa at the liquid limit) and knowing the mean value of R_{wm} (mineralogy function) for highly plastic clays is 21.3 [Vardarega and Heigh 2014]. The remoulded undrained shear strength estimated from Equation [3-1] is c_u=2.6 kPa. Skempton [1954] and Mitchell [1976] proposed Equations [3-2] and [3-3] respectively, relating plasticity index to undrained shear strength c_u, effective vertical stress (σ_v') and friction angle (ϕ'), which can be used to estimate shear strength of clay under various conditions. For this clay the following values were estimated:

$$\frac{c_u}{\sigma_v'} = 0.11 + 0.37 I_p \tag{3-2}$$

$$\sin\phi' = 0.35 - 0.1 \ln I_p = 0.26 \tag{3-3}$$

From Equation [3-3], with a plasticity index (I_p) of 2.45, the frictional angle was ϕ'=15°. Equation [3-2] does not give accurate results for soil with plasticity Index > 100 %, in such cases Equation [3-1] and [3-3] can be used.

3.4 Test procedure

The wind tunnel tests were conducted with two tree saplings (T1 and T2). T1 was tested in the sand and on a force balance with six degrees of freedom [Figures 3-1 and 3-3] and T2 was tested in both sand and clay. The tree saplings were tested with an incremental wind speed loading as shown in Figure 3-7. For the T1 testing, the complete data sampling was done with a 200 Hz sampling rate. Whereas T2 was tested with a 300 Hz sampling rate, to identify any possible electrical noise in the data. The Nyquist frequency is half of the sampling rate. As long as the desired natural frequency estimate is below the Nyquist frequency, the estimate should be reasonable.

The wind velocity profile was set to an "open country" profile. The power law profile for an open country terrain with drag coefficient of 0.00-0.005 (K for open grass land) needs to be taken as suggested by Davenport [1964] for further analysis. For the purpose of the analysis undertaken in this chapter, the wind speed was increased incrementally and recorded by the pitot tubes and the hot wire anemometer near the center of gravity of the tree structure.

After the installation of the strain gauges on the stem and roots, each strain gauge was calibrated. This was conducted using static pull tests; applied bending moment was equated to the Voltage response of the strain gauge. The slope of the volt response line to the applied bending moment was taken as the calibration constant for further calculations. The laser transducers were calibrated using a white strip of paper, which was placed in front of the laser transducer and at each 0.01 m increment, the response in Volts was recorded. The difference in the Voltage response after each increment was taken. The average of Voltage response increment at each 0.01 m displacement increment gave the calibration constant for the laser transducers. Accelerometers, hot wire anemometer and pitot static tubes were used for the testing. The calibrated response of tree saplings T1 & T2 to the applied wind field were measured with increasing incremental wind speeds.

The peak shear strength of the clay mix in the soil box was found using a Pilcon hand vane tester. The shear vane tests were conducted before and after the wind loading tests. The 33

mm diameter vane was used to measure the peak shear strength and the measured shear strength was around 4 kPa, which was the average of 4 tests conducted during the wind tunnel testing. Giving a low sensitivity of approximately 1.5 for the clay.

After the wind tunnel tests, the tree saplings were pruned, measured and weighed. The tree stems were cut in to three equal parts and stored in a refrigerator. Each root and stump were measured, weighed and stored in a lab refrigerator at 5°C. Three-point bending tests were conducted on the stem and root samples in accordance with ASTM D198-09 (Standard Test Methods of Static Tests of Lumber in Structural Sizes). The static bending tests were carried out using the MTS universal testing machine at University of Western Ontario, in the Structures lab. For the three-point bending tests, the distance between the two supports was kept 15 times the mid-point diameter for the stem sample and 60 mm or 100 mm for the roots. Resolution ratio of the test force and the displacement were 0.001 kN and 0.01 mm. A pushing probe of 20 mm radius was attached to the load cell and a lowering rate of 20 mm/min was used and half of the lowering rate was used for the root testing.

3.5 Analysis and results

In this experimental study, the applied wind field and the tree response was recorded in great detail. The flexibility of the experimental techniques provided the opportunity to study the dynamic properties of the tree saplings with complete root systems in different soil media. The dynamic response of the tree stems and roots were examined with varying wind speed, change in soil properties and root architecture. The bending response of different components of the tree saplings T1 & T2 to the applied wind field are shown in Figures 3-8, 3-9 and 3-10.

Each of the bending moment time histories show generally similar results. For example, in Figure 3-8 the lower stem moments are higher than the upper stem moments and leeward root moments are higher than the windward root moments. Windward stem moments are higher than lateral moments and show a positive bias with a non-zero neutral point. The lateral moments of the stem in comparison show two way cycling about the zero axis. The

roots show positive bias and for the windward root approximately the same magnitude of moment in the vertical and lateral direction. The leeward root shows much less lateral response than vertical motion. The cyclic response of the stem shows increasing average and cyclic moment amplitudes with increasing wind speed (approximately proportional to the wind speed). In comparison, the root cyclic amplitudes are initially very small and increase rapidly at higher wind speeds, showing non-linearity indicative of plastic damage to the soil medium.

Changes in tree response with root architecture (by comparing T1 & T2 responses in sand) are shown in Figures 3-8 and 3-10. To examine the changes in response with soil media, T2 responses in sand and clay [Figures 3-9 and 3-10] can be compared. Tree saplings in sand were tested to failure. In clay the tree saplings showed high stability; tests were conducted to the maximum possible loads to avoid stem breakage and not overload the sensors.

The differences in the biomass of tree saplings T1 and T2 are shown in the Table 3-1. T1 weighed 1.51 kg, and T2 weighed 1.59 kg, with only 5.6% increase in total tree weight, yet the failure wind speed increased by 77%. However, inspection of the biomass of the root systems show a much higher root biomass percent for tree T2. The difference in the T1 & T2 response in sand shows the substantial effect that the root system weight and architecture has on tree stability. T2 sustained wind speeds up to 12.2 m/s compared to the T1 failure wind speed of 6.9 m/s.

We can compare the upper and lower stem response of T1 and T2 in sand at similar wind speeds. The lateral moment response of T1 with a more symmetrical root system was much lower compared to the T2 response; the T2 lateral bending moment response was around 15 times higher than the T1 response. The T2 windward moment response was twice as high compared to the T1 response. In comparison with sand and clay, as anticipated, T2 showed much higher stability in clay, and did not fail even at 12.2 m/s wind speed. Further testing with higher wind speeds on clay were not conducted because of strain gauge capacity concerns and also to reduce risks with respect to stem breakage. By comparing the T2 response in clay (cohesive) and sand (non-cohesive) [Figures 3-9 and 3-10], it can

also be seen how a tree with a highly stable root-soil (clay) system responds to the wind loads compared to a less stable root soil (sand) system. The upper stem windward response of T2 was twice as large in clay compared to its response in sand, and the lower stem windward response was almost thrice as much compared to its response in sand. The upper stem lateral response of the T2 sapling showed 20 to 30 % increase in sand compared to the clay case and the lower stem lateral response showed 30 to 40 % increase in sand compared to the response in clay. The T2 roots, 1 and 2 showed up to 3 times the response in sand compared to clay; root 3 showed a much higher response in sand compared to clay.

As stated by James et al. [2006], the key to understanding the complex dynamic response is understanding the energy transfer, as the load applied is directly proportional to the structural response. Considering the strain gauge response in terms of bending moment as a measure of energy transferring from wind to tree sapling and ultimately dissipating through the tree structure and the root components, the stem response for clay was higher compared to the sand and much higher energy was transferred to the root plate in the sand compared to the clay. It is clear that a tree has better chances of survival, if less energy is transferred from the wind to the tree, and if the mass damping is higher (reducing the transfer of wind energy from the trunk to the root system). It is interesting to note that for the same tree sapling with no change in frontal area and the wind speed, higher stem response and lower root response was recorded with a cohesive soil-root system compared to a frictional soil. This suggests that the tree-soil system damped (dissipated) more energy, allowing less energy to be transferred to the root plate. The tree sampling sway response for different scenarios is further analyzed in the next sections and the dynamic properties are examined to improve the understanding of tree stability.

3.5.1 Wind loading and spectral analysis

The wind field for all of the described wind tunnel tests was applied in increments as shown in Figure 3-7. The time period for each load increment was 180 seconds. Turbulence intensity is the ratio of standard deviation to the mean wind speed and gust factor is the ratio of maximum wind speed to the mean wind speed. Data recorded with the hot wire anemometer placed close to the center of gravity of tree structure was used to estimate the turbulence intensity and gust factor. The turbulence intensity and gust factor of the applied

wind field for a typical test are as shown in Figure 3-11. A stabilized wind field in the wind tunnel was observed beyond wind speeds of 1.6 m/s, where the turbulence intensity and gust factor stabilized at values of 0.125 and 1.5 respectively.

In this study, spectral analysis was used to transform the data from the time domain into the frequency domain. The power spectral density (PSD) of the wind load or tree response in time domain is the description of the power distribution over frequency. A Fast Fourier Transformation was used based on Welch's method [Welch, 1967]. This method uses the concept of averaging periodograms to aid noise reduction; a 50% overlap window was used. All of the spectral analysis of this study were performed with the Signal Processing Tool Box of the commercial MATLAB software. Spectral analysis aids the identification of the frequency components, which influence the primary tree responses. A wind spectrum is the distribution of turbulence with frequency. The wind spectrum with increase in wind speed for the T2 test in clay is shown in Figure 3-12, which represents the typical wind data of each test. The wind spectrum at each wind speed relates to data collected for the three minute (180 s) time period of each load increment.

The spectral peak for the turbulence in natural wind events is of the order of 1 cycle per minute and in the wind tunnel it is around 1 Hz (1 cycle per second) or higher [Liu 1991]. The wind spectra show peaks in the range of 0.3-1.8 Hz [Figure 3-12] with increasing wind speeds and generally noisier response at high frequencies. The peak frequency increases with greater wind speeds and the spectra is more stable (more similar) at high wind speeds.

The wind spectra consist of three subranges: i) the energy containing range, where the turbulence is produced by shear and buoyancy; ii) the inertial subrange, where energy is neither produced nor destroyed but shifts from larger to smaller scales and iii) the dissipation range [Baldocchi 2012]. In the measured spectra, the slope of the wind spectrum in the inertial subrange generally show a slope of -2/3 [Figure 3-12], following Kolmogorov's law [Kaimal et al. 1972]. This represents the local isotropy, with no net transfer of turbulence in this subrange.

Assessing the survival of structures and trees for design-level wind events and fatigue loading is important. We need to check to see if fatigue may be important for trees and

roots. For wind loading, fatigue responses can be: 1) narrow band processes (near single frequencies), e.g. slender chimneys or masts with vortex shedding (potential resonance) or 2) wide band processes (with a wide spectrum of frequencies where a fundamental frequency might not easily be observed), with little prospect of resonance occurring. Counting stress cycles for damage estimates is not always straightforward; in the time domain this requires rain flow cycle counting for a wide band process (narrow band processes are much easier to approximate) or for the frequency domain the Dirlik method [Dirlik, 1985] can be used. Thus identifying bandwidth characteristics of random processes gives important insights into phenomena and required analytical approaches.

Catwright and Longuet-Higgins [1956] derived the bandwidth parameter ε of a spectrum, as shown in Equation [3-4] [Ochi, 1990].

$$\varepsilon = \sqrt{1 - \frac{m_2^2}{m_0 m_4}} \qquad [3\text{-}4]$$

Where the moments of the spectra, $m_k = \int_0^\infty n^k S(n) dn$ and S(n) is the power spectrum of the random function at the frequency n.

Bandwidth parameter, ε =0 for a random process with a narrow band spectrum and ε=1.0 for a wide band spectrum. The calculated band width parameters of the wind velocity and moment response spectra are presented in Tables 3-2 and 3-3. These generally show values ε→1.0 across a range of wind speeds for both the wind process and the response of the system (both stem and root). It is therefore reasonable to state that the wind and response spectra are likely to be wide band processes.

3.5.2 Tree sway

To better understand the complex dynamic response of these trees to wind loading, sway motions were tracked. Many researchers [Holbo et al. 1980, Mayer 1987, Mayer et al. 1989, Peltola 1996, James et al. 2006 and Sellier et al. 2008] have previously tracked the swaying motion of tree stems to wind loads. In this chapter, the sway motion of the tree stem and root components is also studied with the aid of the tree saplings which have

different root architecture, different founding soils and with incremental wind speeds. The joint response of the base bending moment in the orthogonal directions was plotted. The stem base and the instrumented root response of the two tree saplings was tracked. Two sets of strain gauges were attached orthogonally to track the response data. T2 movement in sand and clay with increase in wind speeds is presented in Figure 3-13, using the response data of orthogonally attached strain gauges at the stem base.

Even though, detailed quantitative understanding of the complex sway response is not possible from Figure 3-13, the general direction and range of the tree (T2) movement and the relative lateral response with respect to windward response can be observed. The response of tree T2 in the lateral direction is higher in clay compared to sand. The windward response of T2 was higher in the sand compared to clay. As the sway motion is very irregular and complex [Figure 3-13], the sway behavior in this study was further investigated using a bivariate normal probability density function, to visualize and better understand the sway motions. In order to explain the complexity of the sway motion, statistical analysis was performed. The two variants used to track the spatial distribution are the windward (along wind) and lateral (across wind) bending moment response of the stem base with increase in wind load. For the case of the roots, vertical and lateral bending moment response was used to track the root movement.

The response data at each load increment was analyzed statistically and the bivariate (two-dimensional) normal distribution was plotted with a joint probability density function, f(x,y) as shown in Equation [3-5]:

$$f(x,y) = \frac{1}{2\pi\sigma_1\sigma_2\sqrt{1-\rho^2}} \times exp\left\{-\frac{1}{2(1-\rho^2)}\left[\left(\frac{x-\mu_1}{\sigma_1}\right)^2 - 2\rho\left(\frac{x-\mu_1}{\sigma_1}\right)\left(\frac{y-\mu_2}{\sigma_2}\right) + \left(\frac{y-\mu_2}{\sigma_2}\right)^2\right]\right\} \quad [3\text{-}5]$$

$-\infty < x < \infty$, $-\infty < y < \infty$

Where X and Y are the orthogonal response data vectors at each wind load increment, μ_1 and μ_2 are the means, σ_1^2 and σ_2^2 are the variances of X and Y respectively, while ρ is the correlation coefficient of X and Y.

Note: Random variables are usually represented by capital letters; in this study this is X and Y for the orthogonal response data and their values by small letters.

The mean for a continuous type random variable X is, $\mu=E[x]$, variance $\sigma^2 = E[(x-\mu)^2]$, correlation coefficient of two random variables X and Y is $\rho = \frac{cov[x,y]}{\sqrt{\sigma_1^2 \sigma_2^2}}$ and covariance, $cov[x, y] = E[(x-\mu_1)(y-\mu_2)]$.

Each data set has been statistically analyzed and the results are presented with sway plots. Statistical parameters that best describe the sway plots are coefficient of variation, skewness and kurtosis. The ratio of standard deviation (σ) to the mean (μ) is called the *coefficient of variation* and it shows the extent of variation in relation to mean. *Skewness* is the ratio of $E[(x-\mu)^3]$ to σ^3, which is a measure of asymmetry of the system. If skewness is zero, the probability density function is symmetric with respect to its mean value [Ochi 1990]. If the value is positive, the tail of the probability density function is fatter or longer on the right side than the left side and vice versa if the value is negative. *Kurtosis* represents the degree of peakedness of the sway distribution and is the ratio of $E[(x-\mu)^4]$ to σ^4 [Ochi 1990]. For a normal distribution, the kurtosis value is equal to 3. If the value is less than 3, distribution is called platykurtic (mild peak) and if the value is greater than 3, the distribution is called leptokurtic (sharp peak). The results of the statistical analysis of each data set used for the sway plots are shown in the sway plot tables attached to Figures 3-14 and 3-15.

In Figure 3-14, the sway responses of T1 with a symmetrical root system in the sand and the stem base on the force balance were compared with increase in wind speed. Since the root plate in the soil medium and the stem base on the force balance act as a flexible and fixed base respectively, these plots show the difference in sway with flexible and rigid base conditions. Even though both conditions showed similar sway patterns and approximately the same spread (variance), it is clear that the flexible base (root plate in sand) showed

much less lateral (orthogonal to wind direction) shift compared to the fixed base (stem base on force balance) case. In the case of the soil medium, as the soil used is purely frictional, the entire tree sapling moved in the direction of the wind. For the fixed base case, the above ground tree structure bent in the lateral direction to the wind direction and swayed. Skewness (measure of distribution asymmetry) of the probability density distribution in the windward and lateral direction were more symmetric in the case of the flexible base compared to the fixed base. Both scenarios showed approximately the same kurtosis (peakedness of the distribution) in the windward direction, meaning the variance is the same. The probability distribution in the windward direction had a mild peak (kurtosis<3), whereas the response in the lateral direction showed a sharp peak (kurtosis>3), i.e. the sway response in the windward direction has high variance compared to the sway in the lateral direction. Understandably the fixed base case showed a higher linear correlation (as the tree sapling on the fixed base case moved lateral to the wind direction) compared to the flexible base and decreases in correlation with increases in wind speed were observed in both cases.

In Figure 3-15, the sway responses of T2 with an asymmetrical root system in the sand and clay medium were compared with increase in wind speed. T2 located in the frictional soil showed high response in the windward direction compared to the cohesive soil test. The lateral response of the stem base on the cohesive soil is twice as high compared to the frictional soil support. The spread (variance) of the sway in the windward direction is much higher in the frictional soil compared to clay and vice-versa in the lateral direction. Skewness (measure of distribution asymmetry) of the probability density distribution in the windward and lateral direction were more symmetric for sand compared to clay. Negative values of skewness show that the mode of the distribution is located at a value greater than the mean. Both cases showed sharp peak distributions (kurtosis>3), meaning less variance, i.e. the response is highly concentrated at the mode (high probability value). The probability distribution of the stem response in the windward direction had high kurtosis in the sand compared to the clay. The lateral response in clay showed a mixed kurtosis response from a sharp peak to mild peak, whereas the response in sand showed increase in kurtosis with wind speed. General decrease in the correlation coefficient occurs with increase in wind speed for the clay case. It is interesting to note an increase in correlation

coefficient with wind speed in the case of the frictional soil. It was expected for T2 with an asymmetric root system in the frictional soil to be more or less vulnerable to failure even at given wind speeds (dependent on the wind direction). This could be a reason why T2 showed more significant resistance to uprooting than T1 with a more symmetric root system.

The root sway response of T1 and T2 with varying root plate support are as shown in the Figures 3-16 and 3-17. Even though the sway response in each plot has an elliptical form, a significant difference in sway direction is observed with varying root plate support and location of the root. In Figure 3-16, the windward and leeward root sway response of T1 in sand is shown with increase in wind speed. In the case of T1 with symmetrical root system in sand, the windward root showed much higher response compared to the leeward root in both the vertical and horizontal directions. The spread (variance) of leeward root sway is very low as well, compared to the windward root. Windward root sway is observed to be quite asymmetric (higher skewness values). Initial increase and then decrease in kurtosis is observed with increase in wind loading for both windward and leeward root response. In both cases, the sway became more concentrated to well spread in the case of leeward root and the distribution remained leptokurtic (sharply peaked) in the case of the windward root.

In Figure 3-17, the T2 root response in both sand and clay can be observed at a single wind speed. As shown, the root response in sand was much higher than in clay. The sway response in sand was much more asymmetric (higher skewness values) than for the clay except for the lateral response of Root 1 and 2. Root response in clay was more concentrated (higher kurtosis values) compared to the response in sand. Correlation coefficients of the vertical to horizontal response of the roots in clay were quite high compared to the response in sand.

Mayer [1987] and Mayer et al. [1989] presented tree sway plots in response to static pull and release tests. The elliptical spread (sway plots) helped to understand the difference in tree sway response with change in soil conditions. The full complex dynamic sway motion (two dimensional stem response plot with no statistical approximation) was also presented

by Gardiner [1995] and James et al. [2006 & 2013], but the complex sway response graphs can only help recognize the true complexity of sway response and the response direction with respect to the wind direction. The statistical analysis presented in this section can be a useful approach to understand the complexity of the two dimensional tree response to dynamic wind loading. The random data (tree response data) characterization was conducted using a joint probability density function and by evaluating various parameters of the distribution. This methodology can be used to identify the detailed changes in sway responses under different scenarios.

3.5.3 Natural frequency and damping

Natural frequency and damping ratio are the most important dynamic properties of trees that characterize tree response to wind loading. Natural frequency is defined as the number of cycles of oscillation per unit of time and is measured in cycles per second (cps) or Hertz (Hz). Natural frequency shows the rate of energy transfer from the equivalent mass to the spring of a dynamic system. Whereas the damping ratio determines the amount of energy lost in each oscillation of the system. Because of the importance of dynamic properties to model the dynamic response of a tree, many researchers have worked on measuring and modelling tree dynamic properties. As the damping of a tree-like natural system is very complicated to model, velocity proportional (viscous damping) damping is commonly assumed. Moore and Maguire [2004] reviewed and synthesized data on the dynamic properties of trees. The dynamic properties were observed to be governed by the mass distribution and stiffness of the tree system and the excitation frequency of the applied load. In this study, the change in dynamic properties of a tree sapling were examined (with no change in mass and stiffness) with a root system in sand and clay (i.e. with only change in soil) under increasing wind speeds (similar excitation frequency), to investigate the effect of the soil on tree dynamic response.

The damping mechanism of a tree can be sub-divided into two components, 1) internal and 2) external damping [Hoag et al. 1971]. Internal damping is the energy dissipation in the tree root system due to the internal friction of the tree stem, branches and the soil root system and external damping is due to the aerodynamic drag of the crown (in this case of a single tree test). Internal damping is measured using the response data of pull-release

tests. Under undamped or free vibrations, the damping is assumed to be viscous. Milne [1991], Wood [1990] and Moore and Maguire [2004] used the logarithmic decrement method; the half power band width method [Clough and Penzien 1993] can also be used to estimate the damping. Moore and Maguire [2004] and Jonsson et al. [2007] used the Hilbert transformation method to estimate the damping. These three methods were used to estimate the damping of free vibration (pull and release tests) for the first mode of vibration and are used as explained below. For more detailed explanation of these methods please refer to Appendix I. The three methods described below were used in this study and the results are compared to examine the suitability of each method to estimate the damping of a tree.

The logarithmic decrement method is the most useful and an easiest method to estimate the damping from free vibration decay [Clough and Penzien 1993] in the time domain. In this method, the rate at which the amplitude of a damped vibration decreases is measured over one or n number of cycles. If x_1 and x_{n+1} are the amplitudes of vibration of the first cycle and after n number of cycles respectively, the damping ratio (ξ) is given by:

$$\xi = \frac{\delta}{\sqrt{(2\pi)^2 + \delta^2}} \qquad [3\text{-}6]$$

Where $\delta = \frac{1}{n} \ln\left(\frac{x_1}{x_{1+n}}\right)$

As it is a time domain method, this method is not sufficient to estimate the aerodynamic damping also damping ratio cannot be estimated at all excited modes.

The half power band width method was used to estimate the damping of a system in the frequency domain. From the frequency response function, the maximum amplitude (x_{max}) is obtained at the chosen natural frequency (f_n). The two frequencies f_1 and f_2 corresponding to the half power band, i.e. at $\frac{x_{max}}{\sqrt{2}}$ are used to obtain the damping. The ratio of the frequency range between two frequencies at the half power point and twice the natural frequency is given by:

$$\xi = \frac{f_2 - f_1}{f_1 + f_2} = \frac{f_2 - f_1}{2f_n} \qquad [3\text{-}7]$$

Even though this method can be used to estimate the damping at all excited modes, one of the disadvantages of this power spectrum method is that for lightly damped systems the half power bandwidth is small and needs to be measured carefully.

The Hilbert transformation method used in this study is described in Jonsson et al. [2007]. The response data is transformed to the frequency domain using Fourier transformation. At the anticipated mode of vibration, the data is filtered using a Butterworth filter and is transformed to the time domain using the Hilbert transformation. The obtained data is plotted as a function of time. The slope of the envelope divided by the natural frequency at the selected mode of vibration is the damping for that mode of vibration (in this chapter only the first mode of vibration was analyzed). One problem with this method is that it is usually only applied to free vibration damping.

Even though external damping due to aerodynamic drag of the crown was explained by Hoag et al. 1971, Milne 1991 and Wood 1995, none of the literature has included the change in damping with increase in wind speed. In this chapter, the auto correlation method has also been used to estimate the damping with increase in wind speed. The auto correlation method is used because of its simplicity as a logarithmic decrement method (time domain method) and convenience as with the half power bandwidth method or the frequency domain method.

The auto correlation methodology is summarized below [see Figure 3-18]:

- The recorded response data is plotted in the frequency domain using fast fourier transformation (FFT).

- The frequency response data is filtered for the first mode of vibration, i.e. at the first natural frequency band width using a Butterworth band pass filter. The selected band width is the frequency range at which most of the energy is transferred to the first mode of vibration.

- The filtered data is transferred to the time domain using an autocorrelation function [Ochi 1990]

$$Autocorrelation = \frac{E\left[\left(X_{t_1} - \mu_{t_1}\right)\left(X_{t_2} - \mu_{t_2}\right)\right]}{\sigma_{t_1}\sigma_{t_2}} \quad [3\text{-}8]$$

Where E is the expected value operator; the mean for a continuous type random variable X is, $\mu=E[x]$, variance $\sigma^2 = E[(x-\mu)^2]$, and t_1 to t_2 is the shift in the time period.

An example of the auto correlation approach for the first mode of vibration is plotted in the time domain as shown in Figure 3-18 and the damping is estimated using the logarithmic decrement method. To ensure consistency in calculation, five cycles were used for each damping ratio estimate. In the autocorrelation method, the logarithmic decrement estimate gives the accurate measure of slope, which is directly proportional to damping.

The structural damping estimates of each component of the tree saplings T1 and T2 are shown in Tables 3-4 and 3-5 respectively. These damping ratios were estimated from the pull and release test data of each component with rest of the structure attached to the fixed base. The structural damping estimates were completed using the same three methods. Auto correlation showed very similar results to the logarithmic decrement method. The half power band width method showed much higher values compared to other two methods and Hilbert transformation method showed much lower values, also the auto correlation method is the only method which could be used to estimate the damping at various different wind speeds. Hence the auto correlation method is used for further calculations. Tables 3-4 and 3-5 show the natural frequencies of the stems are very similar and in the range of 2.4-2.8 Hz. In contrast, the natural frequencies of the roots are much higher and in the range of 60-100 Hz. The structural damping ratios range from 0.016 to 0.089 for both stem and root and show no clear trends based on component type.

The damping estimates of tree sapling T1 in sand with increase in wind speeds are presented in Figure 3-19. Increase in damping ratio with increase in wind speed is observed for stem windward response, windward root vertical response and the leeward root lateral response. It is interesting to note that the damping ratio trend of the orthogonal responses of stem and the roots are very different especially at high wind speeds. The stem damping ratio varied between 6 % and 11 %, windward response showed higher damping than the

lateral response. Root damping ratios were much higher than the stem damping ratios; the damping ratio varied from 7 to 20 %.

The damping estimates of tree sapling T2 in sand and clay with increase in wind speeds are presented in Figures 3-20 and 3-21. In sand, generally damping appears to increase with wind speed, but this trend is not fully clear. Root damping ratios are a little higher than stem ratios; both structures span the range 0.038-0.155. This compares to the tree structural damping values found in the literature, for example: 0.04-0.15 [Moore and Maguire 2004]; 0.10 [James and Haritos 2010]; 0.08-0.153 [Flesch and Wilson 1999]; 0.06 [Milne 1991]. In the clay, the trends appear to be reversed with the stem damping being higher on average than the roots. This shows the significant effect of soil on the damping. All of the root responses showed higher damping in sand compared to the response in clay, which is understandable as higher energy is transferred to the root plate in sand compared to clay at similar wind speeds [Figures 3-9 and 3-10]. T2 failed at 12 m/s wind speed in the sand, but it did not fail in the clay; the change in damping with increases in wind speed followed the same trend. T2 in sand showed increases in damping at failure wind speeds except for the windward stem response. The windward stem response showed initial increases and then decreases in damping. It is interesting to note that, T2 components which carried higher energy with increases in wind speeds showed higher damping with increases in damping. Similar trends in damping variation were observed with both upper and lower stem windward response and the lateral response in both sand and clay soils.

As the damping estimated from the tree response data at each wind speed gives the total damping for the first mode of vibration, the structural damping alone was estimated using the tree component response from static pull and release (free decay) tests.

The structural damping was also calculated using the auto correlation method:

$$\xi_{struct} = \frac{1}{2\pi n} ln\left[\frac{u_i}{u_{i+n}}\right] \qquad [3\text{-}9]$$

The structural damping and the total damping estimates of each tree sapling are presented in Figures 3-19, 3-20, and 3-21. The structural damping estimates were conducted from the

free decay test data of the tree saplings in sand and clay; the tree sapling was pulled and released at the top of the crown. The stem and root response to the free decay was used to estimate the structural damping.

Once the structural damping is known, the aerodynamic damping can be estimated using:

$$\xi_{aero} = \xi - \xi_{struct} \quad [3\text{-}10]$$

The aerodynamic damping is estimated by subtracting the structural damping (estimated using the autocorrelation method from the free decay test data of the tree sapling response in the soil base) from the total damping (estimated using the autocorrelation method using the filtered data at each wind speed).

The effect of the soil medium on aerodynamic damping was also examined. The results are shown in the Figure 3-22. Aerodynamic damping in both sand and clay showed increasing and decreasing patterns of damping ratio change with increase in wind speed. This may be because for every step of increase in wind speed, the tree deflects and/or shifts to a new position. In the new position because of the resistance offered by the soil or shift that may or may not have happened to the tree with root system in the engineered soil (the clay and sand we used in this experiment), this could impact the sway and hence the damping significantly. In both sand and clay, the stem aerodynamic damping varied from half the structural damping to thrice with changing wind speeds. The structural root damping in clay was on the lower end of the damping estimates, the aerodynamic damping of the roots increased up to four times the structural damping. Milne [1991] examined the ratio between damping due to contact with neighboring trees, aero dynamic damping, and damping in the tree stem and root system as 5/4/1. In this wind tunnel study, with the tests on a single tree sapling at a time, structural damping was on the higher side and aerodynamic damping only increased up to 3 times the structural damping at high wind speeds. It is also important to note here that all damping estimates in this chapter were conducted for the first mode of vibration.

3.5.4 Admittance functions

In this section dimensionless mechanical and aerodynamic admittance functions are examined in detail, with increase in wind speed and change in root architecture and soil medium. Even though the nature of the wind load is defined by its mean speed, turbulence intensity, gust factor and the wind profile, many researchers use the simplified equation of the drag force to estimate the wind load:

$$F = \frac{1}{2}\rho A C_D \bar{V}^2 \qquad [3\text{-}11]$$

Where ρ is the air density, A is the frontal area of the crown, C_D is the drag coefficient and $\bar{V}$ is the mean wind speed. The work in this chapter follows the same approach and Equation [3-11] is used to estimate the wind energy transferred to the tree from the wind. To calculate the drag force on the tree sapling at each wind speed, A and C_D are estimated as given below:

i) The tree sapling (T1) frontal area was estimated using the images taken from the recorded video during the wind tunnel testing. Frontal area at each wind speed is estimated using the pixel counting software with the help of Dr. Stephen Mitchell's team from the University of British Columbia, Canada. T1 frontal area varied from 0.348 m^2 to 0.342 m^2 with increase in wind speed from 0 m/s to 6.98 m/s. An average frontal area of 0.347 m^2 was used for further calculations. Only T1 frontal area was estimated by the forestry department team of University of British Columbia and the rest of the required results are obtained through approximation. The frontal area of T2 was estimated assuming that the frontal area is proportional to the branch mass [Kellomaki 1999]. The estimated frontal area of T2 (from the T1 estimate of 0.347 m^2) was 0.31 m^2.

ii) The response data of T1 from the force balance test was used to estimate the drag coefficient (C_D). The drag coefficient of the tree sapling with increase in wind speed was estimated by equating the recorded force at the stem base from the force balance to the drag force estimate using Equation [3-11] and is as shown in Figure 3-23. This shows the drag coefficient changes non-linearly from 1.1 to 0.65 as the wind speed increased to 10 m/s. The same drag coefficient estimate was used for further analysis in this chapter for

both Norway spruce tree saplings tested. Similar trends in drag coefficient variation with increase in wind speed was also observed by Mayhead [1973b] for various tree species, C_D varied from 0.4 to 0.8 at 10 m/s for different species. For spruce it varied from 0.62 to 0.8 at 10 m/s wind speed. At wind speeds greater than 30 m/s, uniform values of drag coefficient are used [Mayhead 1973b]. For Norway spruce values of 0.35 are used for wind speeds greater than 30 m/s.

The above drag coefficient and frontal area estimates were used to relate the wind pressure on the tree structure to the applied wind velocity in the frequency domain. In this study the response component taken to estimate the response spectra and the mechanical admittance function of the above ground structure is the base bending moment response. The ratio of base bending moment at each wind speed to the wind load on tree sapling estimated using Equation [3-11] was taken as the center of gravity (COG). The change in COG of tree saplings T1 and T2 with increase in wind speed is shown in Figures 3-24 and 3-25 respectively. The T1 response with a symmetrical root system showed no significant change in COG with different stem bases; initial drop in COG and then steady decrease in COG was observed. T1 in sand failed at 6.9 m/s wind speed; it is interesting to note that T1 on the force balance also showed a similar trend in COG variation with increase in wind speed [Figure 3-24]. Even though T2 with an asymmetrical root system in sand and clay also showed similar trends in COG, significant shift in COG can be observed between both cases [Figure 3-25]. At higher wind speeds, 20 to 30 % increase in COG height of T2 was shown in sand compared to the clay base. For the case of the sand, the root base was shifted slightly making the entire tree sapling move and adjust with increase in wind speed, whereas the clay base acted as a fixed base, making the stem bend significantly to compensate for the wind load. This could be the reason why significant shift in COG height is observed with change in soil base, it is also important to note this difference is only observed in the case of T2 with the asymmetrical root system and also the applied wind load direction is different in the T1 and T2 tests [Figure 3-2].

The power spectral density (PSD) of the tree stem base bending moment response was plotted using Fast Fourier Transformation (based on Welch's method [Welch, 1967]). The power spectral densities of tree saplings T1 and T2 are shown in Figures 3-26 and 3-27

respectively. The base bending moment response spectra $S_B(f)$ were plotted for different base condition of each tree sapling with increases in wind speeds. In Figure 3-26, slight increase in natural frequency of T1 is observed from the root plate in sand to stem base on the force balance (fixed base), at 3.6 m/s wind speed natural frequency changed from 2.77 to 2.8; at 4.8 m/s, 2.74 to 2.8; and at 5.8 m/s, 2.6 to 2.98. It seems logical as the trees with low frequencies react more to the wind fluctuations with increased displacements and base bending moments [Baker 1997]. As the resonance peak breadth represents the damping, damping variation with increases in wind and changes stem base conditions can be observed. The T1 root base in sand showed more damping except for the low wind speeds compared to the force balance case. Shift in additional energy peaks can be observed with change in stem base conditions. For the sand case, additional energy was observed from 10 Hz to 60 Hz. For the force balance case, less dominant energy peaks were observed from 10 Hz to 30Hz. The reason could be the root natural frequencies, all of the root plate was engaged at similar wind speeds in the case of sand compared to the fixed base case (force balance), transferring more energy to the tree in the sand case. T1 failed by uprooting at 6.9 m/s with root system in sand because of the high energy transferred to the root plate whereas T1 on the force balance was fixed at the base.

In Figure 3-27, a similar trend of lower resonant frequency in the sand case can be observed, 4 to 8 % with changing wind speeds. High damping in sand at lower wind speeds and at high wind speeds was observed compared to the clay case. Similar energy peaks were observed in both cases from 9 Hz to 60 Hz. In the sand case, the first order resonant frequency was on the lower end compared to the clay case. The rest of the higher order frequencies in the sand case were very similar to the clay case with few energy peaks at little higher and lower frequencies. The plausible reason for the shift in higher order natural frequencies could be because of high response and high deflections for the first mode of vibration in sand (because of low first natural frequencies) are causing the other tree parts to sway a little slower or faster with changing wind speeds. This concept needs to be investigated further with more experimentation.

The wind spectra and the corresponding tree response spectra can be related using transfer functions, the aerodynamic and mechanical admittance functions. Wind force on the above

ground structure of the tree and wind velocity spectrum are related through the aerodynamic admittance of the tree and the tree response to the wind force are related through the mechanical admittance function.

In this study, the aerodynamic admittance was estimated using the approach of Gardiner [1992] and Baker [1995]:

The force on the tree due to wind is found using Equation [3-11], since the wind velocity v is the combination of the mean component ($\bar{v}$) and the fluctuating component (v').

$$v = \overline{v} + v' \qquad [3\text{-}12]$$

Substituting Equation [3-12] in to Equation [3-11], the mean wind speed component is not considered as it contributes to the steady wind loading and $(v')^2$ is not considered as it is much lesser than $2\bar{v}v'$. Hence the power spectrum of the wind force $S_F(f)$ would be [Baker 1995]:

$$S_F(f) = 4\left(\frac{\bar{F}}{\bar{v}}\right)^2 S_v(f)\Gamma(f)^2 \qquad [3\text{-}13]$$

Where, $S_v(f)$ is the power spectrum of the wind speed, and $\Gamma(f)$ is the aerodynamic admittance function.

The theoretical aerodynamic admittance, given by Baker [1995] from Davenport [1964] is

$$\Gamma(f)^2 = \frac{1}{1 + 2.5\left({}^{fD}/_{\bar{v}}\right)^{2.5}} \qquad [3\text{-}14]$$

Where D is the tree canopy diameter. For conifers, Mayer [1987] proposed that the aerodynamic admittance is approximately 1. As this approximation is valid for mature field trees, we investigated the aerodynamic admittance of tree saplings for the wind tunnel testing. The results are as shown in Figure 3-28. The dimensionless experimental aerodynamic admittance was estimated using Equation [3-13] and the theoretical aerodynamic admittance function estimated using Equation [3-14] are as shown in the

Figure 3-28. Both the background and the resonant response (at 2-4 Hz) components can be clearly observed from the experimental results [Figure 3-28].

The concept of aerodynamic admittance is used to filter the high frequency part of the wind spectrum [Baker 1995], as finite size gusts cannot load the canopy at the same time. Most previous studies [Gardiner 1992] only considered the background response component and this is approximated as 1 [Mayer 1987] and the resonant response component is generally considered to be insignificant. For large structures, the gusts cannot load the entire structure because of their lack of correlation, and the aerodynamic admittance tends towards zero at high frequencies and at low frequencies, and for small structures it tends towards 1.0 [Holmes 2001].

However, in this study from Figure 3-28, it is clear that the response to the wind load has a high correlation with the tree sapling natural frequency, this is understandable as the tree on the force balance was moving with wind. What is notable from the Figure 3-28 is that the aerodynamic admittance at low frequency is well below the theoretical value of 1.0. This may be due to a number of issues, but certainly one factor is that the effect of mechanical response (movement) of the tree has not been accounted for in the analysis; this is strictly only possible for rigid structures. To understand these low values of aerodynamic admittance at low frequency values, the normalized wind spectra are plotted against the reduced frequency ($\frac{fD}{\bar{v}}$) in Figure 3-29. As this is a normalized plot, the spectra for each wind speed should collapse onto a single curve. Whilst this is generally the case, few wind speeds show some variation (the wind spectra at 7.9 m/s) [Figure 3-29].

The inverse wave length of gust is $\frac{f}{\bar{v}}$. It is shown in Figure 3-29, that $\frac{fD}{\bar{v}}$ is varying from 0.01 to 10, with wind speeds varying from 3.6 m/s to 10.3 m/s. Hence the, gust wave lengths are of the same order as the size of the tree structure. Typically model scales in the wind tunnel are 1:200 to 500. In this case the model tree is 1:20 or 1:10. Hence the gust sizes are relatively small compared to the size of the tree and will locally excite the structure rather than the whole tree. This may also have some effect on lowering the values of aerodynamic admittance at low frequencies. Davenport [1964] also noted that if $\frac{fD}{\bar{v}}$ is in

the range of 0.01 to 10, the nature of aerodynamic admittance is uncertain. Additionally, the porous structure of the tree sapling will cause bleeding flow and broadening of the bandwidth. Hence a modified aerodynamic admittance factor is considered in this study. This aspect is further discussed in Chapter 4 with respect to Jensen number.

From Figure 3-28, the aerodynamic admittance at low frequencies (< 1.0 Hz) varied from 0.64 to 0.686 with increase in wind speed from 3.6 m/s to 10.3 m/s, for the simplicity of calculations, the aerodynamic admittance factor is approximated to be 0.66.

The base bending moment response spectra, in terms of wind spectra and the admittance function is given in Equation [3-15] and the mechanical admittance in terms of wind spectra and tree response is given by Equation [3-16] [Baker 1995] below:

$$S_B(f) = X^2 \mathrm{H}(f)^2 S_F(f) \qquad [3\text{-}15]$$

$$\mathrm{H}(f)^2 = \frac{1}{[\rho A C_d \bar{v} X]^2} \frac{S_B(f)}{S_v(f)} \frac{1}{\Gamma(f)^2} \qquad [3\text{-}16]$$

The theoretical mechanical admittance function is given by Equation [3-17] [Clough and Penzien 1993]:

$$H(f)^2 = \frac{1}{\left[\left(1 - \left({}^{f}/_{f_n}\right)^2\right)^2 + \left(2\zeta\, {}^{f}/_{f_n}\right)^2\right]} \qquad [3\text{-}17]$$

The transfer function Equation [3-17] is a measure of transferred wind energy to the tree response, even though Equation [3-17] is the theoretical mechanical admittance of a single-degree-of-freedom dynamic system [Holmes 2001] it has been approximated by many researchers [e.g. Holbo et al., 1980; Mayer, 1987, Mayer et al. 1989; Peltola, 1996; Schindler, 2008] that the tree possesses linear elastic material properties. This means the internal response load to the applied external load depends only on the natural frequency and damping, instead of mass or stiffness of the structure individually. The theoretical transfer function, Equation [3-17] with 2.9 Hz natural frequency and varying damping is plotted as shown in Figure 3-30, to better understand the energy transfer at various frequencies. It is clear how the energy is transferred at each frequency with increasing

damping. At the natural frequency of the structure and low damping, the resonance condition can be clearly observed in Figure 3-30 (between 2 and 4 Hz).

Figure 3-31 shows the normalized mechanical admittance of the T1 windward base bending moment response with increase in wind speed. The foundation in this case acts as a fixed base, with the stem base on the force balance. Linear increase in damping with increase in wind speed can be seen [Figure 3-31] with changes in the resonant peak frequency and the width of the peak. As other studies have considered the soil root plate to be fixed for dynamic analysis, it is interesting to see steady change in damping with increase in wind speed. This trend of damping change was only observed in this case (with the fixed base) throughout this study.

The estimated mechanical admittance using the experimental results from Equation [3-16] are compared with the theoretical admittance [3-17] as shown in Figure 3-32, for the T1 root system in sand and stem base in the force balance and the tree T2 with root system in both sand and clay at the same wind speed. Both T1 and T2 showed higher damping in the case of the sand (0.247 and 0.113 respectively) compared to the force balance (0.195) and clay (0.094) base. As clay and the force balance mimic more of a fixed base condition, it is clear that the damping is high in the case of a flexible root base. T1 with a symmetrical root system showed higher damping compared to T2 with an asymmetrical root.

In an effort to quantify the role of the soil and the root plate anchorage on tree response, the stem response of T1 in the sand and on the force balance, and the stem response of T2 in sand and clay are compared. The sway of the tree in the sand box and on the force balance is investigated to understand the influence of root plate on tree dynamics. The stem response of T1 and T2 in sand is investigated to understand the influence of root architecture on tree dynamics and T2 in sand and clay is investigated to understand the influence of soil type on tree dynamics.

In Figures 3-33, 3-34, and 3-35, mechanical admittance of the stem base response of tree saplings T1, and T2 on sand and clay were plotted with increase in wind speeds. The mechanical admittance shows the tree response to different wind frequencies. From the breadth of the resonance peak, damping can also be quantified [Figure 3-30]. Figure 3-33

shows the mechanical admittance of the T1 lower stem windward response up to the failure wind speed (T1 failed at 6.9 m/s wind speed). The breadth of the resonant peak increased with increase in wind speed and decreased before the failure wind speed reached. A similar trend in damping variation can also be observed from the damping estimates of T1 presented in Figure 3-19. Complete reduction in energy at all frequencies and high damping at resonant peak can also be observed at 6.9 m/s wind speed.

Figures 3-34 and 3-35 show the mechanical admittance of T2, lower stem lateral response with increase in wind speed in sand and clay respectively. The T2 response in clay show a general trend of increase in damping with increase in wind speed. A similar trend in damping variation can also be observed from the damping calculations in Section 3.5.3 of this chapter and Figure 3-20. For the case of sand, an initial increase and decrease in damping was observed from the damping estimates and the admittance function in Figure 3-35.

The methodology used to estimate the mechanical admittance of the roots was:

- The ratio of base bending moment to the root bending moment response with increase in wind speed was estimated for each case.

- The dimensionless mechanical admittance function of the root, $H_R(f)^2$ is taken as:

$$\mathrm{H}_R(f)^2 = \frac{1}{[\rho A C_d \bar{v} X (RAF)]^2} \frac{S_{RB}(f)}{S_v(f)} \frac{1}{\Gamma(f)^2} \qquad [3\text{-}18]$$

- The ratio of base bending moment to the root bending moment (1/RAF) is factored, so that the admittance amplitude of the dimensionless mechanical admittance function of root is close to 1 at zero frequency.

- The bending moment response factor (the ratio of stem base bending moment response in windward direction to the respective root bending moment response at each wind speed, 1/RAF)

The root bending moment in the case of the symmetric and asymmetric root systems with increase in wind speed is estimated and compared from Figures 3-36 and 3-37. The bending

moment response factor of the T1 root system in sand was much lower compared to the T2 response factor in sand, hence the root architecture made significant differences in root response to wind loading and consequently the tree stability. For this case not just root architecture [Figures 3-4 and 3-5] but also the tree biomass changes [Table 3-1] of T1 and T2 need to be considered to understand the root response and tree stability variations.

In Figure 3-38, significant amounts (almost 2/3) of the energy was damped before it was transferred to the root plate in the case of clay. The root response for the similar base bending moment response of the tree indicates the effect of soil on tree stability.

Root bending moment response factor of T2 in both sand and clay are presented in Figure 3-39. More than a 50% lower response was observed in clay; it is important to note that in the case of clay, lower response meant lower energy transfer from stem to roots (energy damped [Figure 3-38]), which made the structure (T2 on clay) more stable. In the case of the T1 and T2 root architecture comparison, the root did not respond to the load at the stem base (did not transfer the energy to the ground) [Figures 3-36 and 3-39], which made the tree (T1) fail.

- The results of root admittance of T1 on sand and T2 on sand and clay are as shown in Figures 3-39 and 3-40. The mechanical admittance of the roots shows the transfer of energy to the roots at various frequencies. At the lowest frequencies, the gain is less than 1 indicating that the wind load at low frequencies did not induce any inertial effects. At the tree resonance frequencies, the gain clearly indicates the change in damping in each case with increase in wind speeds as estimated in Section 3.5.3 of this chapter. At higher frequencies, higher energy can be observed in all cases, as these are close to the natural frequencies of the roots [Tables 3-4 and 3-5]; however, this is not the case for the stem response [Figures 3-33, 3-34, and 3-35].

3.6 Discussion

In this study the wind field was analyzed with corresponding motions of the tree sapling components in cohesive and non-cohesive (frictional) soil media with increasing wind speeds. As the tree response to wind loading is an extremely complicated process, the

response characteristics were studied using the three most popular dynamic analyses in windthrow research.

- The tracked sway motion was used to identify the direction of sway with wind and also the change in swaying pattern with varying root architecture, root location in the root plate, soil medium and wind speed.

- Change in dynamic properties in every tested scenario were estimated to assess the effect of the soil and root architecture on the tree dynamic response.

- The admittance spectra were derived to improve understanding of energy transfer from wind to tree to roots and soil.

SWAY

To improve the understanding of the sway response, the response data was plotted using a joint probability density function and the data was statistically analyzed, to make the complex two dimensional tree sway response more understandable.

- The dynamic tree sway appears to be greatly influenced by the root soil support system. The stem response in frictional soil (sand) was more comparable with the wind direction making it more susceptible to failure.

- In the case of the highly stable root soil system (T2 on clay case and T1 on the force balance), the stem response seems to be distributing energy into the lateral response too, helping the tree response with lower stem deflection and higher mass damping and causing much lower energy to transfer to the root plate. With increase in tree root-soil plate stability (on cohesive soil) or the fixed base system (on the force balance), windward and lateral responses also seem more closely correlated.

- The elliptical sway shape of T2 was more elongated because of the root asymmetry compared to T1 with a symmetric root structure. A similar elliptical tree sway response was also observed by Mayer [1987] and Sellier et al. [2008], suggesting that the tree saplings in the experimental setup were behaving more like real trees in the field.

- Root response in sand and on the windward side showed higher responses with increase in wind load. The root response in all of the observed scenarios seems to be more symmetric and highly concentrated meaning the roots stayed in one position for most of the time and moved in a more symmetric pattern.

- As stated by Mayer et al. [1989] trees show three possible types of sway:

i) The tree does not sway much (damped swaying); the tree saplings at low wind speeds and the roots showed this type of sway.

ii) Tree sway enhanced by the sway in the direction of wind load, increasing the deflection considerably with comparatively small wind load increases. This type of sway was demonstrated by the tree sapling in sand.

iii) Tree sway against the direction of the applied dynamic wind load, damping the sway initially and eventually swaying in the direction of the wind load at higher wind speeds. The tree sapling in clay showed similar responses. However, the tree was not tested to failure, so examination of what happens with increase in wind load to failure was not possible.

This indicates that the testing methodology and the analysis techniques we used in this chapter could be used in further studies to investigate tree dynamics under different scenarios, as the sapling response could potentially simulate scaled responses of mature field trees.

DYNAMIC PROPERTIES

The three methods used in this chapter, to estimate the structural damping [Table 3-4] showed that the consistency of damping estimates is highly unlikely, as the fundamental characteristics of each method are very different. To estimate the damping of a structure like a tree with multiple degrees of freedom and the various assumptions made for damping calculations, we need to be very cautious. All three methods showed low damping at the stem base compared to the upper stem with the crown. Autocorrelation showed mid-range

estimates within all of the results and the Hilbert transformation method estimates were on the lower side and the half power band width method estimates were on the higher side.

The auto correlation methodology could be very useful to estimate the damping at various wind speeds. Even though in windthrow research viscous damping is assumed [Jonsson et al. 2007], it needs to be noted that it was only tested with structural damping (from free decay tests). The results from this wind tunnel study shows damping due to aerodynamic load is not a linear function of velocity; similar ideas were also proposed by Moore and Maguire [2004].

The structural and aerodynamic damping estimates in this chapter indicate a twice to thrice variation in aerodynamic damping for the stem with increase in wind speeds in comparison to structural damping. For the roots this was 3 to 4 times the root structural damping. Damping is high for larger trees and also aerodynamic damping varies with wind speed [Milne 1991] and structural damping varies with sway amplitude [Jonsson et al. 2007]. Hence further tests need to be conducted to test aerodynamic damping and corresponding wind load through long-term monitoring. In this chapter damping estimates were only conducted for the first mode of vibration. Further calculations need to be conducted for the second and third modes of vibration; also tests need to be conducted with different soils and the soil water contents to improve our understanding of tree-root soil dynamics.

SPECTRAL ANALYSIS

The spectral analysis helped to identify the tree stem and root component natural frequency and the quantitative energy transferred to the above ground tree structure from the wind field and redistributed to the below ground root structure. Through root response spectral analysis, the energy transfer from wind to tree to roots can be identified. The entire tree and root structure showed resonant response at tree natural frequency. Significant variation in energy transfer and the damping can be clearly observed with change in soil conditions.

The transfer functions of the stem were calculated by dividing the tree base bending movement by the wind speed power spectral density and the bending moment response spectra was also divided by the mean base bending moment at the corresponding wind

speed as part of the non-dimensionalization process. The admittance functions presented [Figures 3-33, 3-34, and 3-35], show the energy transferred to the tree at varying wind speeds and different frequencies. The mechanical admittance functions were very similar to the transfer functions presented by Holbo et al. [1980], Baker [1995] and Hassinen et al. [1998], showing peaks only at resonant frequency. This indicates that the tree sapling in this experimental study behaved similarly to a forest tree (lightly damped harmonic oscillator) [Gardiner 1995].

Root admittance showed high energy peaks at the tree natural frequency and also near the root natural frequencies. Root damping varied with root location and also with wind speed. This is another area that needs to be further explored with coherence and damping estimates at root natural frequency. This will enable more understanding of the correlation and load transfer between the above and below ground tree structure.

3.7 Conclusions

In this study, the tree sapling sway with increase in wind speed in both sand and clay is examined in a new way. Normalized joint probability density distribution along with statistical analysis of the sway response is presented. It not only quantified the orthogonal responses (windward and lateral response) of the trees, it has provided useful insights into the change is tree response with increase in wind loading and change of soil medium.

In this study for the first-time, dynamic properties (natural frequency and damping) of the tree saplings with increase in wind speed is examined. The Autocorrelation method is used to estimate damping at each wind speed. Using structural damping estimates, aerodynamic damping of the tree and root system with increase in wind speed is also examined for the first time. This showed significant variation with change soil medium, but did not show proportional increase in damping with increase in wind load.

In this study, along with stem base, root mechanical and aerodynamic admittances with increase in wind speed and change in soil conditions are calculated for the first time. Once

the established relation in this study is verified, this methodology would help to estimate the energy transfer from wind to tree to root system under various conditions.

3.8 References

ASTM D2395-07a, Standard Test Methods for Specific Gravity of Wood and Wood-Based Materials, *ASTM International*, West Conshohocken, PA, 2007, www.astm.org

ASTM D6913-04, Standard Test Methods for Particle-Size Distribution (Gradation) of Soils Using Sieve Analysis, *ASTM International*, West Conshohocken, PA, 2009, www.astm.org

Baker, C. J. (1995). The Development of a Theoretical Model for the Windthrow of Plants. *Journal of Theoretical Biology*, 175, 355–372. http://doi.org/10.1006/jtbi.1995.0147

Baker, C. J. (1997). Measurements of the natural frequencies of trees. *Journal of Experimental Botany*, 48(310), 1125–1132.

Baldocchi, D. (2012). Lecture 19, Wind and Turbulence, Part 4, *Surface Boundary Layer, Theory and Principles*, 1–24.

Bischetti, G. B., Chiaradia, E. A., Simonato, T., Speziali, B., Vitali, B., Vullo, P., & Zocco, A. (2005). Root strength and root area ratio of forest species in Lombardy, 11–22. https://doi.org/10.1007/s11104-005-0605-4.

Bolton, M.D. (1986) The strength and dilatancy of sands. *Geotechnique*, 36, No. 1, 65-78.

Cartwright, D.E. and Longuet-Higgins, M.S. (1956) The Statistical Distribution of the Maxima of a Random Function. *Proceedings of the Royal Society of London*, Series A, 237, 212-232.

Castro-García, S., Blanco-Roldán, G. L., Gil-Ribes, J. a., & Agüera-Vega, J. (2008). Dynamic analysis of olive trees in intensive orchards under forced vibration. *Trees - Structure and Function*, 22(6), 795–802. http://doi.org/10.1007/s00468-008-0240-9

Ciftci, C., Brena, S. F., Kane, B., & Arwade, S. R. (2013). The effect of crown architecture on dynamic amplification factor of an open-grown sugar maple (Acer saccharum L.). *Trees - Structure and Function*, 27, 1175–1189. http://doi.org/10.1007/s00468-013-0867-z

Clough, R. W., and Penzien, J. (1993). *Dynamics of structures*, McGraw-Hill, New York, NY, USA.

Davenport, A. G. (1964). The buffeting of large superficial structures by atmospheric turbulence. *Annals of the New York Academy of Sciences*, 116(1), 135–160.

Deljoui, P. (2012). *Upheaval Buckling of Offshore Pipelines in Homogeneous and Layered Soils*. PhD. Thesis, University of Western Ontario, Canada.

Dirlik, T. (1985). *Application of Computers in Fatigue Analysis*, 234. Retrieved from http://webcat.warwick.ac.uk/record=b1445503~S9

Feng, T. (2000) Fall-cone penetration and water content relationship of clays. *Géotechnique*, 50(2): 181-187.

Flesch, T. K., & Wilson, J. D. (1999). *Wind and remnant tree sway in forest cutblocks. II. Relating measured tree sway to wind statistics*, 93, 243–258.

Fourcaud, D. S. T., Sellier, D., & Fourcaud, T. (2009). Crown Structure and Wood Properties: Influence on Tree Sway and Response to High Winds. *American Journal of Botany*, 96(5), 1–12. http://doi.org/10.3732/ajb.0800226

Gardiner, B. a, Stacey, G. R., Belcher, R. E., & Wood, C. J. (1997). Field and wind tunnel assessments of the implications of respacing and thinning for tree stability. *Forestry*, 70(3), 233–252. http://doi.org/10.1093/forestry/70.3.233

Gardiner, B.A. (1989). *Mechanical characteristics of Sitka spruce*. Forestry Commission Occasional Paper No. 24, Forestry Commission, Edinburgh.

Gardiner, B. A. (1992). Mathematical modelling of the static and dynamic characteristics of plantation trees. In: Franke J, Roeder A (eds) *Mathematical modelling of forest ecosystems*. Sauerlander,Frankfurt/Main, pp 40–61.

Gardiner, B. A. (1995). The interaction of wind and tree movement in forest canopies. In M. P. Coutts and J. Grace [eds.], Wind and trees, 41–59, Cambridge University Press, Cambridge, UK.

Hassinen, A., Lemettinen, M., Peltola, H., & Gardiner, B. (1998). A prism-based system for monitoring the swaying of trees under wind loading, *Agricultural & Forest Meteorology* 90: 187–194.

Henry Liu (1991). *Wind Engineering: A Handbook for Structural Engineers*. Prentice Hall, Columbia.

Hoag, D. L., Fridley, R. B., & Hutchinson, J. R. (1971). Experimental measurement of internal and external damping properties of tree limbs. *Transactions of the American Society of Agricultural Engineers*.

Holbo, H. R., Corbett, T. C., & Horton, P. J. (1980). Aeromechanical behavior of selected Douglas-fir. *Agricultural Meteorology*, 21(2), 81–91. http://doi.org/10.1016/0002-1571(80)90056-4.

Holmes, J. D. (2001). Wind Loading of Structures. Spon Press, New York

James, K. (2003). Dynamic Loading of Trees. *Journal of Arboriculture*, 29(3), 1–7. http://www.treelink.org.

James, K. R., & Kane, B. (2008). Precision digital instruments to measure dynamic wind loads on trees during storms, *Agric. Meteorol.*, 148, 1055–1061. http://doi.org/10.1016/j.agrformet.2008.02.003

James, K. R., Haritos, N., & Ades, P. K. (2006). Mechanical stability of trees under dynamic loads. *American Journal of Botany*, 93(10), 1522–1530. http://doi.org/10.3732/ajb.93.10.1522

James, K., & Haritos, N. (2010). The Role of Branches in the Dynamic Response Characteristics of Trees. *Australian Earthquake Engineering Society 2010 Conference*, The Institution of Engineers, Australia.

James, K., Hallam, C., & Spencer, C. (2013). Measuring tilt of tree structural root zones under static and wind loading. *Agricultural and Forest Meteorology*, 168, 160–167. http://doi.org/10.1016/j.agrformet.2012.09.009

Jonsson, M. J., Foetzki, a., Kalberer, M., Lundström, T., Ammann, W., & Stöckli, V. (2007). Natural frequencies and damping ratios of Norway spruce (Picea abies (L.) Karst) growing on subalpine forested slopes. *Trees - Structure and Function*, 21(5), 541–548. http://doi.org/10.1007/s00468-007-0147-x

Kaimal, J. C., Wyngaard, J. C., Izumi, Y. and Cote, O. R. (1972). "Spectral characteristics of surface-layer turbulence." *Journal of Royal Meteorological Society*, 98, 563-589.

Kane, B., & James, K. R. (2011). Dynamic properties of open-grown deciduous trees. *Canadian Journal of Forest Research*, 41(2), 321–330. http://doi.org/10.1139/X10-211

Kane, B., Modarres-Sadeghi, Y., James, K. R., & Reiland, M. (2014). Effects of crown structure on the sway characteristics of large decurrent trees. *Trees - Structure and Function*, 28, 151–159. http://doi.org/10.1007/s00468-013-0938-1

Kellomäki, S. (1999). Calculation of Foliage Mass and Foliage Area, European Commission: *Biogenic VOC emissions and photochemistry in the boreal regions of Europe – Biphorep*, Edited by Tuomas Laurila and Virpi Lindfors, 113–126.

Makarova, O. V., Cofie, P., & Koolen, A. J. (1998). Axial stress-strain relationships of fine roots of Beech and Larch in loading to failure and in cyclic loading. *Soil and Tillage Research*, *45*, 175–187. https://doi.org/10.1016/S0933-3630(97)00017-2

Mayer, H. (1987). Wind-induced tree sways. *Trees*, 1, 195–206. http://doi.org/10.1007/BF01816816

Mayer, H., Raupach, M. R., Kohsiek, W., Gardiner, B., Clarke, J. a., Amtmann, R., Milne, R. (1989). Windthrow [and Discussion]. *Philosophical Transactions of the Royal Society B: Biological Sciences*, 324, 267–281. http://doi.org/10.1098/rstb.1989.0048

Mayhead, G. J. (1973a). Sway periods of forest trees. *Scottish Forestry*, 27, 19–23.

Mayhead, G. J. (1973b). Some drag coefficients for british forest trees derived from wind tunnel studies. *Agricultural Meteorology*, 12, 123–130. http://doi.org/10.1016/0002-1571(73)90013-7.

Mergen, F. (1954). Mechanical aspects of wind-breakage and wind firmness. *Journal of Forestry*, 52: 119-125.

Miller, L. A. (2005). Structural dynamics and resonance in plants with nonlinear stiffness. *Journal of Theoretical Biology*, 234, 511–524. http://doi.org/10.1016/j.jtbi.2004.12.004

Milne, R. (1991). Dynamics of swaying of Picea sitchensis. *Tree Physiology*, 9(11976), 383–99. Retrieved from http://www.ncbi.nlm.nih.gov/pubmed/14972849

Mitchell, J. K. (1976), *Fundamentals of Soil Behavior*, John Wiley and Sons, Inc., New York, N.Y.

Moore, J. R., & Maguire, D. A. (2004). Natural Sway Frequencies and Damping Ratios of Trees: Concepts, Review and Synthesis of Previous Studies. *Trees*, 18, 195–203. http://doi.org/10.1007/s00468-004-0387-y

Moore, J. R., & Maguire, D. A. (2005). Natural sway frequencies and damping ratios of trees: influence of crown structure, *Trees*, 19, 363–373. http://doi.org/10.1007/s00468-004-0387-y

Moore, J. R., & Maguire, D. A. (2008). Simulating the dynamic behavior of Douglas-fir trees under applied loads by the finite element method. *Tree Physiology*, 28(1), 75–83. http://doi.org/10.1093/treephys/28.1.75

Reubens B, Poesen J, Danjon F, Geudens G and Muys B (2007) The role of fine and coarse roots in shallow slope stability and soil erosion control with a focus on root system architecture: a review. Trees 21 (4):385-402. doi:10.1007/s00468-007-0132-4.

Ochi, M. K. (1990). *Applied probability and stochastic processes in engineering and physical sciences*. John Wiley and Sons, New York, USA.

Peltola, H. (1996). Swaying of trees in response to wind and thinning in a stand of scots pine. *Boundary Layer Meteorology*, Vol.77, 285–304.

Saunderson S. E. T., England A. H, Baker C. J. (1999) A dynamic model of the behaviour of Sitka Spruce in high winds. *Journal of Theoretical Biology*, 200:249–259.

Schindler, D. (2008). Responses of Scots pine trees to dynamic wind loading, *Agricultural and Forest Meteorology*, 148, 1733–1742. http://doi.org/10.1016/j.agrformet.2008.06.003

Schwarz, M., Cohen, D., & Or, D. (2010). Root-soil mechanical interactions during pullout and failure of root bundles. *Journal of Geophysical Research: Earth Surface*, *115*(4), 1–19. https://doi.org/10.1029/2009JF001603

Sellier, D., & Fourcaud, T. (2005). A mechanical analysis of the relationship between free oscillations of Pinus pinaster Ait. saplings and their aerial architecture. *Journal of Experimental Botany*, 56(416), 1563–1573. http://doi.org/10.1093/jxb/eri151

Sellier, D., & Fourcaud, T. (2009). Crown Structure and Wood Properties: Influence on Tree Sway and Response to High Winds. American Journal of Botany, 96(5), 1–12. https://doi.org/10.3732/ajb.0800226

Sellier, D., Brunet, Y., & Fourcaud, T. (2008). A numerical model of tree aerodynamic response to a turbulent airflow. *Forestry*, 81(3), 279–297. http://doi.org/10.1093/forestry/cpn024

Simiu, E. (1974). "Wind spectra and dynamic along wind response." *Journal of Structural Division*., ASCE, 100(9), 1897-1910

Skempton, A. W. (1954). The pore-pressure coefficient A and B. *Geotechnique*, 4, Issue 4, 143-147.

Spatz, H. C., & Bruechert, F. (2000). Basic biomechanics of self-supporting plants: Wind loads and gravitational loads on a Norway spruce tree. *Forest Ecology and Management*, 135, 33–44. http://doi.org/10.1016/S0378-1127(00)00296-6

Spatz, H. C., & Theckes, B. (2013). Oscillation damping in trees. *Plant Science*, 207, 66–71. http://doi.org/10.1016/j.plantsci.2013.02.015

Spatz, H. C., Brüchert, F., & Pfisterer, J. (2007). Multiple resonance damping or how do trees escape dangerously large oscillations? *American Journal of Botany*, 94(10), 1603–1611. http://doi.org/10.3732/ajb.94.10.1603

Stokes, A, & Mattheck, C. (1996). Variation of wood strength in tree roots. *Journal of Experimental Botany*, 47(298), 693–699. http://doi.org/10.1093/jxb/47.5.693

Sugden, M. J. (1962). Tree sway period—a possible new parameter for crown classification and stand competition. *Forest Chron*, 38(3), 336-344.

Vardanega, P. J., & Haigh, S. K. (2014). The undrained strength – liquidity index relationship. *Canadian Geotechnical Journal*, 5(19), 1073–1086. http://doi.org/10.1139/cgj-2013-0169

Varshoi, A., & Studies, P. (2012). *Response of Foundations to Random Cyclic Loads*. MESc. University of Western Ontario, Canada., 226.

Welch, P. D. (1967), The use of Fast Fourier Transform for the estimation of power spectra: A method based on time averaging over short, modified periodograms. *IEEE Transactions on Audio and Electroacoustics*, AU-15 (2): 70–73, doi:10.1109/TAU.1967.1161901.

Wood, D. (1990). *Soil behaviour and critical state soil mechanics*. http://doi.org/10.1016/0148-9062(92)90570-P

Wood, C.J. (1995) Understanding wind forces on trees. In Wind and Trees. M.P. Coutts and J. Grace (eds). Cambridge University Press, 133 – 64.

Zentar, R., Abriak, N., & Dubois, V. (2009). Applied Clay Science Effects of salts and organic matter on Atterberg limits of dredged marine sediments. *Applied Clay Science*, 42(3-4), 391–397. http://doi.org/10.1016/j.clay.2008.04.003

Table 3-1 Tree sapling biomass

Tree sapling biomass	T1	T2	Percentage difference in T1 biomass with respect to T2
Tree height (m)	1.4	1.2	14.3
Diameter at stump height (m)	0.044	0.048	9.1
Pruning height above ground level (m)	0.5	0.4	20
Total sapling weight (g)	1509.85	1599.68	5.95
Failure wind speed (m/s)	6.90	12.20	76.81
Trunk weight (g)	501.80	511.21	1.88
Branch mass (g)	725.60	640.00	-11.80
Crown frontal area (m^2)	0.35	0.31	-10.66
Root system weight (g)	275.20	435.96	58.42
Stump (g)	150.80	233.30	54.71
Roots without stump (g)	113.80	188.15	65.33

Table 3-2 Band width parameter of the applied wind speed and T2 stem and root response spectra at each wind speed increment (T2 Sand Test)

Wind speed (m/s)	Wind speed spectra band width parameter (ε)	Stem response spectra band width parameter (ε)	Root response spectra band width parameter (ε)
3.8	0.9991	0.9979	0.9625
6.0	0.9993	0.9984	0.9982
8.1	0.9973	0.9976	0.9992
10.2	0.9969	0.9956	0.9985
12.1	0.9943	0.9963	0.9997

Table 3-3 Band width parameter of the applied wind load and T2 stem and root response spectra with increase in wind speed (T2 Clay Test)

Wind speed (m/s)	Wind load spectra band width parameter (ε)	Stem response spectra band width parameter (ε)	Root response spectra band width parameter (ε)
3.8	0.9992	0.9987	0.9939
6.0	0.9993	0.9986	0.9985
8.1	0.9986	0.9969	0.9989
10.2	0.9969	0.9952	0.9985
12.1	0.9939	0.9958	0.9977

Table 3-4 Structural damping estimate of tree T1

Tree 1	Natural frequency	Damping Ratio		
		Method		
		Auto correlation	Hilbert	Half power band width
Upper stem windward	2.5	0.097	0.055	0.187
Lower stem windward	2.6	0.067	0.056	0.139
Upper stem lateral	2.4	0.089	0.045	0.153
Lower stem lateral	2.55	0.066	0.044	0.115

Table 3-5 Structural damping estimate of tree T2

Tree 2	Natural frequency	Damping Ratio		
		Method		
		Auto correlation	Hilbert	Half power band width
Upper stem windward	2.775	0.063	0.060	0.174
Lower stem windward	2.825	0.057	0.050	0.121
Upper stem lateral	2.750	0.053	0.035	0.166
Lower stem lateral	2.800	0.044	0.036	0.116
Root 1 top	61.230	0.066	0.049	0.041
Root 2 top	100.300	0.036	0.044	0.032
Root 3 top	59.950	0.051	0.086	0.007
Root 1 side	68.300	0.060	0.021	0.016
Root 2 side	60.020	0.030	0.044	0.007
Root 3 side	60.020	0.016	0.066	0.007

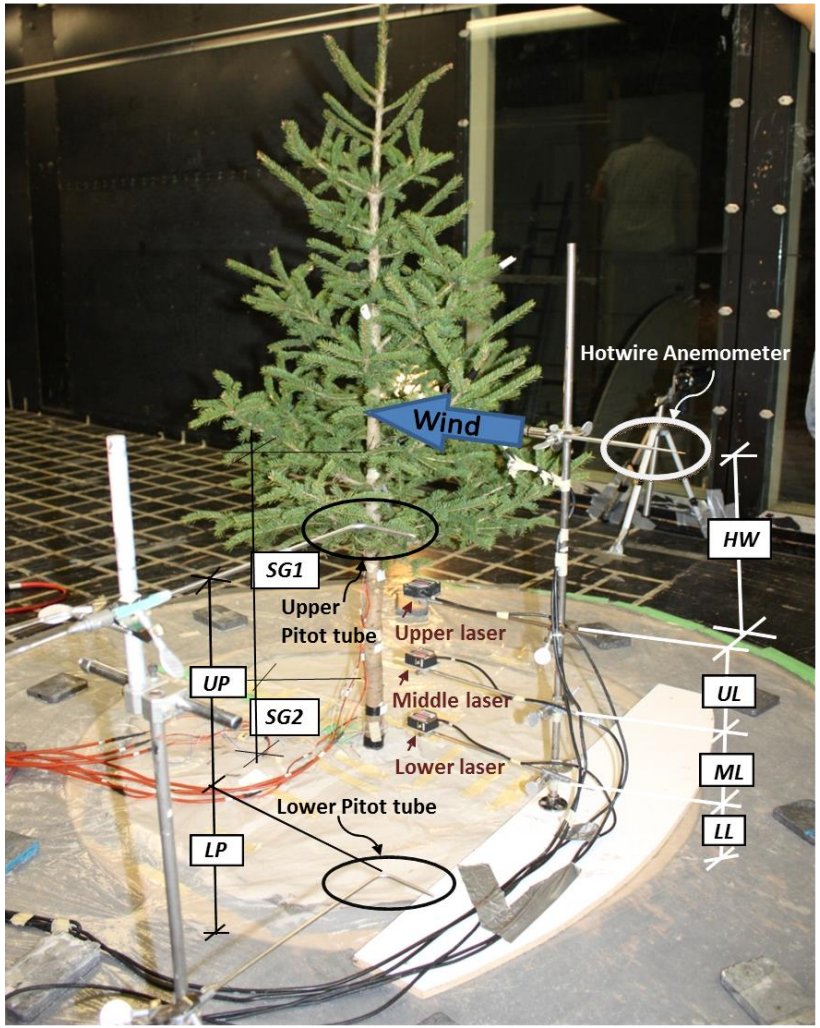

Dimension Description		Setup		
Description	Symbol	T1 in Sand	T2 in Sand	T2 in Clay
Height of hot wire anemometer above wind tunnel floor	HW	68.0	68.0	68.0
Height of upper pitot tube above lower pitot tube	UP	37.0	37.4	37.4
Height of lower pitot tube above tunnel floor	LP	30.8	31.3	31.25
Height of upper laser above middle laser	UL	11.25	12.1	10.0
Height of middle laser above lower laser	ML	12.5	12.8	10.0
Height of lower laser above wind tunnel floor	LL	11	16.5	27.25
Height of strain gauge attachment above lower strain gauge attachment	SG1	49.25	56.5	56.5
Height of lower strain gauge attachment above soil level	SG2	13.25	3.0	3.0

Note: All dimensions in cm

Figure 3-1 Tree sapling in the wind tunnel and instrument positions of the experimental setup

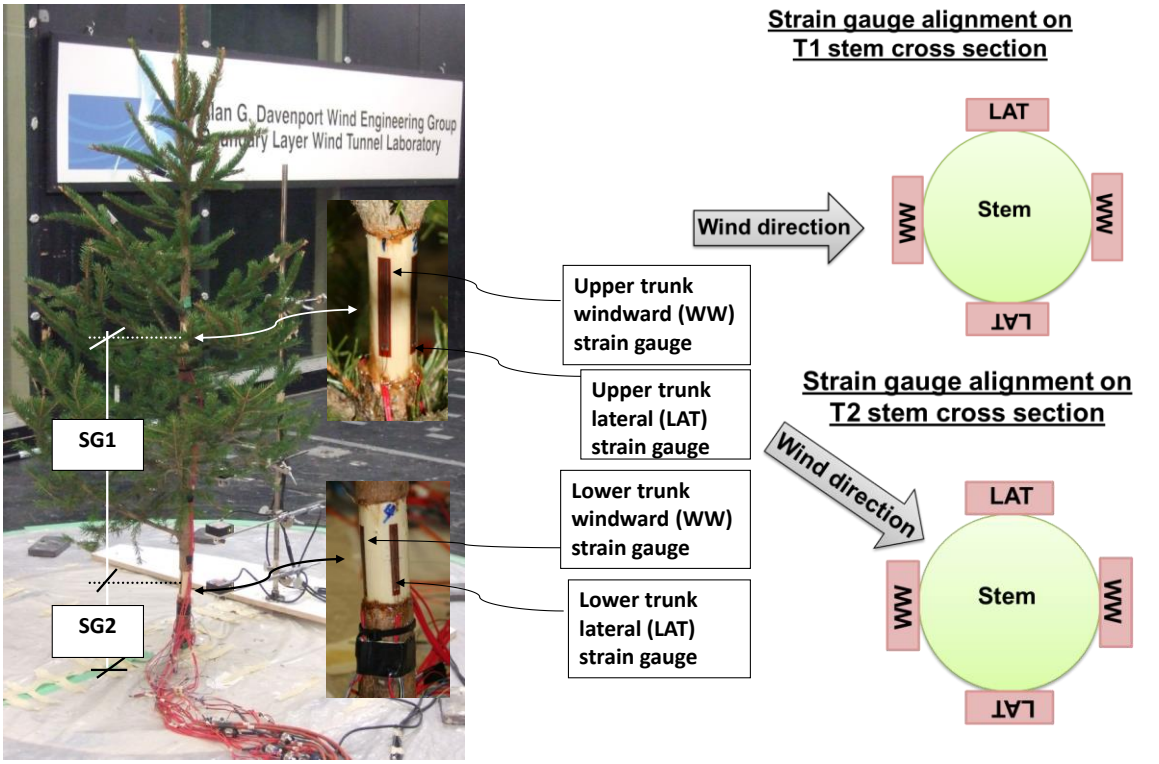

Figure 3-2 Strain gauge setup on the tree stem

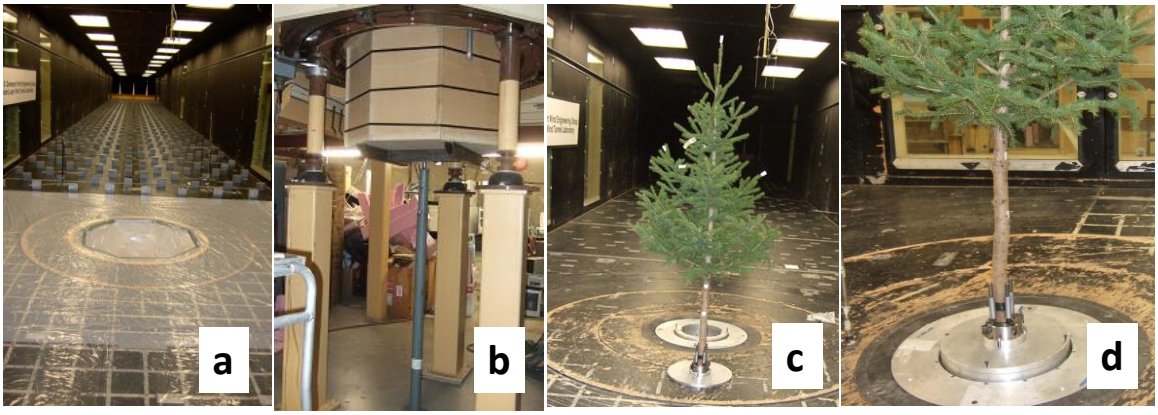

Figure 3-3 Wind tunnel floor with automated floor roughness elements and inserted planter box at the turn table location [a], planter box support system below the wind tunnel floor [b] and the tree sapling setup on the force balance on the wind tunnel turntable [c and d].

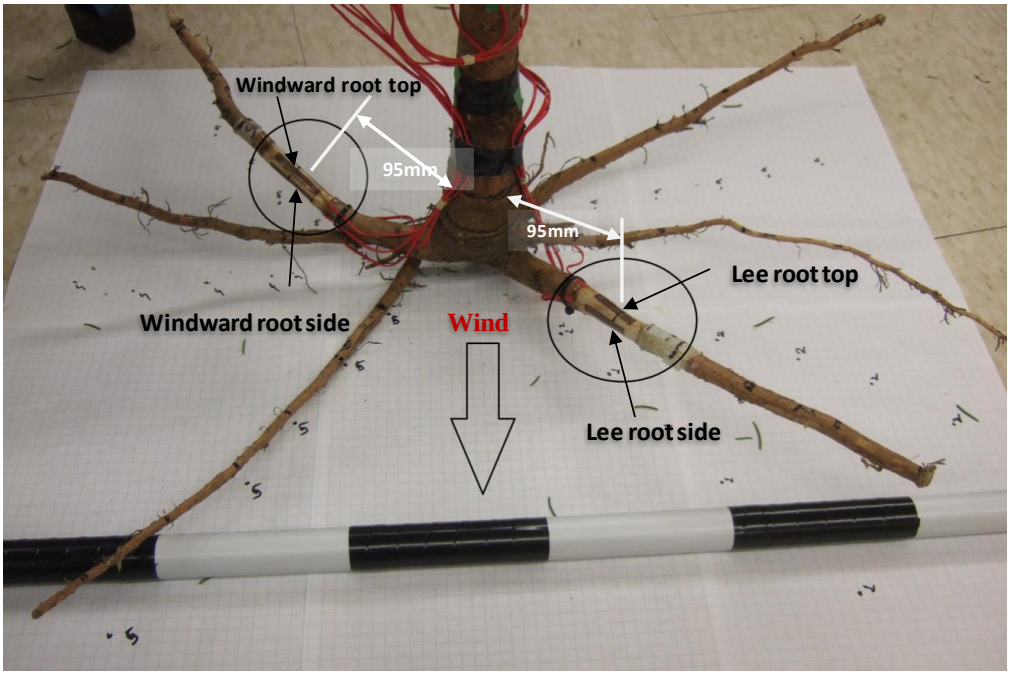

Figure 3-4 Tree T1 root system instrumentation

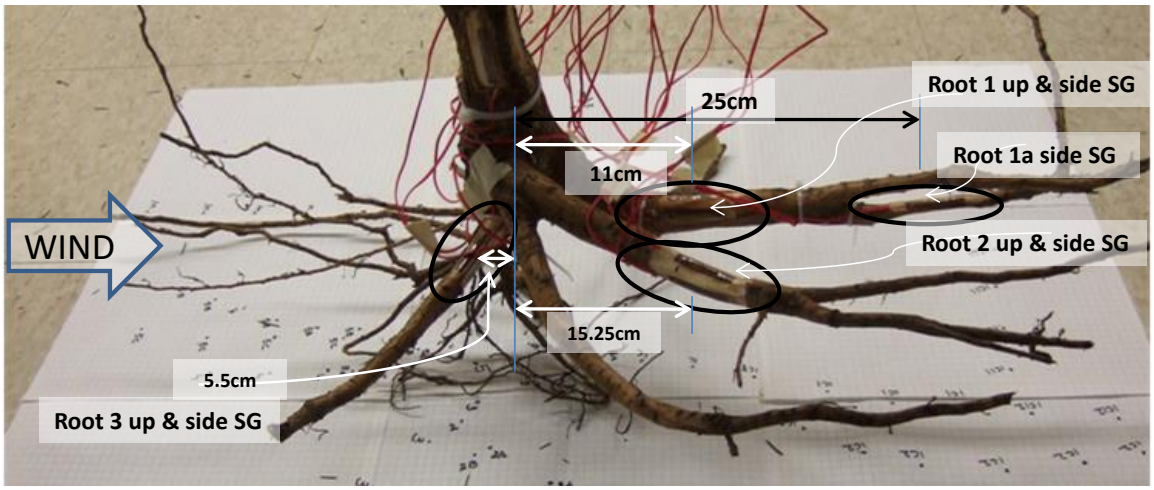

Figure 3-5 Tree T2 root system instrumentation

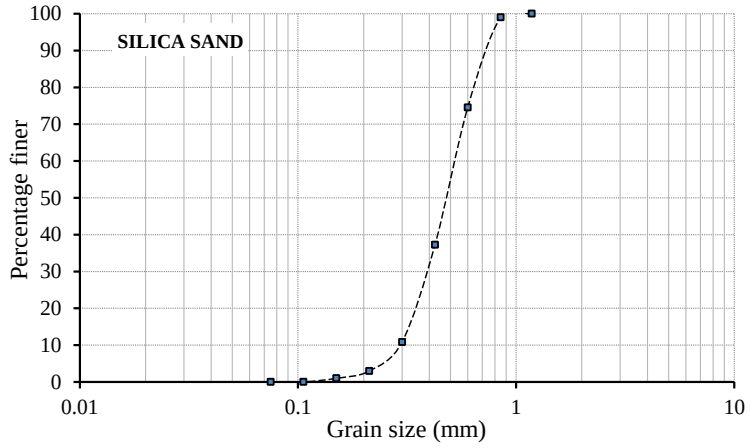

Mineral	Quartz
Solubility	Insoluble
Specific Gravity	2.65
Grain Shape	Sub-angular
Hardness	7 Mohs

Figure 3-6 Particle size distribution curve and characteristics of silica sand

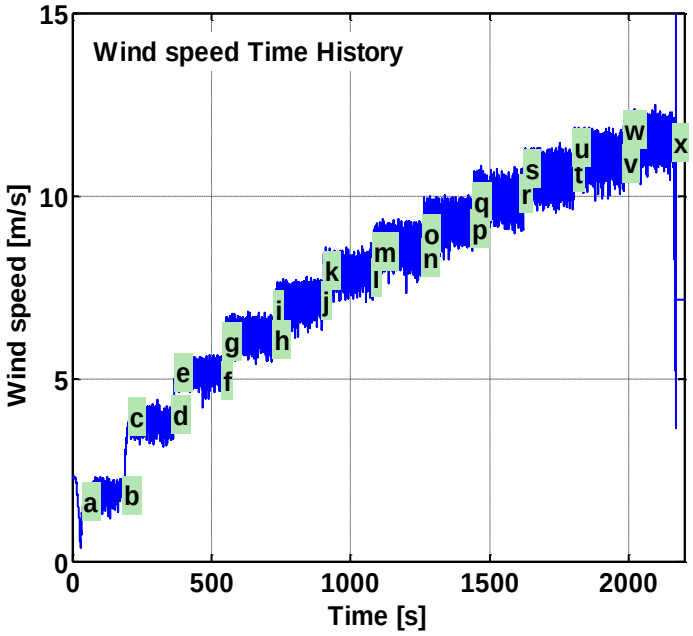

Wind tunnel speed increments [Volts]	Wind speed [m/s]	Variance	Skewness	Kurtosis
a-b(0.5)	0.74	0.00	-0.01	3.04
c-d(1.0)	1.48	0.01	-0.59	3.56
e-f(1.5)	2.63	0.02	-0.15	2.96
g-h(2.0)	3.71	0.04	1.26	8.38
i-j(2.5)	4.79	0.03	-0.26	2.77
k-l(3.0)	5.86	0.04	5.86	3.07
m-n(3.5)	6.93	0.05	6.93	2.71
o-p(4.0)	7.99	0.06	-0.40	3.24
q-r(4.5)	9.05	0.06	-0.21	2.88
s-t(5.0)	10.12	0.08	-0.42	3.37
u-v(5.5)	11.16	0.07	-0.34	3.18
w-x(6.0)	12.22	0.06	-0.39	3.16

Figure 3-7 Typical wind speed increments with time

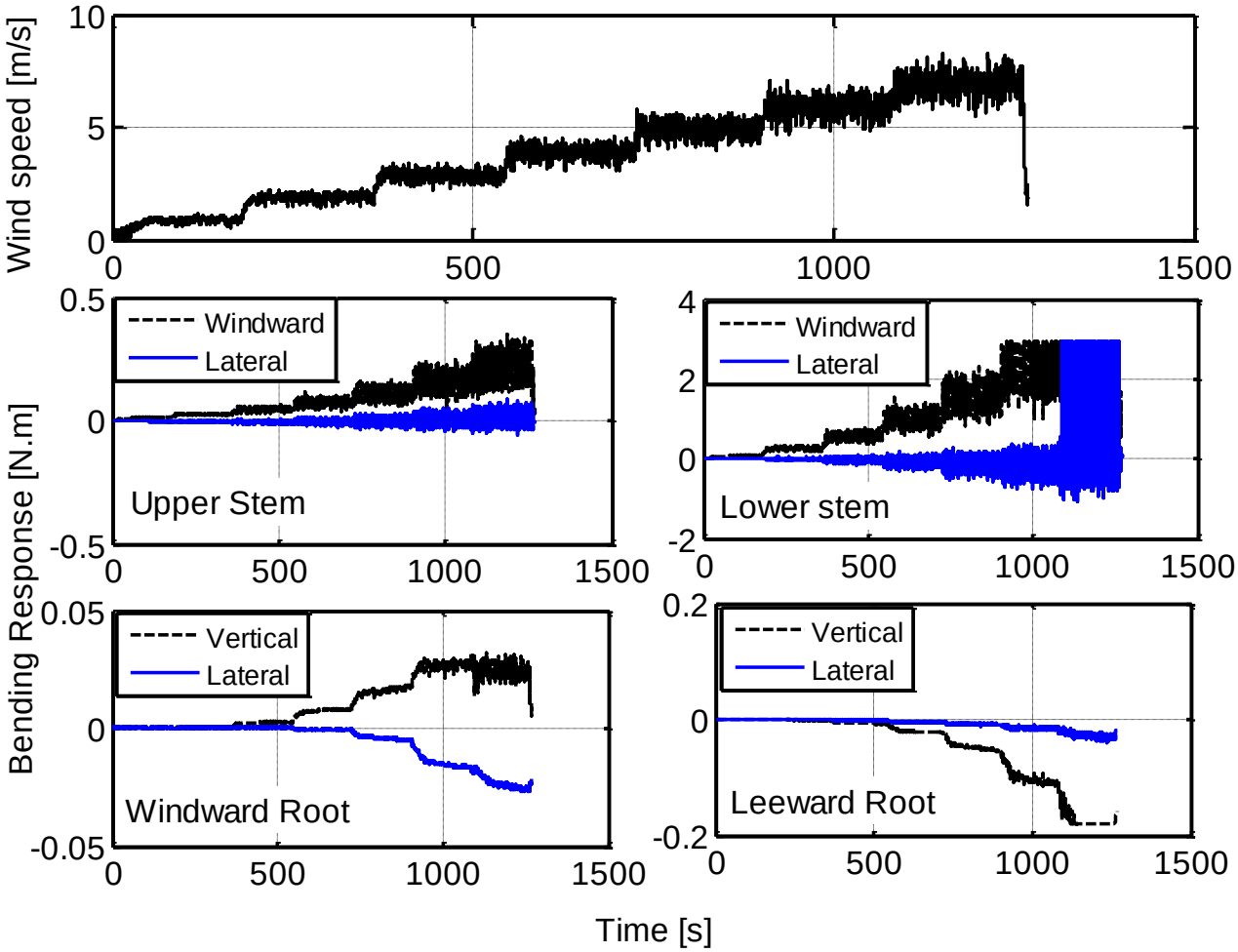

Figure 3-8 Tree sapling T1 response in sand

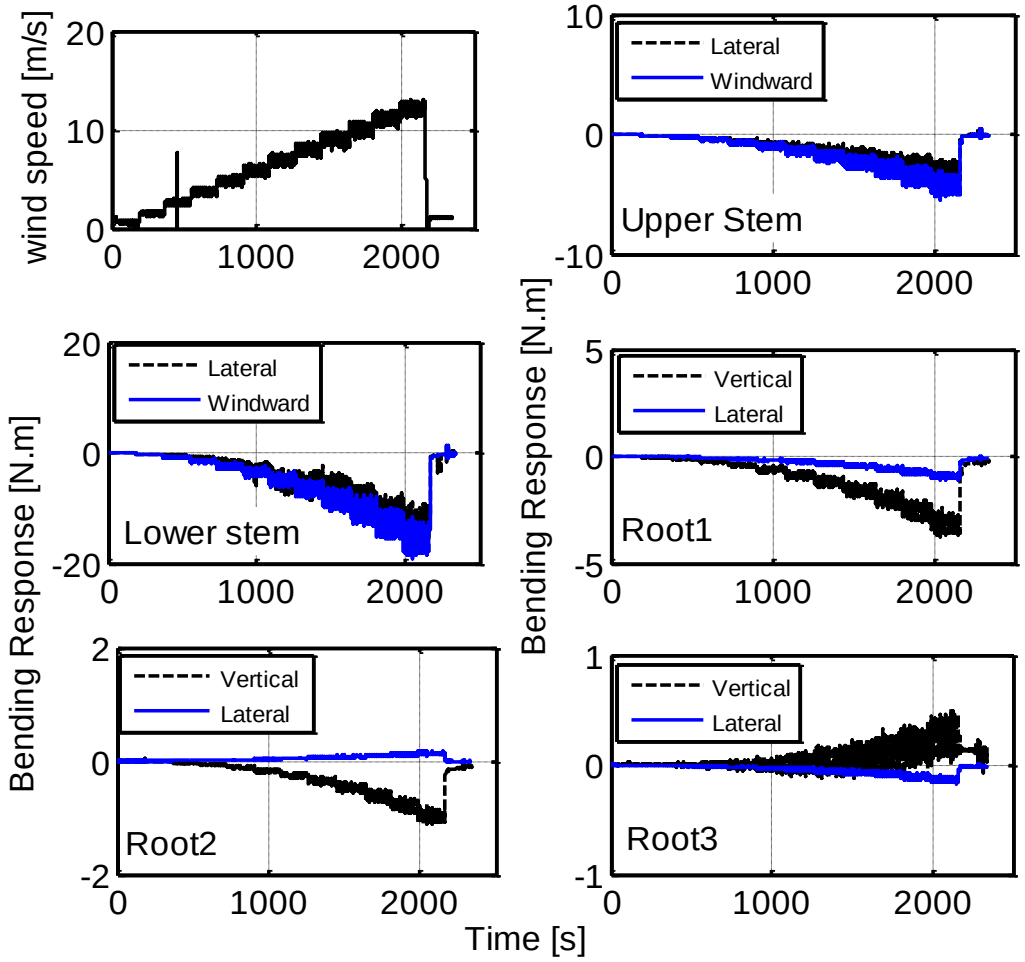

Figure 3-9 Tree sapling (T2) response in clay

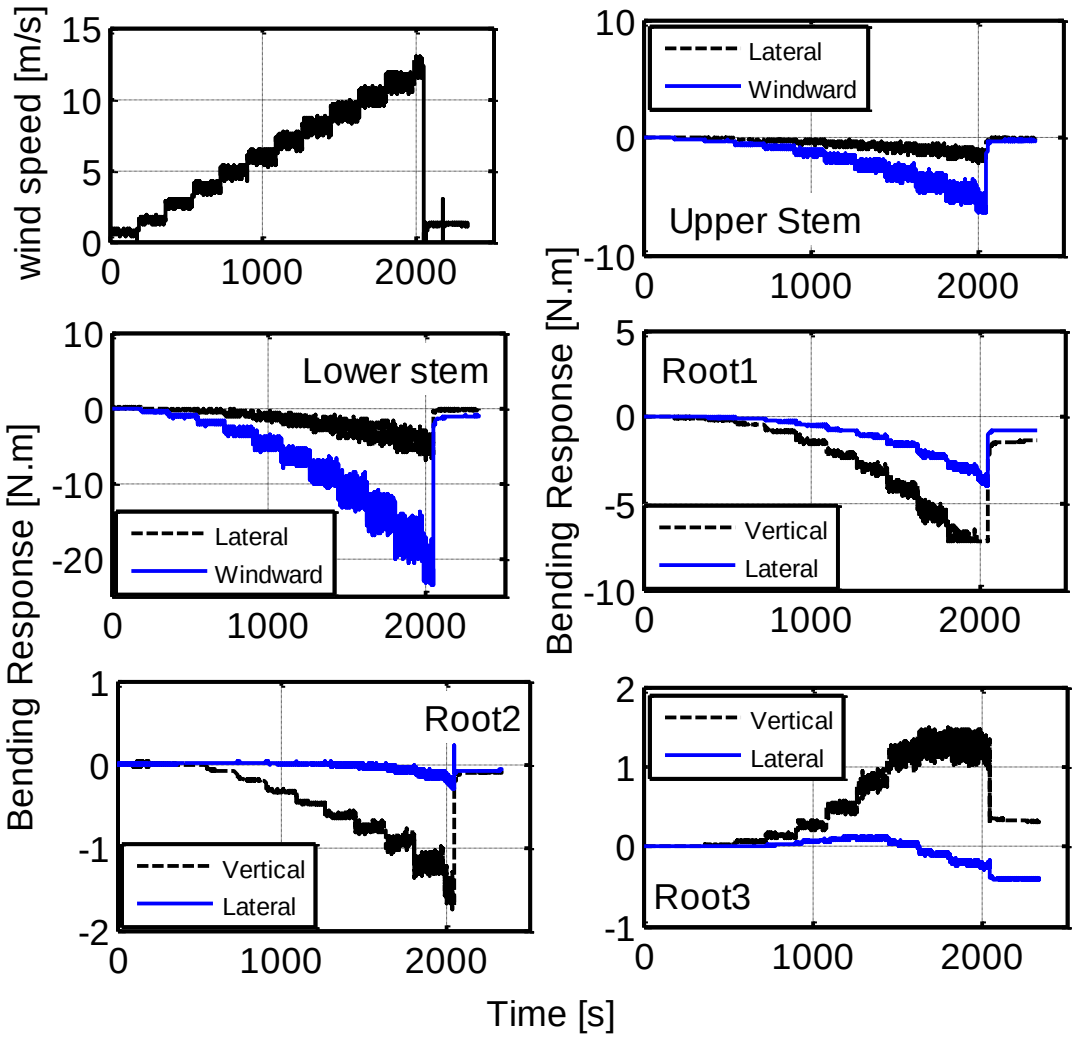

Figure 3-10 Tree sapling (T2) response in sand

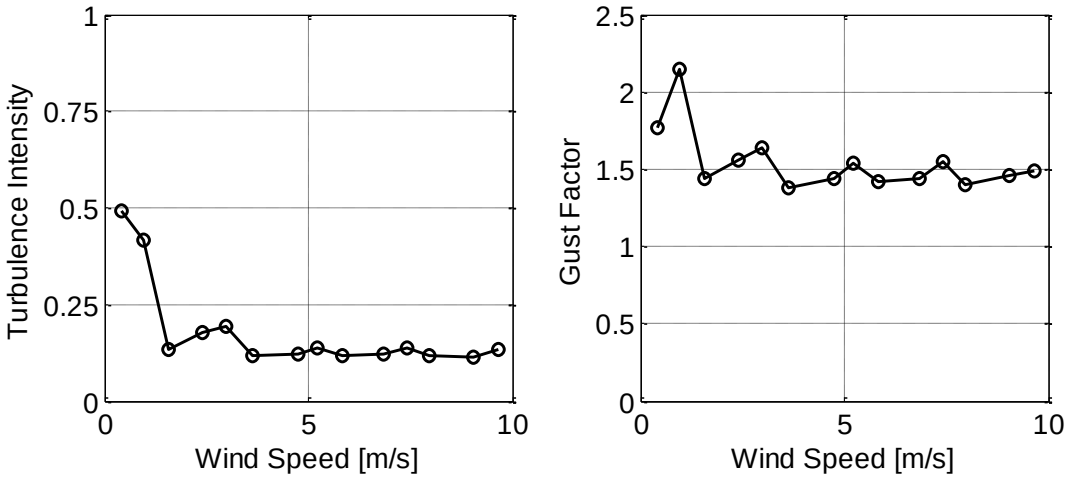

Figure 3-11 Turbulence intensity and gust factor of the applied wind field near the tree center of gravity

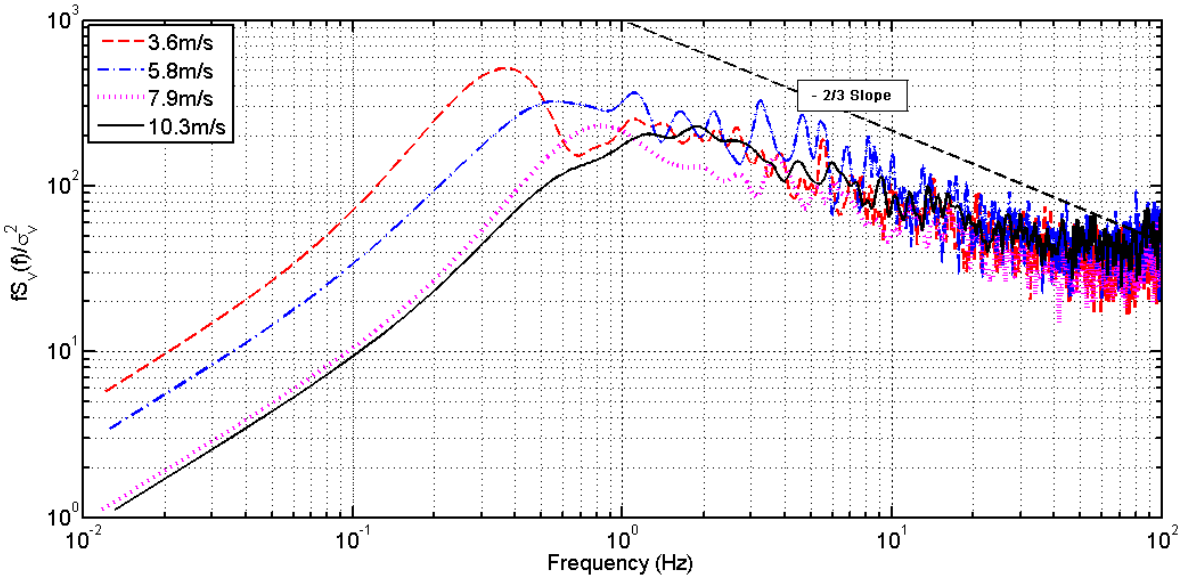

Figure 3-12 Wind speed power spectrum near the tree center of gravity

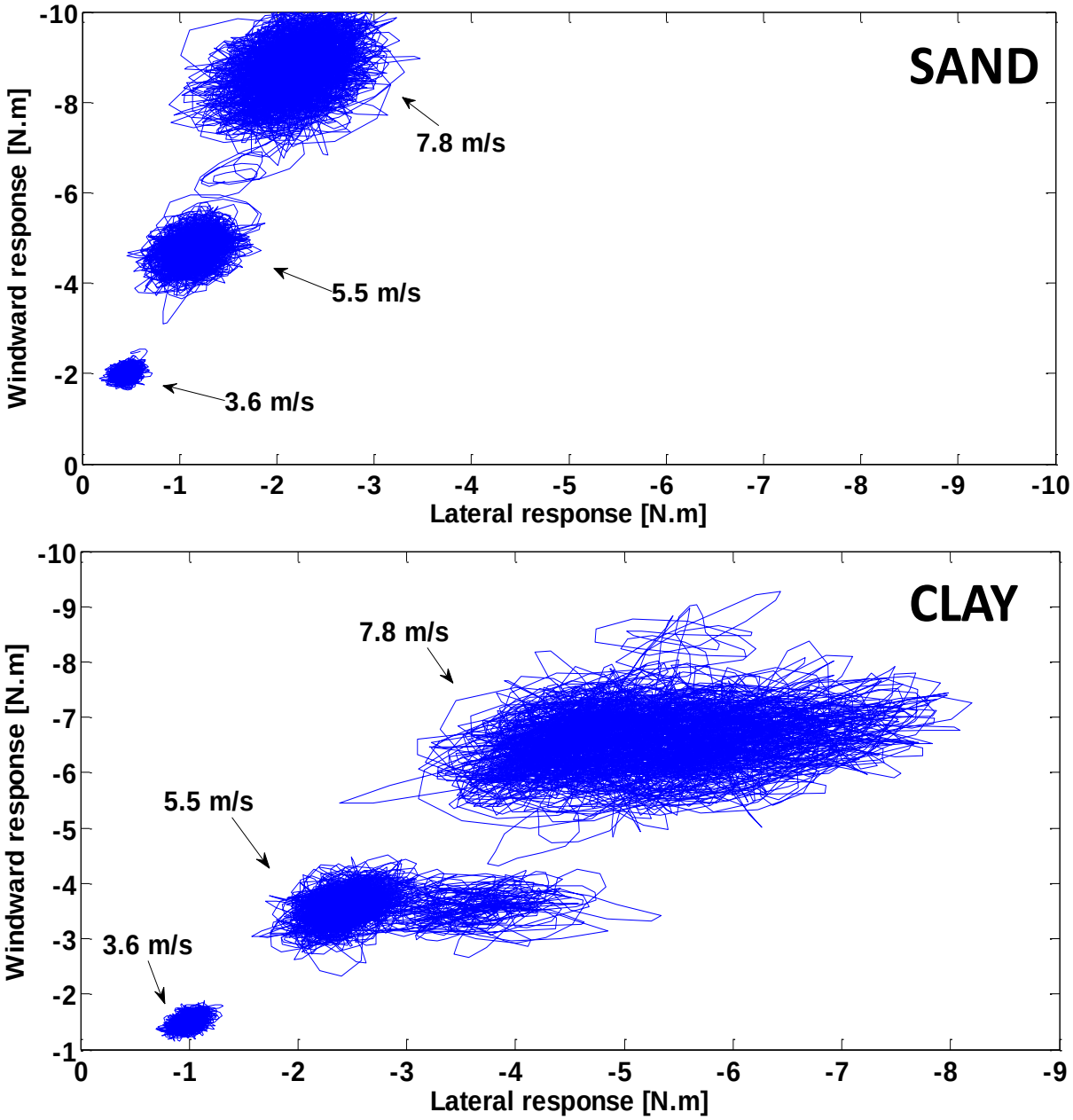

Figure 3-13 Tree (T2) sway with increase in wind speed and change in root plate soil medium

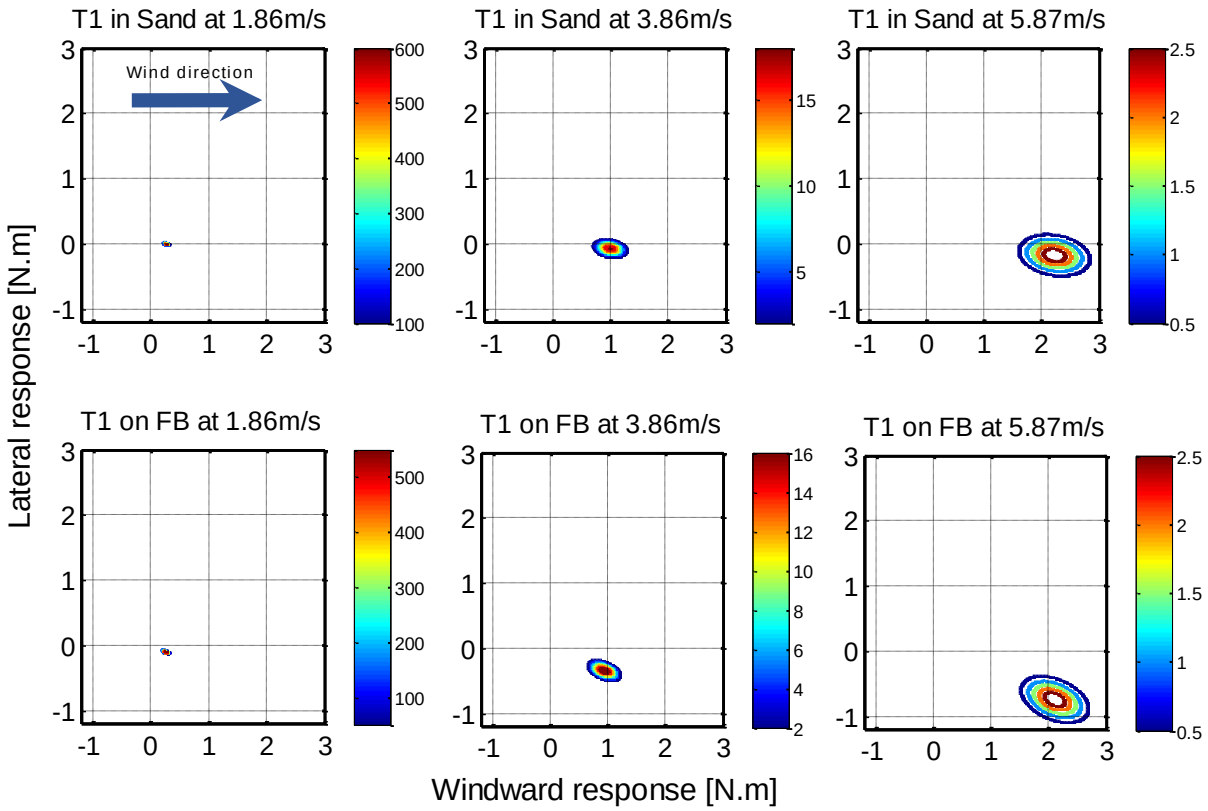

Sway Plot	Variant	Mean	Variance	Coefficient of variation	Skewness	Kurtosis	Covariance	Correlation coefficient
T1 in Sand at 1.86m/s	X axis	0.26	0.00	0.10	0.14	2.59	0.00	-0.23
	Y axis	0.00	0.00	-3.38	-0.12	3.20		
T1 in Sand at 3.86m/s	X axis	0.98	0.02	0.14	0.18	2.72	0.00	-0.21
	Y axis	-0.07	0.00	-0.91	-0.09	3.09		
T1 in Sand at 5.87m/s	X axis	2.21	0.11	0.15	0.03	2.68	-0.01	-0.20
	Y axis	-0.18	0.03	-0.96	-0.03	3.00		
T1 on FB at 1.86m/s	X axis	0.24	0.00	0.12	0.38	2.49	0.00	-0.68
	Y axis	-0.10	0.00	-0.13	-0.17	2.84		
T1 on FB at 3.86m/s	X axis	0.92	0.02	0.14	0.23	2.71	0.00	-0.46
	Y axis	-0.34	0.01	-0.22	-0.22	3.09		
T1 on FB at 5.87m/s	X axis	2.09	0.10	0.15	0.09	2.65	-0.02	-0.40
	Y axis	-0.74	0.04	-0.26	0.00	3.07		

Figure 3-14 Sway response of tree T1 in sand and on the force balance (FB) with increase in wind speed

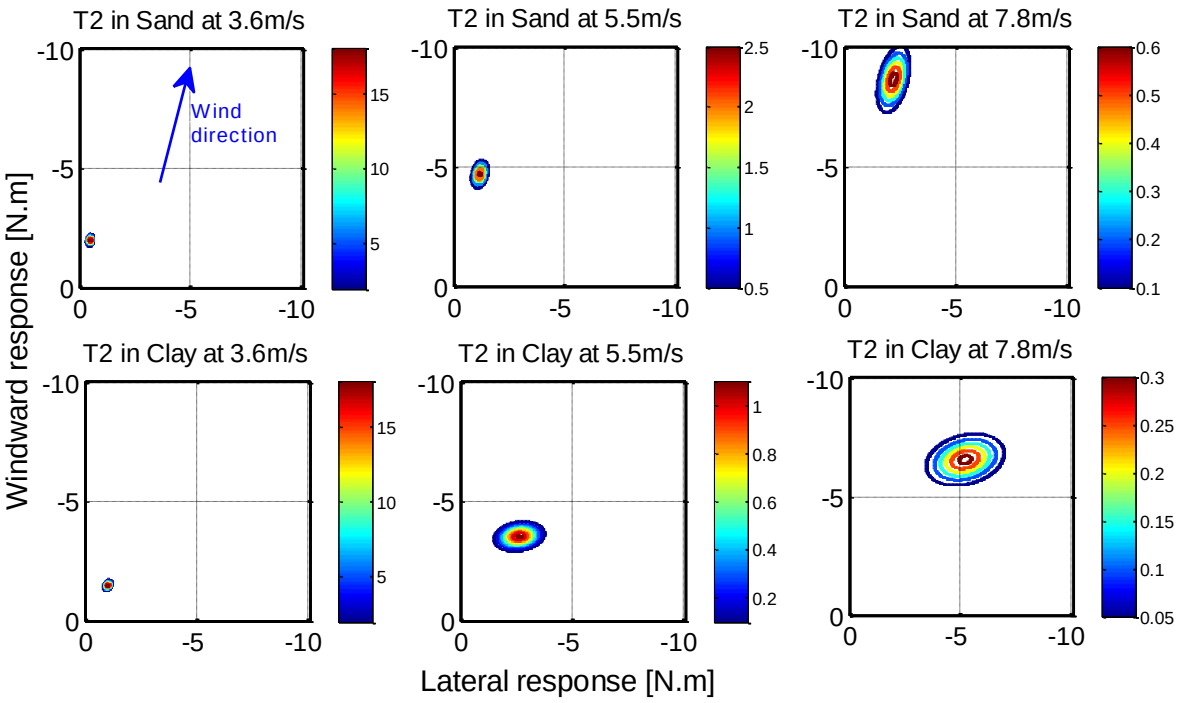

Sway Plot	Variant	Mean	Variance	Coefficient of variation	Skewness	Kurtosis	Covariance	Correlation coefficient
T2 in Sand at 3.6m/s	X axis	-0.45	0.01	-0.16	0.05	3.04	0.00	0.28
	Y axis	-2.01	0.01	-0.06	-0.10	3.02		
T2 in Sand at 5.5m/s	X axis	-1.14	0.04	-0.17	-0.03	3.07	0.02	0.30
	Y axis	-4.74	0.11	-0.07	0.08	3.28		
T2 in Sand at 7.8m/s	X axis	-2.18	0.14	-0.17	-0.08	3.37	0.12	0.43
	Y axis	-8.73	0.53	-0.08	-0.46	5.05		
T2 in Clay at 3.6m/s	X axis	-0.99	0.01	-0.09	-0.06	3.04	0.00	0.39
	Y axis	-1.50	0.01	-0.07	0.00	3.04		
T2 in Clay at 5.5m/s	X axis	-2.60	0.26	-0.20	-1.71	5.96	0.03	0.20
	Y axis	-3.56	0.08	-0.08	0.06	3.06		
T2 in Clay at 7.8m/s	X axis	-5.19	0.84	-0.18	-0.46	2.72	0.13	0.25
	Y axis	-6.60	0.32	-0.09	-0.23	3.95		

Figure 3-15 Tree (T2) sway with increase in wind speed and change in root plate soil medium

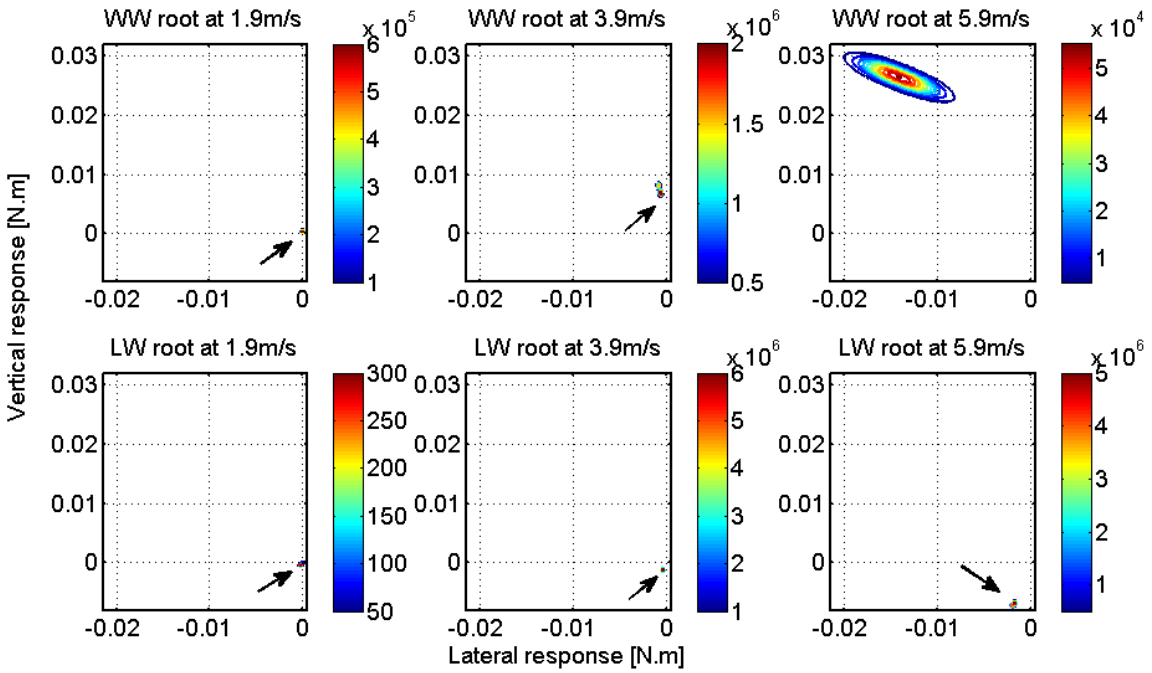

Sway Plot	Variant	Mean	Variance	Coefficient of variation	Skewness	Kurtosis	Covariance	Correlation coefficient
WW root at 1.9m/s	X axis	7.9E-05	6.1E-10	0.32	0.08	2.95	7.6E-10	0.64
	Y axis	3.0E-04	2.3E-09	0.16	-1.04	3.31		
WW root at 3.9m/s	X axis	-6.9E-04	1.7E-08	-0.19	2.12	7.00	-9.6E-08	-0.89
	Y axis	7.4E-03	6.7E-07	0.11	-1.81	5.95		
WW root at 5.9m/s	X axis	-1.4E-02	7.3E-06	-0.19	1.64	4.75	-4.1E-06	-0.82
	Y axis	2.6E-02	3.5E-06	0.07	-1.89	7.74		
LW root at 1.9m/s	X axis	-3.8E-05	1.0E-09	-0.85	-0.19	4.74	5.3E-10	0.41
	Y axis	-2.1E-04	1.6E-09	-0.19	-0.30	3.43		
LW root at 3.9m/s	X axis	-4.1E-04	1.5E-09	-0.09	-1.00	6.40	2.0E-09	0.76
	Y axis	-1.1E-03	4.7E-09	-0.06	-1.02	6.55		
LW root at 5.9m/s	X axis	-1.8E-03	1.4E-08	-0.07	-0.16	2.82	2.2E-08	0.71
	Y axis	-7.0E-03	6.8E-08	-0.04	-0.01	1.79		

Figure 3-16 Windward (WW) and leeward (LW) root sway of tree T1 in sand with increase in wind speed

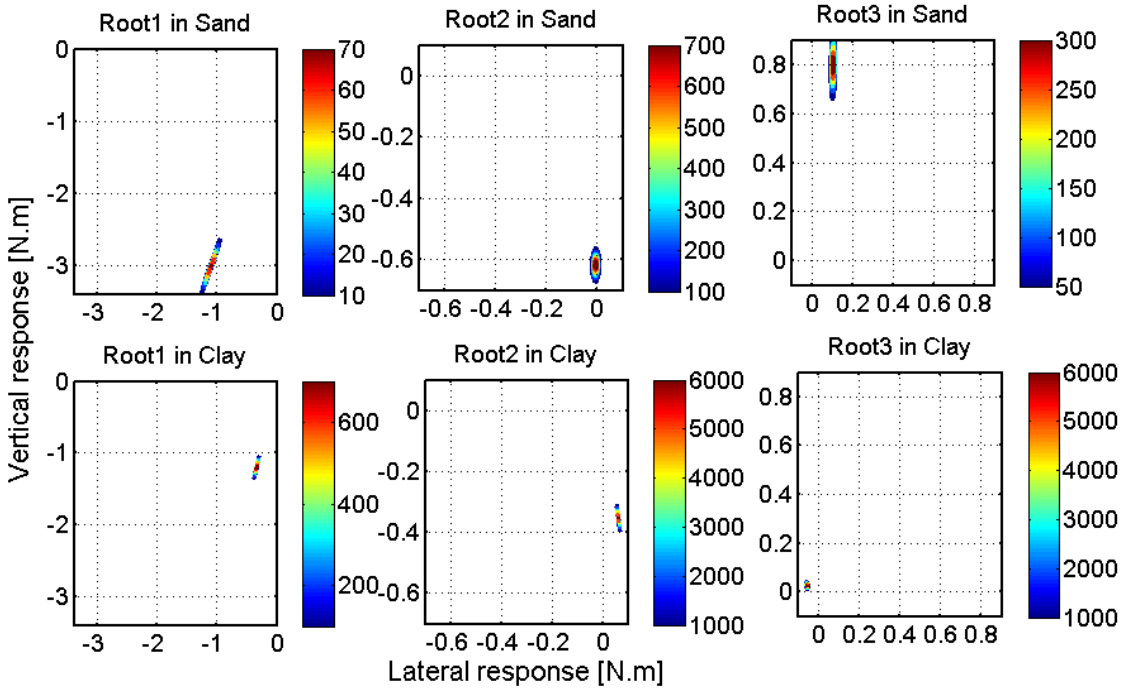

Sway Plot	Variant	Mean	Variance	Coefficient of variation	Skewness	Kurtosis	Covariance	Correlation coefficient
Root1 in Sand	X axis	-1.10	0.01	-0.07	0.38	7.38	0.01	0.99
at 7.8m/s	Y axis	-3.01	0.04	-0.06	-0.01	9.06		
Root2 in Sand	X axis	-0.01	0.00	-1.15	0.95	3.73	0.00	0.05
at 7.8m/s	Y axis	-0.62	0.00	-0.04	-0.01	17.63		
Root3 in Sand	X axis	0.11	0.00	0.06	-0.38	2.98	0.00	0.13
at 7.8m/s	Y axis	0.80	0.01	0.09	-0.84	9.05		
Root1 in Clay at	X axis	-0.34	0.00	-0.07	-0.09	11.43	0.00	0.99
7.8m/s	Y axis	-1.20	0.01	-0.07	-0.20	11.73		
Root2 in Clay at	X axis	0.06	0.00	0.07	0.24	11.47	0.00	-0.97
7.8m/s	Y axis	-0.35	0.00	-0.07	-0.07	11.70		
Root3 in Clay at	X axis	-0.05	0.00	-0.05	-1.03	9.74	0.00	-0.27
7.8m/s	Y axis	0.03	0.00	0.32	0.13	2.95		

Figure 3-17 Root sway of tree (T2) in sand and clay at 7.8 m/s wind speed

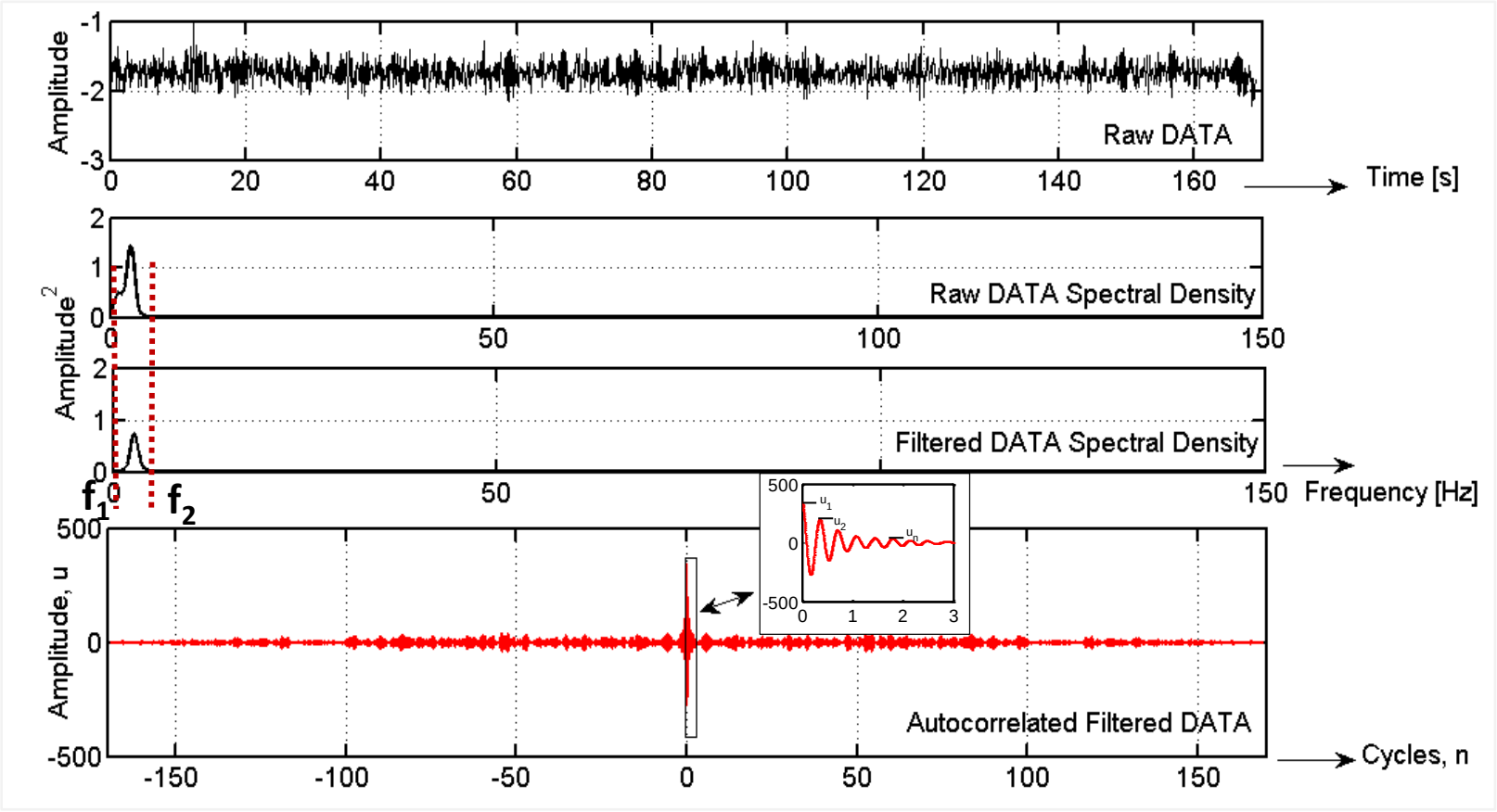

Figure 3-18 Example of typical autocorrelation methodology

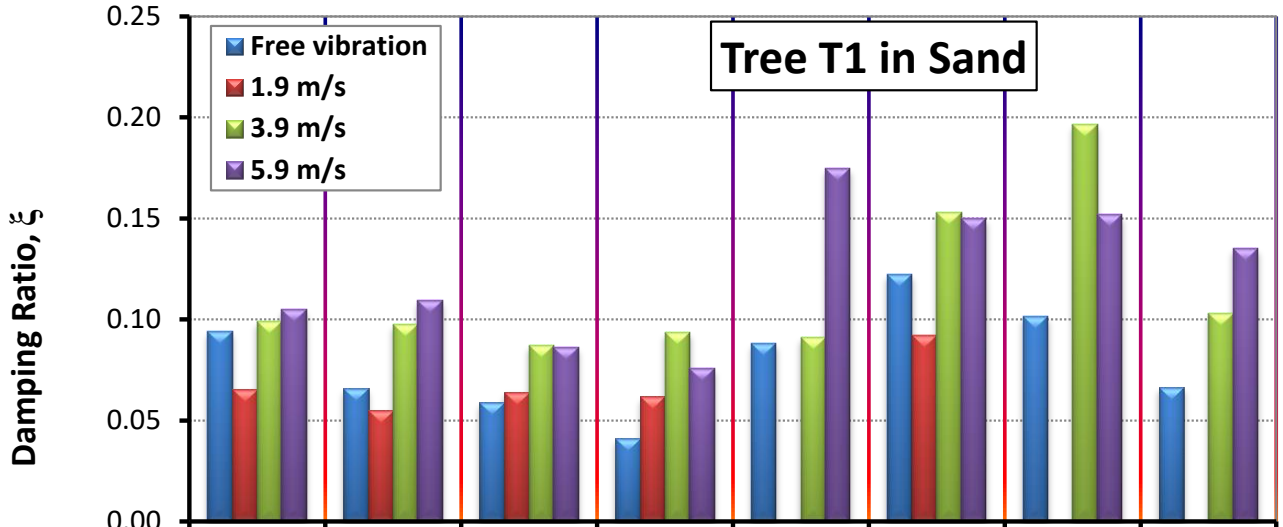

	Upper stem WW	Lower stem WW	Upper stem lateral	Lower stem lateral	Root ww up	Root lw up	Root ww side	Root lw side
Free vibration	0.09	0.07	0.06	0.04	0.09	0.12	0.10	0.07
1.9 m/s	0.07	0.06	0.06	0.06	0.00	0.09	0.00	0.00
3.9 m/s	0.10	0.10	0.09	0.09	0.09	0.15	0.20	0.10
5.9 m/s	0.11	0.11	0.09	0.08	0.17	0.15	0.15	0.14

Figure 3-19 Damping ratio estimated from the strain gauge data with increase in wind speed

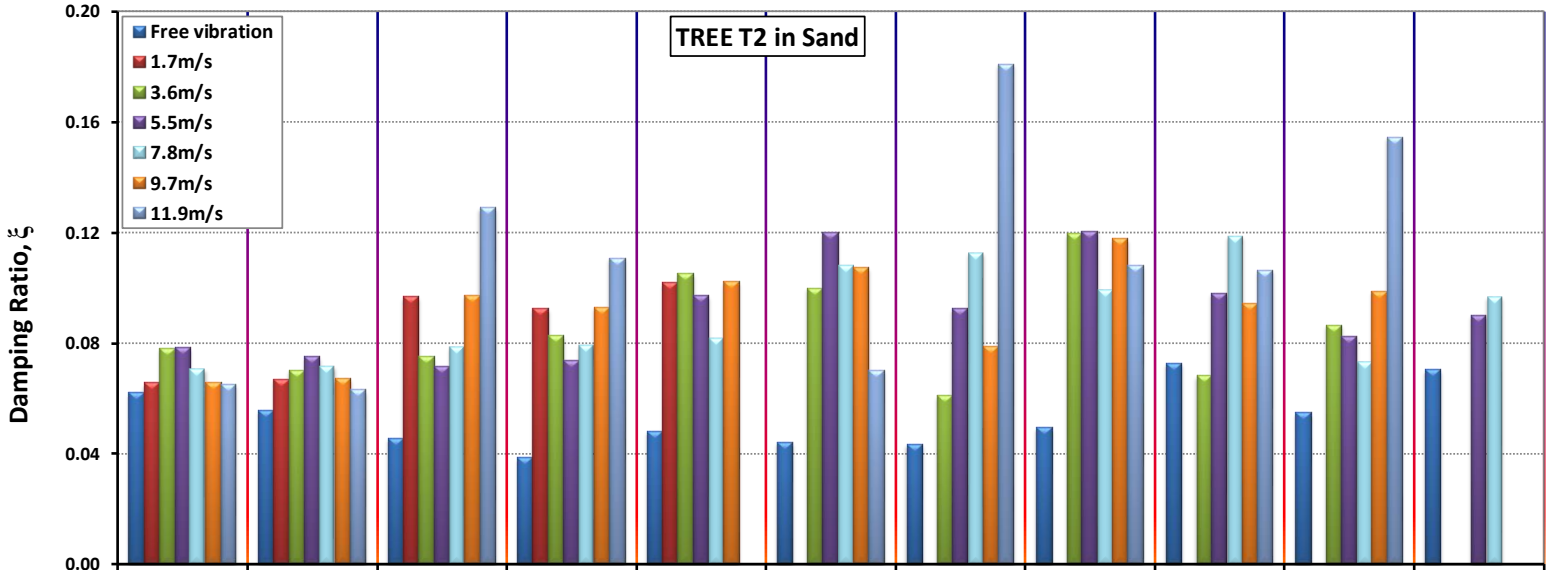

	Upper stem WW	Lower stem WW	Upper stem lateral	Lower stem lateral	Root 1 up	Root 2 up	Root 3 up	Root 1 side	Root 2 side	Root 3 side	Root 1b up
Free vibration	0.062	0.056	0.046	0.038	0.048	0.044	0.043	0.049	0.073	0.055	0.070
1.7m/s	0.065	0.067	0.097	0.093	0.102						
3.6m/s	0.078	0.070	0.075	0.083	0.105	0.100	0.061	0.120	0.068	0.087	
5.5m/s	0.078	0.075	0.072	0.074	0.097	0.120	0.092	0.121	0.098	0.082	0.090
7.8m/s	0.071	0.072	0.079	0.079	0.082	0.108	0.113	0.099	0.119	0.073	0.097
9.7m/s	0.066	0.067	0.097	0.093	0.102	0.107	0.079	0.118	0.094	0.099	
11.9m/s	0.065	0.063	0.129	0.111		0.070	0.181	0.108	0.106	0.155	

Figure 3-20 Damping ratio estimated from the strain gauge response data with increase in wind speed

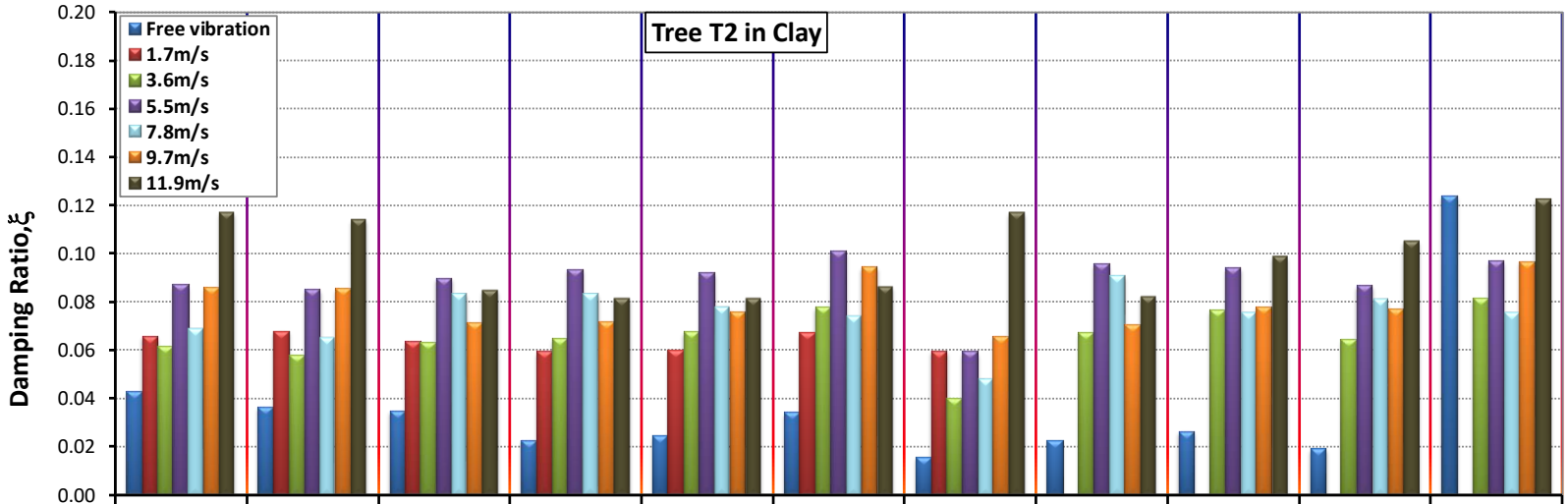

	Upper stem WW	Lower stem WW	Upper stem lateral	Lower stem lateral	Root 1 up	Root 2 up	Root 3 up	Root 1 side	Root 2 side	Root 3 side	Root 1b up
Free vibration	0.042	0.036	0.035	0.022	0.025	0.034	0.015	0.022	0.026	0.019	0.124
1.7m/s	0.066	0.068	0.063	0.060	0.060	0.067	0.060				
3.6m/s	0.061	0.058	0.063	0.065	0.068	0.078	0.040	0.067	0.076	0.064	0.081
5.5m/s	0.087	0.085	0.090	0.093	0.092	0.101	0.059	0.096	0.094	0.087	0.097
7.8m/s	0.069	0.065	0.083	0.083	0.078	0.074	0.048	0.091	0.076	0.081	0.076
9.7m/s	0.086	0.085	0.071	0.072	0.076	0.094	0.066	0.070	0.078	0.077	0.097
11.9m/s	0.117	0.114	0.085	0.082	0.082	0.086	0.117	0.082	0.099	0.105	0.122

Figure 3-21 Damping ratio estimated from the strain gauge data with increase in wind speed

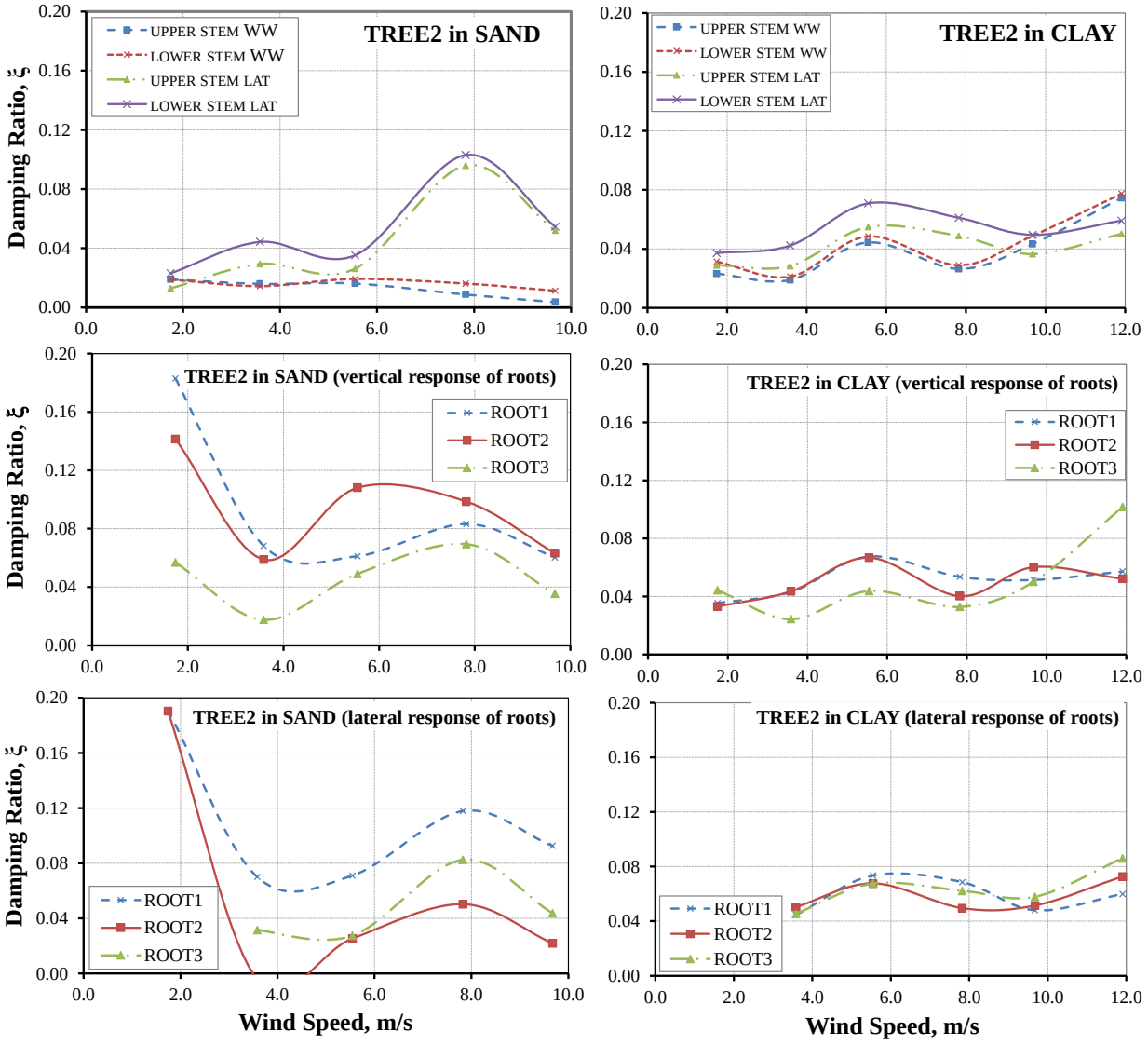

Figure 3-22 Aerodynamic damping ratio with increase in wind speed and change in soil medium

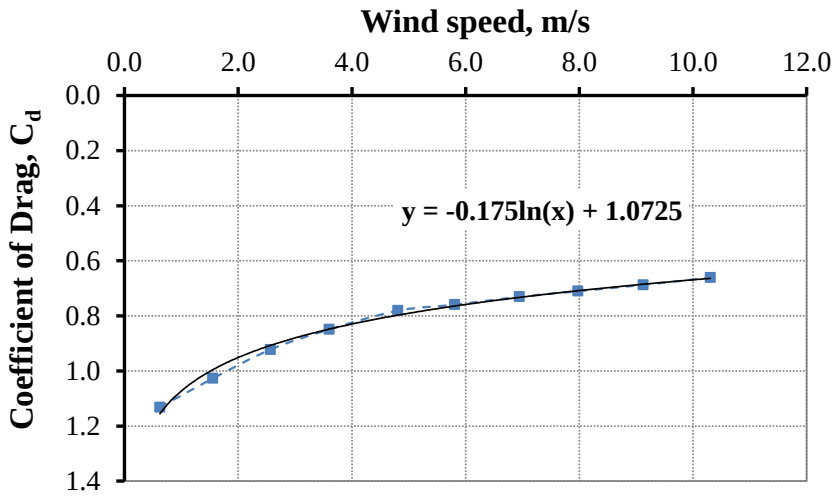

Figure 3-23 Coefficient of drag with increase in wind speed

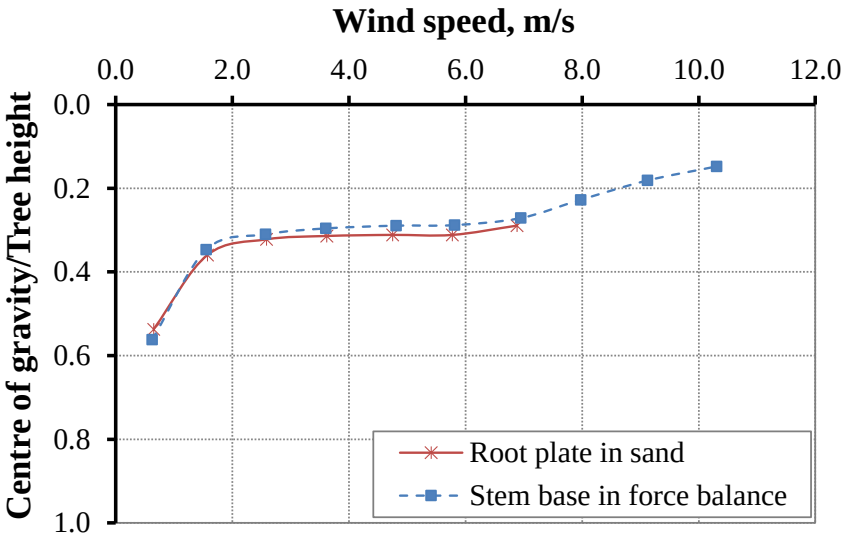

Figure 3-24 Centre of gravity of tree T1 with increase in wind speed

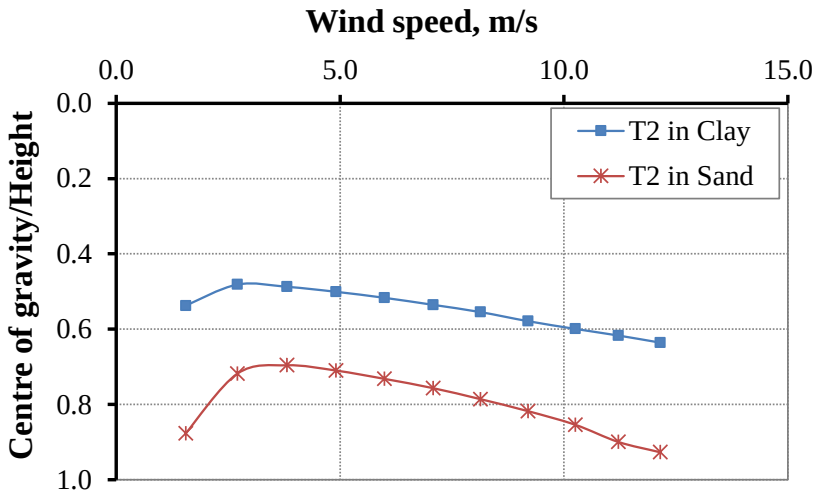

Figure 3-25 Centre of gravity of tree T2 with increase in wind speed

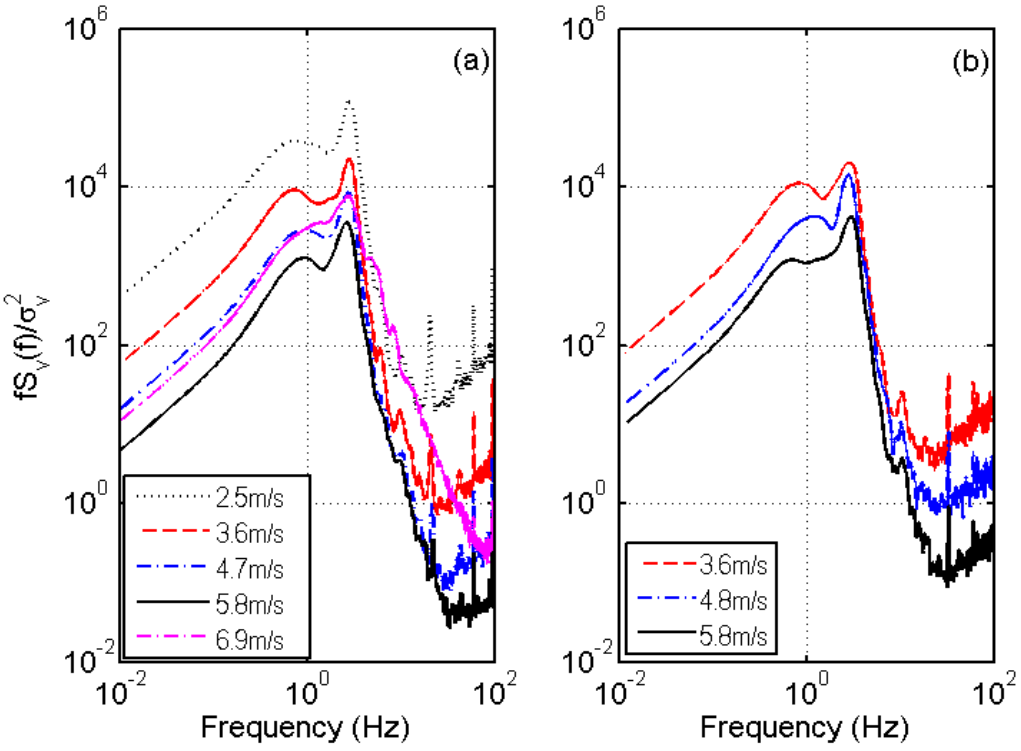

Figure 3-26 Power spectra of the T1 stem base bending moment response with increases in wind speed (a) in sand (b) on force balance

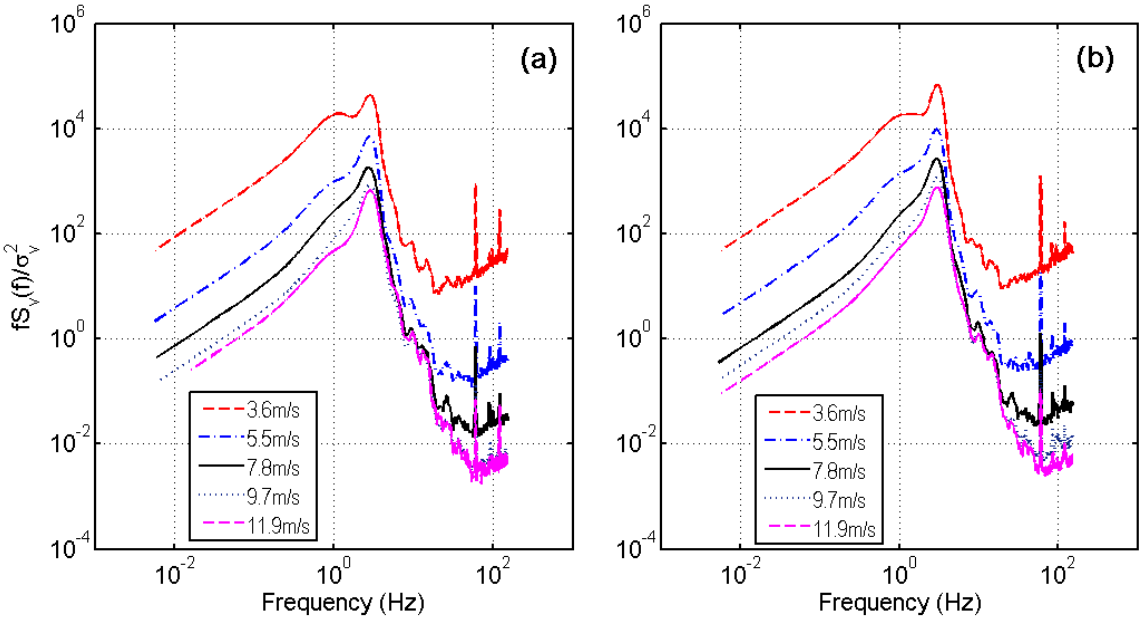

Figure 3-27 Power spectra of T2 stem base bending moment response with increase in wind speed (a) in sand and (b) in clay

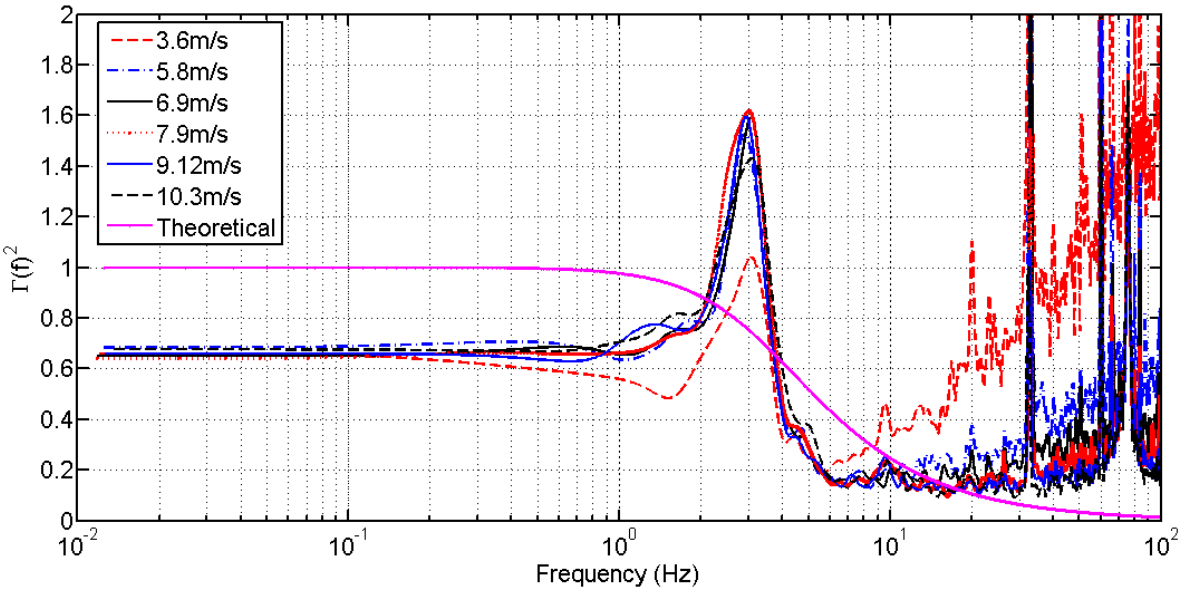

Figure 3-28 Aerodynamic admittance of tree T1 on the force balance with increase in wind speed

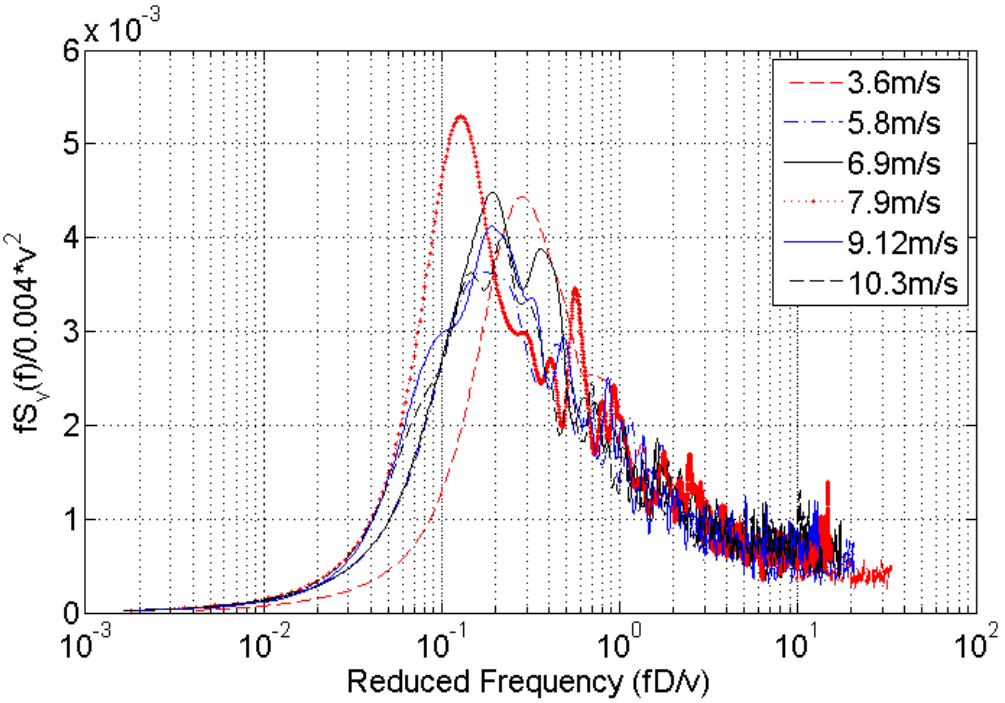

Figure 3-29 Normalized wind spectra with open country surface drag coefficient of 0.004 (Davenport 1964)

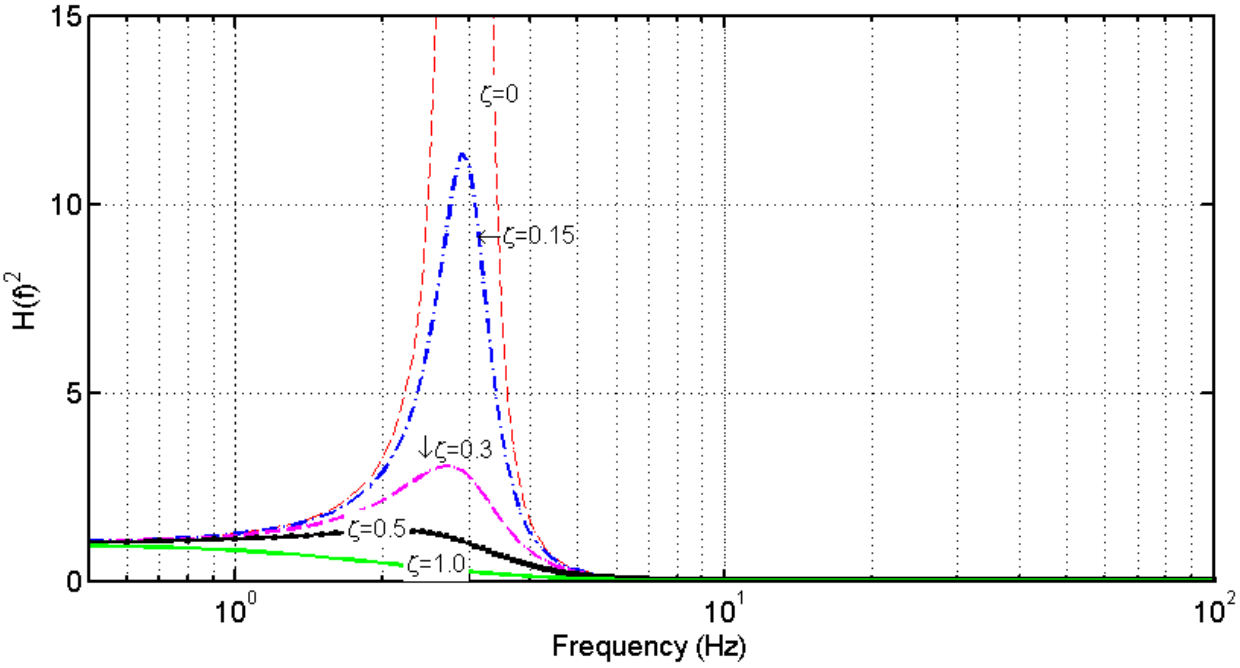

Figure 3-30 Theoretical admittance with increase in damping with 2.9 Hz natural frequency

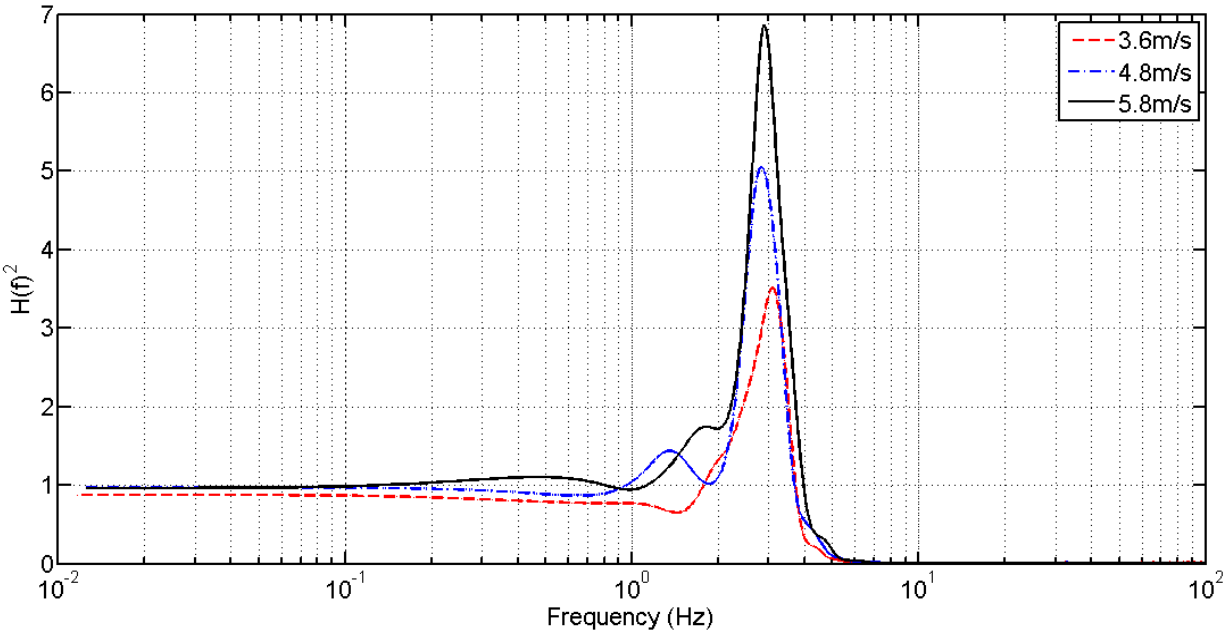

Figure 3-31 Mechanical admittance of windward stem base moment response of tree T1 on the force balance

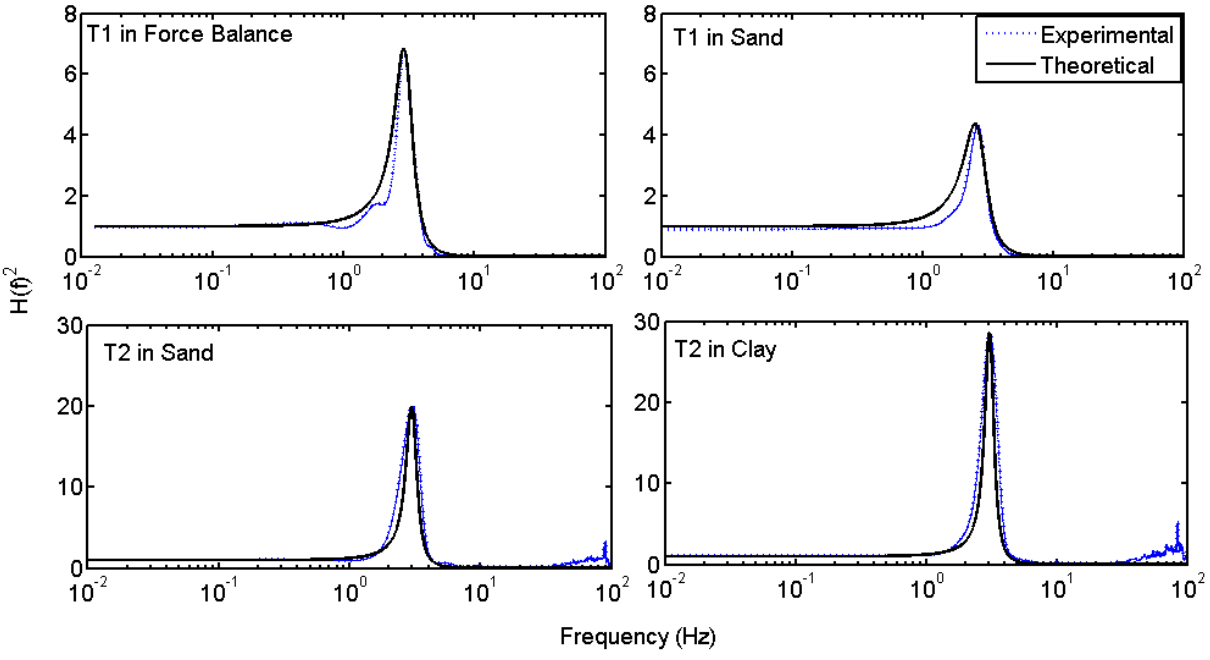

Figure 3-32 Mechanical admittance of T1 and T2 at 5.9 m/s

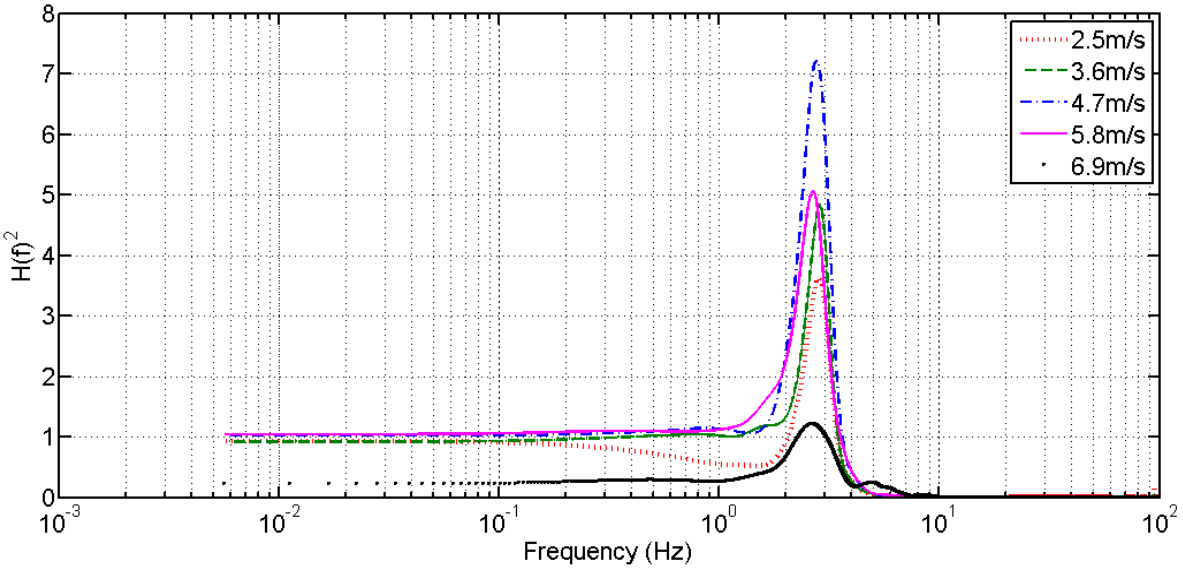

Figure 3-33 Mechanical admittance of stem base moment response of tree T1 in sand

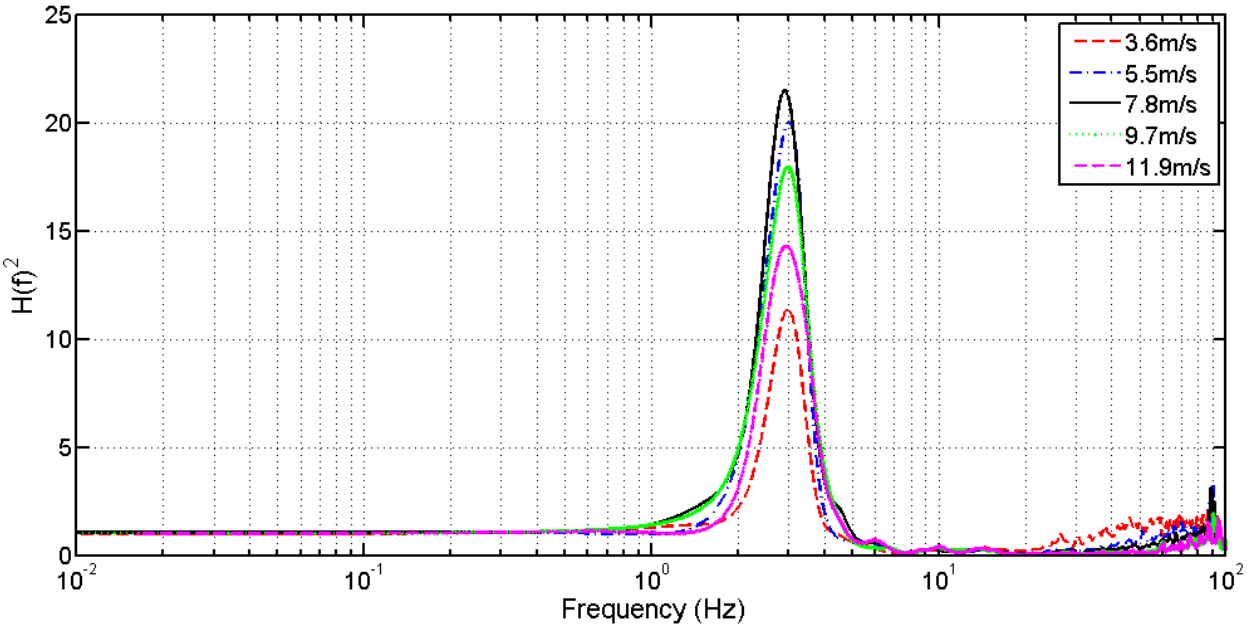

Figure 3-34 Mechanical admittance of stem base moment response of tree T2 in sand

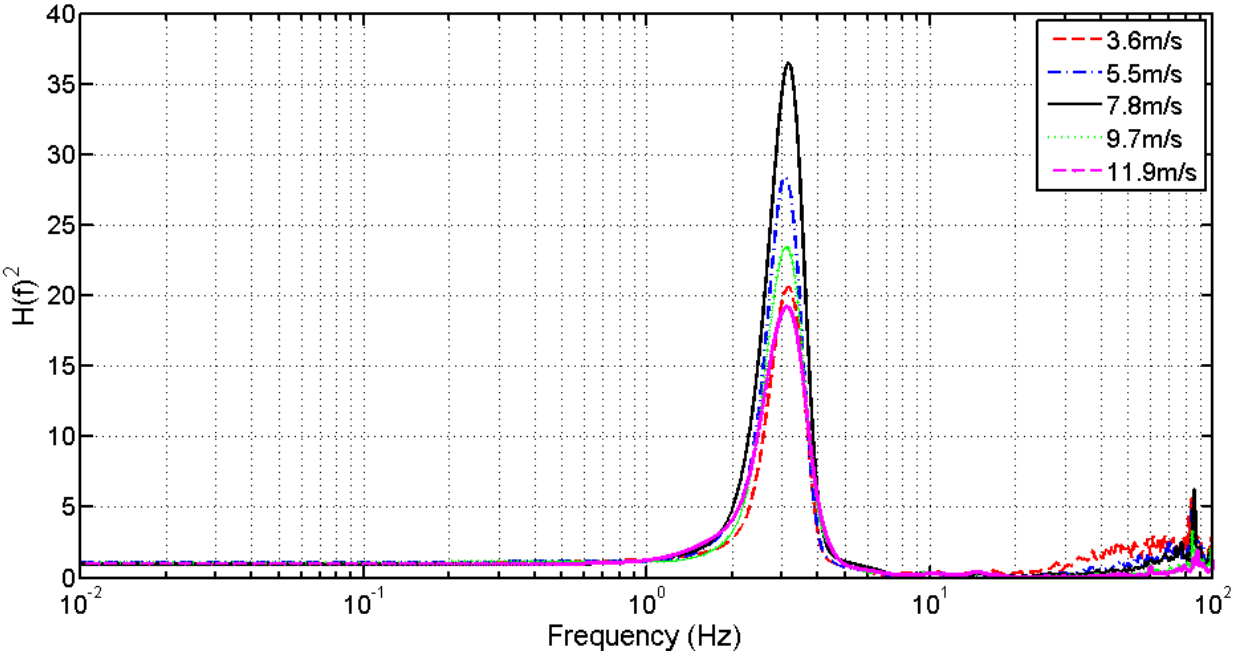

Figure 3-35 Mechanical admittance of stem base moment response of tree T2 in clay

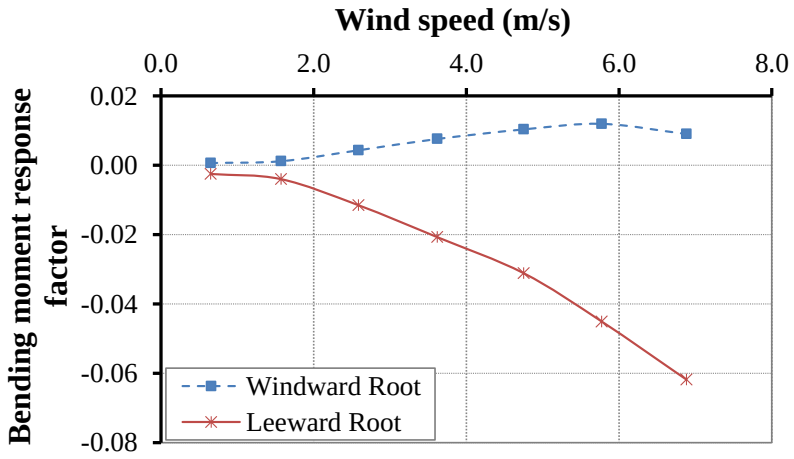

Figure 3-36 Root response factor of tree T1

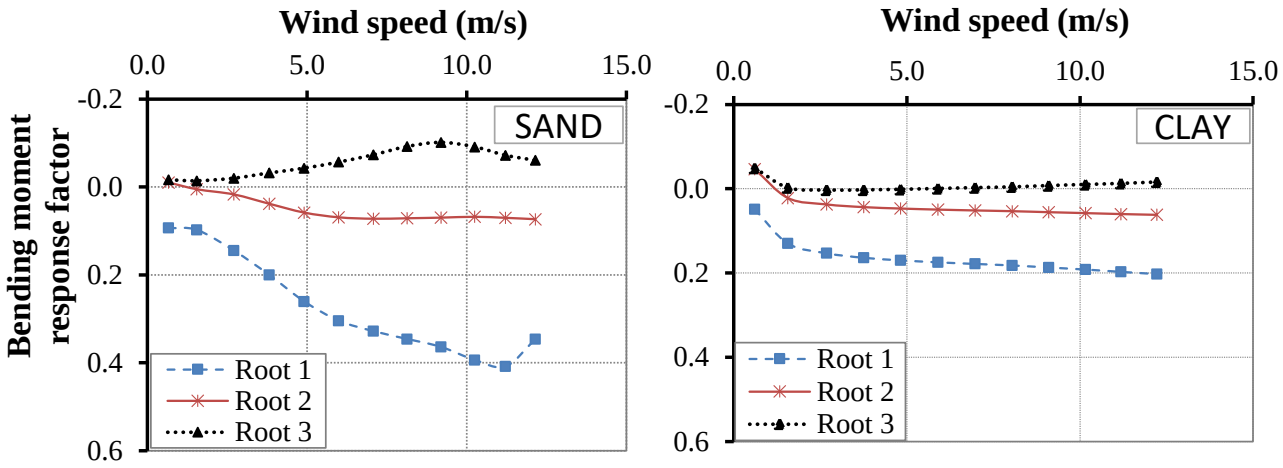

Figure 3-37 Root response factor of tree T2 in sand and clay

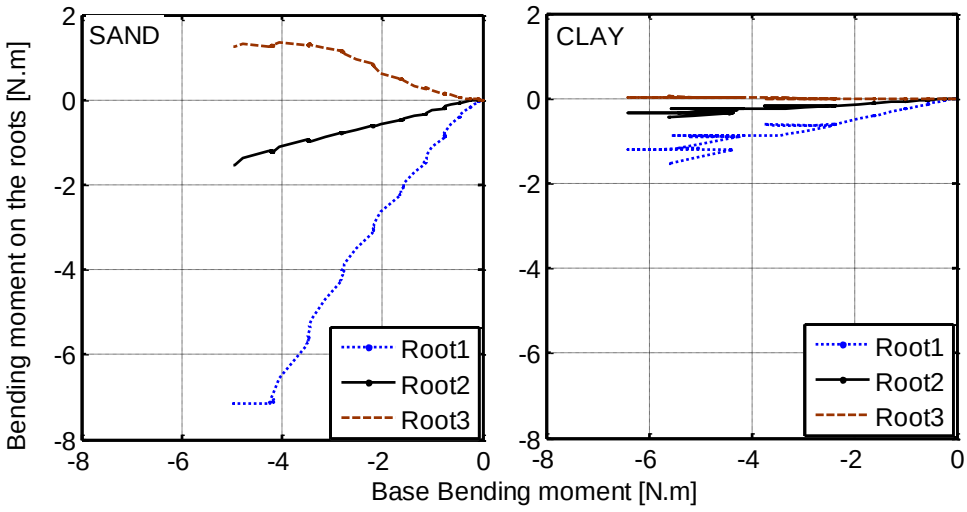

Figure 3-38 Tree T2 root vertical response in sand and clay

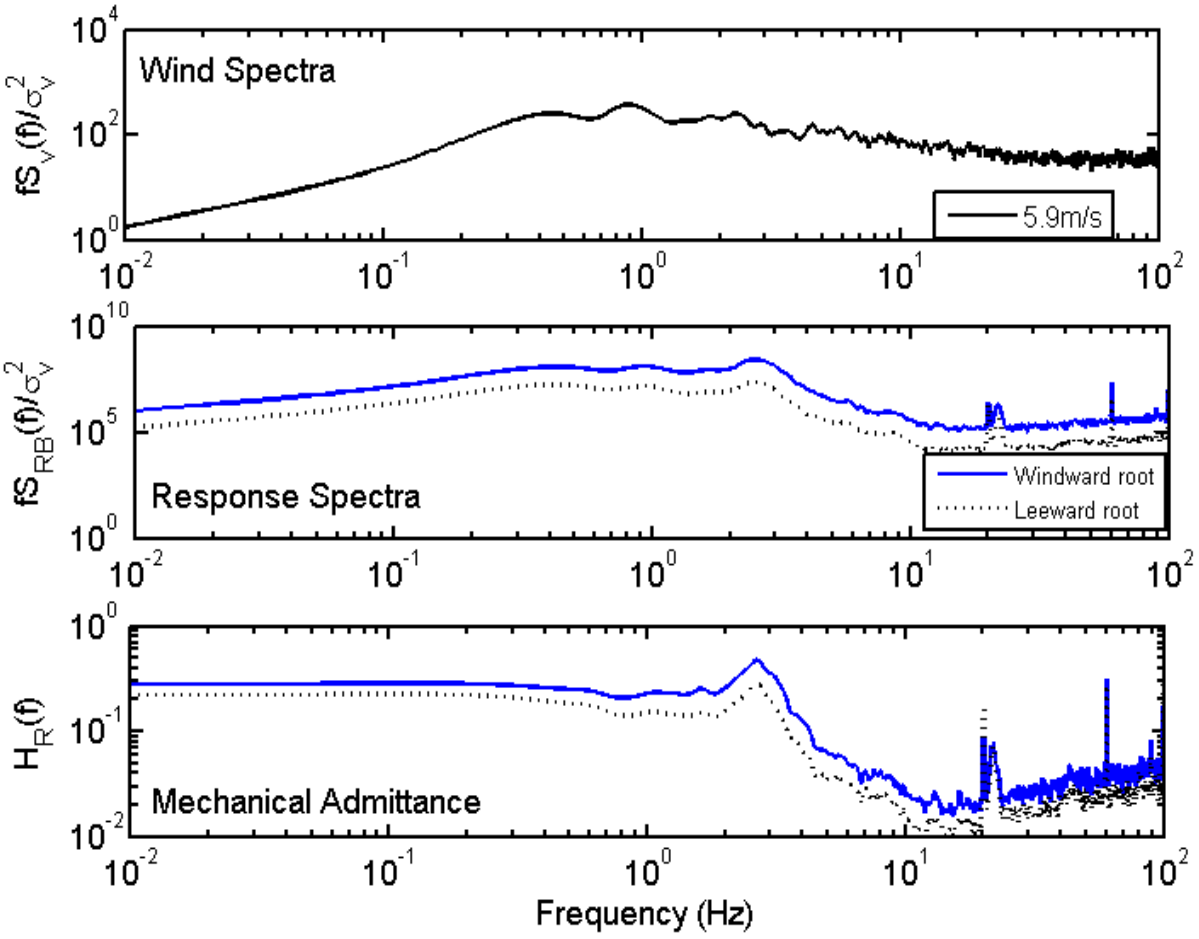

Figure 3-39 Wind spectra at the tree sapling center of gravity, response spectra of the roots and the mechanical admittance spectra of tree T1 roots in sand

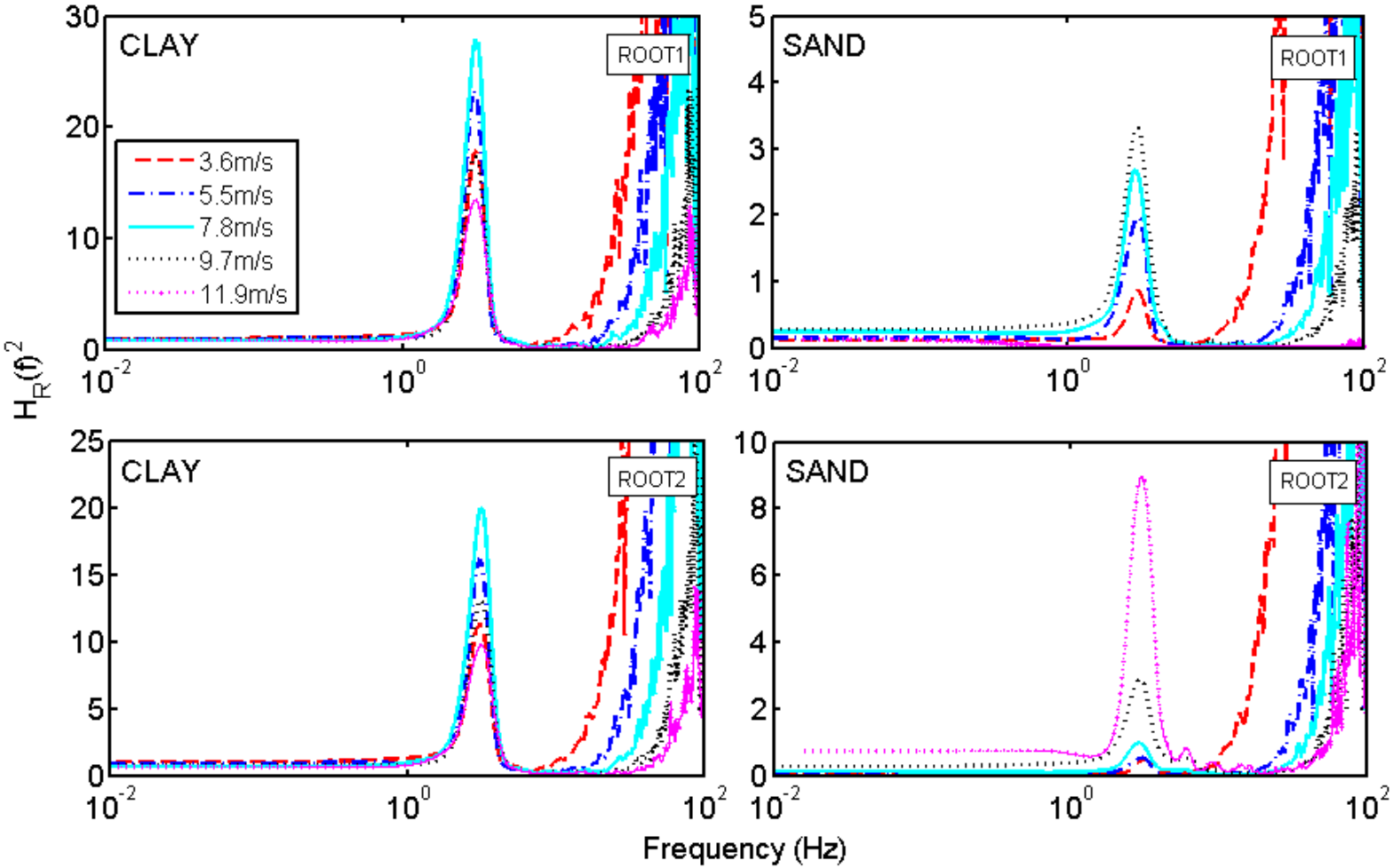

Figure 3-40 Mechanical admittance of tree T2 root vertical response in sand and clay

Chapter 4

4 Scaled physical modelling of windthrow using a wind tunnel

4.1 Introduction

The objective of this study is to examine the similitude of responses between scaled tree (sapling) tests in the wind tunnel and full scale tree responses to winching. The mature Norway spruce field tree response to winching is the “full scale” response to static loading. The Norway spruce tree sapling response in the wind tunnel represent a “scaled” response to dynamic and static loading. The tree saplings in the wind tunnel were tested with root systems in sand and clay under dynamic conditions. Further static pulling tests were also conducted for the saplings for both soil conditions. In this chapter comparisons are made on three different aspects: i) scaling, ii) static to dynamic loading responses and iii) change in root plate soil media.

The similarities and the limitations of using tree saplings to represent full scale tree responses are examined using dimensionless parameters and structural load response comparisons. Equivalent wind speeds and respective load responses of tree saplings in sand and clay soils are studied in detail through the rain flow counting technique. Peak gusts and peak responses are identified, compared and the load and response were correlated to understand the effect of dynamic loading over static loading through load transfer. Static and dynamic loading response comparisons are made using dynamic load factors and secant modulus of rotation and with change in root plate response with change in load direction.

4.2 Background

The field of *windthrow* is a very complex area of study. Research in this subject is quite diverse, and many attempts from different viewpoints have been made to understand tree stability under wind loading. Field experiments on mature trees under both static and dynamic loading conditions and wind tunnel experiments on tree saplings and on model trees are the most widely used experimental techniques for windthrow studies. Mature field

tree response to static loading is generally studied using winching [Fraser 1962; Somerville 1979; Smith et al. 1987; Frederickson et al. 1993; Papesch et al. 1997; Peltola et al. 2000; Bryne and Mitchell 2007], dynamic tree properties through sway tests [Mayhead 1973; Blackburn et al. 1988; Gardiner 1989; Milne 1991; Gardiner 1995 and Flesch and Wilson 1999] and the response to wind loading is studied through long term monitoring [Mayer 1987, Raupach 1994, Gardiner 1992]. Winching and long-term tree response monitoring tests have also been used to track root response to pull loads and wind loading respectively [Fraser and Gardiner 1963, Coutts 1986, Mayer 1987, Watson 2000].

However, it is unlikely that more than a few tree responses and few failures under extreme wind events will be captured in their natural physical surroundings, even with many long-term monitoring data sets. Hence wind tunnel studies may provide a viable alternative. Scaled model tests are less expensive, versatile and easy to conduct. Wind tunnel tests reported in the literature have been conducted on tree saplings and on synthetic forest models to test sub-critical responses under controlled wind loading conditions. Mayhead [1973], Roodbarky et al. [1994], Gillis et al. [2000 and 2002], Rudnicki et al. [2004] conducted wind tunnel experiments on plants, with stem bases that were clamped to the wind tunnel floor to explore the change in drag force with increase in wind speed. Meroney [1968], Stacy et al. [1994], Gardiner et al. [2005] designed a model forest canopy to study the wind flow characteristics in and above forests. As the drag force estimate does not depend on root anchorage, all of these tests ignored the anchorage component. Although the anchorage component does not influence the drag force, it has a significant effect on tree stability. Tree root plate anchorage also varies with root plate architecture, root strength and soil strength. No testing to date has investigated both sub-critical and failure conditions for trees in a wind tunnel. All of the available information on full scale tree failures is based on posteriori post-storm surveys.

Since the tests in the wind tunnel are non in-situ and only the above ground part of the tree response is tested so far in the wind tunnel, it is still problematic to determine or model the uprooting resistance (critical response) of a mature field tree based on wind tunnel test results alone. With the aid of winching tests, the anchorage resistance under lateral pull can be studied (allowing sub-critical and critical failure responses can be estimated). However,

linking the tree response under static loading to dynamic loading is still challenging and is generally empirical in nature. The wind tunnel also has the potential to provide fundamental understanding of windthrow behavior and may provide links between static and dynamic loading (by enabling the same tree and rooting medium to be tested to failure in both states). This poses the question of whether a small sapling tested in a wind tunnel is representative of the behavior of a full scale tree. To answer the question, three different aspects need to be examined: i) scaling, ii) loading and iii) anchorage.

To relate the wind tunnel results to the full scale tree response, the relationships between the model and the prototype in particular need to be established. Similarity of behavior between a model and a prototype is called similitude: geometric, kinematic and dynamic similitude is examined using scaling laws. Geometric similarity is a constant length scale factor relation of corresponding linear dimensions, kinematic similarity is a constant velocity scale factor with no change in direction at corresponding points and the dynamic similarity is a constant force scale factor difference at corresponding points [Jha 2004]. For wind tunnel modelling, aerodynamic, elastic, inertial, damping forces need to be considered. In order to attain similarity between model and the prototype, not just the geometric similarity needs to be considered: model material properties and fabrication also need to be compared to the prototype, method of loading, measurement and the interpretation of the results are also essential factors. It is not possible for the model to be in perfect similitude with a prototype; based on the experimental goals the model similitude is usually designed as per the requirements of the testing [Sockel 1994].

For windthrow research, geometric similarity can be examined based on the mass, branch length and the stem diameter variation along the length of the tree structure. Elastic similarity can be compared based on the variation of bending stiffness along the height of the structure. Stress similarity, based on the variation of load and corresponding response variation can be conducted along the length of the structure. Tree response to dynamic wind loading is dependent upon the dynamic properties of the tree structure. The dynamic properties such as frequency and damping of any structure varies with the magnitude and distribution of mass and stiffness along the structural dimensions. In order to understand the change in tree dynamic response with tree age, the structural scaling needs to be

clarified. Density, stiffness and damping parameters of the model and the prototype needs to be similar to achieve structural and dynamic similarity.

The soil and root system supporting the tree are also important to understand stability and the properties of soil can vary significantly from one location to other. Soil strength depends on two important properties, cohesion and friction. Similarity of this part of the tree system is also important. In the wind tunnel study, sand and clay were chosen as the root plate soil media. The silica sand used was a purely frictional soil and Bentonite clay was a purely cohesive soil. These soils were chosen to help understand the tree response to wind loading for extremes of soil behaviour and consequently root-soil interaction and anchorage.

In engineering, it is a common practice to use dimensional analysis to derive scaling factors. Using the principle of dimensional analysis, various scale factors are derived with three fundamental parameters (mass, length and time). Dimensionless groups (π terms) are generally derived using the principles of the Buckingham Pi theorem [Gibbins 2011]. To achieve similitude, the dimensionless terms must be equal for the model and the prototype. In this study, the physical parameters of the prototype and the sapling are already fixed. An alternative would be to create an artificial tree that is properly scaled, but this presents some significant challenges of material behavior. Thus the aim of this study is to understand and quantify the difference between the two responses (mature field tree and tree saplings) to determine the viability of the approach. To examine the impact of dynamic loading over static loading and consequently the responses, dynamic load and the response were examined in detail. At each wind load segment, the dynamic load responses were divided into number of load cycles, each cycles amplitude and mean were also obtained using rainflow counting technique. Statistical proclivity of response with respect to the load is examined. To compare dynamic load response to static load response and to examine the effect of soil properties on tree stability, tree sapling anchorage strength factors are analyzed in detail.

4.3 Research objectives

The objective of this study is to relate the scaled 'model' tree responses to full scale tree responses. This includes both static and dynamic load response. Changes in tree response to different soil conditions (clay and sand) are also considered.

Instrumented tree saplings with their structural root systems in two different soil media were tested in the wind tunnel and a mature field tree was winched to failure in field. Both data sets used Norway spruce trees. The extensive data collected from both test programs are used:

i. To find appropriate dimensionless groups to assess similitude;

ii. To examine the geometric, elastic and stress similarity between the mature tree and saplings;

iii. To examine the load response changes with scaling;

iv. To examine the influence of dynamic loading and the corresponding response;

v. Compare the static and dynamic load response of tree saplings through anchorage strength factors;

vi. To examine the differences in static and dynamic load responses with change in load direction (difference in tree anchorage because of asymmetry in root plate architecture).

4.4 Comparison of the tree sapling behavior and properties with a mature field tree

Field study: this was conducted at the Davey tree farm in Ohio, USA. during biomechanics week in August 2010. For further details on this field study refer to Chapter 2 of this thesis. This was a tree winching study. This tree was instrumented with strain gauges attached to the stem, windward root and leeward root. Tilt sensors were also attached to the stem on the windward side and lateral side. The concept was to uproot the tree and study the root soil interaction. Tree failure occurred through stem breakage during winching. Dynamic

properties of the tree were calculated using the data collected from the manual pull and release tests. Windward and leeward root movement was tracked during winching. The field tree used for the winching was 24 years old and was 23.1 m in height. The tree DBH (diameter at breast height, around 1.3 m height above the ground) was 0.458 m and was pruned up to the height of 6.45 m above the ground level. The overall center of mass of the tree structure after pruning was 8.3 m above the ground level. The winching height was 9.57 m and was deliberately kept close to the tree center of mass. Overall mass of the stem and crown after pruning was 1612.6 kg. The soil in the field was silty loam with an effective unit weight of 20 kg/m^3 is taken for further calculations. The tilt sensor locations and strain gauge setup of the field tree and the roots are as shown in Figure 4-1 and Figure 4-2.

Scaled wind tunnel study: The tree saplings selected were 5 year old Norway spruce (Picea abies (L.) H.Karst.) utilized as a reference species, since it is ubiquitous in urban and rural Ontario. To ensure simple root architecture, all of the fine roots were pruned, leaving just the structural roots (> 0.4 mm diameter) in place. To avoid the complexity of field based systems, scaled tests were conducted in a Boundary Layer Wind Tunnel. The wind tunnel tests subjected small trees with varying stiffness, mass, geometry (crown, stem and roots) and damping behaviors to different wind velocities and an open country turbulence regime. To create a realistic root-soil system, a large soil box was embedded in the tunnel floor and the tree root systems were embedded in silica sand for some tests and clay (Bentonite+water) for the other tests. The mechanical stability and response of any tree depends on its structure and the tree family. Soil strength also depends on two very important factors, cohesion and friction. To maximize the usability of the results, purely cohesive and frictional soils were used in the wind tunnel testing to provide the widest possible range of soil responses. It should be noted that these reference soils are likely dissimilar to real soils (with variation in particle sizes) and the trees were not grown in-situ. This provides a more tractable analysis of the results and ease of approximation, but may introduce artefacts into the results.

The tree saplings T1 and T2 were 1.37 m and 1.27 m respectively. Tree saplings were carefully uprooted from the tree farm without damaging the structural root system. The

root plates were washed and the roots with diameter less than 0.4 mm were removed leaving the structural roots intact. The wind tunnel experimental setup used was as shown in the Figure 4-3. T1 was tested with its root system in sand and T2 was tested in both sand and clay. T1 has a more symmetrical root system and T2 had an asymmetrical root system as shown in Figure 4-4 & Figure 4-5 more detailed description of the tree saplings T1 and T2 are provided in Chapter 3.

Measurements of the movements and loads on the tree, roots and soil were made with video images, laser range finders, strain gauges and accelerometers. The incoming wind fields were measured using hotwire anemometers and pitot tubes. Wind speeds were increased in step increments until the trees were uprooted. Tree saplings were also tested under static pull loads to failure. For further details on the experimental procedure and test setup, refer to Chapter 3 of this thesis. This experimental study was conducted to understand the dynamics of tree-root-soil interaction under wind loading.

4.4.1 Initial similitude assessments

To assess the similarity between the tree sapling (TS) and the field tree (FT), characteristic variables from both of the experiments need to be compared. Similarity and scaling is studied through few dimensionless parameters, and through geometric, elastic and stress similarity assessments and comparison. As the field tree winching test (Chapter 2 of this thesis) was conducted in its natural physical surroundings and the tree sapling wind tunnel tests (Chapter 3 of this thesis) were conducted using the natural tree saplings (i.e., the model was not fabricated), prototype and the model physical parameters are unalterable. Geometric, mechanical and dynamic properties of the model and the prototype are also unchangeable. Through these two experimental techniques (field tree winching test and tree sapling wind tunnel tests), the goal is not necessarily to equate and scale the response, but to understand the differences between the sapling and a mature field tree response and compare the results. In this section, tree saplings (TS), T1 & T2 used in the wind tunnel experimental study are compared with a mature field tree (FT) to identify the similarities. In both the tests, trees species used were **Norway spruce** (***Picea abies***) species. Morphological and dynamic properties of FT and TS are listed in Table 4-1.

Stem density of the field tree and the tree saplings used for the testing were estimated using the tree geometrical properties and the weight estimates collected from the tests. Also using the Norway spruce biomass function given by Repola et al. [2007]. Stem density (ρ_s) including bark for the winched field tree and the tree saplings are estimated using the following Equation [4-1] (after Repola et al. 2007):

$$y_{ski} = b_0 + b_1 d_{ski} + b_2 \frac{d_{ki}}{t_{13ki}} + u_k + e_{ki} \qquad [4\text{-}1]$$

Where, y_{ski} is the stem density in kgm^{-3}; d_{ki} is the tree diameter at breast height in cm; d_{ski}= 2+1.25d_{ki}; t_{13ki} is the tree age in years and the empirical parameters given by Repola et al. [2007], for the Norway spruce are b_0=442.03, b_1= -0.904, b_2=-82.695, u_k=73.69, e_{ki}=524.74. Both the estimates were very close with less than 5% difference; hence the average values were taken as shown in Table 4-1. Modulus of elasticity of the stem was estimated from the three-point bending tests of the sample collected from the tree stem. Modulus of elasticity of the winched tree was 1.2 GPa and for the tree saplings modulus of elasticity varied from 0.6 to 0.7 GPa; an average of 0.65 GPa is used for further calculations. The remaining morphological properties were as listed in Table 4-1.

Dynamic properties of the mature field tree were estimated using the conducted manual pull and release sway tests, the response data of the tilt sensor which was attached close to the tree centre of mass was used to calculate the dynamic properties. Dynamic properties of the tree saplings presented in this chapter were also estimated using the pull-and-release tests conducted in a similar way as field tree. In both the field tree winching test and the tree saplings wind tunnel tests, the response data of the sensors attached close to the tree centre of mass were used to estimate the tree dynamic properties. Assuming viscous damping (i.e. damping proportional to velocity), damping ratio is estimated using the logarithmic decrement method [Appendix I]. To attain similar conditions in estimating the damping, pull-and-release tests response data was used and in each measurement six cycles were used to estimate the damping decrement. Natural frequency of 0.35 and damping ratio of 0.051 were estimated for the field tree. Damping ratio of the Norway spruce field tree and the tree saplings ranged from 0.041 to 0.069. Among all of the examined trees, the tree sapling with the symmetrical root system (T1) in sand showed the highest damping. The

tree sapling with the asymmetrical root system (T2) in both sand and clay showed lowest damping in the sand.

Critical damping coefficient and the damping coefficient were estimated as shown in Table 4-1, total mass of the tree structure (W) as listed in the Table 4-1 is used for the calculations. Critical damping coefficient and the damping coefficient estimates of the tree and the saplings were as shown in the Table 4-1. The damping coefficient of the mature field tree was 5.87 kg.s/m and for the tree saplings damping coefficient of T1 was 0.041 kg.s/m and T2 damping coefficient in sand was 0.3 kg.s/m and in clay, 0.35 kg.s/m. damping coefficient of T2 with asymmetrical root system was low in sand compared to clay. A drag coefficient of 0.35 is used as given by Mayhead [1973] for the mature Norway spruce trees. In the case of tree saplings, T1 was tested in the wind tunnel with the stem base on the force balance. The drag coefficient estimates were given in Chapter 3; at 5.87 m/s velocity the calculated drag coefficient was 0.76.

Root-soil plate properties are also listed in Table 4-1. The field tree diameter of the root plate was about 3.25 m with an average root plate depth of 0.9 m. The tree saplings had a root plate diameter of 0.6 m and 0.56 m respectively, which scales 1:5.4 and 1:5.8 respectively with the field tree. Modulus of elasticity of the tree sapling roots were around 10 times lower than the field tree root estimates. Anchorage failure loads of the field tree were estimated using the tangent intersection method as given in Chapter 2. The failure base bending moment, vertical load, and the rotation of stem base are as given in Table 4-1.

Since the tree sapling (T2) in clay did not uproot, failure wind load was also estimated using the tangent intersection method as explained in Chapter 2. The root plate anchorage failure ratio (M/θ) of the field tree was 4107 kNm/rad and for the tree saplings varied from 0.037 to 0.75 kNm/rad. The base bending moment failure stiffness of the tree saplings was much lower than the field tree. Two very important points to note here are i) the tree sapling root plate was only the structural part of the root plate, all of the fine fibrous roots were removed (which help to anchor the tree) before the wind tunnel testing, ii) the tree sapling root plate was tested in poor graded dry silica sand which does not have any appropriate

cohesion (c′=0) making the anchorage strength very low. In addition, the field tree anchorage strength was a lot higher than an average forestry tree because of the tree location [Chapter 2].

4.4.2 Geometric, elastic and stress properties

To compare the similarity between model and the prototype, three important similarity requirements were examined: i) geometric ii) kinematic and iii) dynamic similarity. Geometric similarity is examined through structural similarity between the model and the prototype. In this study geometric similarity is examined by comparing the field tree structure to the tree sapling structure. Relative diameter (diameter at the chosen section/ highest diameter of the stem) of the field tree variation across the relative tree height (stem section height above the ground/ total tree height) is compared to the tree sapling in Figure 4-6. Relative diameter of the field tree was low compared to the tree saplings. The tree saplings also showed different variations of relative diameter along the length of the tree height. It is interesting to note, that all of the examined trees showed constant relative diameter of 0.6 at 0.4 relative tree height. As the mature field tree and the tree saplings are Norway spruce trees and have similar structure, decrease in diameter with increase in height can be seen. The mature tree showed lower relative diameter values with increase in relative tree height compared to the tree saplings. It should be noted that for both sets of tests, the above ground positions of the tree structure were pruned at similar relative heights. It can therefore be considered that the structural similarity (geometric similarity) is maintained, but one important factor to note here is that slenderness ratio of the field tree was twice as high for the mature tree compared to the sapling.

Kinematic similarity means similar velocity field and stream line pattern, where as dynamic similarity means similar pressure distribution and wind generated forces are similar [Liu 1991]. As the field tree was only winched and swayed manually, kinematic and dynamic similarity cannot be examined between the model and proto type with the available data for this study. In the wind tunnel testing of the tree saplings, open terrain flow was maintained [Chapter 3] assuming the response would be similar to the field tree response under such wind conditions. For both the wind tunnel and field tree studies, wind pressure and forces were calculated using the same drag force equation with the listed scale factors

in Table 4-1. The kinematic and dynamic similarities are inseparable, as long as the geometric similarity is maintained, if the flow is kinematically similar it also means dynamic similarity is achieved [Liu 1991].

The problem with experimental scale modelling is creating model and test conditions with perfect geometric, kinematic and dynamic similarities. There are always some compromises in all of the studies that were reviewed [Finnigan and Mulhearn 1978, Stacey et al. 1993, Kelly et al. 2006, de Langre 2008, etc.]. In this study, even though kinematic and dynamic similarity cannot be fully compared, making use of available experimental data, elastic and stress similarity between the model and the prototype are compared as shown in the Figures 4-7 and 4-8 respectively.

Elastic similarity of the model and the full scale tree are compared using the bending stiffness along the length of the tree. By assuming the tree to be a cantilever bean, the bending stiffness can be taken as $\frac{3EI}{L^3}$. Modulus of elasticity (E) is taken as constant across the length of the tree. Stiffness is proportional to moment of inertia, i.e. stiffness is proportional to d^4. The comparison was made between the model and the prototype by plotting the relative stiffness $\left(\frac{d_i^4}{DBH^4}\right)$ vs relative height (H_i/H). The bending stiffness comparison of the field tree with the tree saplings is as shown in Figure 4-7. The relative stiffness of the prototype and the tree saplings varied equally up to a relative tree height of 0.25, above the ground level. Relative stiffness of the field tree was very low above a relative tree height of 0.25, indicating mature trees are highly flexible in their upper regions above ground level. Significant decrease in tree relative stiffness above the height of 0.25H with increase in tree age or height (H) is therefore observed.

Stress similarity between the full scale tree and the tree saplings were compared using the variation of base bending response with stem base rotational response [Figure 4-8]. In the stress similarity comparison, one very important point to note is: the maximum load here is not the anchorage strength for every tree compared. Only the tree saplings in sand uprooted at the maximum loads are presented in this comparison, it is the stem failure load for the field tree, and the maximum tested load (neither the stem fracture nor anchorage failure happened at this load) for the tree sapling T2 in clay. The stem rotations presented

here were the stem rotation at a tree height of 0.25H above the ground level about the stem base.

As shown in Figure 4-8, the tree saplings in sand showed higher rotational response at similar base bending moments compared to the response in clay. At around 1/3rd of the relative bending moment, the field tree showed 60% of the ultimate rotation, whereas the tree saplings only showed 15 to 20%. The field tree showed quite high rotational response at low stem base bending moments, even though the maximum bending and rotational responses presented are not the anchorage failure loads.

4.4.3 Physical modelling of flexible structures in wind tunnels

Scaled physical model testing in boundary layer wind tunnels is now a common approach for determining wind loads on tall buildings. Simulation of the inertial forces and the wind forces on these structures are obtained from wind tunnel testing on aeroelastic models that are appropriately scaled to move in a similar manner to a full-scale building. Significant work has been conducted on the development of experimental techniques for wind tunnel testing and appropriate scale modelling of buildings (e.g. Cermak, 1971; Davenport et al., 1985; Whitbread, 1963; Cook, 1990).

Since they are relatively porous, trees are permeable to wind flows. There can be significant differences in the flow fields adjacent to porous bodies compared to classical solid bluff bodies. Wakes can extend further downstream and recirculation zones can be detached. Drag is increased because porous bodies may have much larger surface areas subjected to skin friction. Trees are also flexible, leading to significant fluid-structure interaction. In addition, when trees are in a strong wind field they change shape and have varying aerodynamic properties. Hence similarity criteria that are valid for impermeable rigid buildings may not be as applicable for the modelling of trees. The literature has very few systematic investigations that allow similarity criteria for the aerodynamic modelling of trees to be determined (Gromke and Ruck, 2008).

This section discusses the physical requirements for creating correctly scaled models of trees in boundary layer wind tunnels. The dimensional variables of windthrow will be

expressed using the three fundamental dimensions; length (L), mass (M) and time (T). Hence using the Buckingham Pi theorem, the dimensionless parameters are derived. Dimensional analysis in this study is divided into three categories based on flow properties, structural properties, and load response which are used to derive the following dimensionless parameters. Only the dimensionless numbers governing the physical problem and some of the dimensionless numbers studied by researchers in this problem are considered for the discussion. Length, mass and time scales of the tree saplings tesed in wind tunnel compared to the mature field tree were around 1:17, 1:13 and 1:8 respectively [Table 4-1]. The aspect ratio of the field tree was twice that of the tree saplings.

4.4.3.1 Requirements for modelling structures in atmospheric boundary layers

An important requirement for physical modelling of wind engineering problems is proper simulation of natural wind characteristics and in particular, the formation of a properly scaled boundary layer over the floor of the wind tunnel working section. The general requirements for geometric, dynamic and thermic similarity in wind tunnel models can be derived from inspectional and/or dimensional analysis. Dimensionless groups can be determined from the appropriate equations expressing the fundamental concepts of mass, momentum and energy conservation for the motion of the atmosphere. Some of the more important groups are geometric scaling, the Rossby number, the Richardson number, the Reynolds number, the Prandtl number, the Eckert number, the Jensen number, the Froude number, the Strouhal number and the turbulence intensity. Further discussion of these dimensionless groups is given below.

The Rossby number relates to large scale phenomena in the atmosphere and given the scale of the model this can be ignored. The Richardson number relates to neutrally stratified flows and can be ignored for this type of problem. Since the same fluid is used for the model and full scale testing, both the Prandtl and Eckert numbers are satisfied.

The standard non-dimensional parameters are discussed in Group I and are as listed in Table 4-2, the key non-dimensional parameters for similarity requirements of wind tunnel testing are the following [Cook 1990]:

Strouhal number, π_1 ($f\ell/U_R$): this defines reduced frequency (oscillating flow) and is the ratio of oscillation to the mean wind speed [White 2003]. The length scales, wind speeds, and the natural frequencies of the full-scale and 'model-scale' tree are matched through the Strouhal number. In this study, it is taken as constant for the full-scale and the model value, as the natural frequencies of the model and prototype are known, reference velocity is estimated by equating the Strouhal number of the model trees (tree saplings) to the prototype (field tree).

Strouhal number ($f\ell/U_R$) of T1 is calculated using the reference velocity of 5.87 m/s. Reference velocity of T2 and the field tree are calculated by equating the T1 Strouhal number to the T2 and field tree Strouhal numbers. Hence reference velocities of T2 and field tree were taken as 5.9 and 12.28 m/s respectively.

Reynolds number, π_2 ($\rho U_R D/\mu$): this assesses the relative importance of fluid inertia and viscosity. This is difficult to match at full scale and is around 2 orders of magnitude smaller in most wind tunnel tests. Reynolds number is above 2000 where the flow transitions from laminar to turbulent. This shows the flow is turbulent for all tested wind speeds. However, the Reynolds number can show independence with wind speed. Since the drag coefficient for the saplings is constant for the majority of wind speeds (see Chapter 3), this is likely the case.

Jensen number, $\pi_3(\ell/z_o)$: Relates scale factor of structure to the atmospheric boundary layer simulation. For the open country profile used in this study, the roughness length is 0.012 m [Case and Isyumov 1998]. As the wind tunnel testing of tree saplings was conducted with open country profile and the same is assumed for the field tree, Jensen number would not change. However, with such a small length scale (1:20) a full boundary layer cannot be achieved. Hence the flow profile created will represent the lower parts of the boundary layer and will provide only a boundary layer-like flow with some turbulence but likely not enough shear.

Froude number, π_4 ($g\ell/ U_R^2$): is the ratio of gravitational to the inertial forces of the flow. Field tree Froude number was around four times higher. Indicating higher gravitational forces of the field tree compared to the tree saplings.

Euler number, π_5 ($F_d/\rho\ell^2U_R^2$): gives the reduced drag coefficient estimate. From the Table 4-2. The results were around 2.5 times higher for field tree.

Cauchy number, π_6 ($\rho_f . U_R^2 . \left(\frac{L}{D}\right)^3 / E$): The modified Cauchy number with slenderness factor was also examined by De Langre [2008]. It is a dimensionless number representing the ratio of dynamic pressure and modulus of elasticity. Modulus of elasticity of saplings was half as much compared to the field tree, and the slenderness of the field tree was twice as much compared to the tree saplings. The Cauchy number estimated was one order higher for the field tree compared to the tree saplings, representing higher deformations under the wind load.

4.4.3.2 Dimensional analysis of the above ground components

To derive appropriate dimensionless parameters of a tree structural response to dynamic forcing; the above ground tree structure can be assumed to be acting as a cantilever with frontal area. From structural dynamics, the vibrational response of a cantilever can be expressed with the Equation [4-2]:

$$F(E, I, m, \ell, D, \rho_s, g, \rho, f, U_R, g, c, C_D)=0 \qquad [4\text{-}2]$$

Where as E = stiffness [$ML^{-1}T^{-2}$]; I = mass moment of area [L^4]; m = mass per unit length [ML^{-1}]; ℓ (L)= length [L]; D = diameter [L]; ρ_s = structural density [ML^{-3}]; g = gravitational coefficient [LT^{-2}]; ρ = fluid density [ML^{-3}]; f = frequency [T^{-1}]; U_R = fluid velocity [LT^{-1}]; c = damping coefficient [$ML^{-1}T$]; and C_D = dimensionless drag coefficient.

Dimensionless parameters derived from this group with dimensional analysis are as shown in Table 4-3 and are discussed below in detail. The dimensionless parameters are named based on the characteristic significance. The dimensionless parameters of response in Group II are similar to those found by Finnigan and Mulhearn [1978]; Stacey et al. [1994]; and de Langre [2008].

The following parameters: density (π_7), slenderness (π_8), mass (π_9) and stiffness (π_{10}) ratios of the model and prototype were estimated to understand the geometric scaling and are listed as shown in Table 4-3. Slightly lower values of field tree compared to tree saplings was observed.

Aero-elastic response factor, π_{11} ($\rho . C_D . L^5 . D . f^2 / EI$): It was one order higher for the field tree. In the case of the wheat stalk study by Finnigan and Mulhearn [1978], the ratio varied from 0.7 to 1 with increase in wind speed. This shows that the model (tree sapling) was not a very good aero-elastic model for the prototype (field tree).

Frequency factor, π_{12} (f(m/E)$^{1/2}$): It was around 20% lower for field tree, indicating that high elastic forces will occur for the field tree.

Mass factor, π_{13} (mg/EL): The mass factor listed was around two times higher for the field tree compared to the tree saplings. For the experimental model (synthetic model) developed by Stacey et al. [1994], the mass factor was half as much compared to the field tree. To obtain the desired natural frequency, the mass factor was kept low for the synthetic model with increased bending stiffness by Stacey et al. [1994]. It this study, with the use of natural trees, desired natural frequencies are achieved.

Damping factor, π_{14} (c f^2/(Em)$^{1/2}$): this was slightly higher for field tree compared to tree sapling, T2. This could be because of relatively higher damping of field tree.

Elastic response factor, π_{15} (E/ρU$_R^2$): this was almost twice as much for the model compared to the field tree, because of the lower flow induced forces of tree saplings.

Mode shape factor, π_{16} ($m . L^4 . f^2 / EI$): The mode shape factor was 4 to 5 times higher for the field tree compared to the tree saplings. Modelling of waving crops in a wind tunnel study presented by Finnigan and Mulhearn [1978] showed that the mode shape factor was 4 times higher for a nylon model compared to a prototype. In such a case of higher difference, it is suggested by Finnigan and Mulhearn [1978] to compare the mode shapes to assess the differences.

Damping factor, π_{17} $(c.L^4.f/EI)$: the damping factor of the tree saplings was around two orders of magnitude lower than the field tree. The difference is quite high. The causes could be: i) the damping coefficient was estimated assuming single degree freedom system with viscous damping and ii) root-soil plate strength and weight are very different to the actual scenario. A lot more trial and error experimental and analytical work needs to be conducted to equate the two.

Gravitational factor, π_{18} $(m.g.L^3/EI)$: the gravitational factor of the field tree was around 17 to 30 higher than the tree sapling. As the model physical parameters are unchangeable, these are differences between the field tree and the tree sapling.

4.4.3.3 Dimensional analysis of the below ground components

For all structures that lie within or are made of soil, similarity of soil strain in both vertical and horizontal directions need to be examined [Hamada and Tsuchiya 2004]. To derive the dimensionless parameters of the below ground tree structure, the soil-root plate response can be assumed to be the cyclic response of a foundation and can be expressed as in Equation [4-3]:

$$F(M, V, \theta, \rho, \gamma', D, P_a)=0 \qquad [4\text{-}3]$$

Where, V = vertical load [MLT^{-2}]; θ = rotation, rad; M = moment, [ML^2T^{-2}]; ℓ (L)= length [L]; D = diameter [L]; γ'= Soil unit weight, [$ML^{-2}T^{-2}$]; ρ = fluid density [ML^{-3}]; U_R = fluid velocity [LT^{-1}] and P_a=atmospheric pressure [$ML^{-1}T^{-2}$].

All of the dimensionless parameters (Group III) in Table 4-4 are taken from Kelly et al. [2006] and Stacey et al. [1994]. In this study, to model the below ground structure of the tree, load factors acting on the tree foundation (root-soil plate) are compared between the field tree and the tree sapling tests. The comparison done by Kelly et al. [2006] was between field and laboratory caisson foundations in sand and clay. In this study, similar dimensionless parameters are chosen for comparison.

Bending moment coefficient at stem base, π_8 $\left(\frac{M}{\left(\frac{1}{2}\rho_f U_R^2 L^3\right)}\right)$: It is taken from Stacey et al. [1994], the bending moment coefficient for the stem base was estimated using failure bending moment values for both the field tree and the tree saplings. This was higher for T2

and highest in the sand. In clay, the T2 bending moment coefficient was twice as high compared to the field tree. The lowest was for the T1 test in sand. This is reasonable since T1 showed minimal anchorage strength in sand. The closest representation to the field tree from the tested scenarios would be T2 in clay.

Moment load factor, π_9 $(M/\gamma'.D^4)$: This is 1 to 2 orders of magnitude higher for the field tree compared to the tree sapling. As the estimated failure moment load of the field tree was very high, a few more failure loads of the uprooted trees of similar dimensions also need to compared.

Rotational response factor, π_{10} $(\theta.(P_a/\gamma'.D)^{0.5})$: The failure rotational response factor was 35 to 65% higher for the field tree compared to the tree sapling response. This factor also shows field tree response could be closely represented by the tree sapling and clay setup.

Vertical load factor, π_{11} $(V/\gamma'.D^3)$: The vertical load factor of the field tree was 2 orders of magnitude higher compared to the tree saplings.

From the examined dimensionless factors, it appears the field tree was relatively more flexible and heavy compared to the tree saplings in the wind tunnel. It might be rectified by better maintaining the tree freshness while testing in the wind tunnel, which in tern would improve the tree sapling flexibility. Secondly the possibility of hanging a weight in the middle of the root plate (with out disturbing the tree-root structure) can be experimented, this might help maintain the similitude with respect to gravitational forces and response.

4.4.4 Stem base load transfer to root system

Fundamental to understanding of the complex dynamic response of the tree and its survival strategy is the knowledge of energy transfer [James et al 2006]. An attempt has been made to deduce the energy transfer from the foliage to root system with increase in static pull load and wind speeds. To understand the energy transfer to root system and to compare the full-scale tree response to the tree sapling response, bending moment responses of the tree roots to the respective stem responses were compared as shown in Figure 4-9. Only T1 is

chosen for this comparison, as the T1 root system has a symmetrical root plate architecture, similar to the field tree (FT). Windward and leeward root responses were compared for better understanding of the root anchorage mechanics under wind loading. The strain gauges attached on the roots, close to the field tree stem were used for the presented data in Figure 4-9.

The peak leeward root response of the field tree (FT) was around 9 times higher than its windward root response. In the case of tree sapling (T1) response, the peak bending response of leeward root was around 7 times higher than the windward root response with increase in base bending moment. At around one third of the load increase (base bending moment compared to failure base bending moment), the ratio of load stem (base bending moment) to the root bending moment was estimated for comparison. For the FT, this ratio was 500 for the windward root and 59 for the leeward root; whereas for T1, it was 100 for the windward root and 50 for the leeward root. Thus for the field tree, it is clear that a much lower load was transferred to the root system, especially the windward root compared to the T1 root response. The reason could partly be due to static to dynamic loading differences between the two scenarios, greater stability of a more mature root architecture and the soil rooting medium.

4.5 Static to dynamic load response comparison

In the wind tunnel, the tree saplings were tested through step increments of static and dynamic loading. The response of any structure to any given loading not only varies with the properties of the structure, but is also very much dependent on the type of loading. It is equally important to understand the key differences between loading to compare the response. In this study, the pull load is assumed to be static and the wind loading dynamic. A key difference between the static and dynamic loading in this experiment is that the pull load is increased monotonically, whereas the wind load is applied by a number of gusts, which vary in magnitude with time making the load transfer frequency dependent. It is worth noting that for the sand medium, the soil was dry and therefore represents essentially a drained response, whereas the clay would show undrained response.

The applied wind and the tree sapling responses are studied in detail to better understand the dynamic wind loading and the corresponding response. To examine the effect of soil and root plate architecture on dynamic response, tree sapling (T1 & T2) responses with T1 (symmetrical root system [Figure 4-4]) in sand and T2 (asymmetrical root system [Figure 4-5]) in both sand and clay are analysed.

To examine the difference between static and dynamic load responses, secant modulus of rotation and dynamic load factor are estimated from sand and clay tests of T2 under both static and dynamic conditions. The response comparisons are also made with change in load direction. To examine the load response in both sand and clay, only the T2 sapling tests are analyzed in this comparison.

4.5.1 Dynamic load and response

The aim of this section is to understand the dynamic loading and corresponding tree response. The base bending moment response with respect to the stem rotational response of each tree sapling in each test scenario were analyzed with incremental wind speed. The strain gauge sensors attached to the tree stem base and the laser transducers pointing the tree stem in windward direction [Figure 4-3] were used to track the base bending response and stem deflection respectively. Bending moment responses and the corresponding angle of deflections of T1 in sand, T2 in clay, and T2 in sand with increase in wind loads are as shown in Figures 4-10, 4-15 and 4-20 respectively. These show generally non-linear increases with wind loading. It is clear from the bending and rotational response that for sand sudden rotational responses were seen, where as for the clay, base bending moment responses were correlated with increase in wind load. From the bending moment vs rotational response plots, an interesting pattern can be observed. This pattern is called ratcheting.

Ratcheting is a phenomenon were sudden increases and decreases in rotational or bending moment response occur under instantaneous loads. In soil mechanics, progressive accumulation of plastic deformations under cyclic loading in granular soil is explained by ratcheting behaviour [Alonso-Marroquin 2004, Alonso-Marroquin and Herrmann 2004, Garcia-Rojo et al. 2004, McNamara et al. 2008, Cuellar et al. 2009]. This phenomenon has

been seen in various monotonic and cyclic tests (e.g. Shear box and model piles Cueller et al. [2009]) and is thought to be due to sequential coupled densification and convective soil behaviour phases near rigid boundaries or structures.

In order to better understand the ratcheting, the number of wind load cycles, base bending moment response, the load and responses were separated in to a number of cycles. To count the number of cycles and find the characteristics of each cycle, a RAINFLOW counting algorithm is used.

Rainflow algorithms were originally developed by Matsuishi and Endo [1968], it is a popular cycle counting technique. In this study, cycle counting is conducted using the rainflow counting algorithm of MATLAB software. This algorithm code was developed by Adam [2010] according to ASTM E1049-85 standards. Detailed cycle counting methodology is explained in Appendix II.

To examine the ratcheting patterns and to understand the dynamic load and response: wind load, rotational response and the base bending moment response data sets at three selected incremental wind loads from each experiment were chosen. Using the RAINFLOW counting function, cycles amplitude, cycles mean value and number of cycles from each chosen data set were estimated. Along with counting of the number of load and corresponding response cycles, the effect of increase in load (wind speed) and the corresponding response (stem base bending moment and rotational response) with it were also examined using the cycle mean value data. The rainflow cycles mean value data from each selected load increment from the three experiments is statistically analysed and compared. To examine the peak gusts and the corresponding peak responses of dynamic load and response, rainflow cycles amplitude data of the load and responses are analyzed and compared. The trends of increase in peak loads and the peak responses with increase in wind speed increments are also discussed. To understand the load transfer at different frequencies, the coherence between the wind load and tree sapling (T2) response in sand and clay are examined.

4.5.1.1 Rainflow counting and statistical analysis

The wind loading in the wind tunnel was applied in step increments; load was applied for 180 seconds for each increment. Each load and the corresponding response data sets represent data at constant wind speed for the 180s interval. For each wind speed data set in sand and clay, the total number of cycles estimated using rain flow methodology and are as shown in Figures 4-11, 4-16 and 4-21.

In Figure 4-11, rain flow count test of T1 in sand is presented. The sampling rate of this test was 200 Hz. Wind speed, base bending moment and rotational response about the stem base at the three selected wind speeds are as shown in Figure 4-11. The number of cycles per second of the applied wind speed are higher than the base bending moment response and rotational response cycles. Rotational response cycles about the stem base were found to significantly increase with increase in wind speed.

For the T2 test in clay, the number of cycles were presented as shown in Figure 4-16. The sampling rate of this test was 300 Hz. The number of base bending response cycles of this test have significantly increased with increase in wind speed. Even though the rotational response cycles have also increased with increase in wind speed, the increment was much lower compared to the base bending response cycles.

For the T2 test in sand, the rain flow cycle count is as shown in Figure 4-21. The sampling rate for this test was also 300 Hz. In this test, the number of cycles increased with increase in wind speed for the load and also for the response, as the wind load recorded here are by pitot tube. In this test, the number of bending response cycles significantly increased with increase in wind speed compared to the rotational response cycles. From all of rain flow cycle count results, it is clear that the rotational response had lower number of cycles compared to bending moment responses.

The frequency distribution of the cycle mean values were compared and statistically analysed, as shown in Figures 4-12, 4-17, and 4-22. Along with the mean and variance of the distribution, the non dimensional statistical parameters (moments), such as coefficient

of variation, skewness and kurtosis are presented for each data set [Figures 4-12, 4-17 and 4-22].

If X and Y are taken as the data vectors at each wind load increment, μ1 and μ2 are the means, σ_1^2 and σ_2^2 are the variances of X and Y respectively. For a continuous type random variable X, mean, μ=E[x] and variance, $\sigma_2 = E[(x-\mu)^2]$. The ratio of standard deviation (σ) to the mean (μ) is called the *coefficient of variation* and it shows the extent of variation in relation to mean. *Skewness* is the ratio of $E[(x-\mu)^3]$ to σ^3, which is a measure of asymmetry of the system. If skewness is zero, the probability density function is symmetric with respect to its mean value [Ochi 1990]. If the value is positive, the tail of the probability density function is fatter or longer on the right side than the left side and vice versa if the value is negative. *Kurtosis* represents the degree of peakedness of the sway distribution and is the ratio of $E[(x-\mu)^4]$ to σ^4 [Ochi 1990]. For a normal distribution, the kurtosis value is equal to 3. If the value is less than 3, distribution is called platykurtic (mild peak) and if the value is greater than 3, the distribution is called leptokurtic (sharp peak). The moments, covariance and correlation coefficient of each data set are also presented with each density distribution plot.

The frequency distribution of the cycle mean values of T1 in sand are as shown in Figure 4-12. Variance of both load and response have increased with increase in wind speed. Coefficient of variation (extent of variability from mean) of the wind load decreased with increase in wind speed, but the response data showed initial decrease and increase in the coefficient of variation. Rotational response showed the highest extent of variability from the mean. At the lowest wind speed (1.87 m/s) presented, the wind tunnel is not stable; so discarding those values, the wind load showed normal distribution with skewness values near zero and kurtosis near 3. The bending response had negative skewness and >3 kurtosis, representing higher than mean values and a more outlier prone distribution. Rotational response had positive skewness and higher kurtosis before the failure wind speed, hence a smaller than mean value distribution with more outlier prone data at high wind speeds. For test of T2 in clay as shown in Figure 4-17, variance of load increased slightly with increase in wind speed. Near zero variance of rotational response and significant increase in bending response variance with increase in wind speed are observed. The coefficient of variation

(extent of variability from mean) of wind load and rotational response decreased with increase in wind speed, but the bending response data showed initial increase and then, decrease in coefficient of variation. Bending response showed higher variability from the mean with increase in wind speed compared to the rotational response. Near zero to slightly < 0 values of skewness represent close to mean value to slightly higher than mean value distributions of load and response data. Kurtosis values of the response data were also very close to 3, indicating a normal distribution. For the clay case higher variance, coefficient of variation, and negative skewness values of bending response compared to rotational response indicates sudden increases of bending moment responses compared to rotational response.

In Figure 4-22, test T2 in sand is presented. Mean values of the distributions are as presented. Variance of rotational response was low and significant increase in bending response variance with increase in wind speed was observed. Coefficient of variation of response data remained low except for the rotational response at high wind speed. Near zero skewness values for bending response and slightly >0 skewness values for rotational responses were observed. Kurtosis values of the response data were also very close to 3, indicating normal distribution. Even though in the sand, rotational responses were shown to be more sudden and abrupt [Figure 4-20], statistical analysis did not show much difference. Except for the coefficient of variation being high at high wind speed for the rotational response, no other statistical parameter showed any indication of sudden increases in rotational response data compared to bending moment response. This means any rotational increases for sand were abrupt and occurred over few cycles, unlike the clay conditions.

4.5.1.2 Peak gusts and the trend following the peak gusts

To examine the peak gusts and the peak responses, the rainflow cycle amplitudes of the load and responses are further analyzed and compared. To examine the trend *following* the peak gusts, the load and response data need to be cross-correlated. Since the rainflow cycle data does not follow the sequence i.e. information on cycle order is lost during analysis, correlation between the load and response could not be done using rainflow cycles amplitude data. However significant cycles amplitude statistics of load and response data

are estimated. The concept of significant wave height estimate is taken from ocean engineering; the significant wave height ($h_{1/3}$) is defined as the mean wave height of the highest one third of the waves. This significant wave height in ocean engineering or the significant value is a useful statistical measure to examine the severity of a random process [Ochi 1990]. To learn more about the ratcheting, the highest (peak) of cycle amplitude values of load and response data of each load increment were also compared.

In ocean engineering the wave height distribution is assumed to be a Rayleigh function. The significant wave height estimate is conducted using this Rayleigh distribution. This gives the mean of the highest 33% of the amplitudes. It is given by $1.048\sqrt{R}$, where R is the Rayleigh distribution parameter. As R is also equal to 8 times the variance, it can also be simplified to $h_{1/3} = 4.01\sqrt{m_0}$. where, m_0 is the area under the spectral density function or the zeroth moment of the Rayleigh distribution. The significant cycle amplitude or significant magnitude (significant wave height) of the load and response with increase in wind loads are calculated for tests T1 and T2 as shown in Figures 4-13, 4-18 and 4-23. Peak gusts (maximum amplitude of rainflow cycles amplitude distribution or peak wave height) and the corresponding responses were also compared as shown in Figures 4-14, 4-19, and 4-24.

In Figure 4-13, significant amplitude estimates of T1 in sand from rainflow cycles amplitude distribution are presented with increase in wind speed. Rate of increase in significant magnitude of wind speed with increase in wind speed, i.e. the slope of the trend line fitting the significant magnitude distribution with increase in wind speed was much higher compared to the slope of the response trend lines. The bending response had the lowest slope meaning the increase in significant magnitude with increase in wind speed but only because of the high rotational response at the failure load. In peak magnitude comparison [Figure 4-14], the absence of rotational response value at the failure load showed the lowest slope for the rotational response. In sand, T1 showed significant increase in rotation and decrease in base bending response at failure.

In Figure 4-18, significant magnitude variation of T2 in clay with increase in wind speed is presented. The slope of base bending moment trend line was much higher in this case,

significant increase in bending response with increase in wind speed. The slope of rotational response was negative, indicating the decrease in significant amplitude of rotation with increase in wind speed. Peak magnitude variation in Figure 4-19 also showed similar response but with much higher increase in bending response with increase in wind speed. As in Figure 4-15, T2 in clay clearly showed abrupt increases in bending responses, this clearly explains the significant magnitude variation.

In Figure 4-23, T2 is sand case is presented. The slope of base bending moment trend line was much higher in this case too, meaning significant increase in bending response with increase in wind speed. The slope of rotational response was not-negative, indicating the increase in significant amplitude of rotation with increase in wind speed but the increase was lower compared to the bending response. From Figure 4-24, peak rotational response of T2 in sand was also high at failure wind load similar to T1 response. However, this showed very different peak bending moment response, the increase was not steady but more of increasing and decreasing pattern was seen. As in Figure 4-20, T2 in sand showed abrupt increases in rotational responses. But from the significant magnitude variation of bending response had higher slope. The ratcheting of T2 in sand [Figure 4-20] with asymmetric root system was not as abrupt as the ratcheting of T1 in sand [Figure 4-10]. The reason could be, T2 in sand with asymmetrical root was slowly settling in sand than ratcheting, showing more anchorage strength. Further investigation is needed.

4.5.1.3 Coherence

To further check the correlation between load and response, coherence was examined. As coherence represents the correlation in the frequency domain, it is measured to understand the load transfer from wind to tree to root system at different frequencies and hence the tree stability. From Gardiner [1995], this parameter imitates the real tree properties at different frequencies. Coherence between the load and response data at three increments of wind speed is presented in each case. Coherence of wind speed vs bending response and wind speed vs root response of T2 in sand and clay are presented as shown in Figures 4-25 and 4-26 respectively. High coherence means higher load transfer at that frequency.

As shown in Figure 4-25, T2 in sand showed the highest coherence at the tree natural frequency, root coherences were also higher at root natural frequencies. In the case of clay [Figure 4-26] too, a similar trend was observed, coherences in clay were a bit lower compared to the sand case. This may explain the lesser load transfer to the root system in the clay.

4.5.2 Secant modulus of rotation

Secant modulus is the ratio of stress to strain at a chosen point on the stress-strain curve, with the initial stress and strain values as zero. To calculate the secant modulus of rotation, stem base bending moment was plotted against stem base rotation. Before each test, stem base bending moment and rotation were kept zero, and the secant modulus of rotation is the ratio of base bending moment to the stem base rotation at each selected load. The base bending moment response recorded by the strain gauge sensor attached to the lower tree stem in windward direction, and the rotational responses recorded using the middle laser transducers were used to compute secant modulus of rotation. The T2 instrumentation set-up and the locations are as shown in Figure 4-3. The variation of secant modulus of rotation in clay and sand under static and dynamic loading conditions are as shown in Figures 4-27 and 4-28 respectively. In both cases, sharp initial increase and decrease in secant modulus with increase in rotation was observed. Similar trends in secant modulus variation of Norway spruce tested through winching was also observed by Jonsson et al. [2006].

For the case of clay [Figure 4-27], the initial increase was the same for both loading conditions, until the maximum stiffness value was reached in the static loading case. In the static loading case, decrease in secant stiffness was very low compared to the dynamic loading condition. In the dynamic loading case, secant modulus variation under dynamic loading condition was very high initially and the dropped below the static loading stiffness and increased slightly and again started showing a trend of decrease in stiffness with increase in rotation (two peaks were observed with increase in wind speed). A similar trend was also observed by O'Sullivan and Ritchie [1993] when a tree was subjected to cyclic loading, who suggested the reason was progressive failure. In this case too the tree sapling was showing a similar displacement response. When the wind loading was very high (crossed the anchorage strength) the tree moved to a new position rapidly, hence the sharp

drop. At the new location, the anchorage strength was again high showing increasing stiffness (this appears to be a ratcheting phenomenon).

In the case of sand [Figure 4-28], variation of secant modulus under static and dynamic loading conditions showed similar trends of initially high stiffness and steady drop in stiffness with increase in rotation. In the case of dynamic loading, stiffness was much higher compared to the static loading condition. The reason could be the nature of silica sand used, settlement in sand under cyclic loading (dynamic loading) condition is causing more stiffness.

4.5.3 Dynamic load factor

The concept of the dynamic load factor is taken from Blackburn et al. (1988). The ratio of the deflection caused by the dynamic load to that caused by a static load of the same magnitude is known as the dynamic load factor [Blackburn et al. 1988]. The dynamic load corresponding to static load was therefore taken as:

$$F = \frac{1}{2}\rho_f C_A C_D u^2 \qquad [4\text{-}4]$$

Air density, ρ_f; frontal area,C_A; and drag coefficient, C_D of T2 are as shown in Table 4-1. The dynamic load factor of T2 varied from 0.5 to 0.75 for both sand and clay cases [Figure 4-29]. As the load factor was less than 1, deflection caused by dynamic loading is less than the deflection caused by static loading. Dynamic load factor is high if the dynamic deflection is high or deflection caused by static loading of same magnitude is low and vice versa.

Dynamic load factor of T2 in sand and clay are as shown in Figure 4-29. In the case of clay, steady increase in dynamic load factor with increase in loading is observed, i.e. with increase in load, tree stem deflection caused by dynamic load was increasing compared to the deflection caused by the static load. As the secant stiffness in the case of clay [Figure 4-27] was also showing a similar trend with increase in loading, it is clear that in cohesive soils the deflection caused by wind increases with increase in loading, compared to the

static loading deflection. The opposite trend was observed in the case of sand [Figure 4-29]. Due to the settlement in sand, the stiffness is higher and the deflection is lower.

4.5.4 Change in load direction

Finally, the effect of wind direction was explored by positioning the tree sapling, in 0° and 180° orientations with respect to the load direction. The tree stem and corresponding root responses were examined in detail, for both sand and clay soil media. Root response in terms of bending moment responses of roots with increasing wind speed and static pull load (stem base bending moment) in case of clay and sand are as shown in Figures 4-30 and respectively. The tree sapling T2 had an asymmetrical root system [Figure 4-5], at 0^0 orientation T2 faced the wind in such a way that it was expected to have maximum possible strength from root anchorage.

In both the soil conditions, the load transferred to the root system in the static load case was lower compared to the dynamic load condition. In the case of the clay, T2 showed almost the same strength and load transfer in both the directions. In the case on sand, T2 showed only half the anchorage strength in the 180^0 direction. In the case of clay load transferred to the root system was half as much compared to the load transferred in the case of sand. It is interesting to note, the anchorage strength of the tree sapling (T2) was almost half in the case of sand compared to clay.

It has been studied previously that the tree root systems grow in response to wind action and soil conditions which consequently effects the tree stability [Nicoll and Ray 1996]. This study provides the quantitative difference of load transfer (tree stability/soil-root plate anchorage) with change in load type, and directions, and soil conditions.

4.6 Discussion

4.6.1 Full scale to sapling comparison

In this study, the winching response of a full scale tree is compared to the tree saplings response in a wind tunnel. The comparison was intended to help understand the similarities and differences in responses between the mature tree and tree saplings. The mechanical and physical factors and responses of the full scale and the tree saplings are presented and

compared. Geometric and elastic similarity between the full scale and tree saplings was compared, slenderness ratio (L/D) of the field tree was twice as much compared to the tree sapling. From the stress similarity comparison [Figure 4-8], the tree saplings were much stiffer when tested in the wind tunnel compared to the in-situ field tree. Relative load transferred to the root system was around thirty times higher for the tree sapling in sand compared to the mature tree.

The dimensionless parameters were generally different between the full scale and model. The calculated scaling factors and the dimensionless parameters gave us an idea/boundaries of variation between the full scale tree and the tree saplings. Overall comparison leads to an understanding of relatively lower flexibility and weight of tree stapling compared to the field tree. Sensitivity of tree biomechanical properties with age and drying seems to more significant. A lot more trial and error experimental and analytical work needs to be conducted to equate to achieve more balance in similitude.

The ratio of the model frontal area to the cross section of the wind tunnel is called the blockage ratio. Blockage ratio is preferred to be as small as possible, even with blockage ratio as low as 5% discrepancies with aerodynamic characteristics were noticed by some researchers [Takeda and Kato 1992]. These discrepancies are generally corrected using correction factors. In this study, blockage ratio was around 4% but considering the scope of this work, correction factors were not considered. In this study, only the first mode of vibration is examined, testing the first three modes of vibration would improve the understanding on tree dynamic response even more. By conducting more studies of this kind, boundary conditions can be established and every aspect of the full-scale tree stability can be examined with the flexibility and simplicity of tree sapling wind tunnel tests.

4.6.2 Static and dynamic load response comparison

The most common way described in the literature to understand tree response to wind load has been by winching the tree and the dynamic properties were studied through swaying the tree or by long term monitoring. As it is challenging to identify the exact relation between the static and dynamic load responses, a new approach is presented. Static and dynamic load responses of tree saplings in sand and clay were analysed and compared in

detail. An interesting phenomenon observed during the wind load testing was progressive ratcheting, with the tree experiencing intermittent partial rotational failures, prior to complete windthrow occurring in the case of sand. This is thought to be due to repeated phases of soil densification and convection around the roots during loading. To better understand ratcheting, dynamic loads and responses were analyzed in detail. As the dynamic load is basically a number of random loading cycles which vary in magnitude with time, the rainflow technique was used to count the number of cycles, analyse cycle distribution and identify the peaks gusts and the trend with following peak gusts of load and the resultant response.

The static and dynamic response comparisons were also made using the secant modulus of elasticity and the dynamic load factor. The two soil media showed very different anchorage responses in sand and clay. Even though initial increase in secant stiffness and a sharp decrease was observed in both soil media, the clay showed two peaks under the dynamic loading conditions and was different to the static loading condition. In the sand, the trees showed similar trends in both loading conditions, but stiffness was much higher in dynamic loading conditions. Dynamic load factor also showed very different variation with change in soil media. There is a slight change in the frequency of tree sway in sand and clay. As Strouhal number (fL/V) is the measure of vortex shedding and it changes with frequency, the effect of vortex shedding on the difference in tree sway in sand and clay need to be explored further. As the tree structure is porous, the effect of vortex shedding should be minimal [Belloli et al. 2014].

In this study the root response was also compared under both static and dynamic loadings with change in load direction, for sand and clay. Under static loading the load transferred to the root system was much lower compared to the dynamic loading condition especially in the case of sand. These comparisons give us the clear differences in tree response and hence the stability variation with change in soil media. The saplings showed evidence of optimization for a specific soil type. It would be interesting to air spade the soil from a full-scale tree and replace it with another type to see the differences in anchorage strength to confirm this idea.

4.7 Conclusions

In this chapter, i) scaling and ii) static and dynamic load response differences are examined using new techniques. The response of tree saplings tested in the wind tunnel through novel wind tunnel testing [chapter 3] is compared with a mature tree response tested through winching [chapter 2] using dimensionless parameters. This study showed that, model stiffness properties were on the higher side and gravitational factors on the lower side compared to the prototype. This exercise also indicates that through sensitivity analysis, scaled experimental modelling precision could be improved significantly.

To compare the static and dynamic load response, dynamic load factor and secant modulus of rotation were examined. An interesting phenomenon called ratcheting was observed and is examined in detail using the rainflow technique. The Rainflow technique was shown to be useful to compare the static and dynamic load response. These quantified results would be invaluable in future modelling techniques.

4.8 References

Alonso-Marroquin, F. (2004). Micromechanical investigation of soil deformation: incremental response and granular ratcheting. Uni- versität Stuttgart.

Alonso-Marroquin, F., Herrmann, H.J. (2004) Ratcheting of granular materials. Phys. Rev. Lett. 92(5).

ASTM E 1049-85. (Reapproved 2005). "Standard practices for cycle counting in fatigue analysis". *ASTM International*.

Belloli, M., Fossati, F., Giappino, S., & Muggiasca, S. (2014). Vortex induced vibrations of a bridge deck: Dynamic response and surface pressure distribution. *Journal of Wind Engineering and Industrial Aerodynamics*, *133*(0), 160–168. https://doi.org/http://dx.doi.org/10.1016/j.jweia.2014.06.005

Blackburn, P., Petty, J. A., & Miller, K. F. (1988). An assessment of the static and dynamic factors involved in wind throw. *Forestry*, 61(1), 29–43. http://doi.org/10.1093/forestry/61.1.29

Byrne, K. E., & Mitchell, S. J. (2007). Overturning resistance of western red cedar and western hemlock in mixed-species stands in coastal British Columbia. *Canadian Journal of Forest Research*, 37(5), 931–939. http://doi.org/10.1139/X06-291.

Case, P. C. and Isyumov, N. (1998) Wind loads on low buildings with 4:12 gable roofs in open country and suburban exposures. Journal of Wind Engineering and Industrial Aerodynamics, 77&78 (1998), pp. 107–118.

Cermak, J. E. (1971). Laboratory simulation of the atmospheric boundary layer, A.I.A.I. J., vol. 9, pp. 1746.

Cook, N.J. (1990), *The designers guide to wind loading of building structures - Part 2: Static structures*, Butterworths, London UK.

Counihan, J. (1969). An improved method of simulating an atmospheric boundary layer in a wind tunnel, J. Fluid Mechanics, vol. 3, pp. 197-214.

Coutts, M. P. (1986). Components of tree stability in Sitka spruce on peaty gley soil. *Forestry*, 59(2), 173–197. http://doi.org/10.1093/forestry/59.2.173.

Cuéllar, P., Baeßler, M., & Rücker, W. (2009). Ratcheting convective cells of sand grains around offshore piles under cyclic lateral loads, 379–390. https://doi.org/10.1007/s10035-009-0153-3.

Davenport, A. G. (1964). The buffeting of large superficial structures by atmospheric turbulence. *Annals of the New York Academy of Sciences*, 116(1), 135–160.

De Langre, E. (2008). Effects of Wind on Plants. *Annual Review of Fluid Mechanics*, 40(1), 141–168. http://doi.org/10.1146/annurev.fluid.40.111406.102135

Downing, S.D., Socie, D.F. (1982). *Simple rainflow counting algorithms*. International Journal of Fatigue, Volume 4, Issue 1, January, 31-40.

Finnigan, J. J., & Mulhearn, P. J. (1978). Modelling waving crops in a wind tunnel. *Boundary-Layer Meteorology*, 14(2), 253–277. http://doi.org/10.1007/BF00122623

Flesch, T. K., & Wilson, J. D. (1999). Wind and remnant tree sway in forest cutblocks. II. Relating measured tree sway to wind statistics, *Agricultural and Forest Meteorology*, 93, 243–258.

Fraser, A. I. (1962). The soil and roots as factors in tree stability. *Forestry*, 34, 117–127. http://doi.org/10.1093/forestry/34.2.117

Fraser, A.I., and Gardiner, J.B.H. (1963). Rooting and stability in Sitka spruce. *Forestry*. Commission Bull. 40, HMSO, London.

Frederickson TS, Hedden RL, Williams SA (1993) Testing loblolly pine windfirmness with a simulated wind stress. *Canadian Journal of Forest Research*, 23:1760–1765

García-Rojo, R., McNamara, S., Herrmann, H.J. (2004). Discrete element methods for the micro-mechnical investigation of granular ratchet- ing. Proceedings of the ECCOMAS.

Gardiner, B. a, Stacey, G. R., Belcher, R. E., & Wood, C. J. (1997). Field and wind tunnel assessments of the implications of respacing and thinning for tree stability. *Forestry*, 70(3), 233–252. http://doi.org/10.1093/forestry/70.3.233

Gardiner, B., Marshall, B., Achim, A., Belcher, R., & Wood, C. (2005). The stability of different silvicultural systems: a wind-tunnel investigation. *Forestry*, 78(5), 471–484. http://doi.org/10.1093/forestry/cpi053

Gardiner, B.A. (1989) Mechanical characteristics of Sitka spruce. *Forestry Commission Occasional Paper* No. 24. Forestry Commission, Edinburgh.

Gardiner, B. (1992). *Mathematical modelling of the static and dynamic characteristics of plantation trees*. In: Mathematical Modelling of Forest Ecosystems (Franke, J. & Roeder, A. eds) Frankfurt.

Gardiner, B.A. (1995) Wind – tree interactions. *In Wind and Trees*. M. Coutts and J. Grace (eds). Cambridge University Press, Cambridge, pp. 41 –59.

Gibbings, J.C. (2011). Dimensional Analysis. Springer. *ISBN 1-84996-316-9*.

Gillies, J. A., N. Lancaster, W. G. Nickling, and D. Crawley, Field deter- mination of drag forces and shear stress partitioning effects for a desert shrub (Sarcobatus vermiculatus, Greasewood), *J. Geophys. Res*., 105(D20), 24,871–24,880, 2000.

Gillies, J. a., Nickling, W. G., & King, J. (2002). Drag coefficient and plant form response to wind speed in three plant species: Burning Bush (Euonymus alatus), Colorado Blue Spruce (Picea pungens glauca.), and Fountain Grass (Pennisetum setaceum). *Journal of Geophysical Research*: Atmospheres, 107(24), 1–15. http://doi.org/10.1029/2001JD001259.

Gromke, B. and Ruck, B. (2008) Ruck Aerodynamic modelling of trees for small-scale wind tunnel studies, *Forestry*, 81, pp. 243–258.

Henry Liu (1991). *Wind Engineering: A Handbook for Structural Engineers*. Prentice Hall, Columbia.

Hunt, J. C. R. and Fernholz, H. (1975). Wind-tunnel simulation of the atmospheric boundary layer: a report on Euromech 50, J. Fluid Mechanics, vol. 70, pp. 543-559.

James, K. R., Haritos, N., & Ades, P. K. (2006). Mechanical stability of trees under dynamic loads. *American Journal of Botany*, 93(10), 1522–1530. http://doi.org/10.3732/ajb.93.10.1522.

Jha, A. (2004). *Dynamic Testing of Structures using Scale Models*. M.A.Sc Thesis, Concordia University, Montreal, Canada.

Jonsson, M. J., Foetzki, a., Kalberer, M., Lundström, T., Ammann, W., & Stöckli, V. (2006). Root-soil rotation stiffness of Norway spruce (Picea abies (L.) Karst) growing on subalpine forested slopes. *Plant and Soil*, 285(1-2), 267–277. http://doi.org/10.1007/s11104-006-9013-7

Kelly, R. B., Byrne, B. W., & Houlsby, G. T. (2006). A comparison of field and laboratory tests of caisson foundations in sand and clay. *Géotechnique*, 56(9), 617–626. http://doi.org/10.1680/geot.2006.56.9.617

Matsuishi, M. & Endo, T. (1968) *Fatigue of metals subjected to varying stress*, Japan Soc. Mech. Engineering.

Mayer, H. (1987). Wind-induced tree sways. *Trees*, 1, 195–206. http://doi.org/10.1007/BF01816816

Mayhead, G. J. (1973). Sway periods of forest trees. *Scottish Forestry*, 27, 19–23.
Milne, R. (1991). Dynamics of swaying of Picea sitchensis. *Tree Physiology*, 9(11976), 383–99. Retrieved from http://www.ncbi.nlm.nih.gov/pubmed/14972849

McNamara, S., García-Rojo, R.,Herrmann, H.J.(2008). Microscopic origin of granular ratcheting. Phys. Rev. E, 77.

Nicoll B. C., and Ray D. (1996) Adapative growth of tree root systems in response to wind action and site conditions. Tree Physiol 16:891-898.

Ochi, M. K. (1990). *Applied probability and stochastic processes in engineering and physical sciences*. John Wiley and Sons, New York, USA.

O'Sullivan, M. F., & Ritchie, R. M. (1993). Tree stability in relation to cyclic loading. *Forestry*, 66(1), 69–82. http://doi.org/10.1093/forestry/66.1.69.

Papesch, A. J. G., Moore, J. R., & Hawke, A. E. (1997). Mechanical stability of Pinus radiata trees at Eyrewell forest investigated using static tests. *New Zealand Journal of Forestry Science*, 27(2), 188–204.

Peltola, H., Kellomäki, S., Hassinen, A., & Granander, M. (2000). Mechanical stability of Scots pine, Norway spruce and birch: An analysis of tree-pulling experiments in Finland. *Forest Ecology and Management*, 135, 143–153. http://doi.org/10.1016/S0378-1127(00)00306-6

Meroney. R. N. (1968). Characteristics of Wind and Turbulence in and above Model Forests.pdf. *Journal of Applied Meteorology*, 7, 780–788.

Raupach, M. R. (1994). Simplified expressions for vegetation roughness length and zero-plane displacement as functions of canopy height and area index. *Boundary-Layer Meteorology*, 71(1-2), 211–216. http://doi.org/10.1007/BF00709229

Reinhold, T. A. (ed.) (1982) Wind tunnel modelling for civil engineering applications, *Proc. of the international workshop on wind tunnel modelling criteria and techniques in civil engineering applications*, Gaithersburg, Maryland, USA, Cambridge University Press.

Repola, J., Ojansuu, R., & Kukkola, M. (2007). Biomass functions for Scots pine, Norway spruce and birch in Finland. *Working Papers of the Finnish Forest Research Institute*, 53, 27. Retrieved from http://www.metla.eu/julkaisut/workingpapers/2007/mwp053.pdf

Roodbarky, H. J., C. J. Baker, A. R. Dawson, and C. J. Wright, (1994). Experimental observations of the aerodynamic characteristics of urban trees, *J. Wind Eng. Ind. Aerodyn.*, 52(1–3), 171–184, 1994.

Rudnicki, M., Mitchell, S. J., & Novak, M. D. (2004). Wind tunnel measurements of crown streamlining and drag relationships for three conifer species. *Canadian Journal of Forest Research*, 34(3), 666–676. http://doi.org/10.1139/X03-233

Rychlik, I. (1987) *A New Definition of the Rainflow Cycle Counting Method, Int. J. Fatigue* 9:2, 119-121.

Schluter, L. (1991). *Programmer's Guide for LIFE2's Rainflow Counting Algorithm*. Sandia Report SAND90-2260.

Smith, V.G., Watts, M., and James, D.F. (1987). Mechanical stability of black spruce in the clay belt region of northern Ontario. *Can. J. For. Res*. 17: 1080–1091.

Sockel, H. (1994). *Wind-Excited Vibrations of Structures* (Vol. 335). Technical University Vienna, Vienna, Austria: International Centre for Mechanical Sciences.

Somerville, A. (1979). Root anchorage and root morphology of Pinus radiata on a range of ripping treatments. *N.Z. J. For. Sci*. 9: 294–315.

Stacey, G. R., Belcher, R. E., Wood, C. J., & Gardiner, B. A. (1994). Wind flows and forces in a model spruce forest. *Boundary-Layer Meteorology*, 69, 311–334.

Takeda, K., and M. Kato. 1992. “Wind Tunnel Blockage Effects on Drag Coefficient and Wind-induced Vibration.” Journal of Wind Engineering and Industrial Aerodynamics 42 (1–3): 897–908. doi:10.1016/0167-6105(92)90096-S.

Watson, A. (2000). Wind-induced forces in the near-surface lateral roots of radiata pine. *Forest Ecology and Management*, *135*(1–3), 133–142. https://doi.org/10.1016/S0378-1127(00)00305-4.

Whitbread, R.E. (1963) Model simulation of wind effects on structures. Proceedings, International Conference on Wind Effects on Buildings and Structures, Teddington, UK, 26–28 June, pp. 284–302.

Table 4-1 List of tree characteristics, scaling aspects and dimensionless parameters

Morphological and dynamic properties		Field Tree (FT)	Tree Sapling	
			Tree1 (T1)	Tree2 (T2)
Description	**Symbol**			**Clay** / **Sand**
Height of the tree, (m)	ℓ	23.1	1.37	1.27
Stem diameter, DBH or DSH (m)	D	0.458	0.044	0.048
Total mass above stump, (kg)	W	1612.6	1.2	1.15
Mass/unit length, kg/m	m	69.81	0.876	0.905
Crown mass (after pruning), (kg)	M_{crown}	540.6	0.725	0.64
Crown area, (m^2) **	C_A	3054.39	4.09	3.616
Stem Modulus of Elasticity, GPa	E	1.2	0.65	0.65
Stem wood density, kg/m^3	ρ_s	850	950	950
Moment of area at DBH height, m^4	$I=\frac{\pi}{64}D^4$	$2.16X10^{-3}$	$1.84X10^{-7}$	$2.61X10^{-7}$
Flexural rigidity of the stem, $N.m^2$	J =EI	$2.59X10^{6}$	$1.2X10^{2}$	$1.69X10^{2}$
Flow properties				
Air density, kg/m^3	ρ	1.2754	1.2754	1.2754
Air viscosity, kg m^{-1} s^{-1}	μ	$1.8X10^{-5}$	$1.8X10^{-5}$	$1.8X10^{-5}$
Atmospheric pressure (kN/m^2)	P_a	101	101	101

Note: **crown area= C_A =5.65 m^2 per kg crown mass [Kellomaki 1999]

Dynamic properties of the stem					
Natural frequency, (Hz)	ω	0.35	2.9	3.0	3.1
Damping ratio from the sway tests	$\zeta = c/c_c$	0.051	0.069	0.041	0.048
Critical damping coefficient, (kg.s/m)	$c_c = 2\left(\frac{W}{g}\right)f$	115.07	0.71	0.7	0.73
Damping coefficient, (kg.s/m)	c	5.87	0.049	0.03	0.035
Frontal area, (m^2)	F_A	261.4	0.35	0.31	0.31
Drag coefficient	C_D	0.35	0.76	0.76	0.76
Root-soil plate properties					
Plate radius, (m)	R	1.6	0.30	0.28	0.28
Root plate depth, (m)	d	0.9	0.1	0.15	0.15
Soil unit weight, (kN/m^3)	γ'	20	16.4	14.7	16.4
Root Modulus of Elasticity, (GPa)	E_R	3.57	0.15-0.5	0.15-0.5	0.15-0.5
Horizontal load, (N)	H	34091	7.1	40.9	17.5
Vertical load, (N)	V	20175	11.8	11.3	11.3
Moment, (kNm)	M	345	0.0037	0.045	0.021
Rotation, (rad)	θ	0.084	0.1	0.06	0.12
Scaling					
Length (L)= L_m/L_p	λ_L	1	0.059	0.055	0.055
Mass (m)= M_m/M_p	λ_m	1	7.44E-4	7.13E-4	7.13E-4
Time (s) = $T_m/T_p = (1/f_m)/(1/f_p)$	λ_t	1	0.124	0.12	0.12

Table 4-2 Group I dimensionless parameters (flow properties)

E = stiffness [$ML^{-1}T^{-2}$] ℓ (L)= length [L] D = diameter [L] g = gravitational coefficient [LT^{-2}] z_o=roughness length (0.01 m for open country terrain) [L] ρ = fluid density [ML^{-3}] μ = dynamic viscosity [$ML^{-1}T^{-1}$] f = frequency [T^{-1}] U_R = fluid velocity [LT^{-1}] F_d = drag force [$ML^{-1}T^{-2}$]	**Note**: Strouhal number for T2 and FT are taken constant as of T1 at 5.87 m/s reference wind speed (U_R). For T2, U_R =5.9 m/s and for FT, U_R =12.28.

Number	*Name and phenomena*	*Equation*	*Field tree (FT)*	*Tree sapling*			*Comments*
				Tree1 (T1)	*Tree2 (T2)*		
					Clay	*Sand*	
π_1	Strouhal	$f\ell / U_R$	0.677	0.677	0.677	0.677	Reduced frequency
π_2	Reynolds	$\rho U_R \ell / \mu$	2.0E7	5.7E5	5.3E5	5.3E5	Inertia/viscosity
π_3	Jensen	ℓ / z_o	1925	1925	1925	1925	Scale factor
π_4	Froude	$g\ell / U_R^2$	1.5	0.39	0.36	0.36	Gravitational forces/inertial forces of flow
π_5	Euler	$F_d / \rho \ell^2 U_R^2$	0.086	0.033	0.034	0.034	Reduced drag coefficient
π_6	Cauchy	$\rho . U_R^2 . \left(\frac{L}{D}\right)^3 / E$	0.021	0.002	0.0013	0.0013	Elastic forces/inertia forces of flow

Table 4-3 Group II dimensionless parameters (super structure response)

F (E, I, m, ℓ, D, ρ_s, g, ρ, f, U_R, g, c, C_D)=0						
E = stiffness [$ML^{-1}T^{-2}$] I = mass moment of area [L^4] m = mass per unit length [ML^{-1}] ℓ (L)= length [L] D = diameter [L] ρ_s = structural density [ML^{-3}] g = gravitational coefficient [LT^{-2}]		ρ = fluid density [ML^{-3}] μ = dynamic viscosity [$ML^{-1}T^{-1}$] f = frequency [T^{-1}] U_R = fluid velocity [LT^{-1}] c = damping coefficient [$ML^{-1}T$] C_D = dimensionless drag coefficient				
Number	*Name and phenomena*	*Equation*	*Field tree(FT)*	*Tree sapling*		
				Tree1 (T1)	*Tree2 (T2)*	
					Clay	*Sand*
π_7	Density ratio	ρ_s/ρ	666.67	769.23	769.23	769.23
π_8	Slenderness ratio	D/ℓ	0.02	0.03	0.04	0.04
π_9	Mass ratio	$m/\ell^2\rho$	0.103	0.366	0.44	0.44
π_{10}	Stiffness ratio	I/ℓ^4	7.6E-9	5.2E-8	6.5E-8	6.5E-8
π_{11}	Aero-elastic response factor	$\rho C_D \ell^5 D f^2/EI$	0.064	0.007	0.004	0.004
π_{12}	Frequency factor	$f.(m/E)^{1/2}$	8.5E-5	11E-5	11.7E-5	12E-5
π_{13}	Mass factor	$mg/E\ell$	2.5E-8	1.1E-8	1.2E-8	1.2E-8
π_{14}	Damping factor	$c f^2/(Em)^{1/2}$	2.5E-6	1.8E-5	1.2E-5	1.4E-5
π_{15}	Elastic response factor	$E/\rho U_R^2$	6.24E6	1.35E7	1.35E7	1.35E7
π_{16} (π_{12}^2/π_{10})	Mode shape factor	$m f^2 \ell^4/EI$	0.94	0.216	0.125	0.134
π_{17} ($\pi_{12}.\pi_{14}/\pi_{10}$)	Damping factor	$f^3 c\ell^4/EI$	0.028	0.035	0.013	0.016
π_{18} (π_{13}/π_{10})	Gravitational factor	$mg\ell^3/EI$	3.26	0.18	0.11	0.11

Table 4-4 Group III dimensionless parameters (sub-structure response)

F (M, V, θ, ρ, γ', D, P_a)=0						
V = vertical load [MLT^{-2}] θ = rotation, rad M = moment, [ML^2T^{-2}] ℓ (L)= length [L] D = diameter [L] γ'= Soil unit weight, [$ML^{-2}T^{-2}$]		ρ = fluid density [ML^{-3}] U_R = fluid velocity [LT^{-1}] P_a= atmospheric pressure [$ML^{-1}T^{-2}$]				
Number	*Name and phenomena*	*Equation*	*Field tree(FT)*	*Tree sapling*		
				Tree1 (T1)	*Tree2 (T2)*	
					Clay	*Sand*
π_{19}	Bending moment coefficient at stem base	$M/\left(\frac{1}{2}\rho U_R^2 L^3\right)$	0.29	0.07	1.0	0.46
π_{20}	Moment load factor	$M/\gamma'.D^4$	0.1645	0.0017	0.0311	0.013
π_{21}	Rotational response factor,	$\theta.(P_a/\gamma'.D)^{0.5}$	0.338	0.192	0.118	0.223
π_{22}	Vertical load factor	$V/\gamma'.D^3$	0.03078	0.00333	0.00438	0.00392

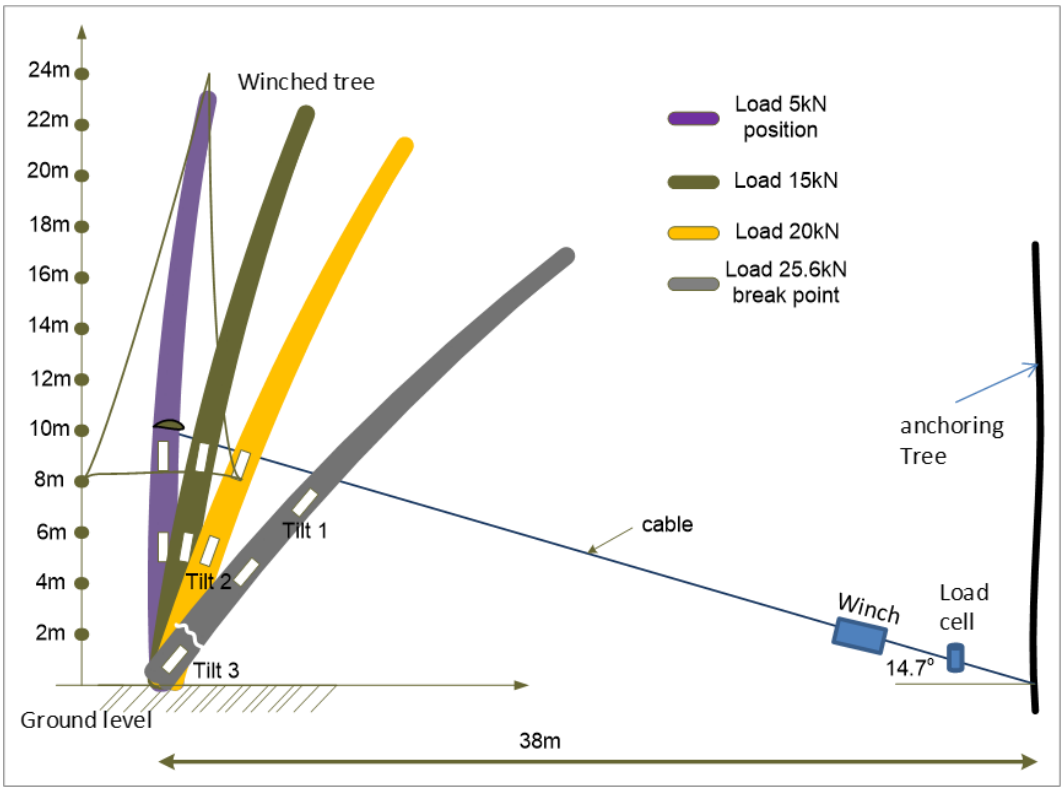

Figure 4-1 Field tree stem deflection with increase in winch load

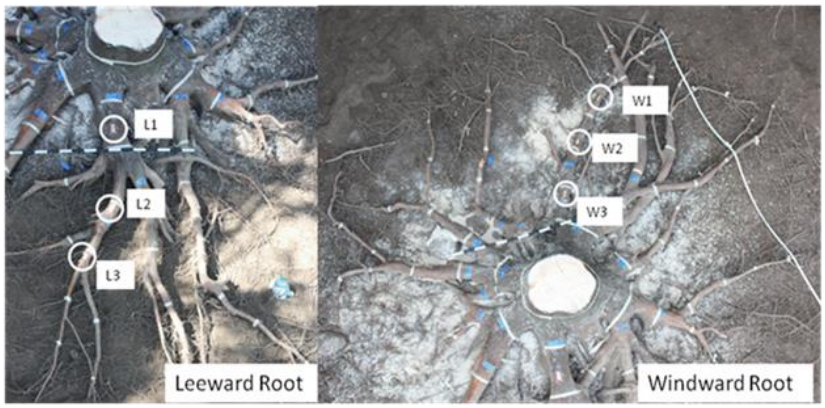

Strain gauge location	Distance from trunk centre (m)
W1	1.4
W2	0.9
W3	0.4
L1	0.6
L2	0.9
L3	1.13

Figure 4-2 Strain gauge locations on the field tree roots

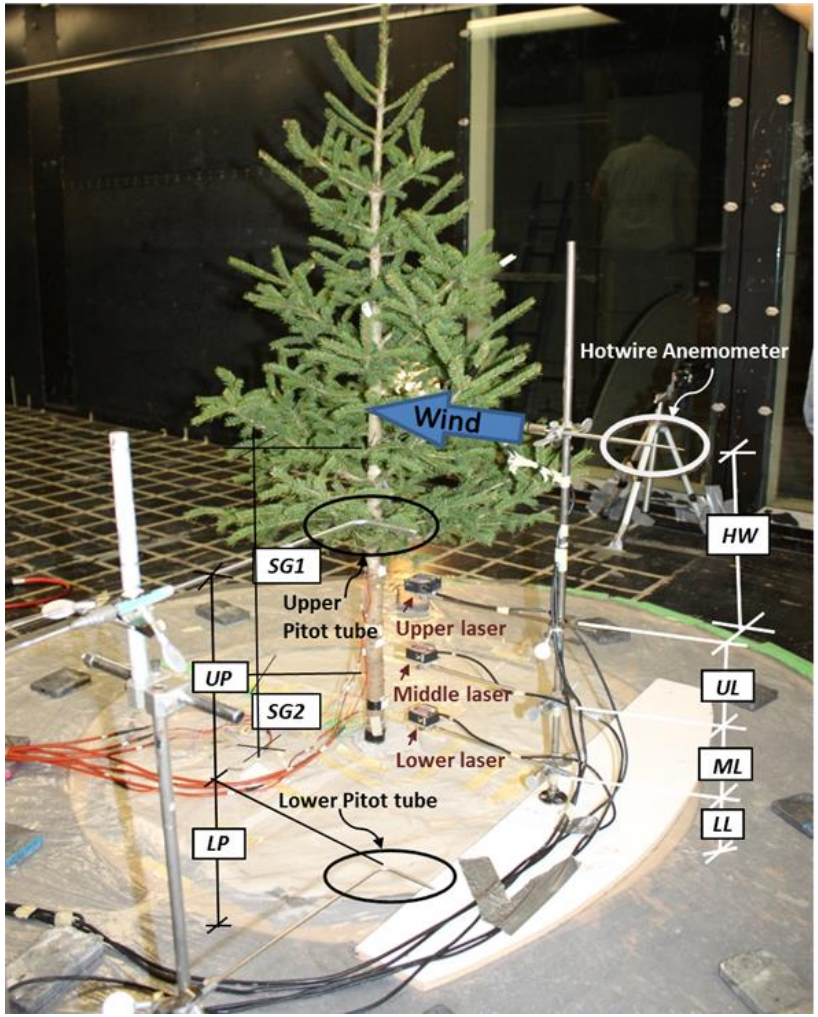

Dimension Description		Setup		
Description	Symbol	T1 in Sand	T2 in Sand	T2 in Clay
Height of hot wire anemometer above wind tunnel floor	HW	68.0	68.0	68.0
Height of upper pitot tube above lower pitot tube	UP	37.0	37.4	37.4
Height of lower pitot tube above tunnel floor	LP	30.8	31.3	31.25
Height of upper laser above middle laser	UL	11.25	12.1	10.0
Height of middle laser above lower laser	ML	12.5	12.8	10.0
Height of lower laser above wind tunnel floor	LL	11	16.5	27.25
Height of strain gauge attachment above lower strain gauge attachment	SG1	49.25	56.5	56.5
Height of lower strain gauge attachment above soil level	SG2	13.25	3.0	3.0

Note: All dimensions in cm

Figure 4-3 Tree sapling in the wind tunnel and instrument positions of the experimental setup

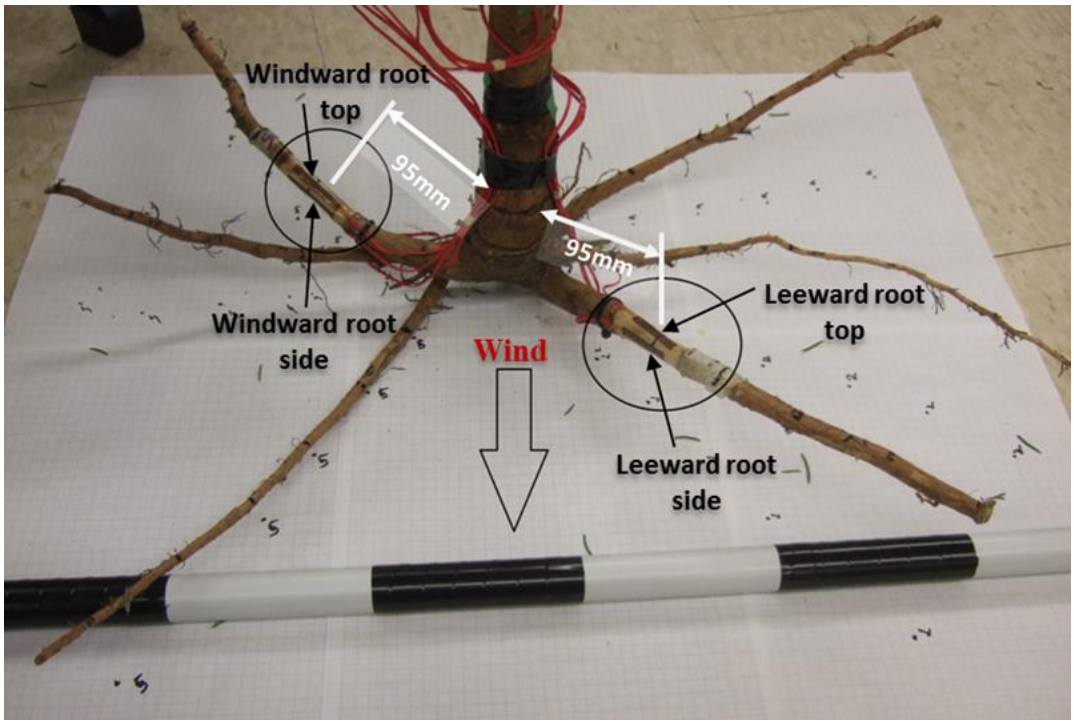

Figure 4-4 Tree sapling T1 root system instrumentation

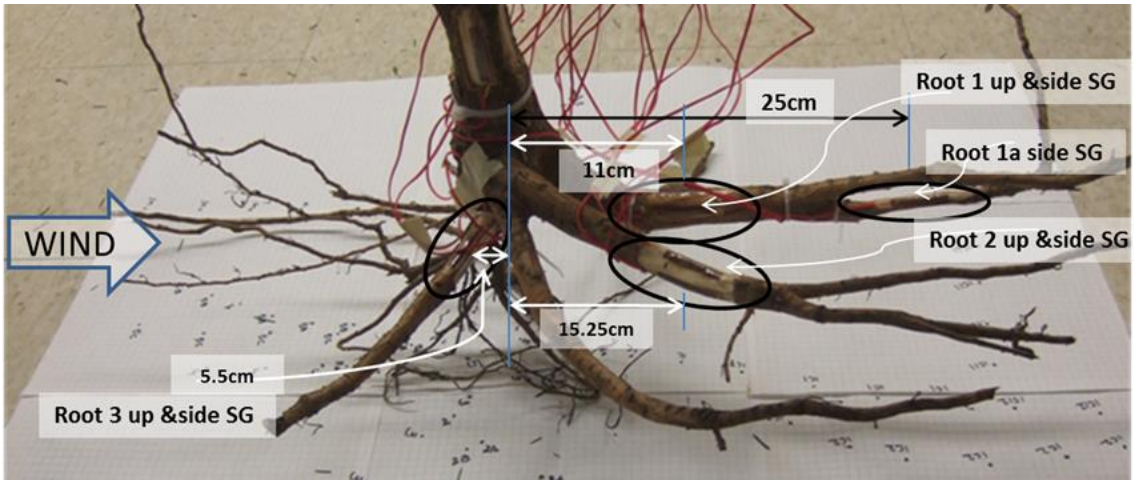

Figure 4-5 Tree sapling T2 root system instrumentation

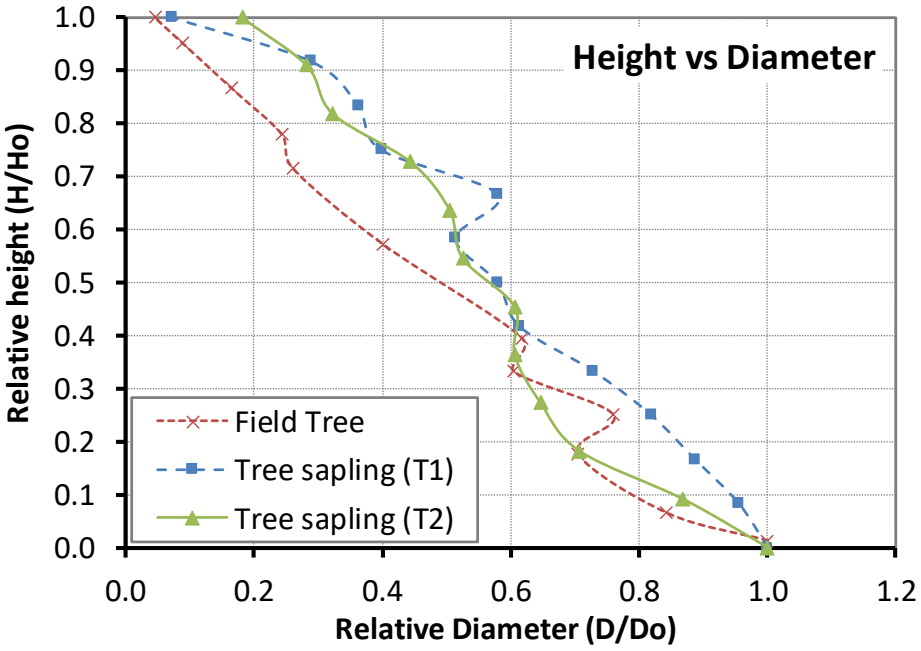

Figure 4-6 Geometric similarity

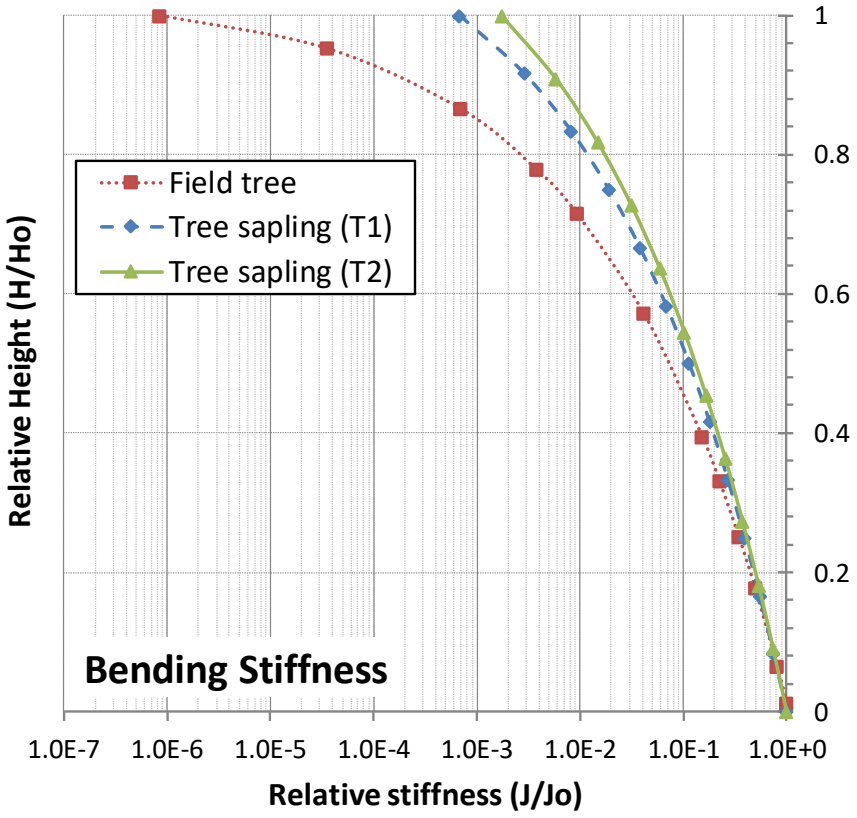

Figure 4-7 Elastic similarity

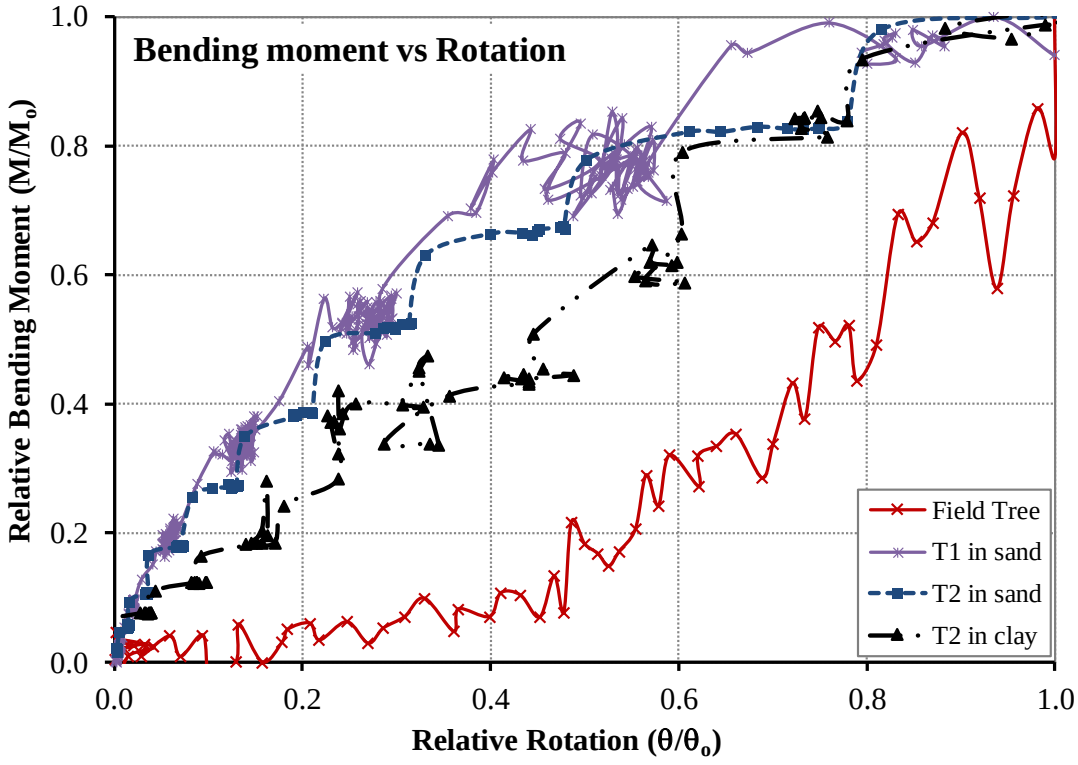

Figure 4-8 Stress similarity

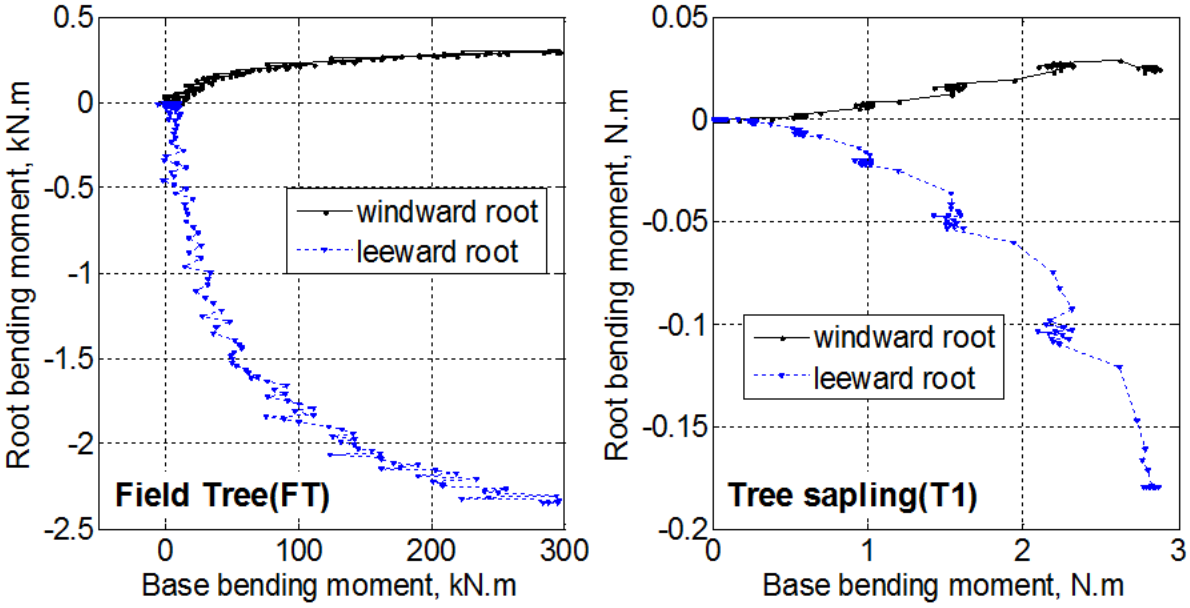

Figure 4-9 Load transfer to root system from stem

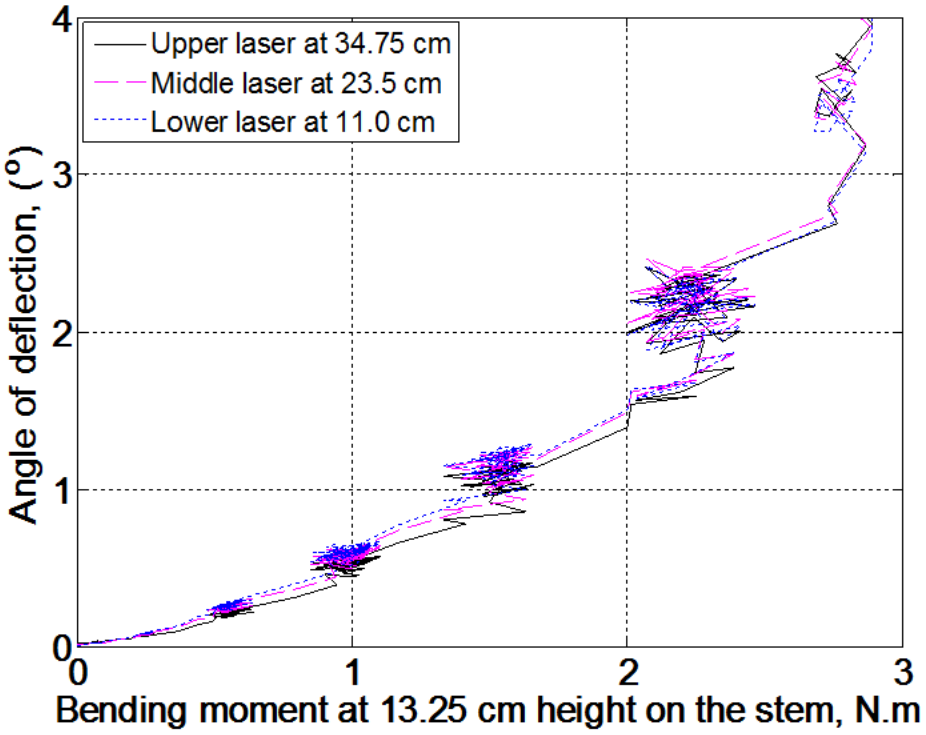

Figure 4-10 Ratcheting pattern of T1 in sand

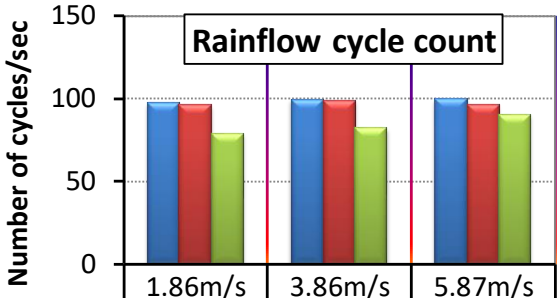

	1.86m/s	3.86m/s	5.87m/s
Wind speed	97.4	99.2	99.5
Base bending moment response	96.1	98.8	96.6
Rotational response at stem base	79.0	82.0	90.2

Figure 4-11 Number of rainflow cycles of T1 in sand with increase in wind speed

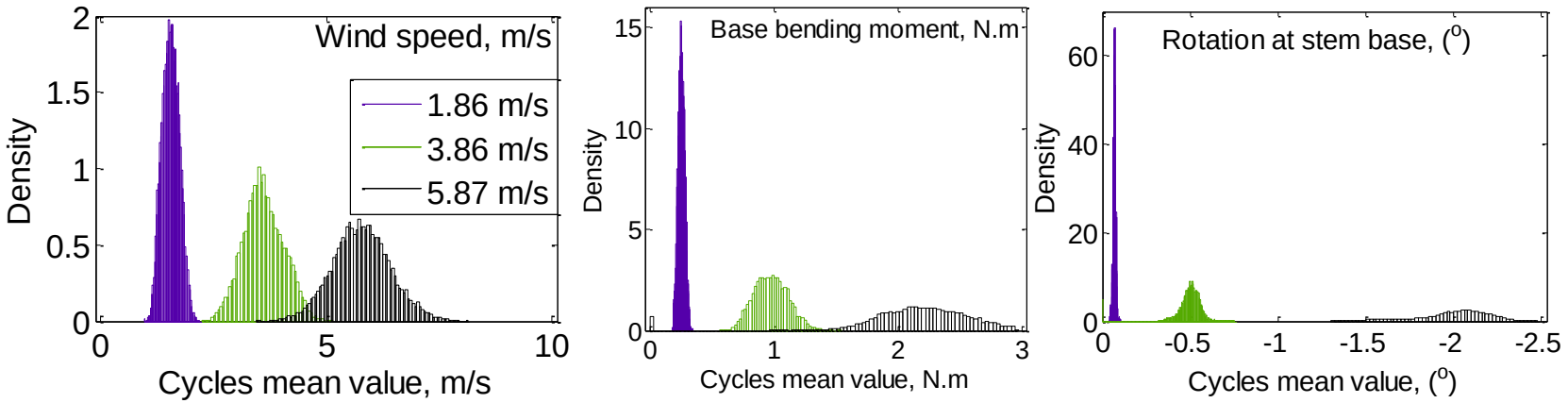

T1 in Sand	Variant	Mean	Variance	Coefficient of variation	Skewness	Kurtosis
1.86 m/s	Wind speed	1.57	0.05	0.14	-0.97	10.63
	Base bending moment	0.25	0.00	0.22	-2.45	14.18
3.86 m/s	Wind speed	3.61	0.19	0.12	0.13	2.75
	Base bending moment	0.98	0.03	0.16	-0.50	8.57
5.87 m/s	Wind speed	5.79	0.40	0.11	0.09	3.01
	Base bending moment	2.17	0.20	0.21	-2.23	12.10
1.86 m/s	Wind speed	1.57	0.05	0.14	-0.97	10.63
	Rotational response	-0.06	0.00	-0.43	1.59	4.49
3.86 m/s	Wind speed	3.61	0.19	0.12	0.13	2.75
	Rotational response	-0.42	0.04	-0.47	1.52	3.70
5.87 m/s	Wind speed	5.79	0.40	0.11	0.09	3.01
	Rotational response	-1.85	0.38	-0.33	2.30	7.38

Figure 4-12 Cycles mean value density distribution of T1 in sand with increase in wind speed

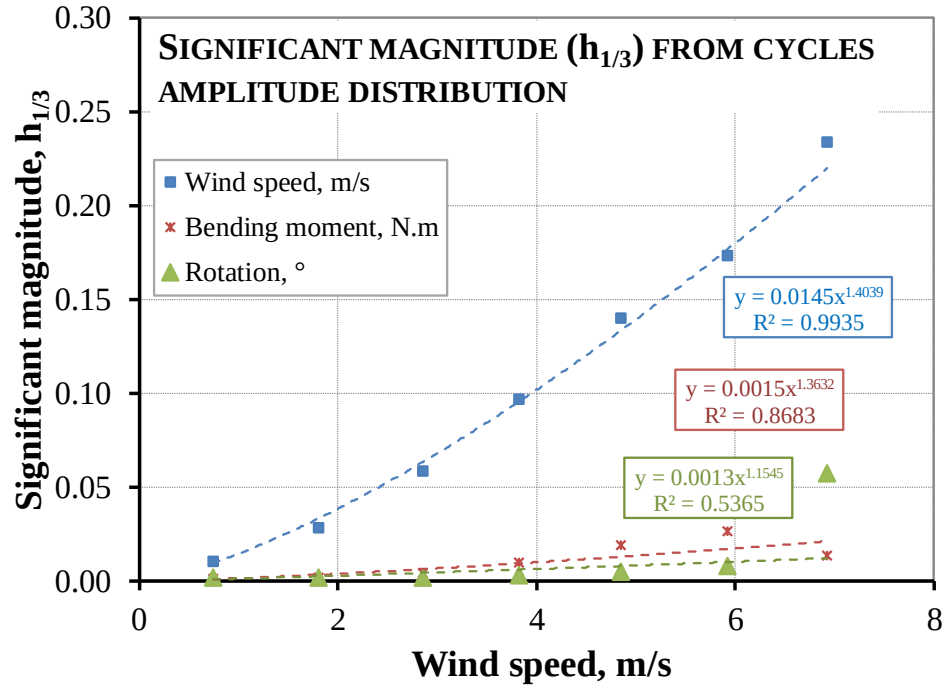

Figure 4-13 Significant wave height of T1 in sand

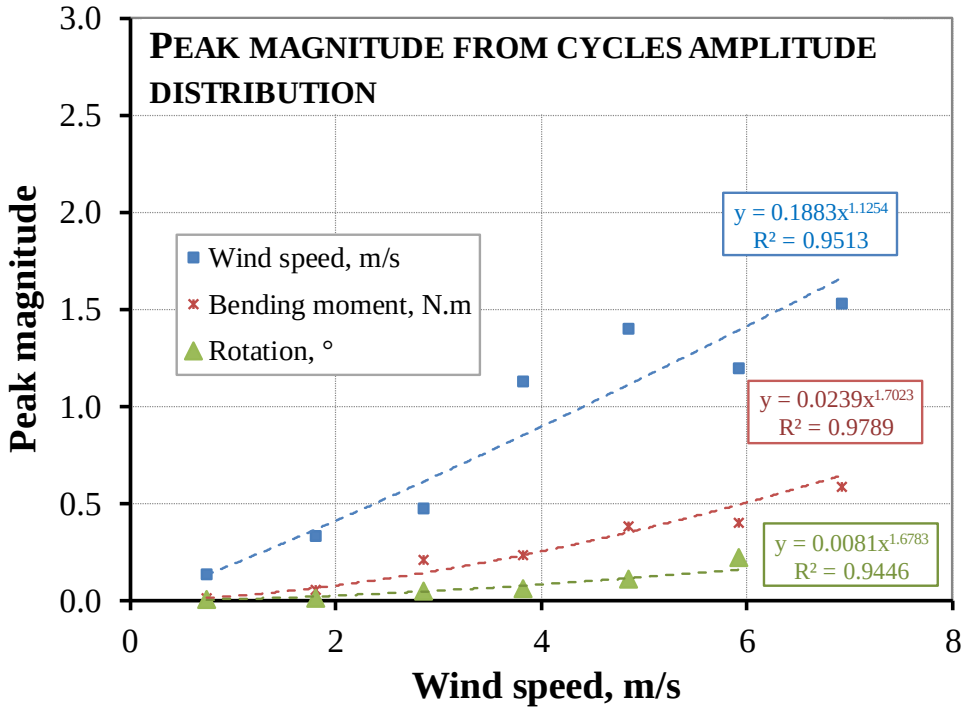

Figure 4-14 Peak wave height of T1 in sand

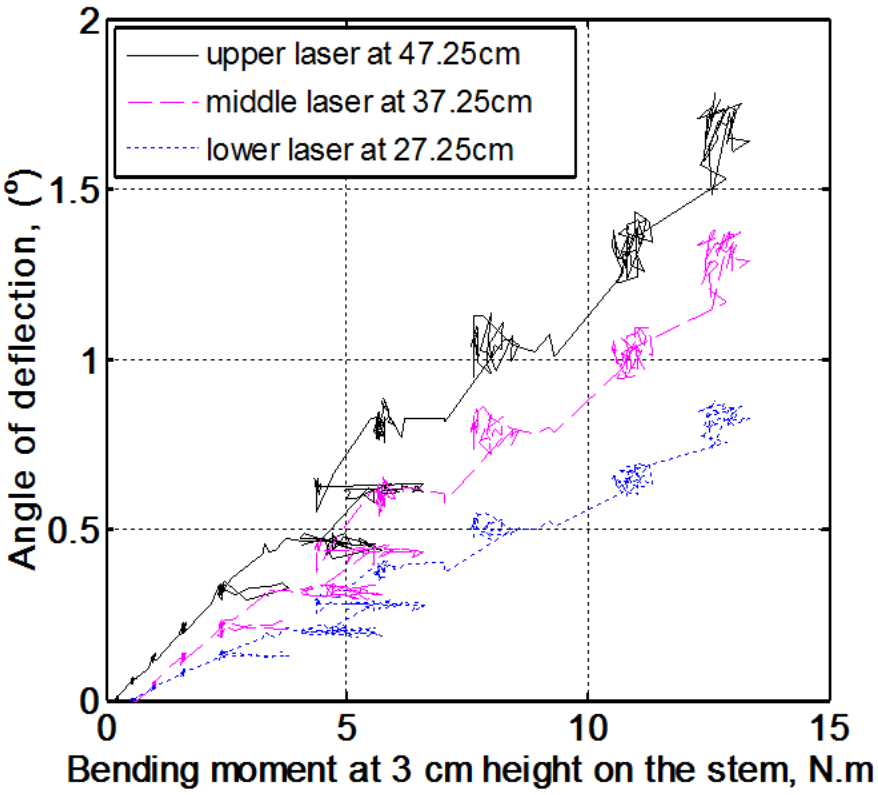

Figure 4-15 Ratcheting pattern of T2 in clay

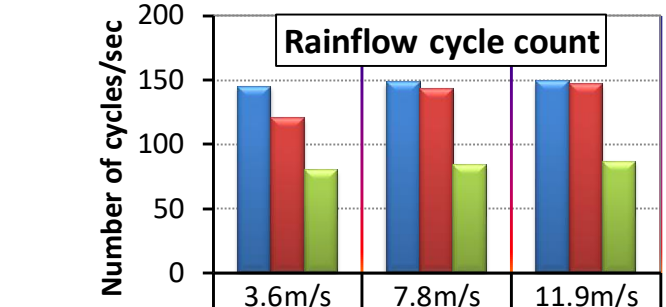

	3.6m/s	7.8m/s	11.9m/s
Wind speed	145.1	148.5	149.0
Base bending moment response	120.6	143.4	146.8
Rotational response at stem base	79.7	84.0	87.1

Figure 4-16 Number of rainflow cycles of T2 in clay with increase in wind speed

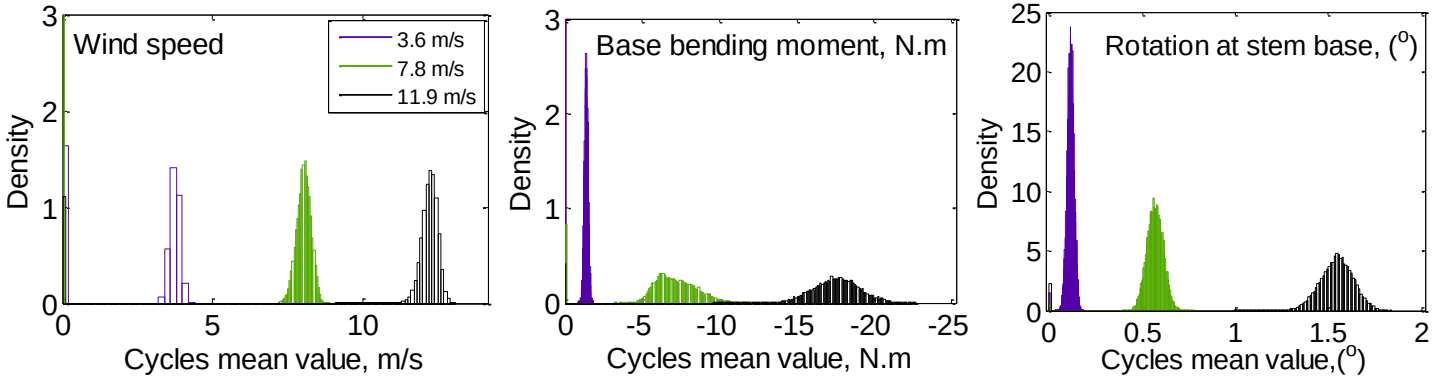

T2 in Clay	Variant	Mean	Variance	Coefficient of variation	Skewness	Kurtosis
3.6 m/s	Wind speed	3.75	0.03	0.04	-0.20	2.76
	Base bending moment	1.37	0.01	0.09	-0.08	3.30
7.8m/s	Wind speed	8.03	0.05	0.03	-0.13	2.85
	Base bending moment	7.60	1.51	0.16	0.24	2.68
11.9m/s	Wind speed	12.23	0.07	0.02	-0.35	3.17
	Base bending moment	17.65	2.04	0.08	0.02	2.87
3.6 m/s	Wind speed	3.75	0.03	0.04	-0.20	2.76
	Rotational response	0.11	0.00	0.16	-0.06	3.12
7.8m/s	Wind speed	8.03	0.05	0.03	-0.13	2.85
	Rotational response	0.56	0.00	0.08	-0.01	2.87
11.9m/s	Wind speed	12.23	0.07	0.02	-0.35	3.17
	Rotational response	1.54	0.01	0.06	-0.20	3.07

Figure 4-17 Cycles mean value density distribution with increase in wind speed of T2 in clay

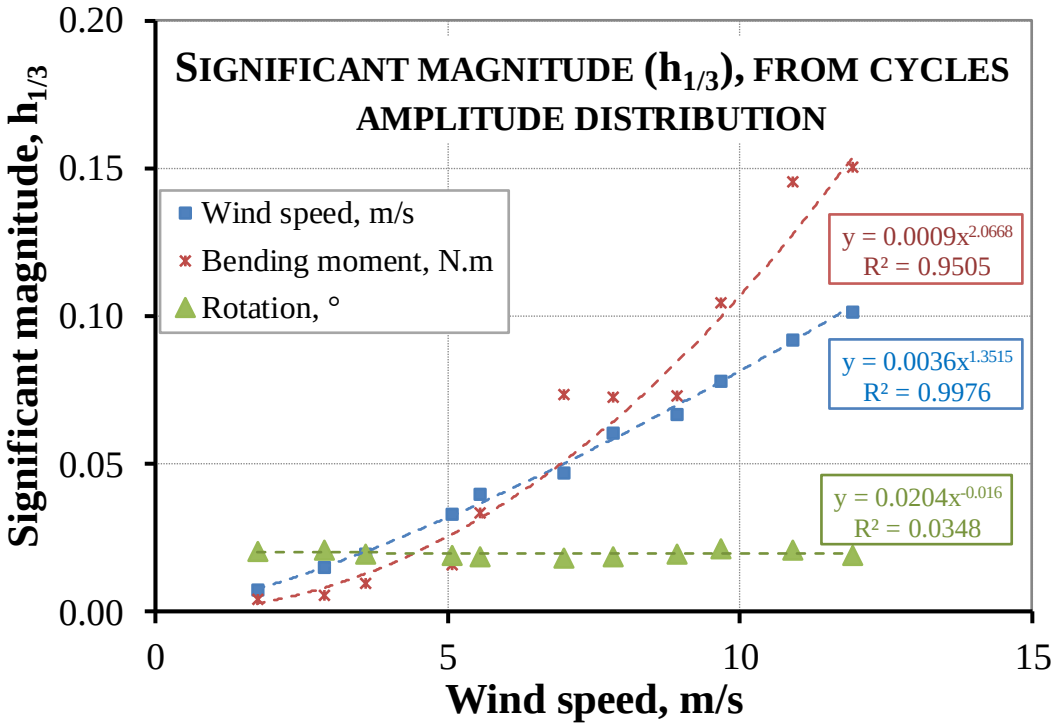

Figure 4-18 Significant wave height of T2 in clay

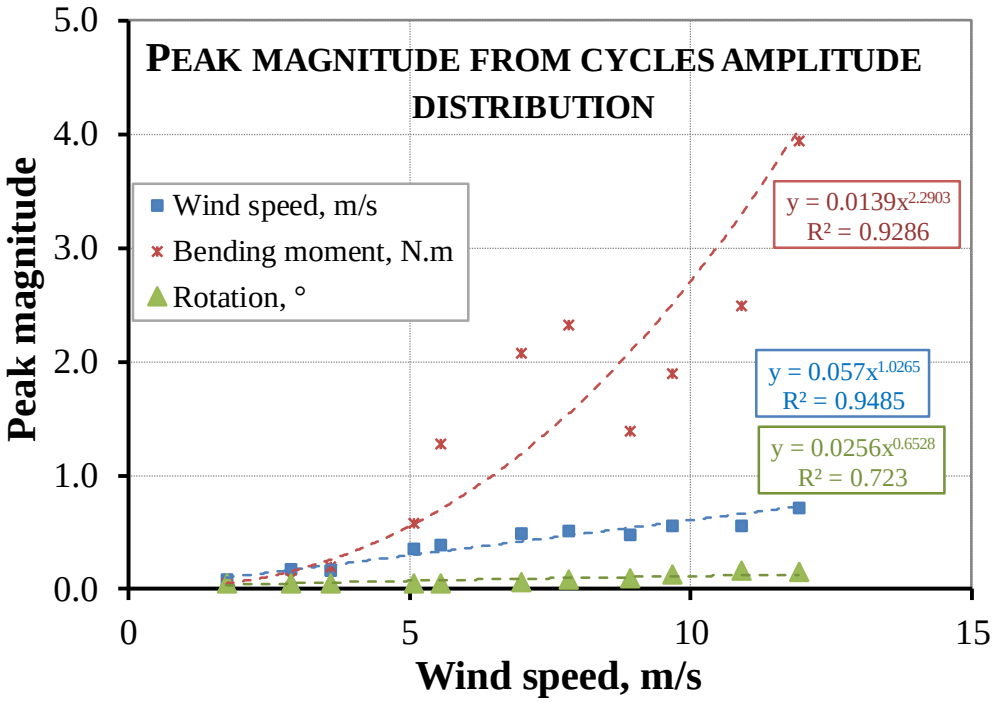

Figure 4-19 Peak wave height of T2 in clay

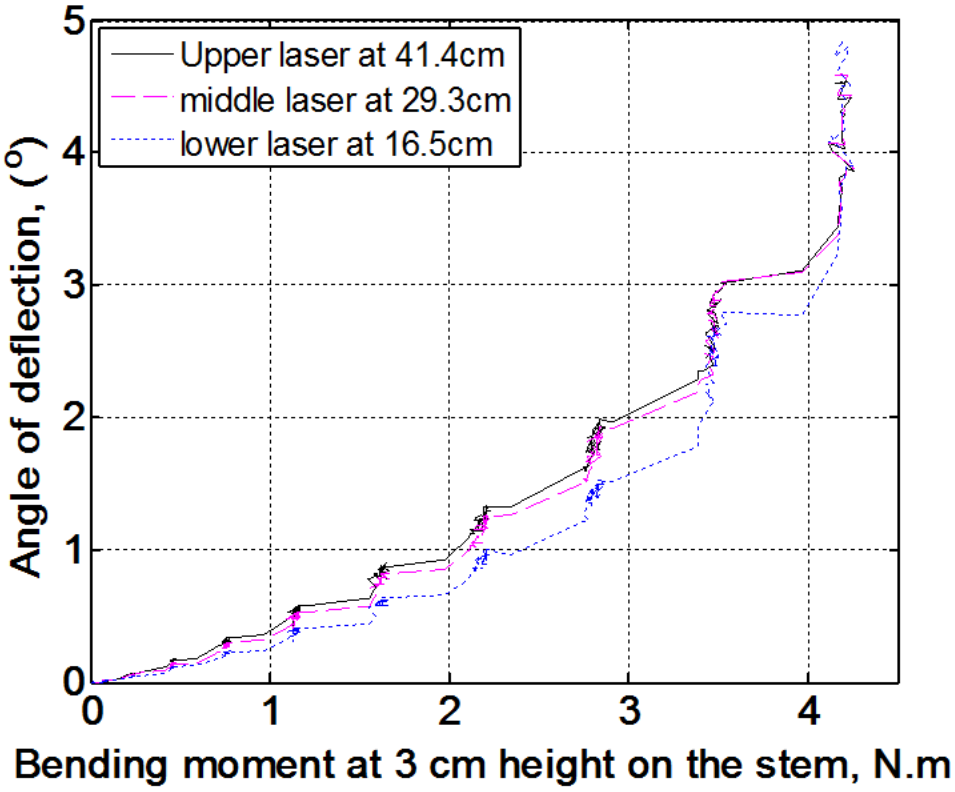

Figure 4-20 Ratcheting pattern of T2 in sand

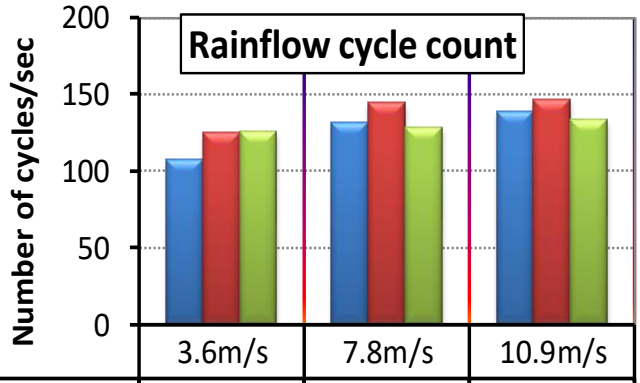

	3.6m/s	7.8m/s	10.9m/s
Wind speed	107.0	132.0	138.8
Base bending moment response	125.1	144.3	146.6
Rotational response at stem base	125.6	128.6	133.2

Figure 4-21 Number of rainflow cycles of T2 in sand with increase in wind speed

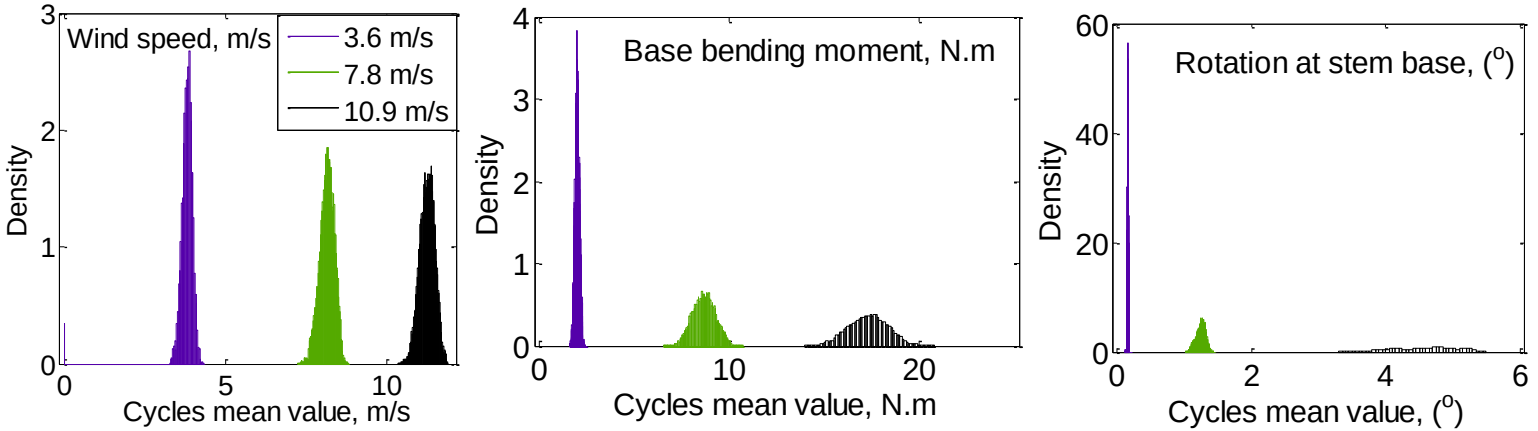

T2 in Sand	Variant	Mean	Variance	Coefficient of variation	Skewness	Kurtosis
3.6 m/s	Wind speed	3.77	0.17	0.11	-7.73	70.20
	Base bending moment	-2.01	0.01	-0.06	0.00	2.80
7.8m/s	Wind speed	8.13	0.05	0.03	-0.36	3.04
	Base bending moment	-8.67	0.37	-0.07	0.05	2.77
10.9m/s	Wind speed	11.23	0.05	0.02	-0.22	2.91
	Base bending moment	-17.31	1.06	-0.06	0.05	2.71
3.6 m/s	Wind speed	3.77	0.17	0.11	-7.73	70.20
	Rotational response	-0.15	0.00	-0.06	0.24	2.90
7.8m/s	Wind speed	8.13	0.05	0.03	-0.36	3.04
	Rotational response	-1.24	0.00	-0.06	0.38	2.74
10.9m/s	Wind speed	11.23	0.05	0.02	-0.22	2.91
	Rotational response	-4.57	0.23	-0.11	0.31	2.28

Figure 4-22 Cycles mean value density distribution with increase in wind speed of T2 in sand

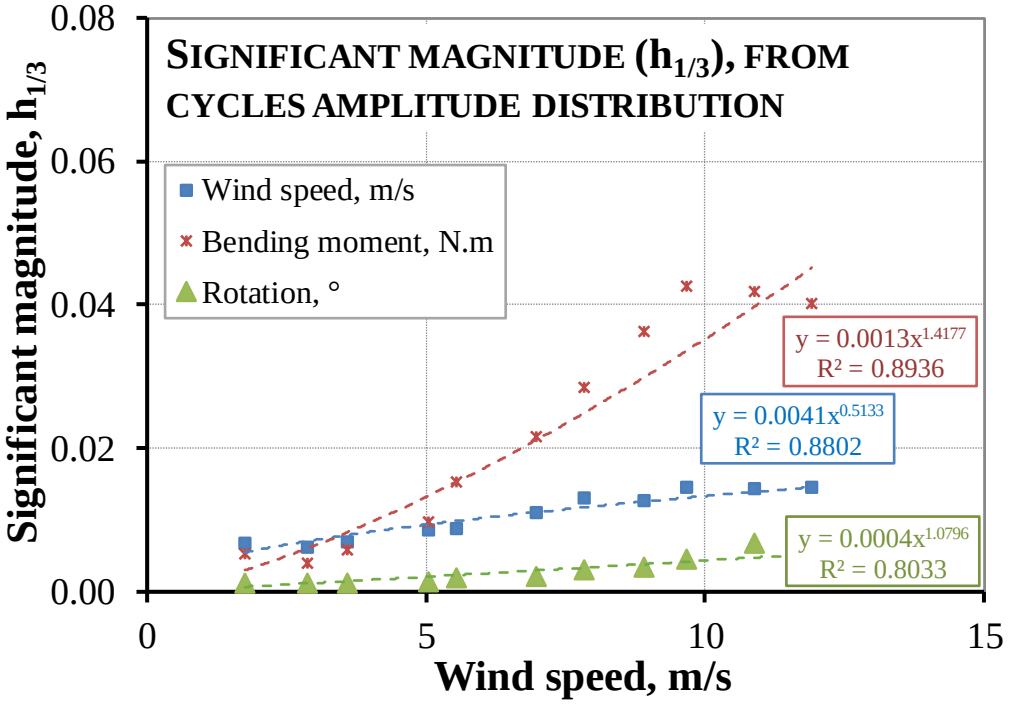

Figure 4-23 Significant wave height of T2 in sand

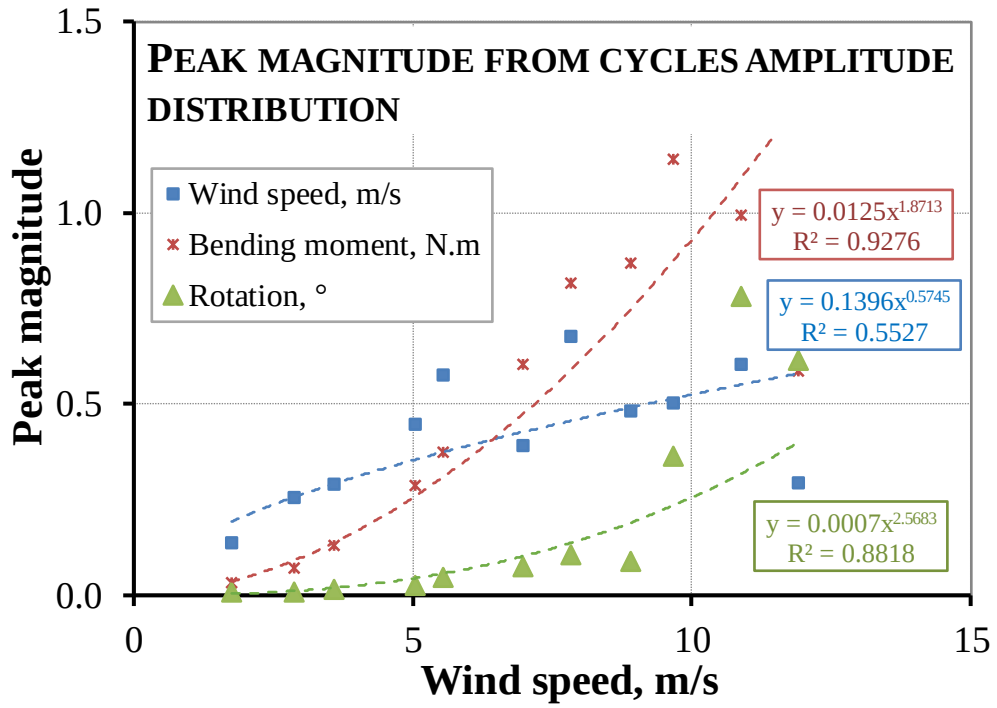

Figure 4-24 Peak wave height of T2 in sand

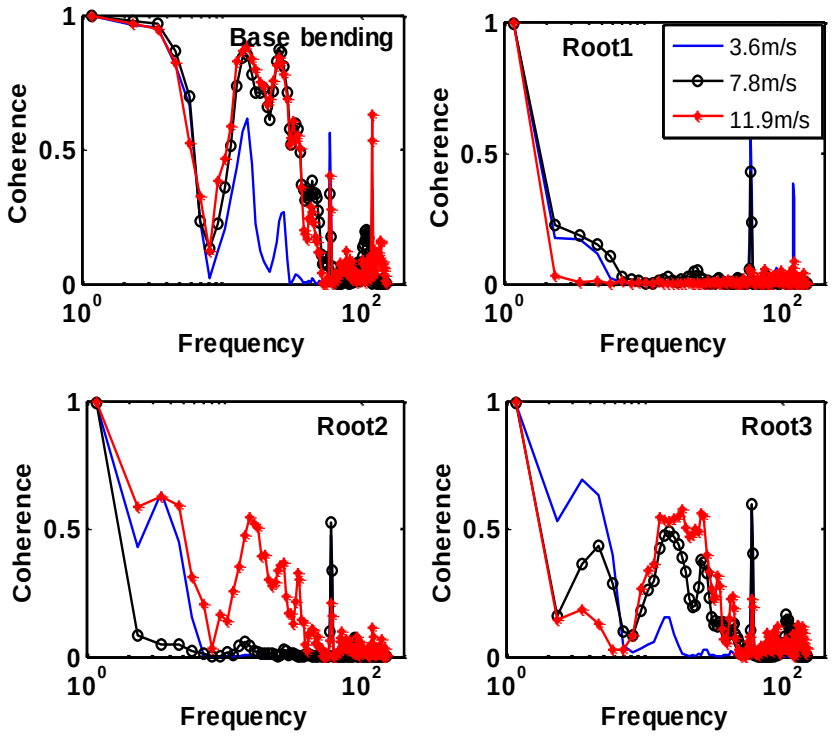

Figure 4-25 Root response with change in wind direction (sand)

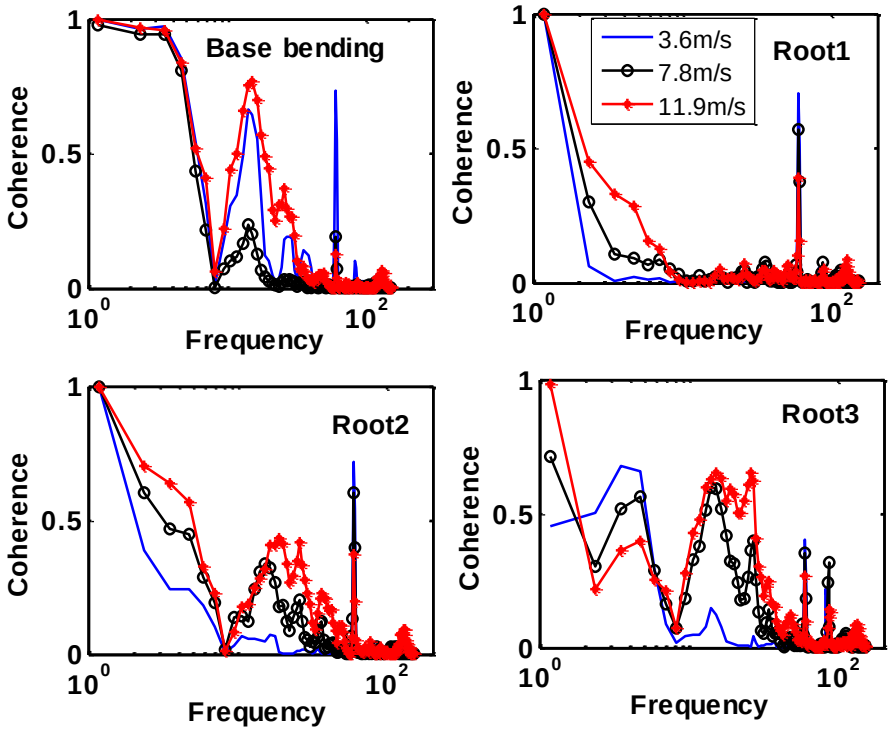

Figure 4-26 Root response with change in wind direction (clay)

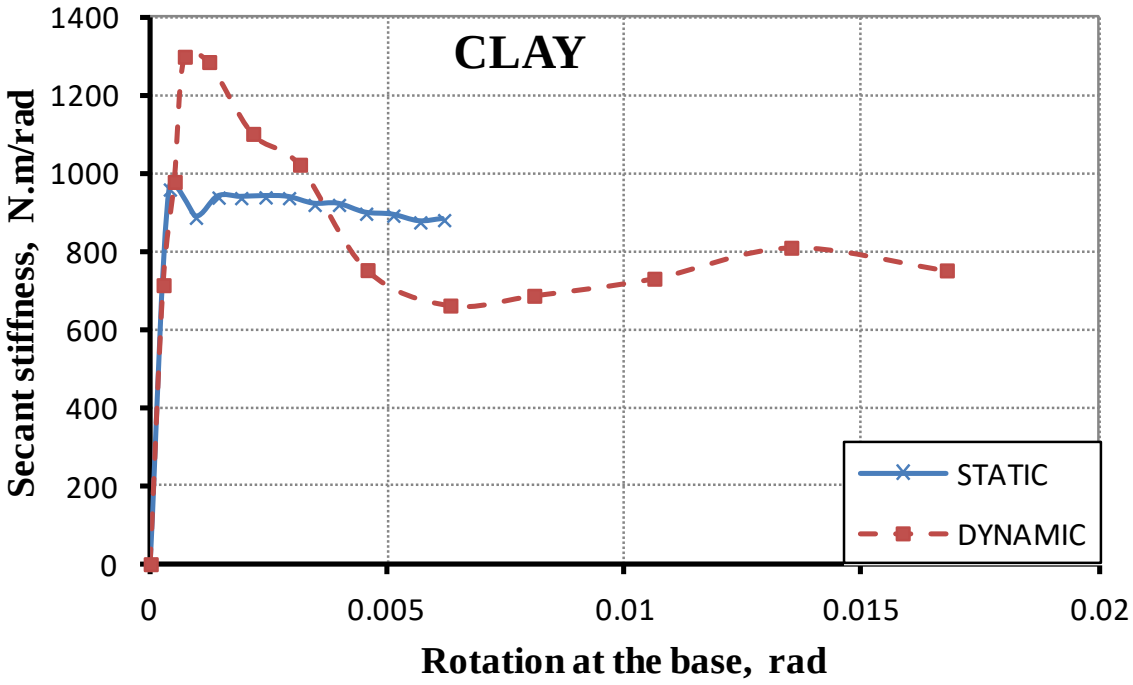

Figure 4-27 Secant modulus of rotation under static and dynamic loading

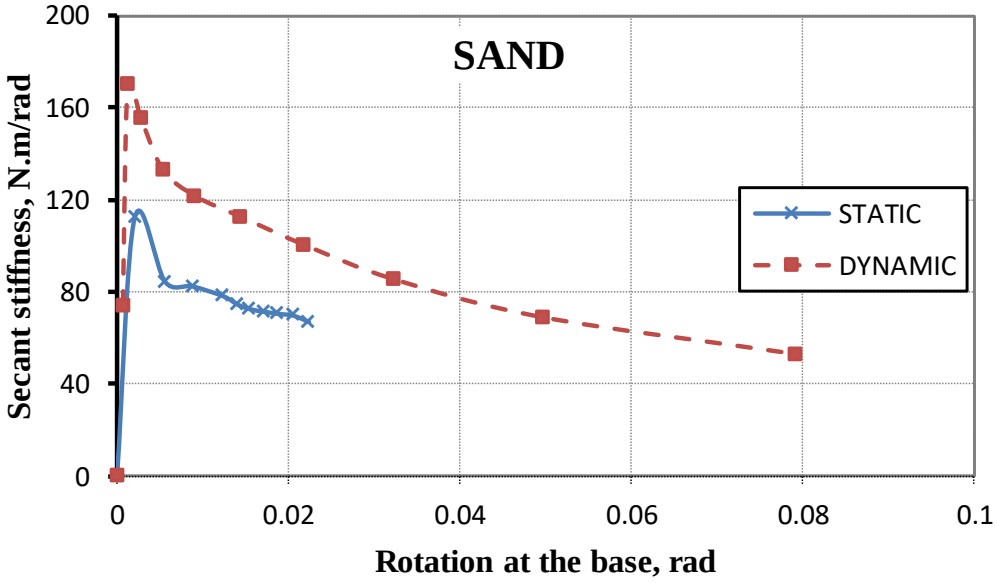

Figure 4-28 Secant modulus of rotation under static and dynamic loading conditions

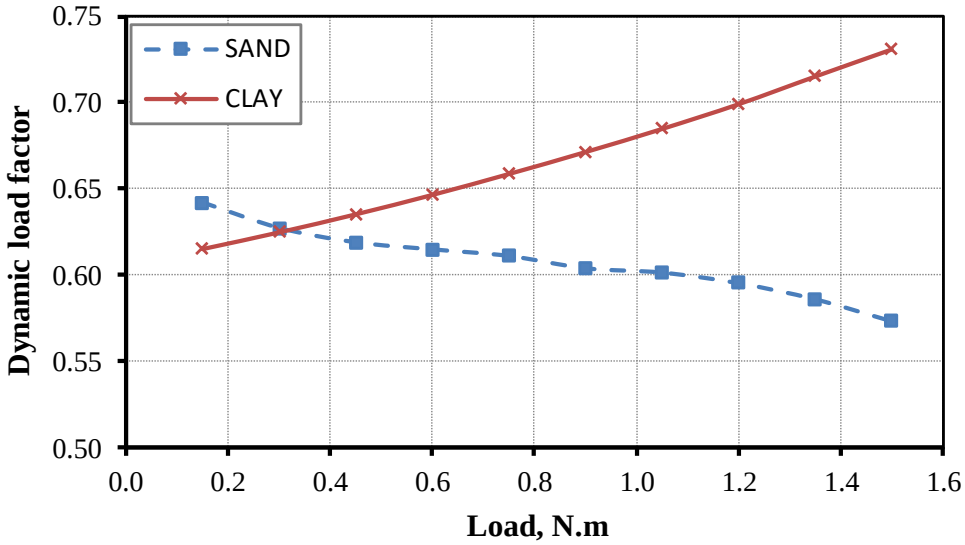

Figure 4-29 Dynamic load factor with increase in wind load

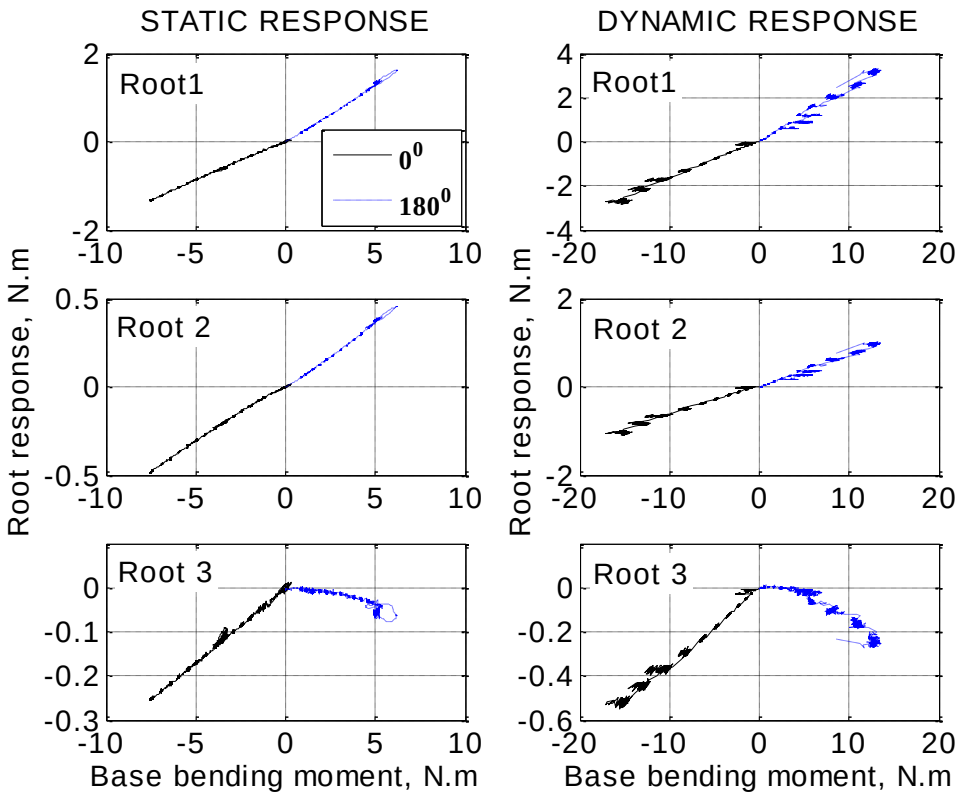

Figure 4-30 Root plate response of T2 in clay

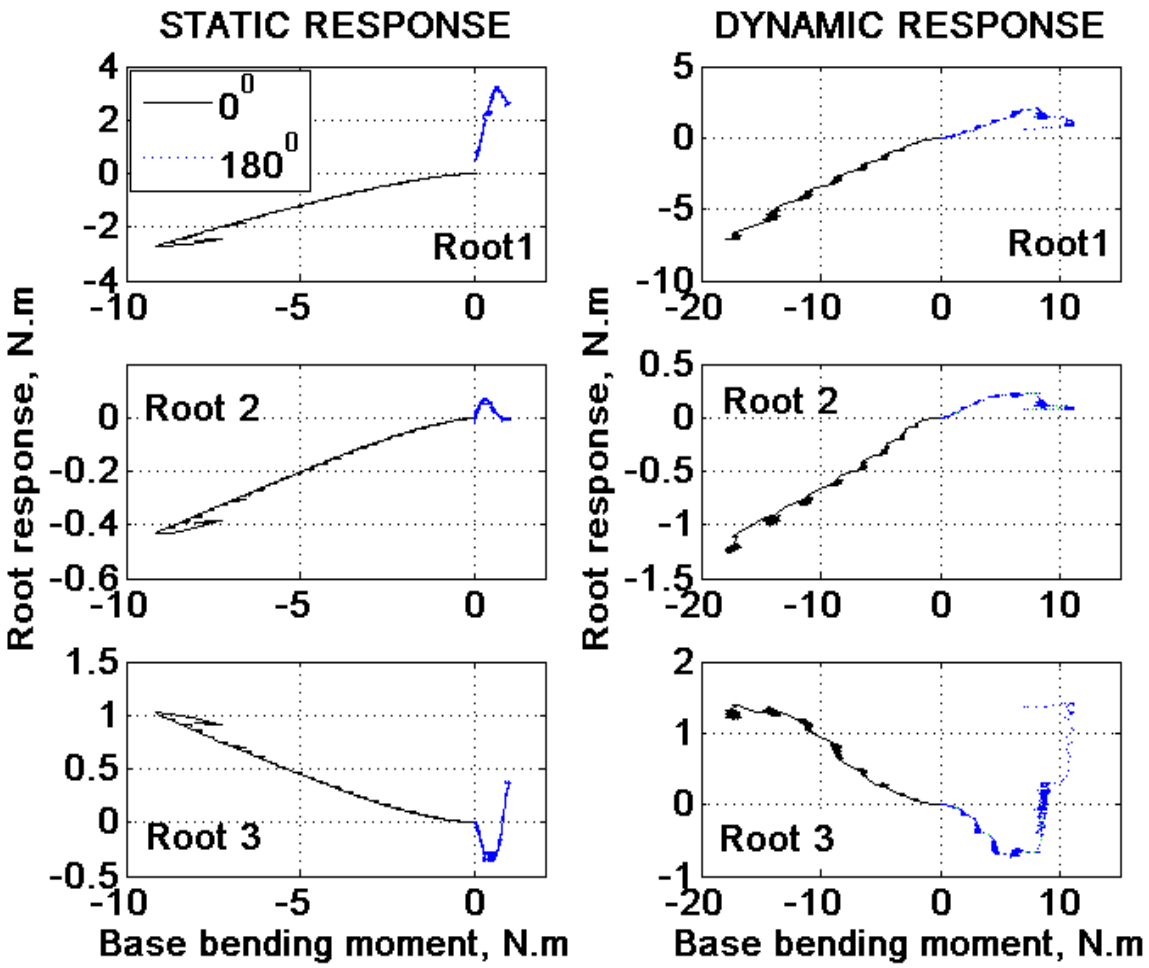

Figure 4-31 Root plate response of T2 in sand

Chapter 5

5 Wind Tunnel Experiments on Trenching

5.1 Introduction

It is often necessary to create engineering structures adjacent to trees in the urban environment. In particular, the wind stability of a tree will be potentially affected by the creation of a trench and loss of any root mass. Arborists have a number of empirical approaches for determining the appropriate distance from the stem where the tree root system can be safely compromised. In this study the effect of trenching on the biomechanics of small Norway Spruce trees is conducted to investigate the problem. Tree saplings with a full structural root system were placed in a custom built sunken planter box fitted into a wind tunnel floor. Clay and sand soil mediums were used for cohesive and frictional trenching conditions respectively. The tree saplings were subjected to incremental wind velocities in a boundary layer wind tunnel. Trenches were excavated at different distances (from 7 to 2 tree diameters) from the tree stem on the leeward side. Pull-release (free decay), static pullover and cyclic failure tests were conducted on the trees to investigate the changes to the load-displacement behavior, critical bending moments, natural frequency and damping with increasing trench size. This approach has enabled confirmation of current empirical methods for determining safe trenching distances from trees and further insight into the effective width and performance of tree root systems.

5.2 Background

The stability of urban trees under wind loading is an important issue to ensure the safety of people and to avoid property damage because of the tree failure. Environmental, ecological and economic benefits of having trees in the urban environment are endless [Bernatzky 1978, Thomas 2000, Ferrini et al. 2008] and are also very much dependent on tree longevity [Koeser et al. 2013]. Not only that the urban environment increases the vulnerability of trees [Matheny and Clark 1998, Jim 2003], the urban tree failure is also a huge liability. Even though urban tree stability requires special attention, urban trees are

less studied than forest trees [Gardiner et al. 2016]. Infrastructure, construction and space restrictions often cause significant impact on tree stability [Miller and Neely 1993, Jim 2003, Fini et al 2013]. Construction and service related trenching is often necessary in urban areas. As the soil and roots are big factors in tree stability [Fraser 1962], trenching causes a twofold loss to the tree anchorage strength due to loss in root mass and soil support.

A key aspect of tree stability is the root-soil plate anchorage strength [Smiley 2008]. According to a major tree failure data base, 35% of tree failures are due to roots [ITFD 2013]. Root anchorage strength varies with root plate architecture, root tensile strength and soil shear strength which changes with soil properties and water content [Coutts et al. 1983, 1986; Crook and Ennos 1998, Stokes and Mattheck 1996, Stokes et al. 1996, Crook et al 1997]. The shape and size of root system not only depends on tree species, but also depends on the soil it is growing in and the forces the plant had to withstand while growing [Ennos and Fitter 1992, Stokes and Mattheck 1996]. Tree lateral roots are usually spread in the uppermost layers of soil [Sutton 1969, Somerville 1979, Stokes and Guitard 1997] and act like guy ropes [Ennos 1993] to support the tree. Vertical sinker roots develop into the ground and provide a valuable component of the anchorage system [Stokes and Mattheck 1996]; these anchor the tree centrally. Soil shear strength may obstruct root growth [Taylor and Gardner 1963], but can also provide high anchorage strength. Soil shear strength also increases with increase in root embedment length, root diameter and angle of distribution [Wu et al. 1988, Yu et al. 2011]. However, high soil compaction and water logging can often restrict root growth and weaken the anchorage strength. Missing or poorly developed roots on one side can also significantly reduce the tree stability [Coutts 1983, 1986]. Another important factor influencing anchorage strength is the variation of root wood strength [Stokes and Mattheck 1996]. Roots must be strong enough to transfer the tensile and shearing forces on the windward side, and the compressive forces on the leeward side to the soil [Coutts 1983, 1986]. Root anchorage strength is a complex interaction and combination of various factors; as long as the tree transfers wind loads safely to the root system and the root system to the soil, the tree remains stable.

Urban trees are more susceptible to windthrow because of low anchorage strength due to shallow root systems (because of space limitations and unfavorable soil conditions), risk of root loss (because of side walk replacements, utility related trenching and root pruning conducted to avoid foundation damage of homes), and compromised anchorage strength (because of the strains associated with the urban environment) [Miller and Neely 1993, Wessolly and Erb 1998, Brudi and Wassenaer 2001, Jim 2003, Day et al. 2010]. In particular trenching in urban environment is unavoidable, making it very important to know the tolerable root loss limit which does not affect the tree stability [O'Sullivan and Ritchie 1993, Fini et al 2013].

Guidelines are available for arborists, based on tree height, branch spread and trunk diameter at breast height (DBH) [Miller and Neely 1993, Miller et al. 1993, Mattheck and Breloer 1995]. The American Society of Consulting Arborists (ASCA) [1989] recommends 0.3 m for each 0.025 m DBH and the British Standards Institute (BSI) [1989] and Watson [1990] recommends a distance of 0.2 m for each 0.025 m DBH [Miller and Neely 1993]. Based on trenching tests conducted by Miller and Neely [1993] on four shade species, only 15% growth reduction occurred in three of the four examined species with trenching higher than the BSI recommendations. From these results Miller and Neely [1993] also recommend ASCA and BSI guidelines. These guidelines though helpful are based on tree site characteristics and tree failure data, because of lack of robust research arborist are often in a dilemma to save trees in urban areas with competing requirements for urban development [Ghani et al. 2009].

Literature on root pruning and trenching studies are minimal and the literature on the effect of dynamic loading on tree stability with trenching is even more rare. As tree failure often occurs due to the dynamic wind loads [O'Sullivan and Ritchie 1993, James et al. 2006], this is of major concern to society. Smiley [2008] and Smiley et al [2014] studied the effect of root pruning on the stability of Young willow oak (Quercus phellos) and Red maple (Acer rubrum) respectively through trenching and root severance. From winching tests of Young Willow Oaks with trenching [Smiley 2008], one-degree pull-testing data showed 15% reduction with a trench within two times the trunk diameter, 23% reduction at one

trunk diameter distance and 35% when the trench was cut tangential to the trunk. With mature red maple trees [Smiley et al. 2014] the failure force was highly variable, on an average 13% of the force was reduced by cutting one root, by cutting 1/3rd of the roots 35% of force was reduced and by cutting half of roots the force was reduced by 47%. It was noted by Smiley et al. [2014], that smaller willow oaks might have more efficient oblique roots compared to mature red maple tree roots making them more vulnerable to root severance compared to young willow oaks. Ghani et al. [2009] studied the effect of trenching on root system anchorage, trenches were dug at different distances from the trunk and the trees were uprooted through winching. Root systems were extracted and analyzed to relate the performance to architectural parameters. Among 25 trees examined, tree height, DBH, crown spread, and root plate depth and diameter did not differ much between the groups. They also saw only 13% decrease in anchorage strength with trenching as close as 0.5 m for 0.21±0.02 m DBH trees. The reason for less variability in the anchorage strength was because of the presence of tap roots (high root plate depth). Fourcaud et al. [2008] also suggested that taproot or rooting depth is the major component of anchorage; hence trenching lateral roots would have little effect on anchorage if tap roots are present.

The only work available on cyclic loading with trenching is O'Sullivan and Ritchie [1993], who investigated the soil-root plate mechanism of Sitka spruce trees (around 0.2 m DBH) growing on a peaty gley (highly organic water logged clay with low ash content and high lignite coal content) soil were examined. About 33% decrease in overturning moment with trenching (with a semi-circular trench around windward side, about one meter from the stem center) of and 26% decrease in soil resistance component due to cyclic loading was observed. Reduction in peak anchorage strength with repeated loading was observed; associated reasons were noted as progressive anchorage failure and energy dissipation. It was also discussed by O'Sullivan and Ritchie [1993] that since windthrow is a dynamic process and loading of a tree's root system is not static and the expected soil strength decreases with cyclic loading [Carter et al. 1982], dynamic loading tests would provide better guidelines.

The surveyed literature clearly indicates the importance of dynamic loading tests on tree stability with trenching. In this study, we tried to quantify the impact of soil strength and root loss on tree stability using Norway spruce saplings. Trenching tests were conducted in both cohesive and non-cohesive soils in a wind tunnel. The tests monitored and analyzed the effect of root loss on tree anchorage strength in two very different soils with increase in trenching size proximity and wind loading.

5.2.1 Research objectives

The purpose of this study is to assess the impact of soil strength and root loss on the mechanical stability of trees with increase in wind loading and trenching. This experimental study was designed to relate and quantify these changes in tree stability with change in soil properties, trenching, proximity and wind speed. Two very different soils (clay and sand) were used as on root medium. The instrumented tree root structure was subjected to incremental trenching and incremental wind loading was used to take the trees to failure in the wind tunnel.

Extensive sapling tree response data was collected from this novel experimental study and was used:

i. To investigate tree stem response by tracking and comparing the stem displacement, base bending moment response and the tree sway;

ii. To investigate root-soil plate response by examining the root bending response and the root plate anchorage strength;

iii. To investigate the variation in tree dynamic properties through the assessment of natural frequency, damping and mechanical admittance;

iv. To investigate the variation in root plate failure mechanism and tree stability.

5.3 Experimental setup and test procedure

To study and understand the dynamic response of trees to trenching and incremental wind loading, wind tunnel tests were conducted with tree saplings (S1 & S2) in a custom built sunken planter box. The experiments were conducted in the Boundary Layer Wind Tunnel (BLWT) laboratory at the Western University, Ontario, Canada. The tree sapling test setup in the wind tunnel is as shown in the Figures 5-1 and 5-3 respectively for tree saplings S1 and S2 respectively. The floor exposure used was "open country" for all the tests, wind velocity during the tests was recorded using five pitot tubes and a hot wire anemometer. Three pitot tubes at ceiling height (2 m above wind tunnel floor) recorded the reference wind speed. Two pitot tubes were used to record the wind speed at two different heights of the tree structure as shown in Figure 5-1 . A hot-wire anemometer was placed at a height close to the center of gravity of the tree, to measure the turbulence of the wind field. Three laser transducers were used to measure the deflection of the stem at three different levels as shown in Figure 5-1. LB series, Keyence laser displacement transducers were used with ± 10 cm measuring range and 180 µm resolution.

The tree saplings (S1 & S2) were 1.2 m and 1.29 m tall Norway spruce (Picea abies [L.] H.Karst.) trees. Both S1 and S2 had an asymmetrical root system; the root systems are as shown in Figures 5-2 and 5-4 respectively. Both the tree saplings (S1 & S2) were pruned up to the height of 0.4 m above the ground level. The DSH (diameter at stump height) of the tree saplings S1 and S2 were 42 mm and 48 mm respectively. The structural root system of the saplings was generally kept intact. To ensure a simple root architecture, all of the fine roots were pruned leaving just the structural roots (> 0.4 mm diameter) in place, as shown in Figures 5-2 & 5-4.

KFG-30-120-C1-11L1M2R type strain gauges were used to track the stem and root response, these strain gauges are two wire lead gauges with 30 mm gauge length and 120 ohm resistance. To attach the strain gauges, bark was removed carefully without damaging the stem and root wood fibers; strain gauges were glued to the stem and roots as shown in Figures 5-1 to 5-4 using Cyanoacrylate adhesive (CC-35X5). This is best suited to porous materials with an operating temperature range of -30 to 120^{o}C. Strain gauges were attached

at two locations along the stem length of each tree sapling to track the lateral and windward strain response with increase in wind load. A ring of four gauges were attached at each location; two located opposite one another to track the windward strain for the stem and vertical in the case of the roots. The other two were placed 90 degrees from the previous ones, to track the lateral responses. Each set of two gauges were placed diametrically opposite one other, so that one gauge would track the tension response and the other would track the compression response. These were connected to the logger in a basic Wheatstone bridge configuration using a half bridge arrangement. A similar ring of four gauges was attached at various locations on the S1 and S2 root systems as shown in Figures 5-2 and 5-4. These were used to track the vertical and lateral response of the roots during wind loading. Because of lack of diametrical size only one set of two strain gauges were in some locations [Figures 5-2 and 5-4], to track response in that direction.

A custom built octagonal sunken planter box, with sides measuring 0.36 m and depth of 1.2 m was built to fit the turntable in the downwind section of the wind tunnel. The planter box was filled with soil leaving 0.1 m depth unfilled. A tree sapling with root plate was placed in the middle of the planter box and the root plate was carefully buried in soil by filling the remaining soil box without causing any significant strain to the root plate and the attached instrumentation. Two soil media with contrasting states and properties were chosen to gain insight into the effect that soil has on tree response to wind loading. Sand tests were conducted with Barco #32 silica sand (Barco, 2015) in a dry state, to test the root response to wind loading in a purely frictional soil. The maximum and minimum dry density of the silica sand based on void ratio estimates and specific gravity are 17.7 kN/m^3 and 15.9 kN/m^3. The clay soil was prepared using Bentonite (sodium form) and water (~ 300%). For every 25 % of Bentonite in weight, 75 % of water in weight was added and blended in a laboratory mixer; care was taken to ensure that the clay was blended effectively. The peak shear strength of the clay mix in the soil box was found using a Pilcon hand vane tester. The shear vane tests were conducted before and after the wind loading tests. The 33 mm diameter vane was used to measure the peak shear strength and the measured shear strength was around 4 kPa, which was the average of 4 tests conducted during the wind tunnel testing.

In this experimental study, the applied wind field and the tree response was recorded in great detail. Typical incremental wind loading applied to the tree sapling in the wind tunnel was as shown in Figure 5-5. Each load increment lasted for 180 seconds, wind load was increased manually which took about a second. The open country profile used had a turbulence intensity of 0.18.

The differences in the biomass of tree saplings S1 and S2 are shown in the Table 5-1. S1 weighed 1.6 kg, and S2 weighed 3.7 kg, with 130% increase in total tree weight. However, inspection of the biomass of the root systems show a much lower increase root biomass percent for tree S2 compared to above ground biomass of S2. S1 was used for trenching tests in clay and S2 was used for trenching tests in sand alone. But S1 was once tested with no trenching in sand to have the comparative anchorage strength between S1 and S2 in sand. Considering the differences in S1 and S2 biomass, it was surprising to see both S1 and S2 failed at 11.9 m/s wind speed with root systems in sand. In this study wind speed was only increased up-to 11.9 m/s, S1 in clay did not fail at maximum tested wind speed.

The flexibility of the experimental techniques described provided the opportunity to study the dynamic properties of the tree saplings with complete root systems and following trenching in different soil media. Trenching in clay and sand were carried out in a different manner as explained below. For the sets of tests (trenching in clay and sand), the tree orientation was chosen based on the root asymmetry as shown in Figures 5-2 and 5-4. The orientation providing the highest anchorage strength (more roots on the leeward side) was chosen for testing.

5.3.1 Trenching in clay

In clay the soil medium was removed and roots were left in place as shown in Figure 5-6. For each test, the distance form the edge of the tree stem on the leeward side of the tree was measured in terms of tree stem diameter (D or DSH). For S1, DSH was 4.2 cm, trenches were dug at 7D (29.4 cm) to 2D (8.4 cm) from the stem edge parallel to the wind tunnel front/back wall (perpendicular to the direction of wind flow), with 4.2 cm (1D) intervals as shown in Figure 5-6.

5.3.2 Trenching in sand

In the case of sand, as sand can not be removed in sections as with the clay, along the length of the root plate on the leeward side was cut incrementally from 7D to 2D as shown in Figure 5-7. For S2, DBH was 4.7 cm. Each test was conducted after the roots were cut up to the distance of 7D (32.9 cm) to 2D (9.6 cm) from the stem edge and placed in the sand carefully without causing any strain to the strain gauges attached to the root plate. The pruned root mass at each trench was as shown in Table 5-2. Almost half of the root mass was removed by the creation of the 2D trench.

5.4 Tree stem response with trenching volume

5.4.1 Displacement time history

The stem displacement response to the applied wind loading was recorded by the laser transducers arranged at three different heights of the stem as shown in Figures 5-1 and 5-3. The displacement time history of tree saplings in clay and sand with increase in trenching and wind loading is presented in Figures 5-8 and 5-9 respectively.

The tree sapling, S1 did not fail in the clay, the position was kept the same throughout the trenching from 7D to 2D, i.e., the tree sapling was not repositioned after each test. The tree sapling experienced cyclic and incremental wind loading from each test from 7D to 2D trenching and finally failed for the 2D trench test at 11.9 m/s wind speed. The laser transducers and the strain gauges were adjusted to zero after each test. From Figure 5-8, clear and steady increases in displacement with increase in trenching volume can be observed. Deflection of the tree doubled from the 7D to the 3D trench for the same amount of loading and was almost tripled for the 2D trench. From the 7D to the 4D trench decreases in overturning resistance and hence increases in deflection were minor for the same amount of loading. However, for the 3D trench, drastic increase in deflection was observed for the same amount of loading.

In contrast, the tree sapling S2 in sand was tested to failure for each trench. In Figure 5-9, the S2 displacement time history with increase in trenching and wind speed is shown. Based on the load increment for the given loading, it is clear that the overturning resistance

did not decrease with increase in trenching from 7D to 6D. The resistance started decreasing for the 5D trench. The resistance significantly reduced with 3D trench. For the cohesive soil (clay), the S1 deflection [Figure 5-8] with increase in trenching volume was increasing gradually up until 3D trench. In the case of frictional soil (sand), S2 deflection did not increase significantly from 7D to 3D at the same amount of wind loading, the deflection was even lower for the 4D trench compared to the 7D trench deflection [Figure 5-9], the tree sapling might be settling in instead of deflecting with the pruned root structure. Similar trend (no loss in resistance with increase in trenching volume) was observed for the 5D and 4D trenches with a slightly lower anchorage resistance compared to the 7D and 6D trenches. In cohesionless soil (sand), the tree sapling failed at low deflections with increase in root pruning.

5.4.2 Stem base bending response with increase in trenching volume

To understand the rotational stiffness, the stem base rotational response (angle of deflection about stem base) with increase in stem base bending moment was plotted with increase in trenching volume for S1 and S2 in the clay and sand respectively.

Tree sapling bending response to the applied wind load was recorded with the strain gauges attached to the stem base in the leeward direction. Angular deflection of the stem base (θ) was estimated using the equation below:

$$\theta = \tan^{-1}\frac{d_l}{h_l} \qquad [5\text{-}1]$$

Where d_l is the lateral deflection of stem in the leeward direction from the laser transducer and h_l is the height of the laser transducer.

Rotational response of S1 in clay with increase in base bending response and trenching is shown in Figure 5-10. The rotational stiffness (inverse of base bending moment vs angle of deflection slope) of S1 gradually decreased with increase in trenching volume from 7D to 4D; the 3D trench caused significantly higher rotational movements for given moments. Almost 20% loss in stem base rotational stiffness occurred from the 7D to the 3D trench

and 60% loss for the 2D trench. In the case of sand [Figure 5-11], the S2 rotational stiffness did not vary much with increase in trenching volume. However, the tree failed at lower wind loads with increases in trenching volume.

Stem base rotation with increase in wind speed and trenching is plotted as shown in Figures 5-12 and 5-13 for the clay and sand respectively. The stem base rotation of S1 in clay for each trench with increase in wind speed can be clearly seen in Figure 5-12. Deflection for the 3D trench was significantly higher. For the case of sand [Figure 5-13], S2 seems to be sinking into the sand with the pruned root architecture and the tree is failing at lower and lower wind speeds with increase in trenching volume.

5.4.3 Change in tree sways with increase in trenching volume

To better understand the complex dynamic response of the trees to wind loading, the sway motion of the tree stem was plotted for each trench. Holbo et al. 1980, Mayer 1987 & 1989, Peltola 1995, James et al. 2006 and Sellier et al. 2008 previously tracked the swaying motion of tree stems to wind loads. Two sets of strain gauges attached orthogonally near stem base were used to track the response data. The joint response of the base bending moment in the orthogonal directions was plotted to track the tree stem sway.

In order to explain the complexity of the sway motion, statistical analysis was performed, and the sway behavior was investigated using a bivariate normal probability density function, to visualize and better understand the sway motions. The two variants used to track the spatial distribution are the windward (along wind) and lateral (across wind) bending moment response of the stem base with increase in trenching for selected wind loads.

The response data at each load increment was analyzed statistically and the bivariate (two-dimensional) normal distribution was plotted with a joint probability density function, f(x,y) as shown in Equation [3-5]:

$$f(x,y) = \frac{1}{2\pi\sigma_1\sigma_2\sqrt{1-\rho^2}} \times exp\left\{-\frac{1}{2(1-\rho^2)}\left[\left(\frac{x-\mu_1}{\sigma_1}\right)^2 - 2\rho\left(\frac{x-\mu_1}{\sigma_1}\right)\left(\frac{y-\mu_2}{\sigma_2}\right) + \left(\frac{y-\mu_2}{\sigma_2}\right)^2\right]\right\} \quad [5\text{-}2]$$

$-\infty < x < \infty$, $-\infty < y < \infty$

Where X and Y are the orthogonal response data vectors at each wind load increment, μ_1 and μ_2 are the means, σ_1^2 and σ_2^2 are the variances of X and Y respectively, while ρ is the correlation coefficient of X and Y.

The mean for a continuous type random variable X is, $\mu=E[x]$, variance $\sigma^2 = E[(x-\mu)^2]$, correlation coefficient of two random variables X and Y is $\rho = \frac{cov[x,y]}{\sqrt{\sigma_1^2\sigma_2^2}}$ and covariance, $cov[x, y] = E[(x-\mu_1)(y-\mu_2)]$.

Each data set has been statistically analyzed and the results are presented with sway plots. Statistical parameters that best describe the sway plots are coefficient of variation, skewness and kurtosis. The ratio of standard deviation (σ) to the mean (μ) is called the *coefficient of variation* and it shows the extent of variation in relation to mean. *Skewness* is the ratio of $E[(x-\mu)^3]$ to σ^3, which is a measure of asymmetry of the system. If skewness is zero, the probability density function is symmetric with respect to its mean value [Ochi 1990]. If the value is positive, the tail of the probability density function is fatter or longer on the right side than the left side and vice versa if the value is negative. *Kurtosis* represents the degree of peakedness of the sway distribution and is the ratio of $E[(x-\mu)^4]$ to σ^4 [Ochi 1990]. For a normal distribution, the kurtosis value is equal to 3. If the value is less than 3, distribution is called platykurtic (mild peak) and if the value is greater than 3, the distribution is called leptokurtic (sharp peak). The results of the statistical analysis of each data set used for the sway plots are shown in Figures 5-14 and 5-15.

S1 with an asymmetrical root system in the clay, with most of the roots in line with the wind direction and on the leeward side [Figure 5-2] was trenched from 7D to 2D distances as explained in Section 5.3. The sway responses of the S1 stem base were compared with increase in trenching at 11.9 m/s wind speed, as shown in Figure 5-14. The root plate in the soil medium (clay) lost soil support with each trenching increment, even though the sway pattern looks similar there are some important fine details to note from the statistical analysis [Figure 5-14] as explained below. Note: for the 2D trench the sway plot does not fully represent the data statistically analyzed. The sway plot in this case included the failure response to depict the sway pattern of tree failure response. The data statistically analyzed was taken up-to, but not including, the failure point, to uncover the statistical details leading up-to failure. The following statistical observations can be made.

Mean: the mean response of the tree stem in windward and lateral direction indicates the S1 tree resistance to the applied wind force. For the same amount of applied load, the windward response decreased from 12.5 N.m to 8.4 N.m, a total one third loss in windward resistance with increase in trenching from 7D to 2D can be observed. In the lateral direction the stem response did not lose much resistance from 7D to 2D trench sizes.

Variance: the variation in response from the mean indicates the spread in the sway plot. The variance in the windward direction showed significant decreases from 7D to 6D, 4D to 3D, and from 3D and 2D trenches. In the displacement time history [Figure 5-8], these were clearly the critical trenching distances. In the lateral direction not much difference was observed.

Skewness: this gives the measure of probability density distribution symmetry. All of the skewness this values were close to zero indicating more or less symmetry in distribution. Skewness was shifted from 0.1 to -0.1 in the windward direction, i.e. the tail of the probability density function is fatter or longer on the right side and shifted to the left side. This is feasible as the distribution is moving with mean values from -12.5 to -8.4 N.m. Surprisingly the lateral distribution became more symmetric with increase in trenching, changing from 0.13 to 0.06.

Kurtosis: the peakedness of the distribution was close to 3 in most of the cases except for the lateral response of the 2D trench where the tree failed. The probability distribution in the lateral direction at 6D had a sharp peak (kurtosis>3), and changed to a mild peak (kurtosis<3) at 2D meaning. the response changed from a highly concentrated mode to low variance distribution.

Decrease in covariance and correlation coefficient between the orthogonal responses of the S1 stem was observed with increase in trenching volume.

In Figure 5-15, the sway responses of the S2 stem base in sand were compared for increases in trenching from 7D to 3D at 7.8 m/s wind speed. The statistical analysis of the response data is also presented. S2 also had an asymmetrical root system (similar to S1), but S2 also had a strong tap root as shown in Figure 5-4. S2 was also tested through trenching from 7D to 2D distances (note the root plate in the sand was pruned from 7D to 2D) as explained in Section 5.3. The tree failed for the 2D trench before the load point was reached (7.8 m/s), so only the sway response from 7D to 3D are presented in Figure 5-15. Detailed discussion on the changes in the sway properties of S2 with increase in trenching from 7D to 3D is presented below:

Mean: the mean response of the tree stem in the windward direction decreases slightly, but did not vary much. In the lateral direction it varied significantly with no order, the explanation could be that the tree was settling in the soil and as the root plate was pruned. Significant difference was observed for the 5D trench at 5.09 N.m compared to 0.69 N.m at 7D trench [Figure 5-15].

Variance: the variation in response from mean indicates the spread in sway plot. It is interesting to note that no significant variation was observed in either direction.

Skewness: this gives the measure of probability density distribution symmetry. All the skewness values were slightly below zero or close to zero indicating a more or less symmetrical distribution.

Kurtosis: the peakedness of the distribution was close to 3 in most of the cases except for the windward response at 5D, where relatively lower kurtosis can be seen. This indicated that the peak was milder than the rest of the distributions.

No orderly change in covariance and correlation coefficient between orthogonal responses of stem was observed in the sand with increase in trenching.

For the case of clay, a more systematic change in distribution was observed, even though S2 in sand showed more similar and symmetric distributions in each trenching case, any change in response in sand seemed sudden and unpredictable at this point.

5.5 Root plate response with trenching volume

5.5.1 Change in root bending moments with increase in trenching

The tree sapling response of the roots is examined with increase in trenching and wind speed to understand the anchorage mechanism. Root response was tracked by the strain gauges attached to the roots of S1 and S2 as shown in Figures 5-2 and 5-4 respectively.

In Figure 5-16, the S1 root response in clay for the 7D and 3D trenches is shown. The root architecture of S1 was as shown in Figure 5-2. Root 1 was in the direction of wind load on the leeward side and was fatter compared to any other root in the system. Root 2 orientation was about 20 degrees to the Root 1 direction. Both Root 1 and 2 were subdivided from the mid length. Root 3 was more oblique and was in the middle of leeward and lateral direction, but provided depth to the root plate. Root response of S1 changed significantly from the 7D to 3D trenches. For the 7D trench most of the root anchorage resistance was done by Root 1. Root 2 and 3 carried only $1/3^{rd}$ and $1/10^{th}$ of the loads compared to the Root 1 resistance. For the 3D trench, the Root 1 load response decreased to almost $1/3^{rd}$ of its value compared to its response in the 7D trench and the Root 3 response increased to three times its value from the 7D to 3D trench. The response of Root 2 was flat because the strain gauge attached area of the root was not covered by soil medium at 3D trench [Figure 5-6]. In the clay with increases in trenching, redistribution of the loads in the root system was significant.

The root response of S2 in sand with increase in trenching is as shown in Figure 5-17. The root architecture of S2 was asymmetric; it has a strong tap root as shown in Figure 5-4. Root 1, 3 and 9 were strain gauged as shown in Figure 5-4. In Figure 5-17, the response plotted was from the strain gauges attached close to the tree stem on Roots 1, 3 and 9. Root 1 was in the direction of wind load and was on the leeward side. Root 2 was oriented around 90^0 from Root 1. Root 9 was fully bent downward and was acting as an anchor in the frictional soil. Root system response in both the 7D and 3D trenches showed the same response variation, except that the tree failed at 25% lower wind load for the 3D case. Root system load does not seem to redistribute with trenching in sand, but the Root 1 response reduced 90% from 7D to 3D, where as Root 3 showed the same amount of response for 7D even at 25% lower wind load than the 3D trench. The response of the Root 9 was reduced around 25% with increase in trenching from 7D to 3D.

These results give an indication that if the soil support in strong, load gets redistributed in the root system (as in the case of clay of this study) with trenching, providing more anchorage strength to the tree.

5.5.2 Secant modulus of rotation

Secant modulus is the ratio of stress to strain at the chosen point on the stress-strain curve, if the initial stress and strain values are zero. To calculate the secant modulus of rotation, stem base bending moment was plotted against stem base rotation. Before each test stem base bending moment and rotation were at zero, and the secant modulus of rotation is the ratio of base bending moment to the stem base rotation at each selected load. Base bending response of the tree stem from strain gauge attached in the windward direction and the lower laser to estimate the rotational response were used for secant modulus of rotation.

In Figure 5-18, secant modulus of rotation variation of S1 with increase in wind load and trenching in clay is shown. An initial peak in secant modulus occurred from 7D to 3D for all tests at around 2 m/s wind speed. Variation in secant modulus showed at least two peaks with increase in wind load to 12 m/s for all trenching cases except 6D. Similar trends in stiffness variation were also observed by O'Sullivan and Ritchie [1993] when the tree was

subjected to cyclic loading, who suggested the reason was progressive failure. In this case it seems that the tree sapling was showing similar displacement nature. With increase in load, displacement was slowly increasing with increase in wind load. When higher displacement occurred with increase in wind load, the tree moved to a new more stable location and the soil in the new location showed higher stiffness, and the response continued to show this trend.

In Figure 5-19, secant modulus of rotation variation of S2 with increase in wind load and trenching in sand is shown. The stiffness peak occurred at around 2 m/s wind speed for all of the trenching cases. 80% reduction in secant stiffness occurred at the failure wind speed. Similar trends in stiffness variation was observed for all of the cases, with decrease in failure wind load with increase in trenching volume.

5.6 Change in tree dynamic properties with trenching volume

5.6.1 Natural frequency and damping summary with increase in trenching volume

Natural frequency and damping ratio are very important dynamic properties of trees that characterize tree response to wind loading. Natural frequency gives the dominant number of oscillations of a structure per second, whereas the damping ratio determines the amount of energy lost in each oscillation of the system.

The logarithmic decrement method is the most useful and an easiest method to estimate the damping from free vibration decay [Clough and Penzien 1993] in the time domain. In this method, the rate at which the amplitude of a damped vibration decreases is measured over one or n number of cycles. If x_1 and x_{n+1} are the amplitudes of vibration of the first cycle and after n number of cycles respectively, the damping ratio (ξ) is given by:

$$\xi = \frac{\delta}{\sqrt{(2\pi)^2 + \delta^2}} \qquad [5\text{-}3]$$

Where $\delta = \frac{1}{n}\ln\left(\frac{x_1}{x_{1+n}}\right)$

Pull-release (free decay) tests were conducted before each trenching test to estimate the dynamic properties of the tree. The stem base response data is used to calculate the dynamic properties.

As shown in Tables 5-3 and 5-4, the general trend of decrease in natural frequency and increase in damping was observed in both clay and sand with increase in trenching volume. In clay, around 5% decrease in natural frequency and 40% increase in damping was observed; in sand 6% decrease in natural frequency and almost 50% increase in damping was observed. The decrease in natural frequency indicates the loss in tree stability, as the S2 stability was decreasing at higher phase the natural frequency of S2 was showing lower natural frequency compared to S1 in clay. Higher damping increase of S2 compared S1 could be the tree survival strategy of losing as much energy as possible when it is approaching to failure.

5.6.2 Change in spectral response and mechanical admittance with trenching volume

The power spectral density (PSD) of the tree stem base bending moment response was plotted using Fast Fourier Transformation (based on Welch's method [Welch, 1967]). The power spectral densities of tree saplings S1 and S2 are shown in Figures 5-20 and 5-21 respectively at 7D and 3D. The base bending moment response spectra, $S_B(f)$ in terms of wind spectra, $S_v(f)$ and the mechanical admittance function, $\mathrm{H}(f)^2$ is given in Equation [3-15] and the mechanical admittance in terms of wind spectra, and tree response is given by Equation [3-16] [Baker 1995] below:

$$S_B(f) = h_{cg}^2 \mathrm{H}(f)^2 S_F(f) \qquad [5\text{-}4]$$

$$\mathrm{H}(f)^2 = \frac{1}{\left[\rho A C_D \bar{v} h_{cg}\right]^2} \frac{S_B(f)}{S_v(f)} \frac{1}{\Gamma(f)^2} \qquad [5\text{-}5]$$

Where ρ is the air density (1.218 kg/m^3), A is the frontal area of the crown [Table 5-1], C_D is the drag coefficient (0.7 [chapter 3]) and $\bar{V}$ is the mean wind speed (11.9 m/s for S1 and 7.8 m/s for S2 analysis). A Norway spruce tree sapling was tested on a force balance and

analyzed in Chapter 3 to estimate the drag coefficient of Norway spruce tree saplings with similar dimensions and incremental wind loading as used in this chapter. The C_D value at the wind speeds was found to be 0.7 from Chapter 3 and the same value is used in these calculations too. The aerodynamic admittance ($\Gamma(f)^2$) value of 1.0 is taken for the mechanical admittance estimates.

Along with the resonance at tree natural frequency another important information to observe from the mechanical admittance is the energy transfer at various frequencies. As shown if Figures 5-21 and 5-22, low transfer in energy with increase in trenching volumes was observed in clay at higher frequencies (>tree natural frequency) and in sand at lower frequencies (<tree natural frequency). As observed from this study, S2 stiffness did not vary much with increase in trenching volumes, that could be the why S2 was not showing loss in energy transfer at high frequencies.

5.7 Failure loads (with increase in trenching volume)

5.7.1 Clay

In clay, soil strength degradation appears to be progressive as the failure occurred because of excessive yield and displacement. The soil wedge resisting the tree movement failed at 2D trench at 11.9 m/s as shown in [Figure 5-22]; resisting shear stress is from skin friction around the roots and shear strength of the soil around the tree stem base. Socketing was observed at the stem base as shown in Figure 5-22.

As S1 did not fail in the clay with increase in trenching, the probability of failure of S1 in clay with increase in trenching volume is studied. Applied wind load to the tree sapling was estimated as shown in Equation [5-6] below:

$$BM_{wind\ load} = S = F \times h_{cg} = \left[\frac{1}{2}\rho A C_D \bar{V}^2\right] h_{cg} \qquad [5\text{-}6]$$

Tree center of gravity (h_{cg}) was estimated based on the S1 mass distribution; it was 0.6 m above the tree stem base strain gauge. and ρ is the air density (1.218kg/m^3), A is the frontal area (0.35 m^2) of the crown [Table 5-1], C_D is the drag coefficient (0.7) and $\bar{V}$ is the mean

wind speed (11.9 m/s). The response (resistance) data was from the stem base bending resistance recorded by the strain gauge attached at the stem base with increase in wind load for each trench. A Gaussian fit of wind load and stem base strain gauge response at 11.9 m/s at each trench was estimated as shown in Figure 5-23. The comparison shows the difference between 'load' and 'resistance' of the system. From the overlap of the two distributions, the S1 probability of failure with increase in trenching was estimated and plotted as shown in Figure 5-23.

The probability of failure from the load and response data was estimated using Equation [5-7] [Melchers, R. E. 1999] below:

$$P_f = \Phi\left(-\frac{\mu_R - \mu_S}{\sqrt{\sigma_R^2 + \sigma_S^2}}\right) \quad [5\text{-}7]$$

Where S and R are the load and resistance data vectors at each wind load increment, μ_S and μ_R are the means, σ_S^2 and σ_R^2 are the variances of S and R respectively, Φ $\left(\Phi(z) = \frac{1}{\sqrt{2\pi}}\int_{-\infty}^{z} e^{-z^2/2}dz\right)$ [Ochi 1990] is a standard normal distribution function and P_f is the probability of failure.

As shown in Figure 5-23, significant increase in probability of failure started from the 4D trench. Probability of failure jumped from 0.08 to 0.17 for the 4D to 3D trench and was 0.85 by the 2D trench. As the tree failed for the 2D trench, the statistical analysis presented in this section could be useful to predict tree stability with increase in trenching volumes.

5.7.2 Sand

In the case of the S2 tree in sand, the tree sapling was tested to failure. As shown in Figure 5-24, it appears that the failure load, the root structure was rotated inside the sand. The leeward roots were pushed in and the windward roots were exposed slightly from the sand as shown in Figure 5-24. The maximum resistance offered by the S2 stem base bending moment at each trench increment was as shown in Figure 5-25. S2 did not lose any failure resistance up to and including the 6D trench, it lost 8% resistance at 5D and maintained that strength up to the 4D trench. It lost 25% failure resistance for the 3D trench and 45%

for the 2D trench. This tree also showed significant strength considering that the root structure was supported by silica sand only and trenched 45% by the point of the 2D trench. The reason could be the strong structural tap root it had [Figure 5-4]. Fourcaud et al. [2008], Ghani et al. [2009], Smiley et al. [2014] also observed similar increase in root anchorage strength in trees with tap roots.

5.8 Comparison and discussion

This novel testing approach has helped understanding of the tree response to trenching and with increase in wind loading in two very different soils. This potentially provides the tree response variation limits with extreme difference in soil properties (frictionless clay & cohesion less sand). Flexibility and ease of this novel technique has allowed the study of the complex tree response variation with increase in trenching. Extensive data collected from these experiments has allowed detailed analysis of the tree stem, root, dynamic and failure responses.

STEM RESPONSE

In this study, displacement, rotational response and sway response of the tree stem in different soils were studied in great detail with increase in trenching and wind loading. In clay with increase in trenching the S1 stem displacement was doubled from the 7D to the 3D trench and was tripled for the 2D trench. In the case of sand, the sapling did not show much variation in deflection compared to its response for 7D trench for the same load. With increase in loading, the pruned root structure started settling slightly and showed no change in resistance, but did fail at lesser loads with increase in trenching volume.

The rotational response of S1 in the clay showed, a 20% decrease in stem base rotational stiffness for the 7D to 3D trench and 60% for the 2D trench. In the case of sand, there was not much variation in rotational stiffness, but S2 failed at lower wind loads with increase in trenching volume. The reason could be as that the root structure on the leeward side was getting pruned (the decrease in compressive strength) on the leeward side, through the slight settlement of pruned root structure the tree was maintaining similar stiffness at low wind loads in sand.

For the variation in the S1 sway response in clay, the statistical response changes were gradually varying with increase in trench size, but in sand the S2 response changes were sudden and unpredictable. In sand, the S2 root structure with pruning for each trench increment was tilting and settling slightly in the sand to provide the maximum anchorage strength possible and was responding according. In the case of clay, the response could be progressive degradation of soil strength with gradual loss in correlation between windward and lateral response of the stem base with increase in trenching. The same response was observed by O'Sullivan and Ritchie [1993] from cyclically loaded Sitka spruce trees.

ROOT RESPONSE

The root response of the tree saplings was observed from the strain gauge responses of roots. An interesting phenomenon observed from this study was load redistribution occurred in the S1 root system in clay, but not the S2 root system in sand. Mattheck and Breloer [1994] suggested that trees have a 'safety factor' of 5, indicating that trees develop stronger than necessary structure as not to fail under high winds. This study supports and gives clues on how trees survive with minimal support. It also shows with stronger soil support, loads in the root system redistribute and anchor the tree, but not if the soil support is weak.

Secant modulus of rotation variation in clay showed more than one peak in stiffness variation with increase in wind load but the S2 root plate in sand showed one peak stiffness at around 1/3rd of the failure load. The S2 response trend was consistent with increase in trenching. S1 in clay showed various peaks in stiffness response and the trend also varied with different trenches. O'Sullivan and Ritchie [1993] also observed similar trends in Sitka spruce response when trenched and subjected to cyclic loading. In this study bentonite clay seems to showing a similar response indicating progressive failure response.

DYNAMIC PROPERTIES

Dynamic properties estimated in this study from the free decay response of tree saplings for each trench in both clay and sand gave great insights. In any soil, the tree natural frequency seems to be decreasing and damping seems to be increasing with increase in

trenching indicating the decrease in resistance. In cohesion less soils this variation seems to be high compared to the response in cohesive soils. Mayhead et al. [1975] also observed changes in dynamic properties with change in soil media and noted that tree stability can be assessed using dynamic properties. It was also observed from the admittance response of S1 and S2, drop in energy transfer with increase in trenching volumes. In the case of clay, energy transfer drop was at higher frequencies and in the case of sand the energy drop was at lower frequencies indication stiffness variations observed with increase in trenching in both the soil media.

FAILURE RESPONSE

This approach has helped understand and confirm the current empirical methods for determining the safe trenching distances from trees [American Society of Consulting Arborists (ASCA) 1989, British Standards Institute (BSI) 1989, Watson 1990, Miller and Neely 1993, Ghani et al. 2009]. Tree failure because of dynamic loading and trenching occurred because of progressive soil strength degradation and excessive deformation in clay and by overturning in silica sand. With the presence of a strong structural tap root in S2, surprisingly high strength for S2 provided further insight into the effective root plate depth similar to Fourcaud et al. [2008], Ghani et al. [2009] and Smiley et al. [2014].

In this study a statistical analysis is presented to examine the tree stability with increase in trenching. With the sheer availability of load and response vectors, very critical tree stability can be obtained. This method could be potentially used to determine the tree stability in practical situations with simple tree sway tests.

5.9 References

American society of Consulting Arborists (1989) *Protecting trees during construction*. Answer to frequently asked questions for builders and property owners. Weat Ridge, Colorado.

Baker, C. J. (1995). The development of a theoretical model for the windthrow of plants. *Journal of Theoretical Biology*. 175, 355-372.

Bernatzky, A. (1978). *Tree ecology and preservation*. Elsevier, New York.

British Standard Institute (1989) *British standards guide for: trees in relation to construction*. British Standards Institute, Publication #10285

Brudi, E., & Wassenaer, P. Van. (2001). *Trees and Statics: Non-Destructive Failure Analysis*, In: E. Thomas Smiley and K. Coder (Eds.). 2001. Tree Structure and Mechanics Conference Proceedings: How Trees Stand Up and Fall Down. Savannah, Georgia, U.S. pp. 53–69.

Clough, R. W., and Penzien, J. (1993). *Dynamics of Structures*, McGraw-Hill, New York, NY, USA.

Coutts, M. P. (1983). Root architecture and tree stability. *Plant and Soil*, 71, 171–188. http://doi.org/10.1007/BF02182653

Coutts, M. P. (1986). Components of tree stability in sitka spruce on peaty gley soil. *Forestry*, 59(2), 173–197. http://doi.org/10.1093/forestry/59.2.173

Crook, M. J., & Ennos, A. R. (1998). The Increase in Anchorage with Tree Size of the Tropical Tap Rooted Tree Mallotus wrayi, King (Euphorbiaceae). *Annals of Botany*, 82(3), 291–296. http://doi.org/10.1006/anbo.1998.0678

Crook, M. J., Ennos, A. R., & Banks, J. R. (1997). The function of buttress roots: a comparative study of the anchorage systems of buttressed (Aglaia and Nephelium ramboutan species) and non-buttressed (Mallotus wrayi) tropical trees. *Journal of Experimental Botany*, 48(314), 1703–1716. http://doi.org/10.1093/jxb/48.9.1703

Davenport, A. G. (1967) Gust Loading Factors. *ASCE Journal of the structural division*, 93:11-34.

Day, S. D., Wiseman, P. E., Dickinson, S. B., & Harris, J. R. (2010). Tree Root Ecology in the Urban Environment and Implications for a Sustainable Rhizosphere. *Arboriculture & Urban Forestry*, 36(5), 193–205.

Ennos, A. R. (1993). The Scaling of Root Anchorage. *Journal of Theoretical Biology*. http://doi.org/10.1006/jtbi.1993.1040

Ennos, A.R. and Fitter, A.H. (1992). Comparative functional morphology of the anchorage systems of annual dicots. *Functional Ecology*. 6, 71-78.

Ferrini, F., Fini, A., Frangi, P., & Amoroso, G. (2008). Mulching of ornamental trees: Effects on growth and physiology Mulching of Ornamental Trees: Effects on Growth and Physiology. *International Society of Arboriculture*, (May).

Fini, A., Francesco, F., Frangi, P., & Gabriele, A. (2013). Effect of root severance by excavation on growth, physiology and uprooting resistance of two urban tree species. *Acta Horticulturae*, 990(990):487-494.http://doi.org/10.17660/ActaHortic.2013.990.63

Fourcaud, T., Ji, J. N., Zhang, Z. Q., & Stokes, A. (2008). Understanding the impact of root morphology on overturning mechanisms: A modelling approach. *Annals of Botany*, 101(8), 1267–1280. http://doi.org/10.1093/aob/mcm245

Fraedrich, B.R., and Smiley, E.T. (2002) Assessing the failure potential of tree roots. Tree structure and Mechanics Conference Proceedings. *International society of Arboriculture*, Champaign, IL.184pp.

Fraser, A. I. (1962). The soil and roots as factors in tree stability, *Forestry*, 35: pp.117-127

Gardiner, B., Berry, P., & Moulia, B. (2016). Review: Wind impacts on plant growth, mechanics and damage. *Plant Science*, *245*(July), 94–118. https://doi.org/10.1016/j.plantsci.2016.01.006

Ghani, M. A., Stokes, A., & Fourcaud, T. (2009). The effect of root architecture and root loss through trenching on the anchorage of tropical urban trees (Eugenia grandis Wight). *Trees - Structure and Function*, 23(2), 197–209. http://doi.org/10.1007/s00468-008-0269-9

Holbo, H. R., Corbett, T. C., and Horton, P. J. (1980). Aeromechanical behavior of selected Douglas-fir. Agricultural Meteorology, 21(2), 81–91. http://doi.org/10.1016/0002-1571(80)90056-4

ITFD. (2007). *International Tree Failure Database web site*.

James, K. R., Haritos, N., & Ades, P. K. (2006). Mechanical stability of trees under dynamic loads. *American Journal of Botany*, 93(10), 1522–1530. http://doi.org/10.3732/ajb.93.10.1522

Jim, C. Y. (2003). Protection of urban trees from trenching damage in compact city environments. *Cities*, 20(2), 87–94. http://doi.org/10.1016/S0264-2751(02)00096-3

Koeser, A. K., Hauer, R., Forestry, U., & Greening, U. (2013). Factors influencing long-term street tree survival in Milwaukee, WI, USA. https://doi.org/10.1016/j.ufug.2013.05.006

Matheny, N. and Clark, J. (1998). *Tree and development:a technical guide to preservation of trees during land development*. International society of Arboriculture, Lisle, IL, U.S.

Mattheck , C., and Breloer, H. (1994) *The body language of trees, a handbook for failure analysis*. London, England

Mayer, H. (1987). Wind-induced tree sways. Trees, 1, 195–206. http://doi.org/10.1007/BF01816816

Mayer, H., Raupach, M. R., Kohsiek, W., Gardiner, B., Clarke, J. A., Amtmann, R., and Milne, R. (1989). Windthrow [and Discussion]. Philosophical Transactions of the Royal Society B: Biological Sciences, 324, 267–281. http://doi.org/10.1098/rstb.1989.0048

Mayhead , G.J. , Gardiner , J.B.H. and Durrant , D.W. 1975 Physical Properties of Conifers in Relation to Plantation Stability . Unpublished Report. Forestry Commission, Edinburgh, U.K.

Melchers, R. E. (1999), *Structural Reliability Analysis and Prediction*, John Wiley and Sons, Inc., New York, N.Y.

Miller, F. D. J., & Neely, D. (1993). The effect of trenching on growth and plant health of selected species of shade trees. *J. Arboriculture*. http://doi.org/10.1080/03071375.1994.9747030

Miller, N.L., Rathke, D.M., Johnson, G.R., (1993) *Protecting trees near construction damage*. Publication NR-FO-6135-S. Minnesota Extension Service, St Paul.

O'Sullivan, M. F., & Ritchie, R. M. (1993). Tree stability in relation to cyclic loading. *Forestry*, 66(1), 69–82. http://doi.org/10.1093/forestry/66.1.69

Ochi, M. K. (1990). *Applied probability and stochastic processes in engineering and physical sciences*. John Wiley and Sons, New York, USA.

Peltola, H. (1996). Swaying of Trees in Response to Wind and Thinning in A Stand of Scots Pine, Boundary-Layer Meteorol, 77: 285–304.

Sellier, D., Brunet, Y., and Fourcaud, T. (2008). A numerical model of tree aerodynamic response to a turbulent airflow. Forestry, 81(3), 279–297. http://doi.org/10.1093/forestry/cpn024

Smiley, E. T. (2008). Root pruning and stability of young willow oak. *Arboriculture and Urban Forestry*, 34(March), 123–128.

Smiley, E. T., Holmes, L., & Fraedrich, B. R. (2014). Pruning of buttress roots and stability changes of red maple (Acer rubrum) Pruning of Buttress Roots and Stability Changes of Red Maple (Acer rubrum). *Arboriculture & Urban Forestry*, 40(4), 230–236.

Somerville, A. (1979). Root anchorage and root morphology of Pinus Radiata on a range of ripping treatments. *New Zealand Journal of Forest Science* 9, 294-315.

Stokes, A, & Mattheck, C. (1996). Variation of wood strength in tree roots. *Journal of Experimental Botany*, 47(298), 693–699. http://doi.org/10.1093/jxb/47.5.693

Stokes, A., and Guitard, D. (1997). *Tree root response to mechanical stress*. In Biology of root formation and development, Altman, A., and Waisel, Y. (eds), Plenum Press, New York, pp227-236.

Stokes, A., Ball, J., Fitter, A. H., Brain, P., & Coutts, M. P. (1996). An experimental investigation of the resistence of model root systems to uprooting. *Annals of Botany,* 78, 415–421.

Sutton, R.F. (1969). Form and development of conifer root systems. *Commonwealth Agricultural Bureaux*, Tech. Comm. No.7.

Taylor, H.M., and Gardner, H.R. (1963). Penetration of cotton seedling tap roots as influenced by bulk density, moisture content and strength of soil. *Soil Science,* 96, 153-156.

Thomas, P. (2000). *Trees: their natural history*, Cambridge University Press, UK.

Watson, G. W. (1990). *Preventing construction damage to trees*. The Morton Arboretum information leaflet #36, Lisle.

Welch, P. D. (1967), "The use of Fast Fourier Transform for the estimation of power spectra: A method based on time averaging over short, modified periodograms", IEEE Transactions on Audio and Electroacoustics, AU-15 (2): 70–73, doi*:*10.1109/TAU.1967.1161901

Wessolly, L., and Erb, M. (1998). Baum *static*, baum kontrolle. Berlin-Hannover: Patzer Verlag.

Wu, T. H., McOmber, M. R., Roland, E. T., & Beal, E. P. (1989). Study of Soil Root interaction. *Journal of Geotechnical Engineering*, 114(12), 1351–1375.

Yang, J. C. S., Aggour, M. S., Dagalakis, N., & Miller, F. (n.d.). (1981). Damping of an offshore platform model by “random dec” method. *In Proc. ASCE EMD Specialty Conference—Dynamic Response of Structures*, Atlanta, Georgia, pp. 819–832.

Yu, H., Chen, C., & Lo, W. (2011). Mechanical Behavior of the Soil-Root System, *Soil Science*, 176(2), 99–109. http://doi.org/10.1097/SS.0b013e318206478a

Table 5-1 Biometrics of S1 and S2

Tree sapling biometrics	S1	S2	Percentage difference in S2 with respect to S1
Tree height (m)	1.2	1.27	5.83
Total sapling weight (g)	1599.68	3673.88	129.66
Trunk weight (g)	511.21	1157.87	126.50
Branch mass (g)	640	1825	185.16
Crown frontal area (m^2)	0.31	0.88	183.87
Root system weight (g)	435.96	691	58.50
Stump weight (g)	233.3	489.24	109.70
Roots without stump (g)	188.15	201.77	7.24

Table 5-2 Pruned root mass of S2 with increase in trenching

Trenching in SAND	Pruned root mass, (g)	Percentage of pruned root mass, (%)
7D	5.15	2.55
6D	6.61	3.28
5D	9.22	4.57
4D	14.16	7.02
3D	25.83	12.80
2D	23.66	11.73

Table 5-3 Dynamic properties of S2 in clay

Trench	Natural frequency	Damping at the base
No trench	3.17	0.048
7D	3.04	0.056
6D	3.19	0.053
5D	3.28	0.055
4D	3.04	0.064
3D	3.01	0.068
2D	2.79	0.05

Table 5-4 Dynamic properties of S2 in sand

Trench	Natural frequency	Damping at the base
No trench	2.41	0.047
7D	2.5	0.043
6D	2.46	0.046
5D	2.6	0.046
4D	2.4	0.064
3D	2.3	0.056
2D	2.26	0.088

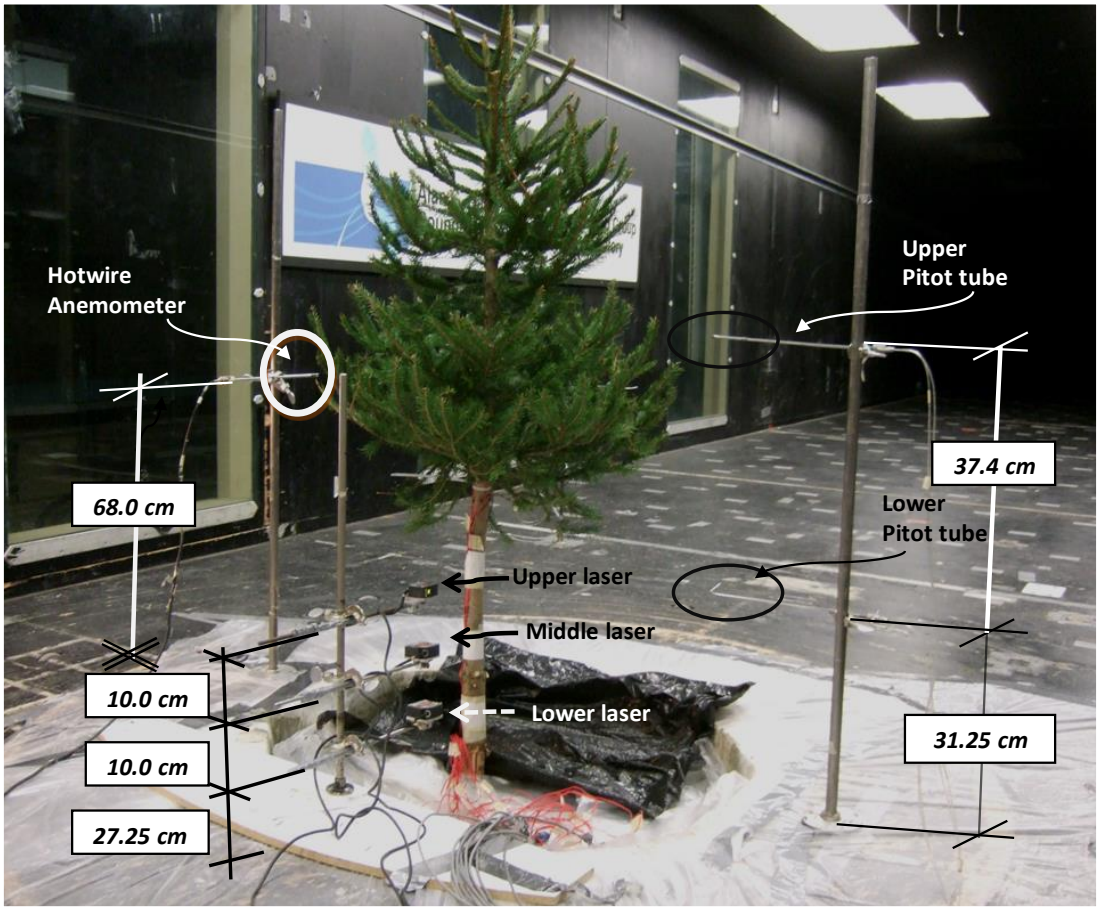

Figure 5-1 Experimental setup, S1 in clay

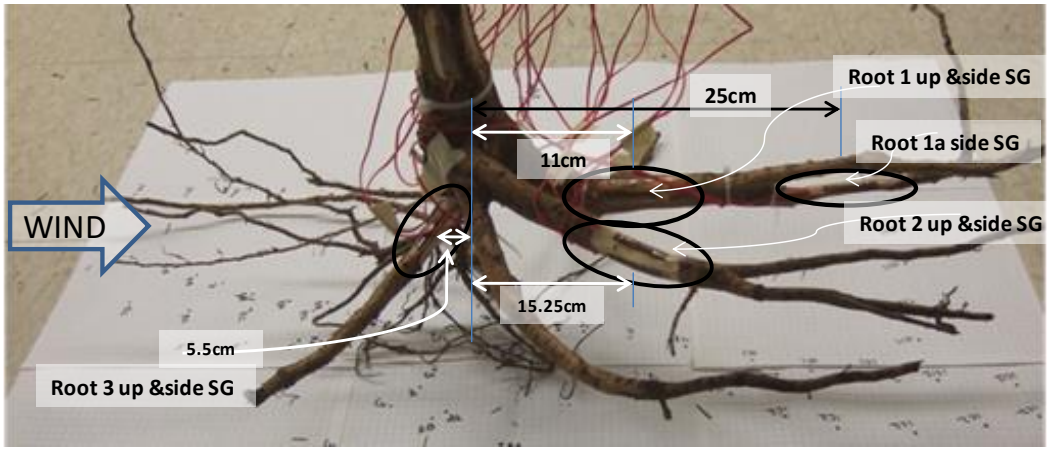

Figure 5-2 Tree 1 (S1) root system and strain gauge setup

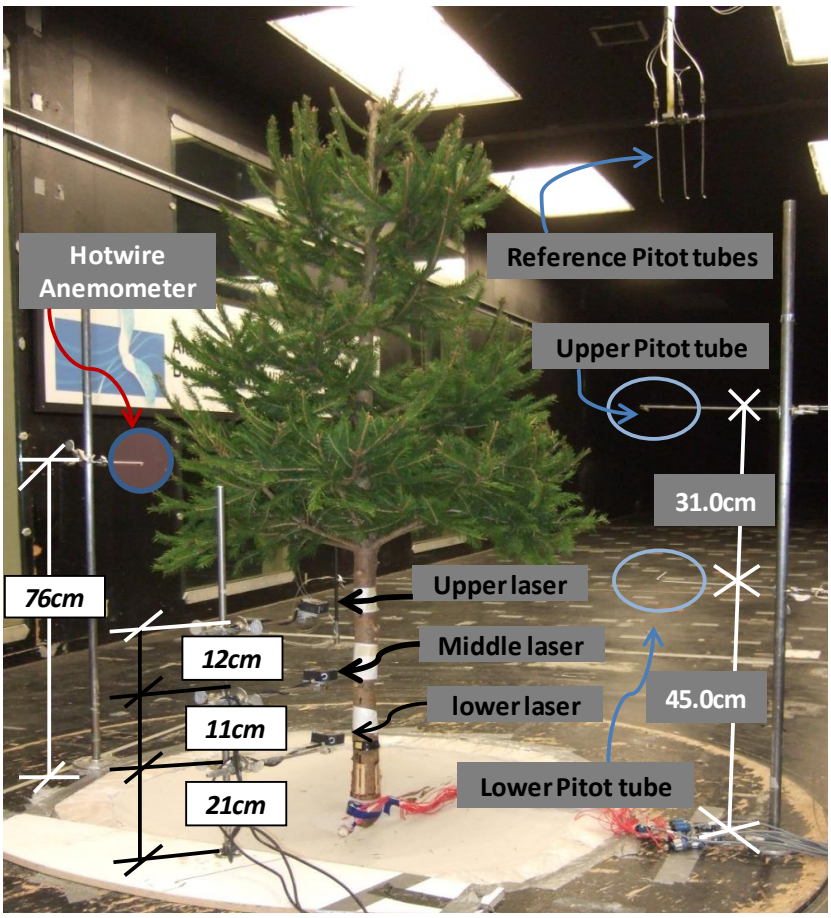

Figure 5-3 Experimental setup, S2 in sand

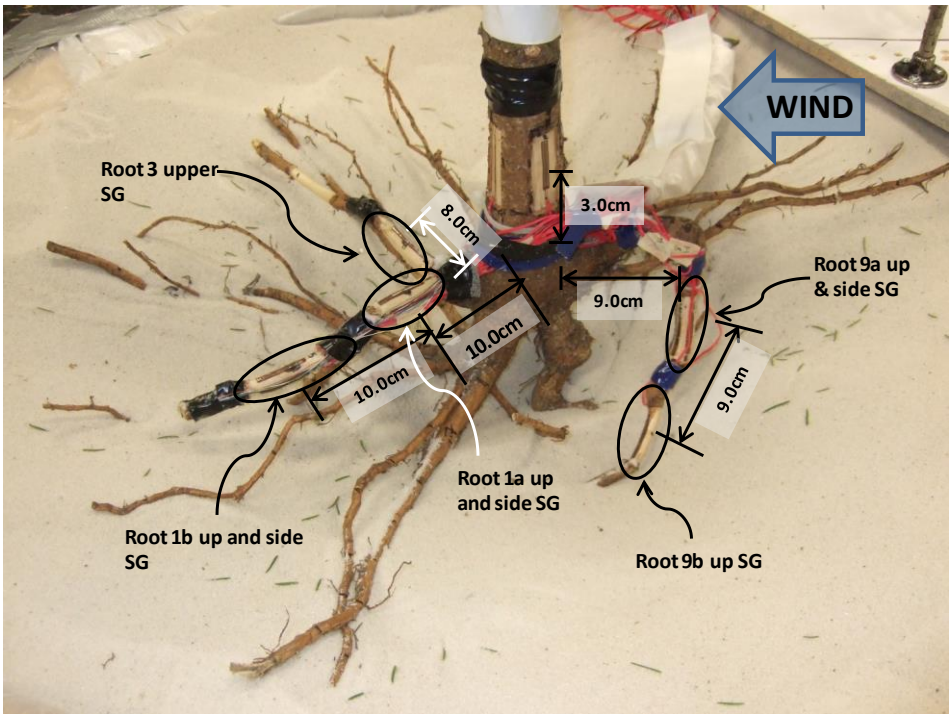

Figure 5-4 Tree 2 (S2) root system and strain gauge (SG) setup

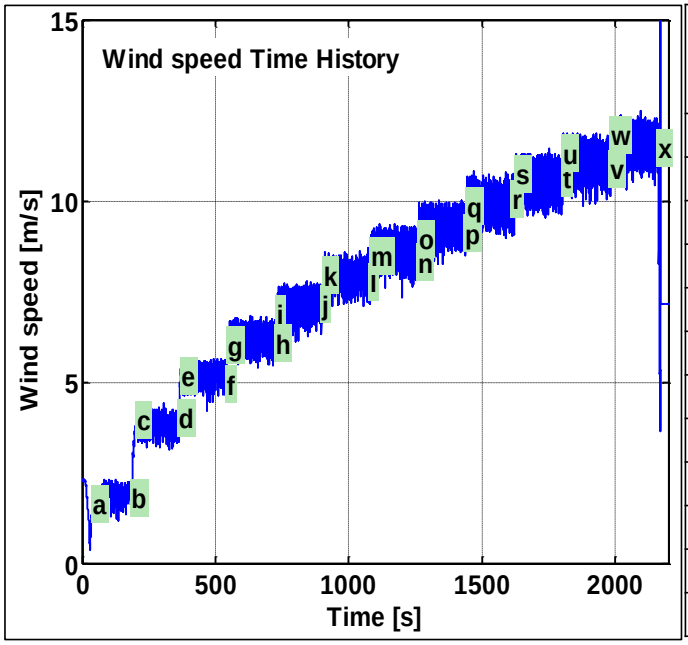

Wind tunnel speed Increments	*Wind speed m/s*
a-b(0.5v)	0.7
c-d(1.0v)	1.7
e-f(1.5v)	2.9
g-h(2.0v)	3.6
i-j(2.5v)	5.1
k-l(3.0v)	5.5
m-n(3.5v)	7.0
o-p(4.0v)	7.8
q-r(4.5v)	8.9
s-t(5.0v)	9.7
u-v(5.5v)	10.9
w-x(6.0v)	11.9

Figure 5-5 Incremental wind load

Figure 5-6 S1 Trenching in clay

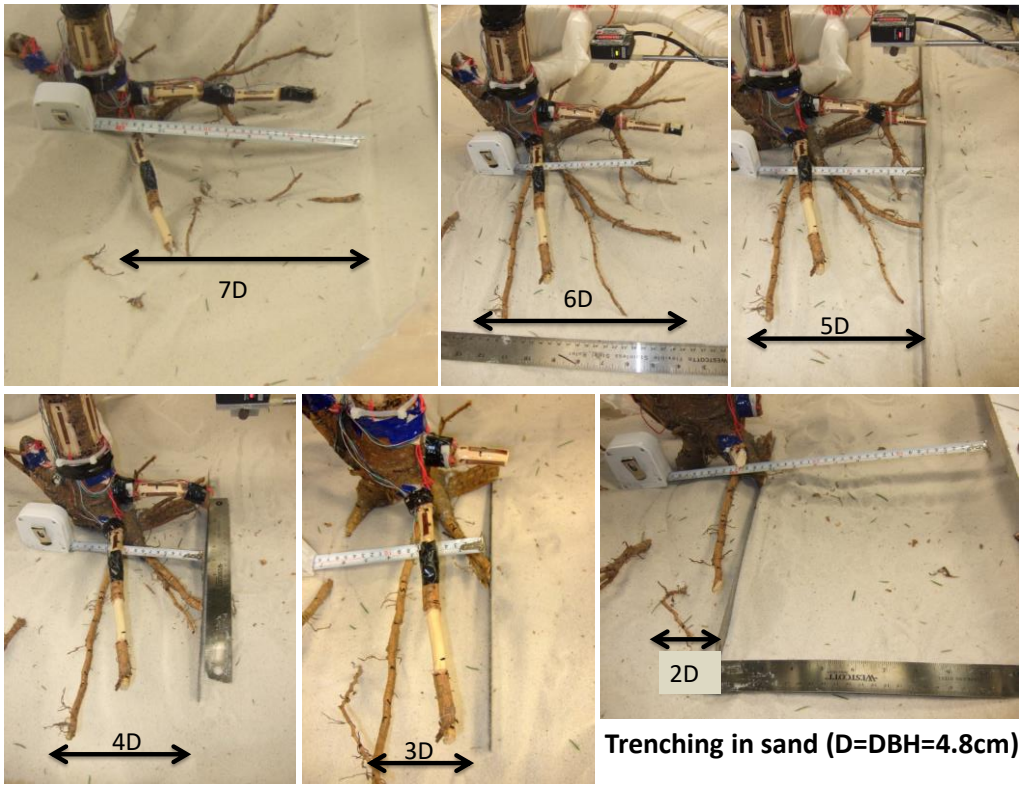

Figure 5-7 S2 Trenching in sand

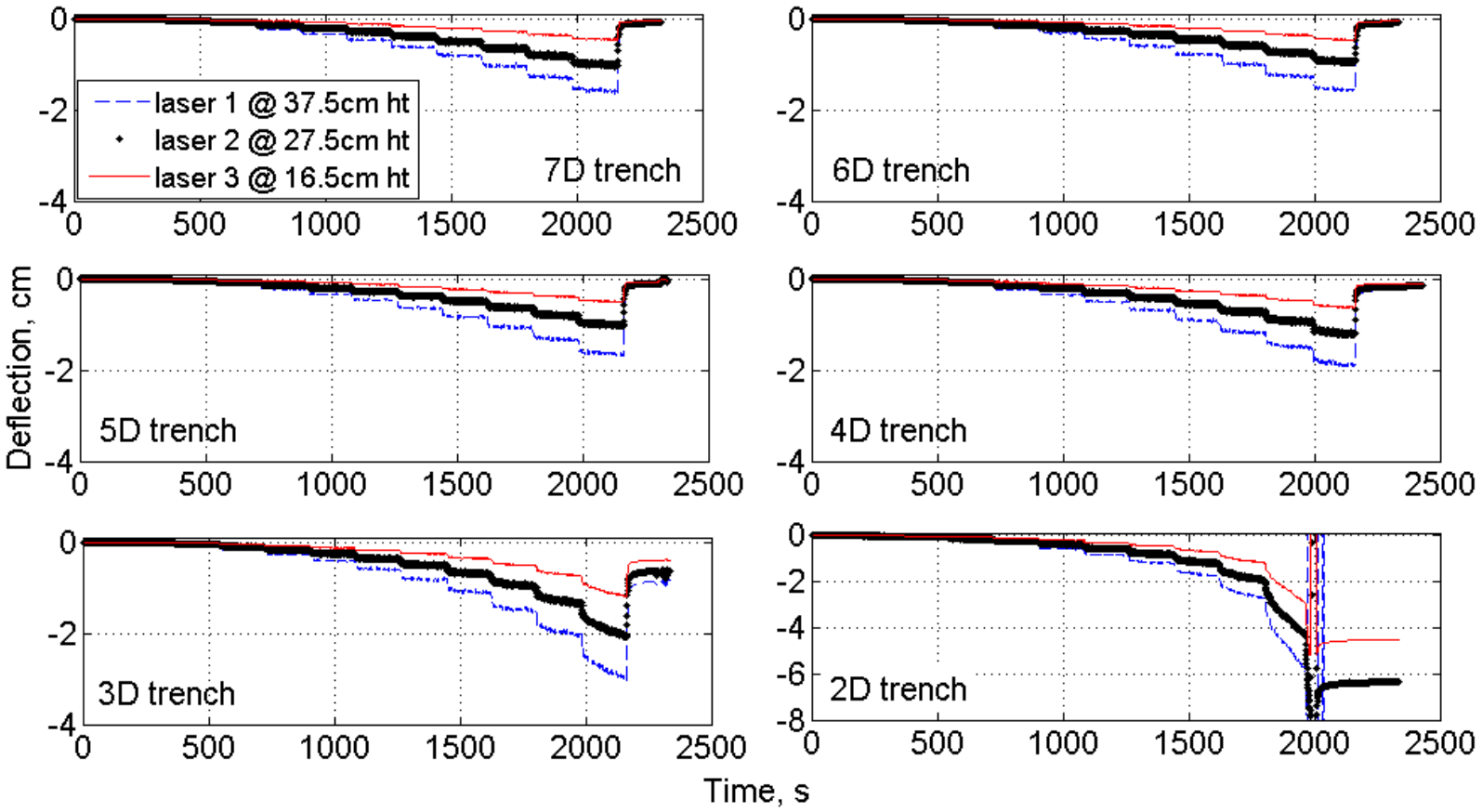

Figure 5-8 Displacement time history of S1 in clay

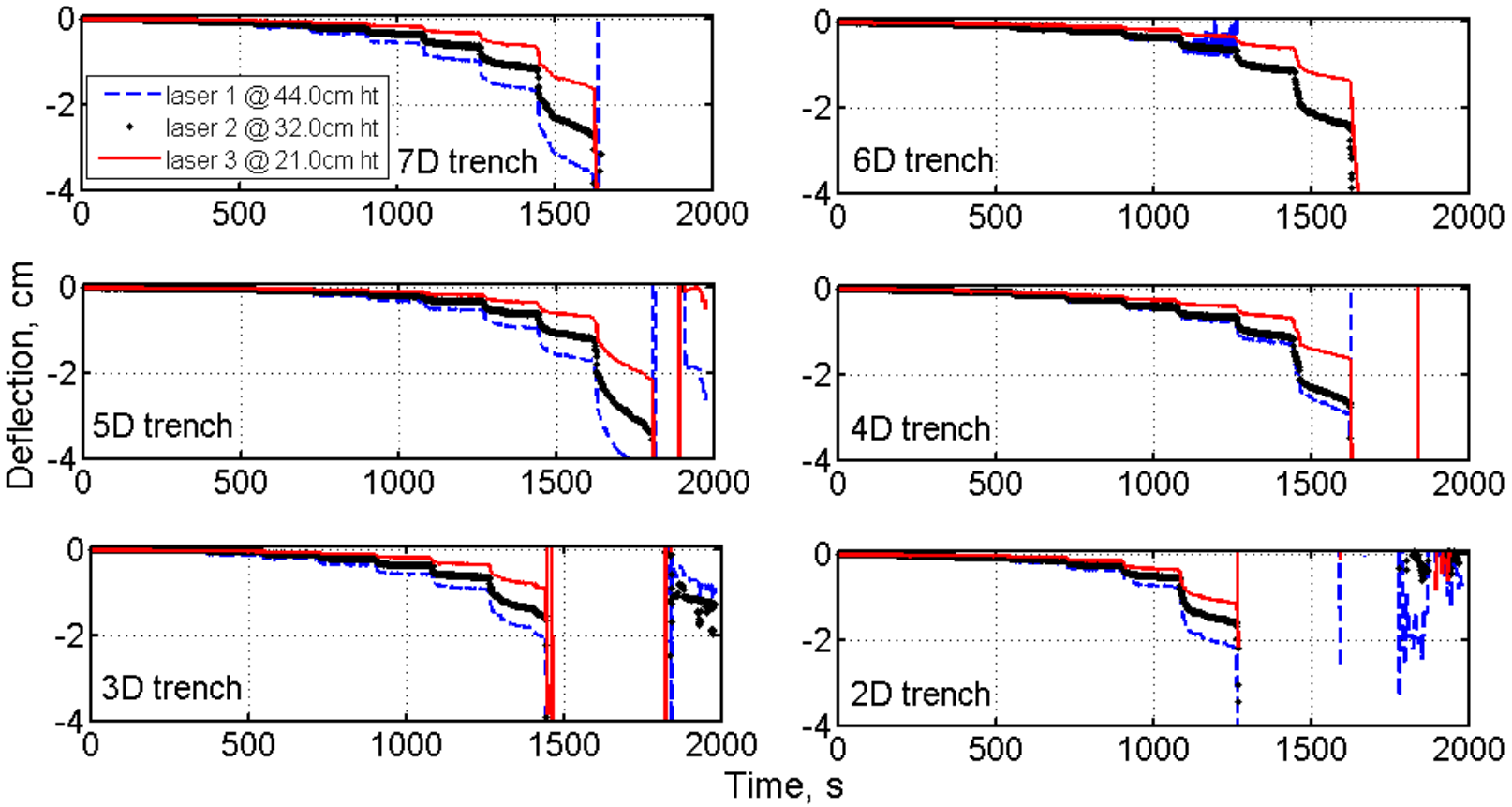

Figure 5-9 Displacement time history of S2 in sand

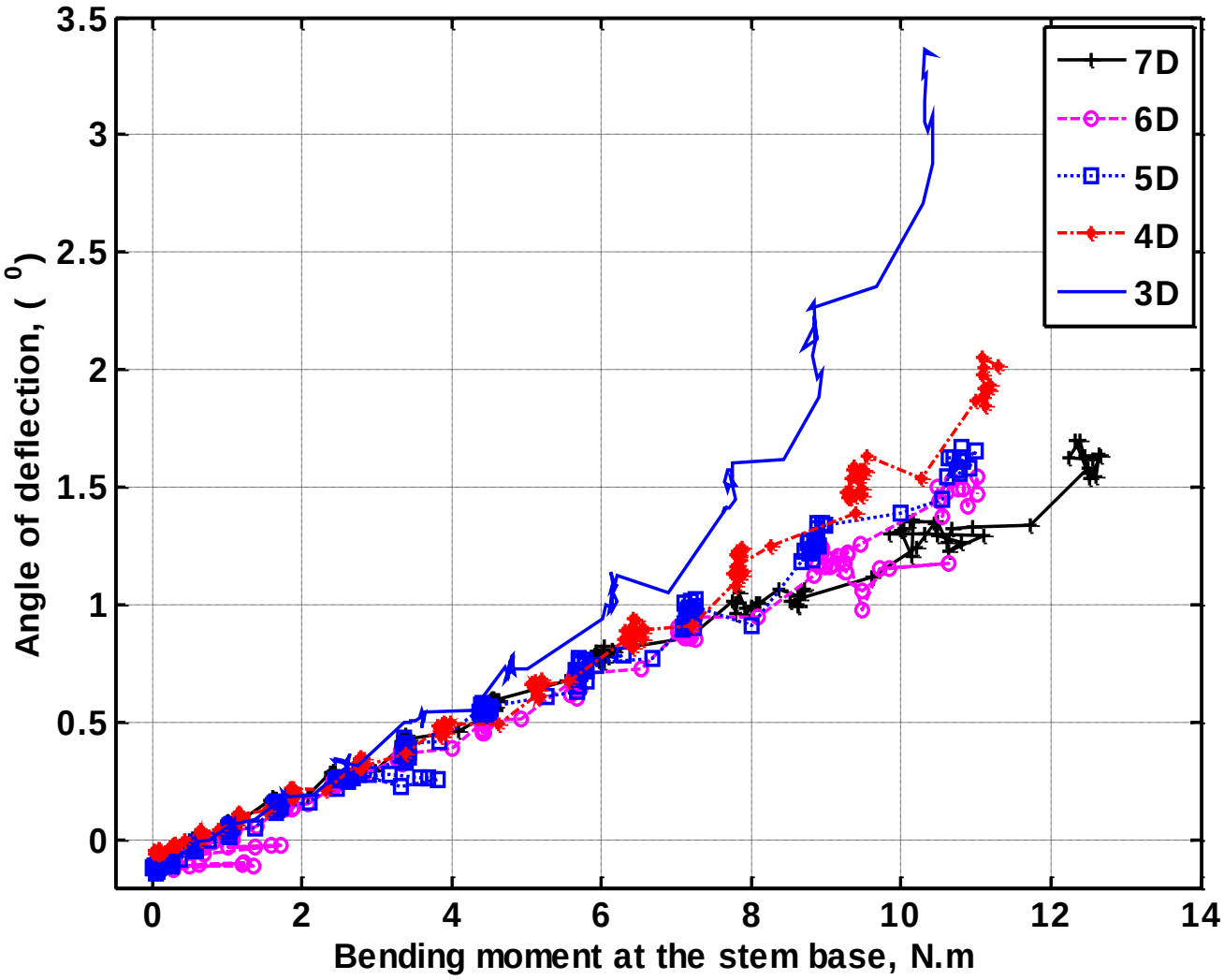

Figure 5-10 Base bending moment with increase of S1 stem rotation at 29.3 cm height

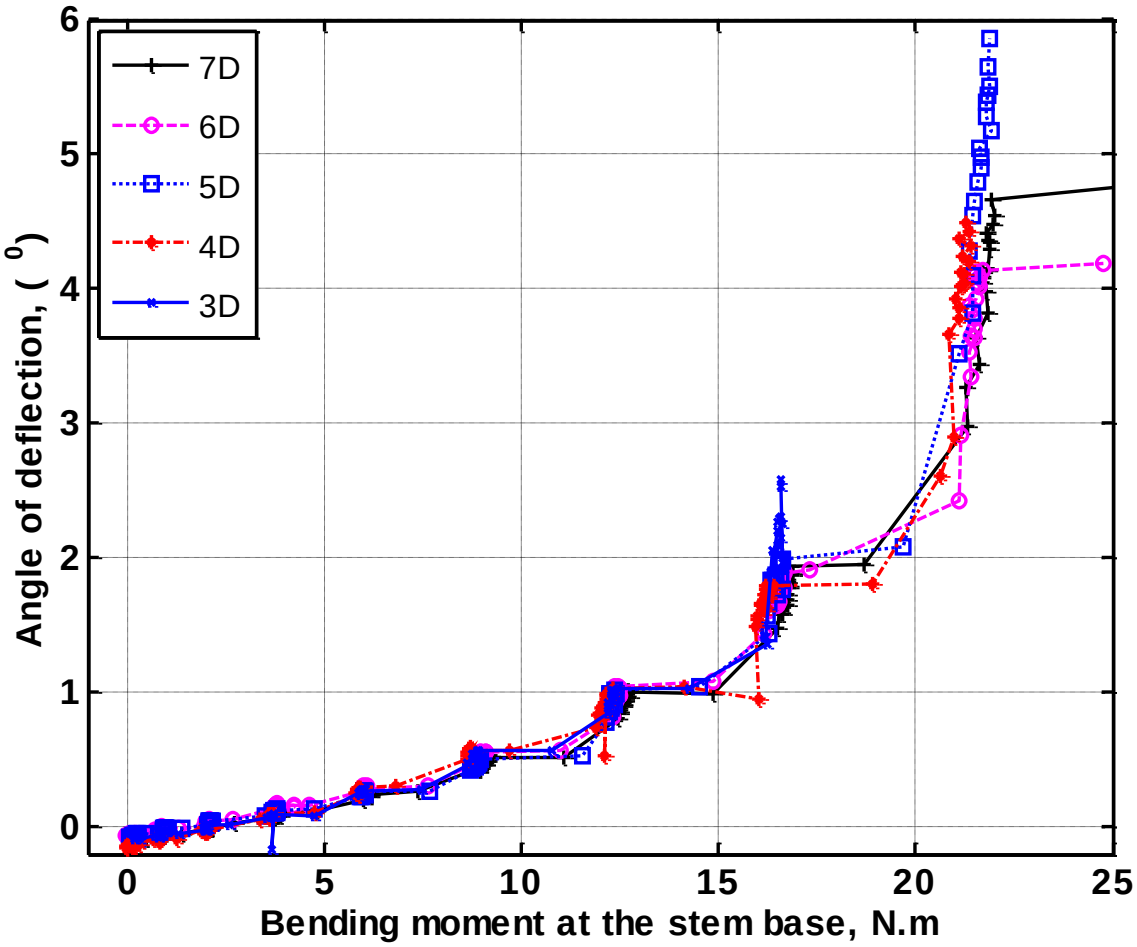

Figure 5-11 Base bending moment with increase of S2 stem rotation at 32.0 cm height in sand

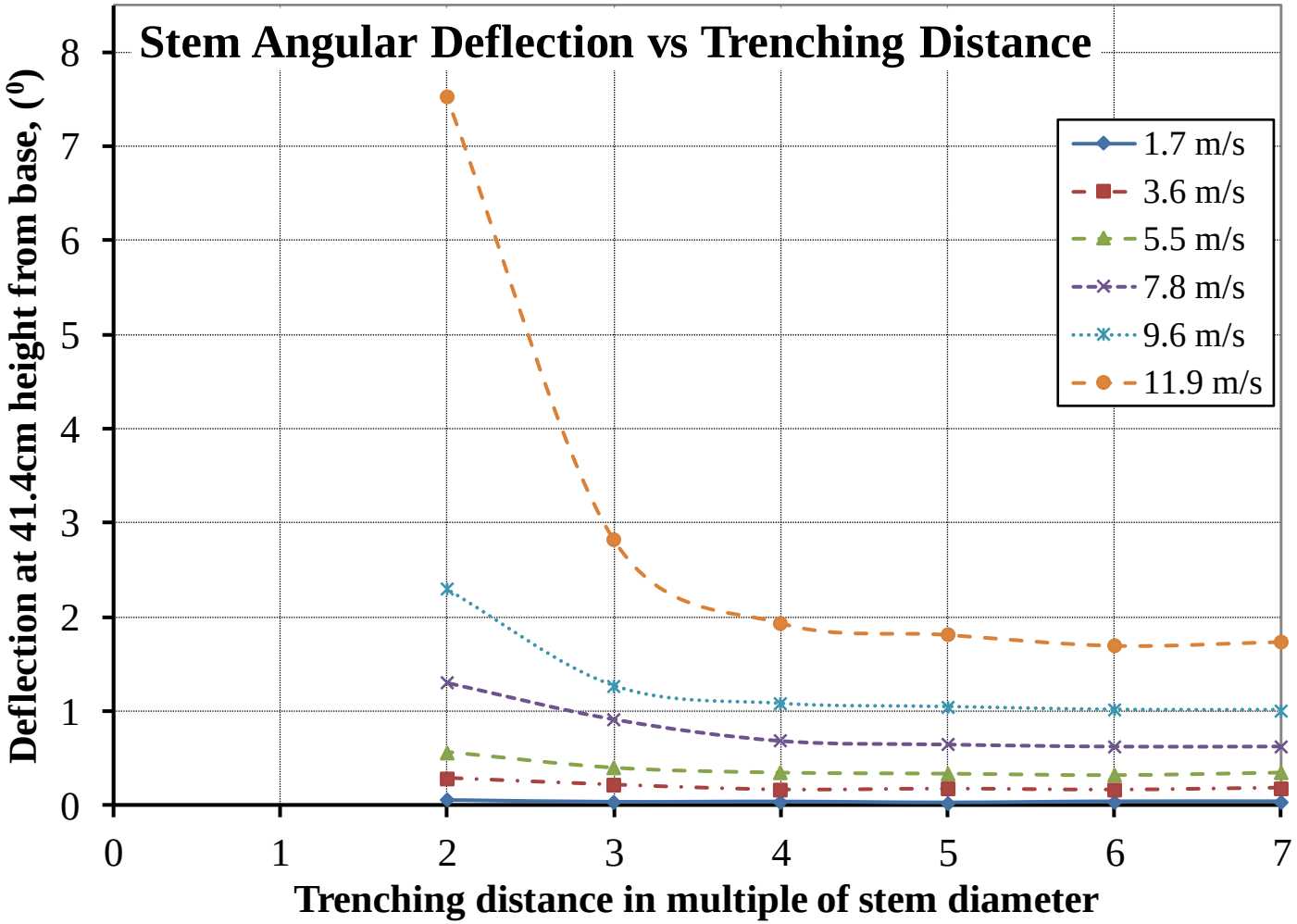

Figure 5-12 Stem angular deflection of S1 with increase in trenching and wind speed

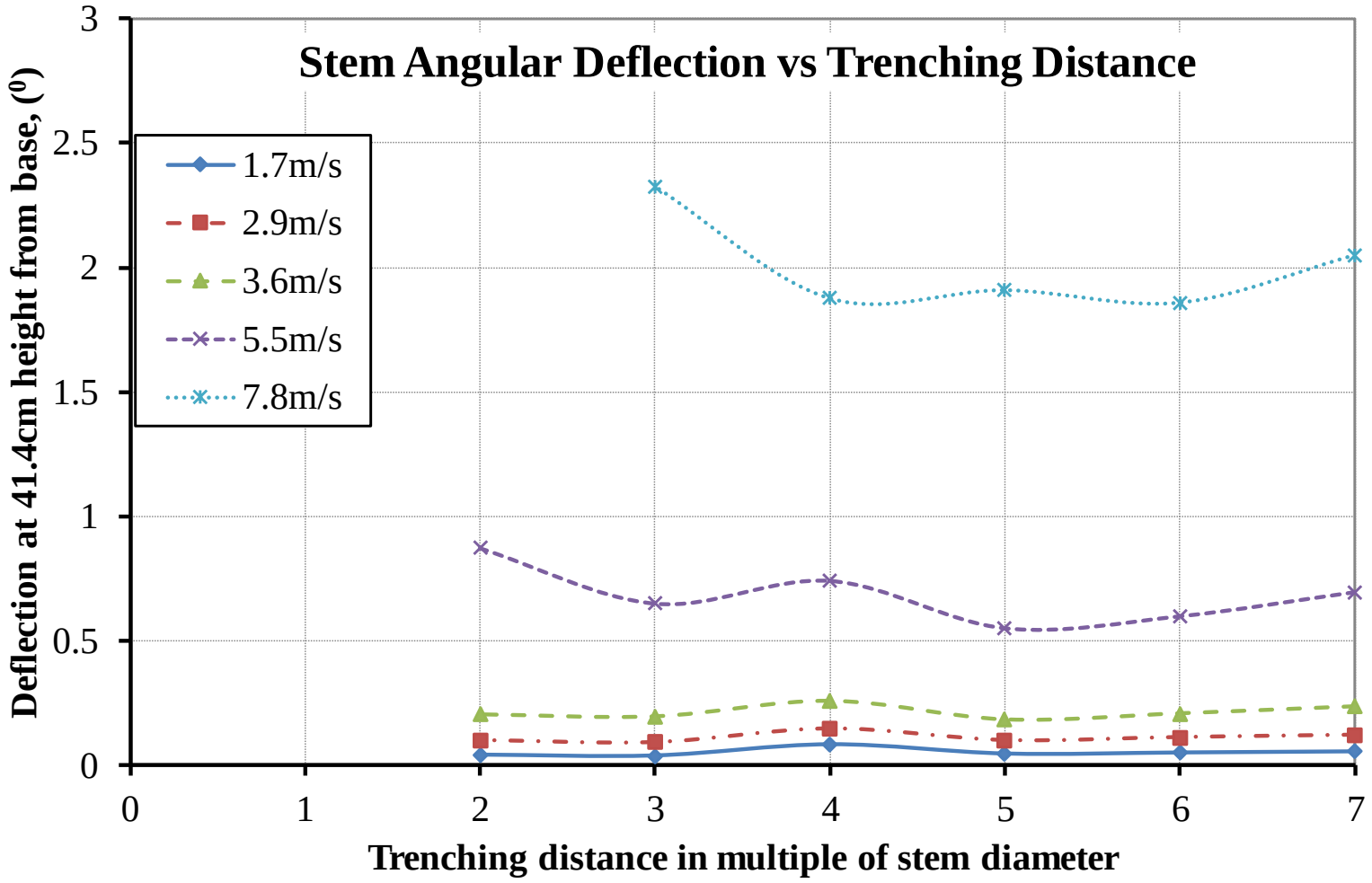

Figure 5-13 Stem angular deflection of S2 with increase in trenching and wind speed in sand

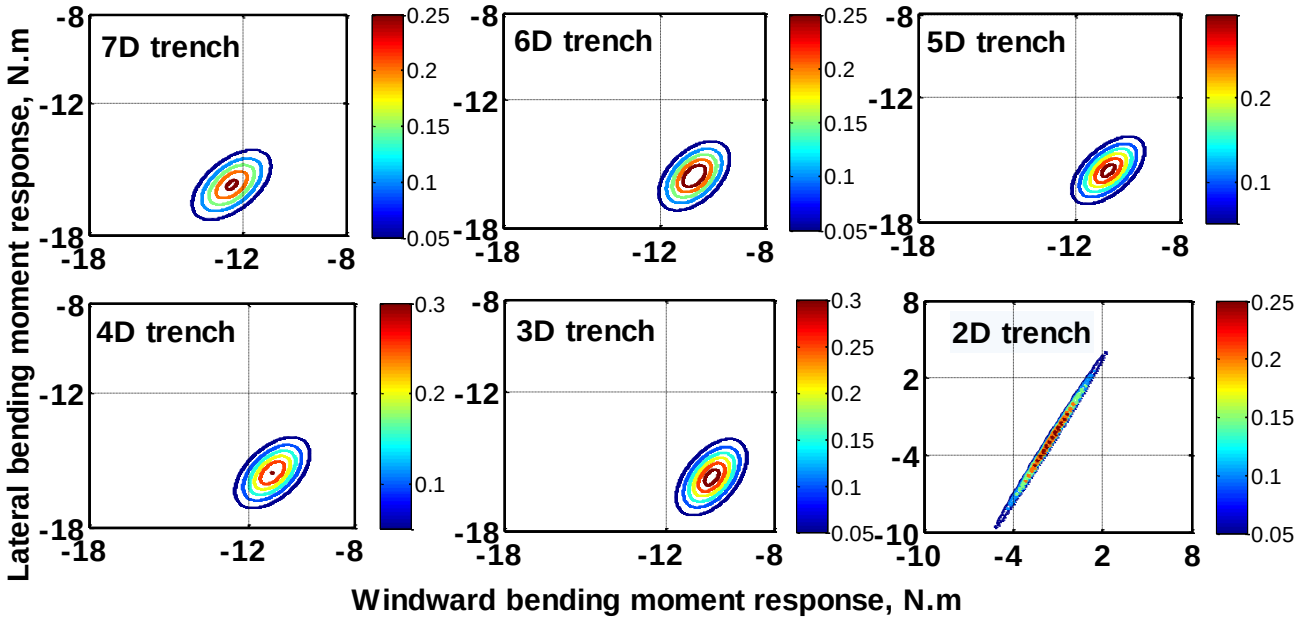

Sway Plot	Variant	Mean	Variance	Coefficient of variation	Skewness	Kurtosis	Covariance	Correlation coefficient
7D	X axis	-12.5	0.72	-0.07	0.10	2.79	0.4	0.54
	Y axis	-15.7	0.76	-0.06	0.13	2.96		
6D	X axis	-10.7	0.51	-0.07	-0.05	2.93	0.3	0.49
	Y axis	-15.6	0.73	-0.05	0.03	3.26		
5D	X axis	-10.8	0.52	-0.07	0.06	2.78	0.35	0.58
	Y axis	-15.5	0.71	-0.05	0.01	3.00		
4D	X axis	-11.1	0.56	-0.07	-0.05	3.17	0.33	0.52
	Y axis	-15.6	0.70	-0.05	0.05	2.96		
3D	X axis	-10.3	0.46	-0.07	-0.12	3.12	0.3	0.52
	Y axis	-15.7	0.73	-0.05	0.09	2.81		
2D	X axis	-8.4	0.23	-0.06	-0.10	2.87	0.12	0.43
	Y axis	-15.5	0.36	-0.04	0.06	2.09		

Figure 5-14 Sway response of S1 at 11.9 m/s wind speed in clay with increase in trenching

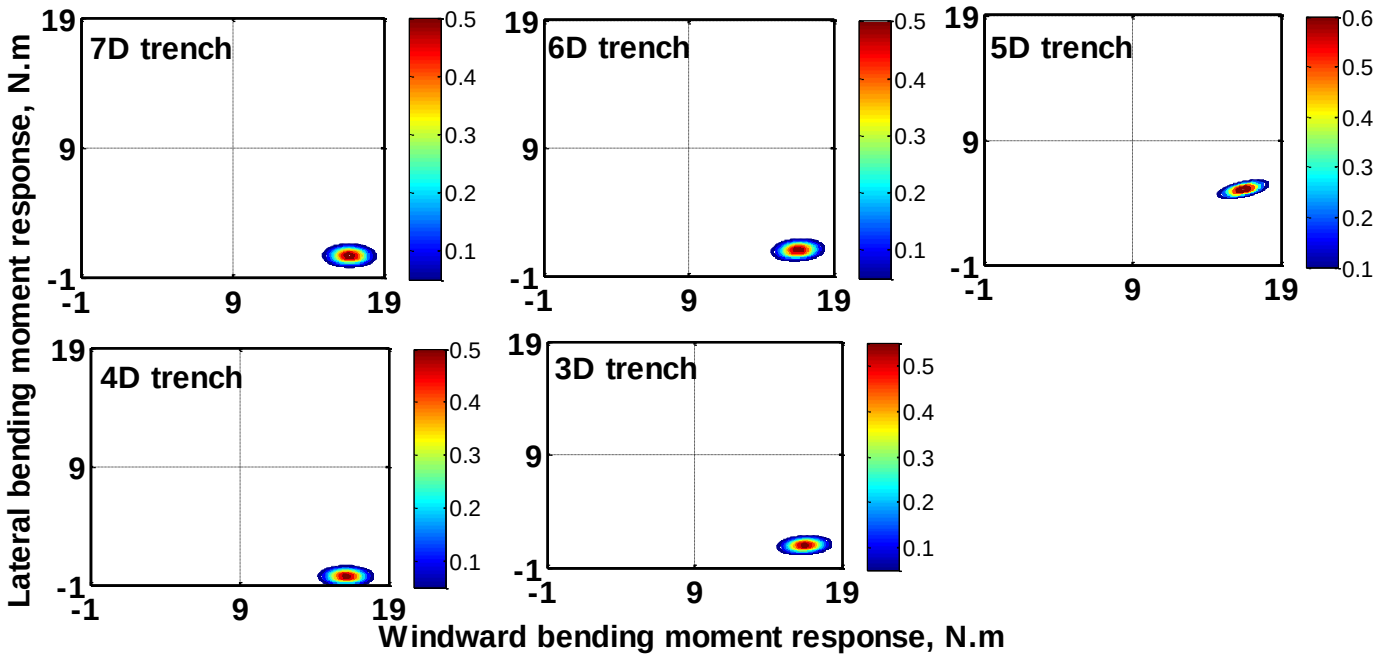

Sway Plot	Variant	Mean	Variance	Coefficient of variation	Skewness	Kurtosis	Covariance	Correlation coefficient
7D	X axis	16.67	0.60	0.05	-0.07	2.76	0.0012	0.0041
	Y axis	0.69	0.15	0.56	-0.01	3.06		
6D	X axis	16.50	0.65	0.05	-0.16	2.87	0.05	0.16
	Y axis	1.06	0.14	0.35	0.00	2.83		
5D	X axis	16.39	0.71	0.05	-0.01	2.59	0.18	0.61
	Y axis	5.09	0.13	0.07	-0.06	2.74		
4D	X axis	16.09	0.68	0.05	-0.18	2.92	0.005	0.02
	Y axis	-0.22	0.14	-1.70	-0.01	2.94		
3D	X axis	16.41	0.66	0.05	-0.14	2.79	0.05	0.17
	Y axis	1.02	0.13	0.35	-0.02	3.11		

Figure 5-15 Sway response of S2 at 7.8 m/s wind speed in sand with increase in trenching

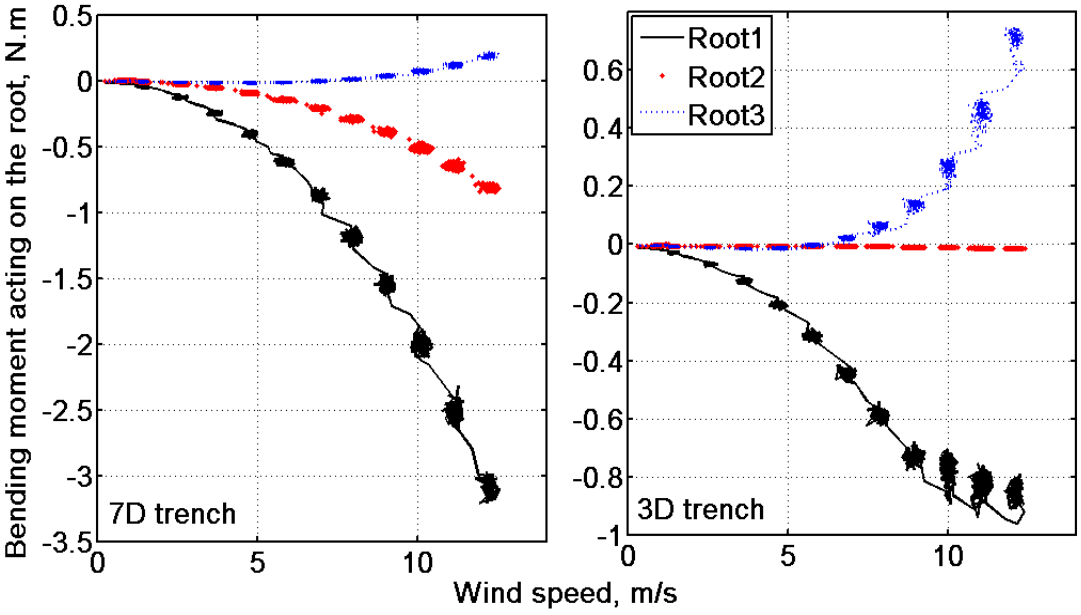

Figure 5-16 Root response of S1 with increase in wind speed

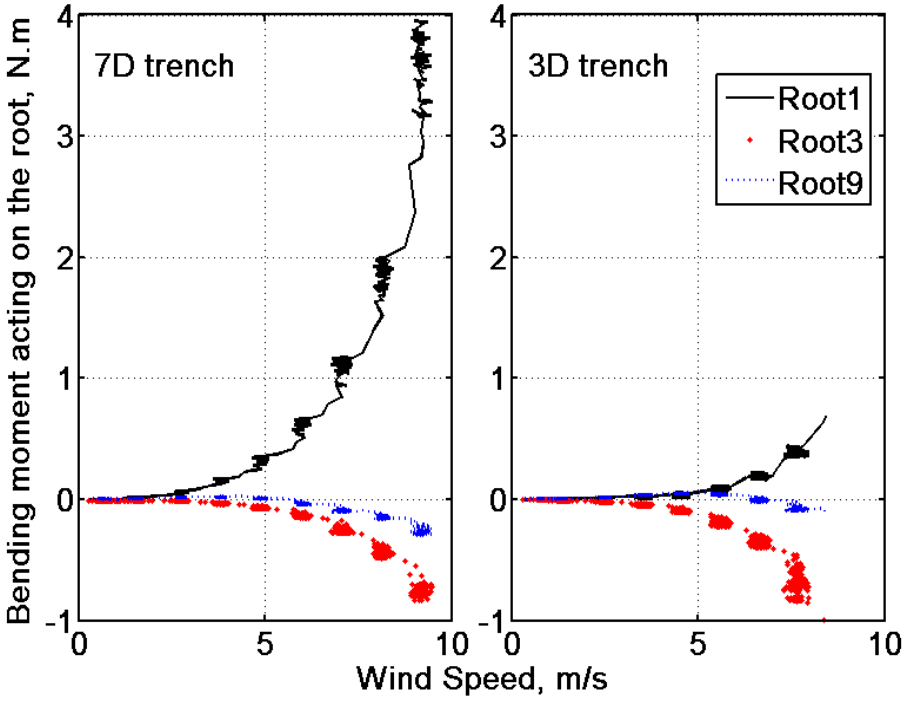

Figure 5-17 Root response of S2 with increase in trenching in sand

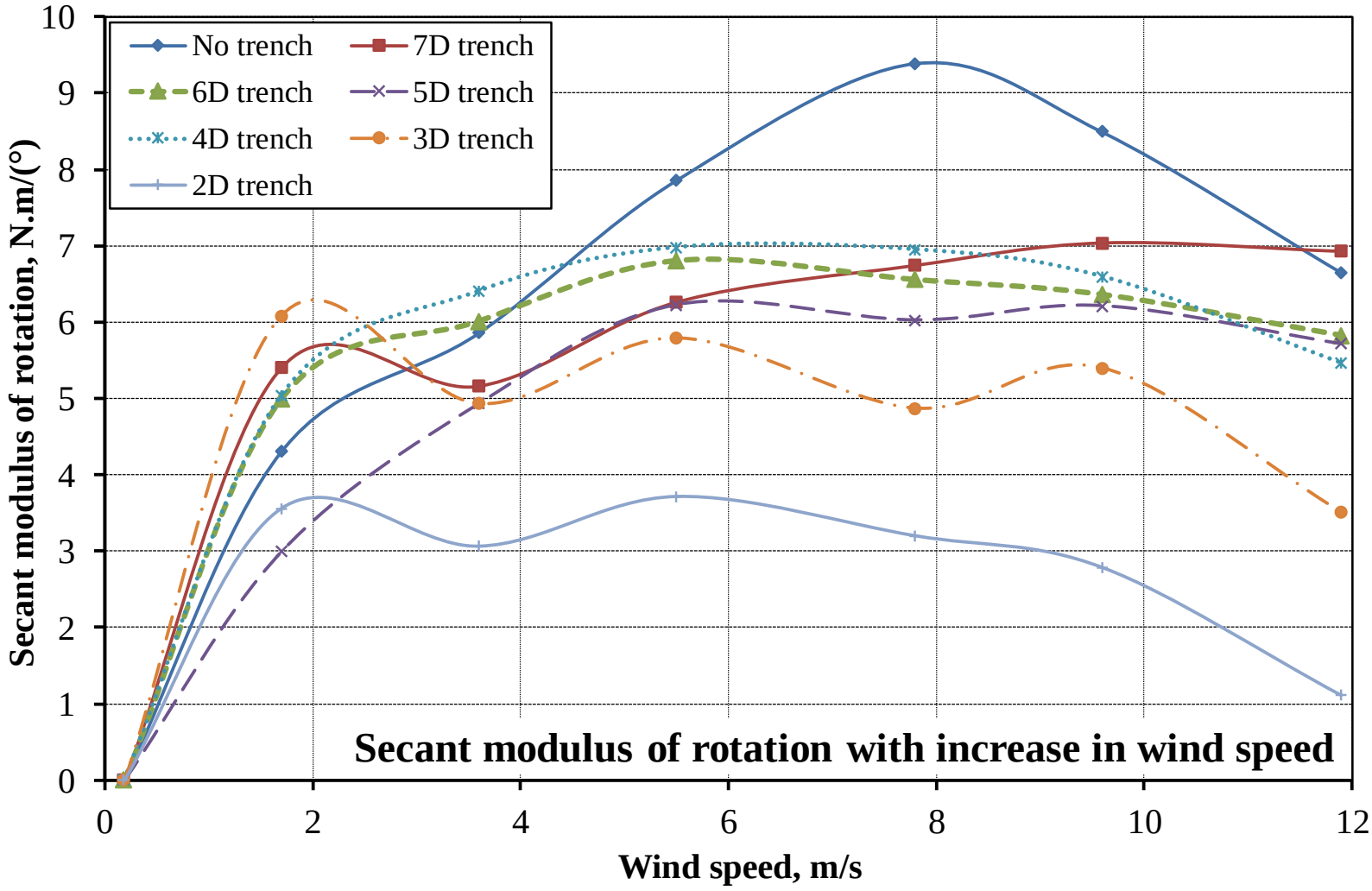

Figure 5-18 Secant modulus of base rotation of S1 with increase in wind speed and trenching in clay

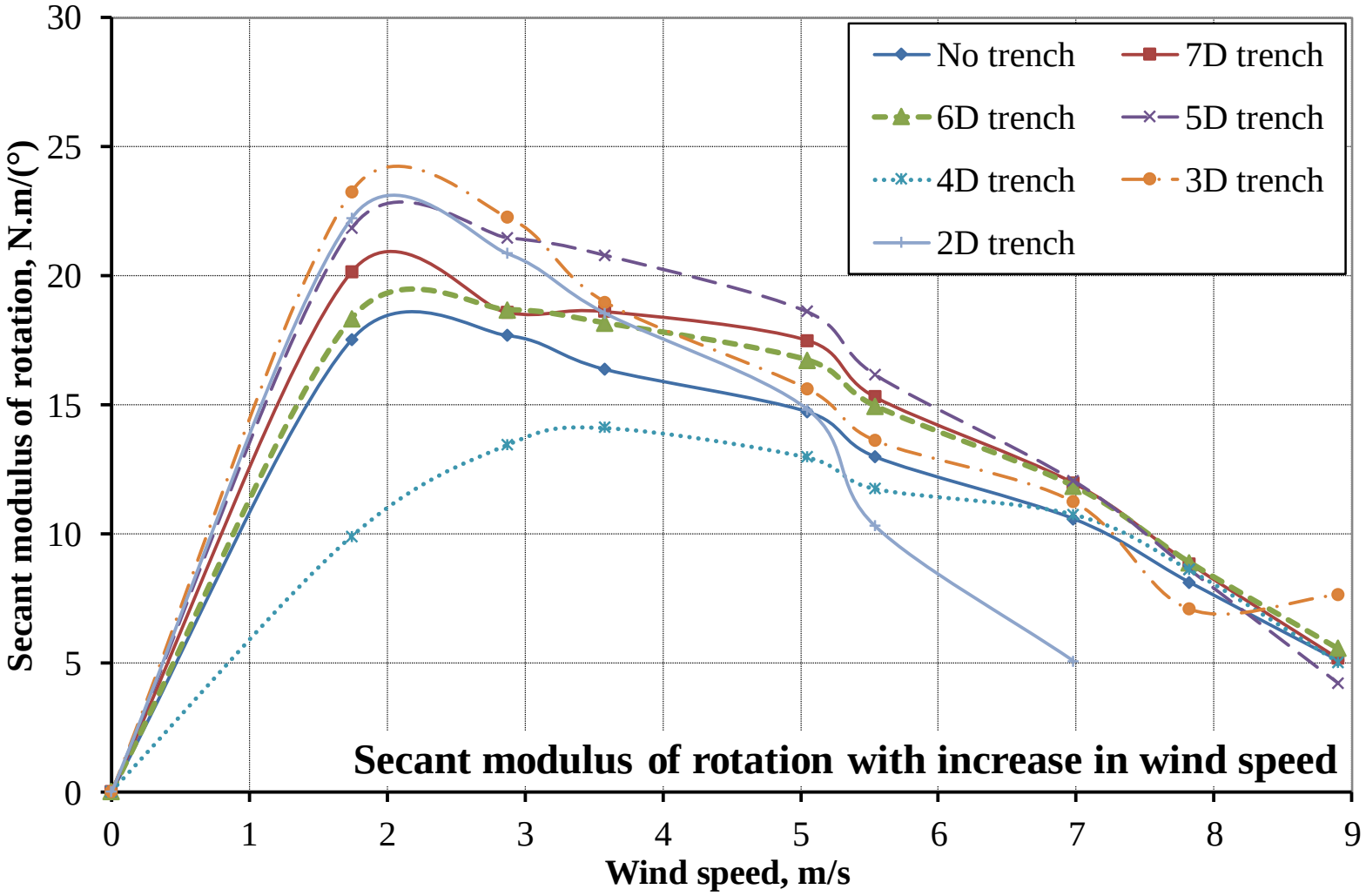

Figure 5-19 Secant modulus of base rotation of S2 with increase in wind speed and trenching in sand

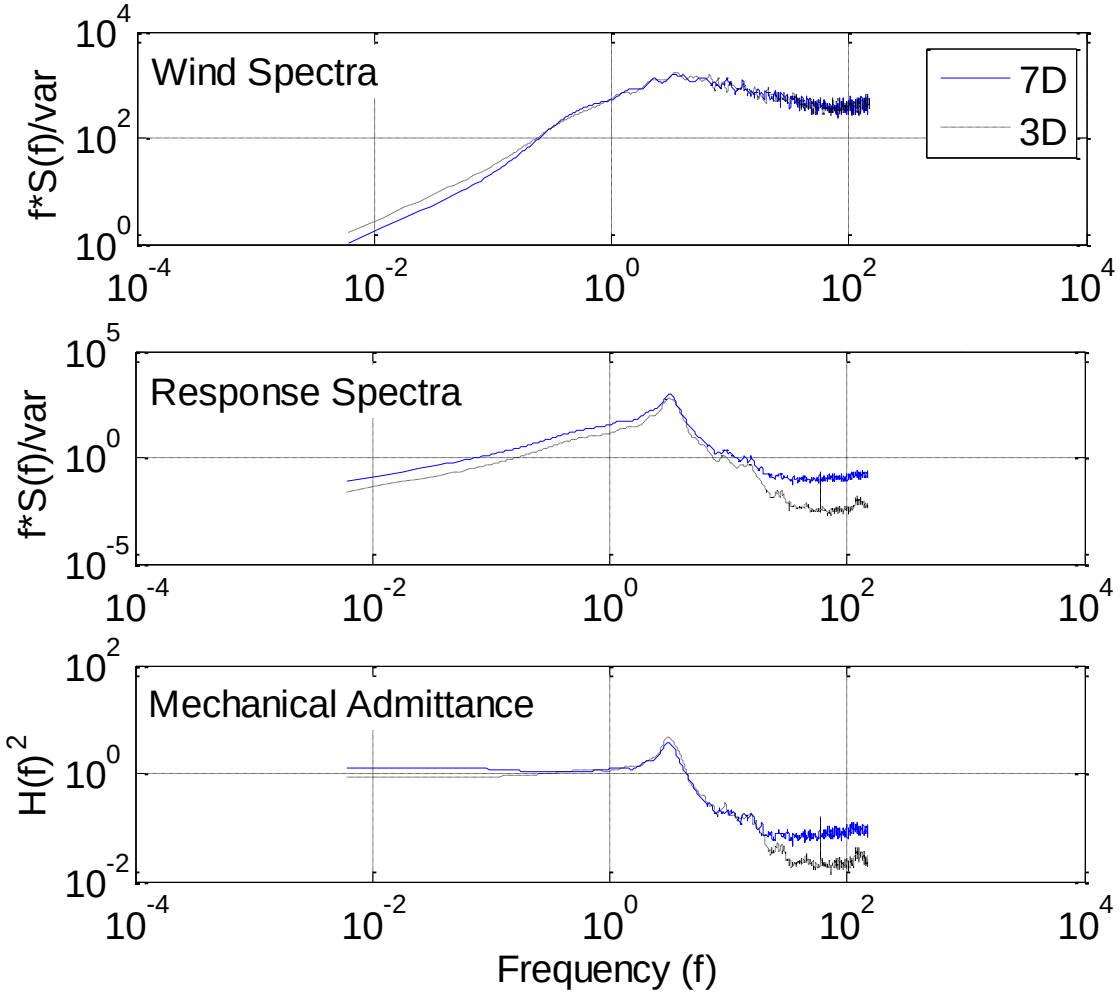

Figure 5-20 Spectral response of S1 in clay at 11.9 m/s wind speed

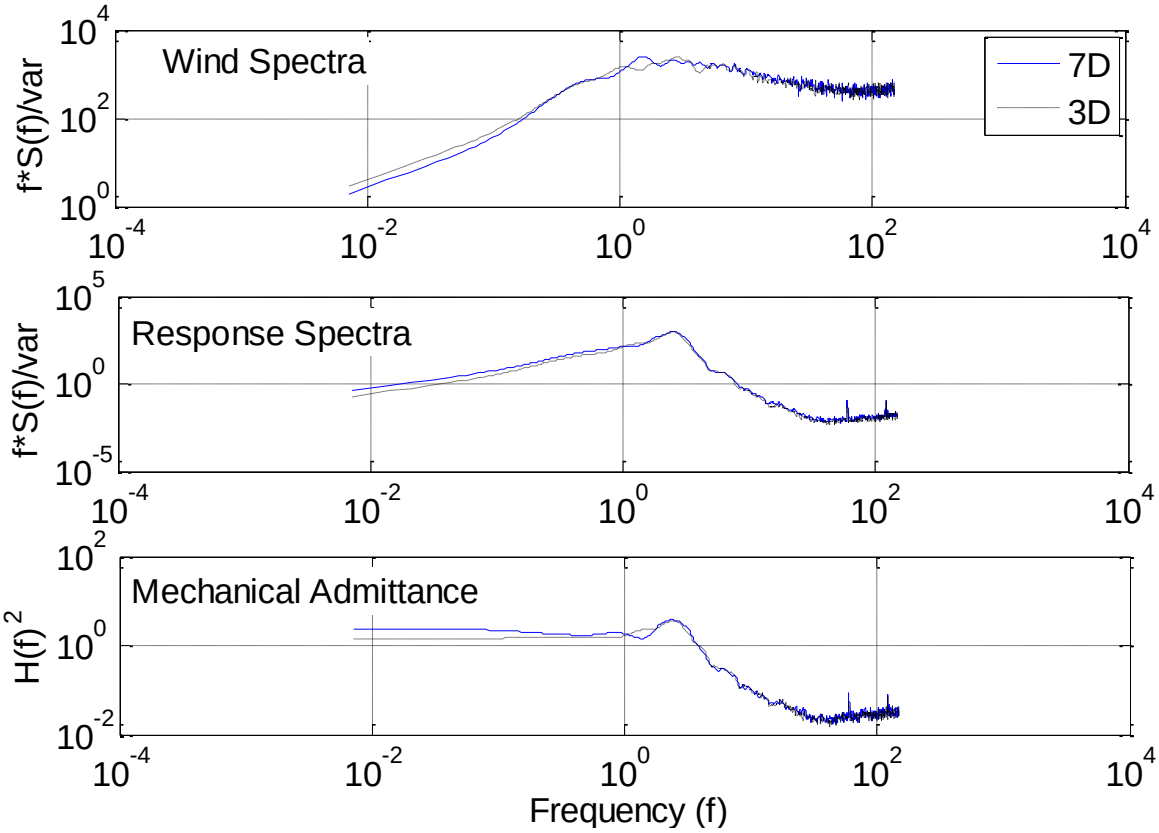

Figure 5-21 Spectral response of S2 in sand at 7.8 m/s wind speed

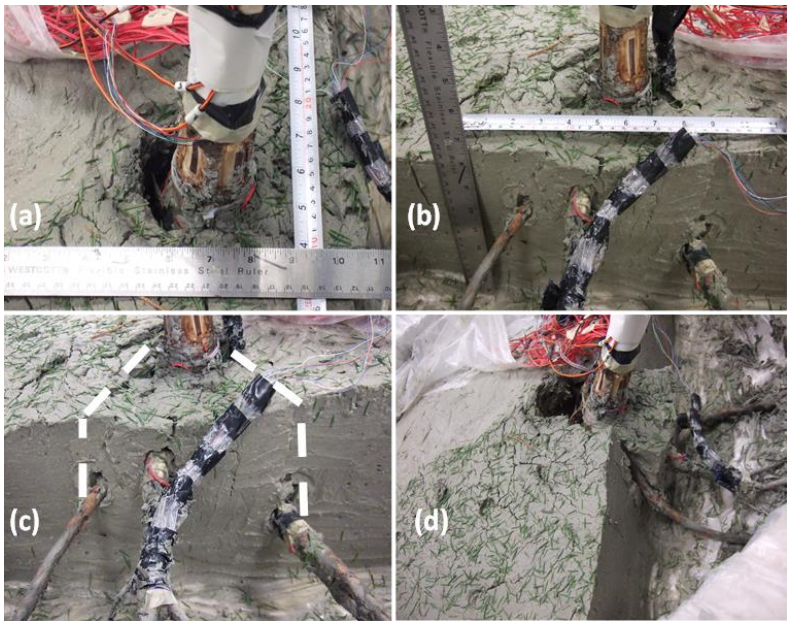

Figure 5-22 S1 soil-root plate failure in clay

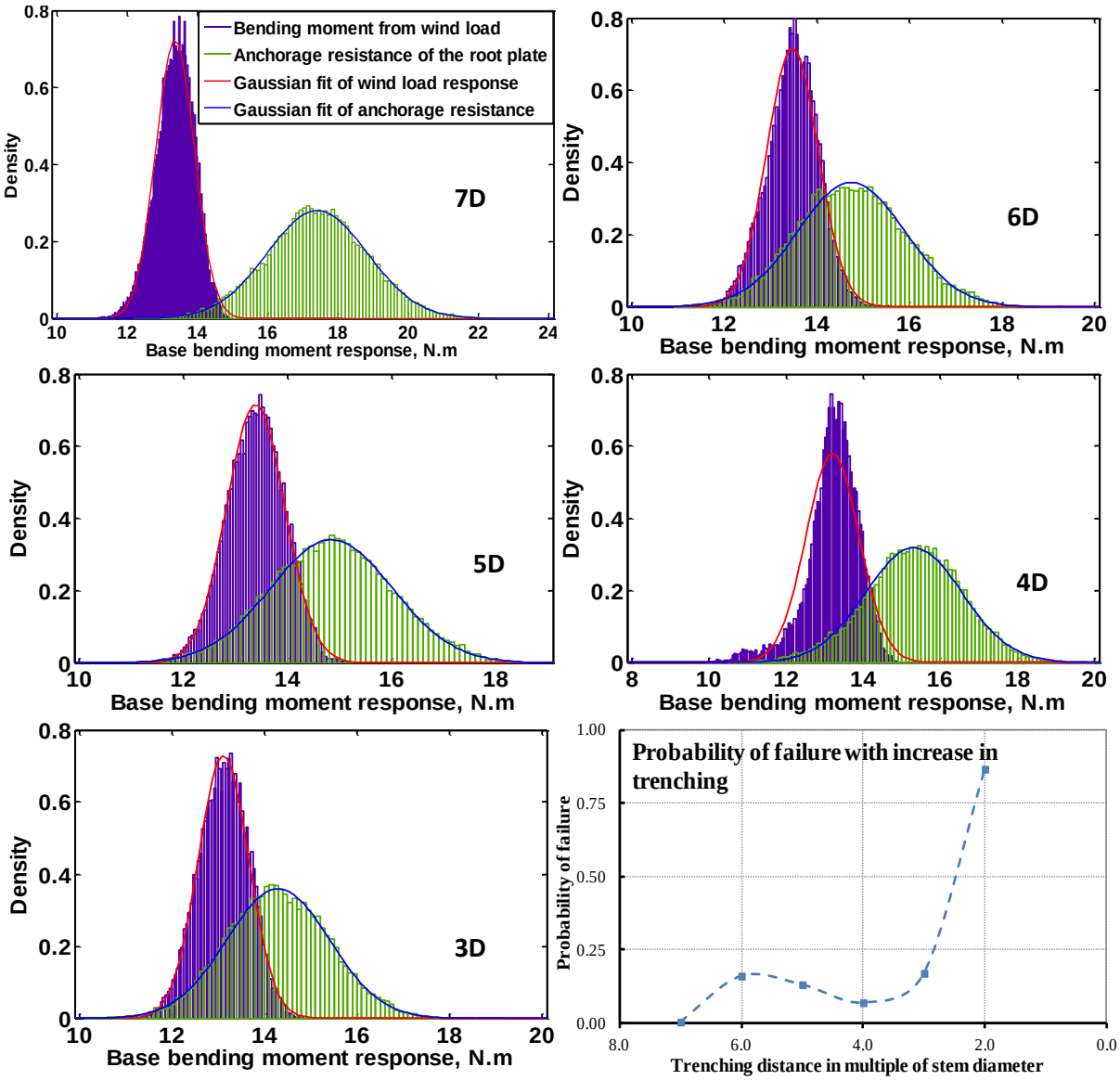

Figure 5-23 S1 tree stability analysis with increase in trenching at 11.9 m/s wind speed

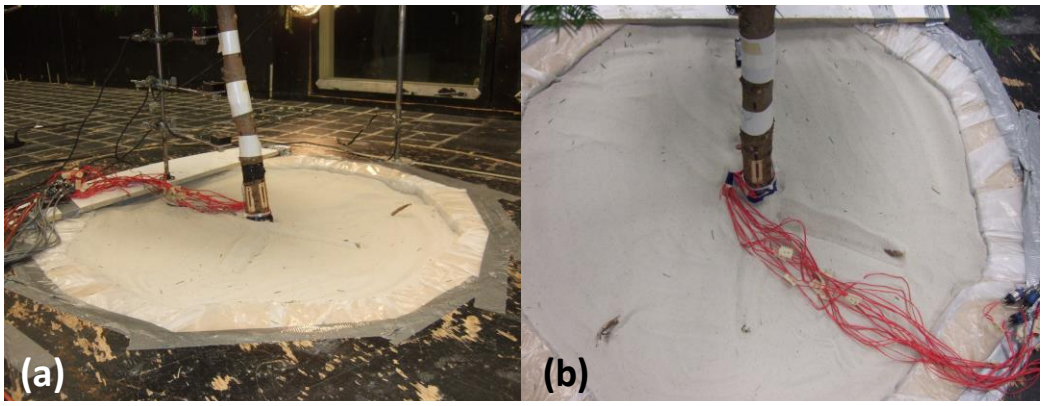

Figure 5-24 S2 soil-root plate failure in sand

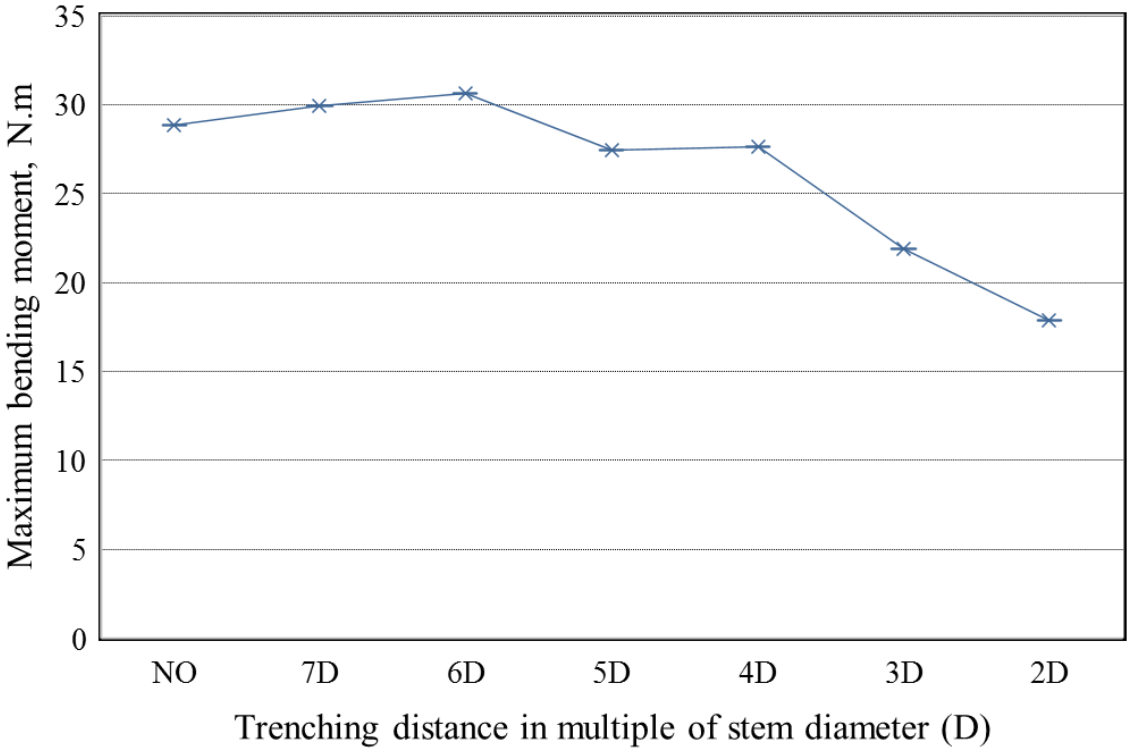

Figure 5-25 S2 failure response in sand with increase in trenching

Chapter 6

6 General discussion and conclusions

6.1 Summary

This chapter presents a brief discussion of the objectives and novelty of the experiments presented in the previous chapters, limitations of the experimentation and analysis, recommendations for the future work and the significance of the presented work in this thesis. Given the complexity of windthrow, for this study the experiments and tree stability analysis were conducted from different viewpoints. A mature field tree was winched to failure; the tree was sufficiently equipped with various sensors to efficiently track the tree-root response to loading and was analyzed in detail. Wind tunnel tests were conducted using tree saplings, with strain gauges attached along the stem and roots. Tests were conducted with two different root soil media (sand and clay). Extensive analysis of the tree dynamic sapling response was conducted with incremental wind loading conditions. The similarities or differences between the 'full scale' and 'model' tree was examined; static and dynamic load responses of the different trees was compared quantitatively. Finally, novel trenching tests were conducted in the wind tunnel with the structural root systems in sand or clay soil media. Major aspects of the tree-root response were studied extensively to examine tree stability.

The primary objectives of this study were:

1) To track and understand the response of a mature tree and root system to lateral loading and examine the applicability of simple engineering principles to this study.

2) To understand the tree sapling dynamic response through wind tunnel testing with changes in major components of tree stability (root architecture, soil media and wind load) and understand the parameter sensitivity of windthrow.

3) To assess the similitude between mature field tree response and tree sapling response to loading. Identify the key differences between static and dynamic loading and corresponding tree responses.

4) To examine the effect of trenching, change in soil media and root architecture and increase in wind loading on tree stability.

Novelty of this study was:

1) A mature field tree stem and root response was studied with various instrumentation, for the first time in windthrow research, root-soil interaction parameter was estimated using the Winkler foundation model.

2) For the first time, well instrumented tree saplings response with increase in wind load and change soil media with intact structural root system is tested in the wind tunnel.

3) Tree sapling dynamic response with increase in wind load is estimated. A new auto-correlation method to estimate the damping with increase in wind load is presented.

4) Detailed analysis of dynamic responses with both stem and root response admittance functions, rainflow and new statistical analysis techniques which are new to windthrow research are presented.

5) A novel trenching technique in the wind tunnel is presented.

6) A new statistical technique which can estimate the tree safety factor with the availability of minimal response data is presented.

6.2 Conclusions

The following major conclusions were derived from this study:

- Assuming the tree stem response to be similar to a cantilever beam is a reasonable assumption. The curvature profile could be a useful means to estimate the stem breakage height.
- Mature tree root bending moment and shear force responses tracked by strain gauges and examined through structural analysis were qualitatively the same as presumed by Niklas [2000], and strain and deflection profiles of the mature tree roots were same as observed by Crook and Ennos [1996] and Stokes [1999].
- The Winkler foundation model proposed could be a feasible way to examine the effect of soil on tree anchorage strength. This method could also be extended to wind loading problems (dynamic properties of the root plate can also be implemented). The stiffness estimates of the mature tree roots were found to be higher for the middle of the root structures.
- The dynamic tree sapling sway appears to be greatly influenced by the root soil support system. With increase in tree root-soil plate stability (with cohesive soil) or a fixed base system (on the force balance), windward and lateral responses of stem seem more closely correlated. Root response in sand and on the windward side showed higher responses with increase in wind load.
- The structural and aerodynamic damping estimates in this study indicate, twice to thrice the variation in aerodynamic damping for the stem with increase in wind speeds compared to the structural damping. For the roots, this was 3 to 4 times the root structural damping. However, damping is high for larger trees and also aerodynamic damping varies with wind speed [Milne 1991] and structural damping varies with sway amplitude [Jonsson et al. 2007]. This indicates the need of further field tree testing through wind loading, to verify the variation in damping with increase in wind loading and to compare the tree responses.
- The mechanical admittance functions of the saplings were very similar to the transfer functions presented by Holbo et al. [1980], Baker [1995] and Hassinen et al. [1998], showing peaks only close to the resonant frequency. This indicates that

the tree sapling in this experimental study behaved similarly to a forest tree (i.e. a lightly damped harmonic oscillator) [Gardiner 1995].

- The dimensionless parameters were generally different between the full scale and model trees. The calculated scaling factors and the dimensionless parameters gave an impression of the range of responses for the full-scale tree and the tree saplings. By conducting more studies of this kind, improved understanding will be achieved of scaling.
- The tree saplings were stiffer when tested in the wind tunnel compared to the in-situ field tree. Relative load transferred to the root system was around thirty times higher for the tree sapling in sand compared to the mature field tree.
- For the tree sapling tests in clay soil, the load transferred to the root system from the stem base was half as much compared to the load transferred for the sand, indicating that the anchorage strength of the tree sapling was almost half as much for sand soil compared to clay. Both soil conditions the load transferred to the root system for the static load condition was lower compared to the dynamic load condition.
- For the trenching in clay, the responses could be due to progressive degradation of soil strength with gradual loss in correlation between the windward and lateral response of the stem base with increase in trenching volume. The same response was observed by O'Sullivan and Ritchie [1993] from cyclically loaded Sitka spruce trees.
- An interesting phenomenon was observed from the trenching tests; the root soil plate load redistributed in the clay, but not in the sand. Mattheck and Breloer [1994] suggested that trees have a 'safety factor' of 5, indicating that trees develop stronger anchorages than necessary so as not to fail under high winds. This study supports and gives clues on how trees survive with minimal support. It also shows with stronger soil support, loads in the root system redistribute and anchor the tree, but not if the soil support is weak or if no redundancy in the system exists.
- Tree failure with increase in wind loading and trenching volume was due to progressive soil strength degradation and excessive deformation in clay, and by overturning in silica sand.

- With the presence of a strong structural tap root in test S2, there was surprisingly high anchorage strength despite the weaker soil media (sand). This provides further insight into the effective root plate depth concept similar to Fourcaud et al. [2008], Ghani et al. [2009] and Smiley et al. [2014].

6.3 Limitations

Major limitations of this experimentation and analysis has been the lack of data to validate the results presented in this study. Also, as most of these experimental techniques are attempted for the first time some of the key components were simplified.

For the mature tree winching test, above ground and below ground tree system responses were recorded using different data loggers with low sampling rates. This significantly limited the capability to examine the energy transfer in the tree-root-soil system.

Even with the care taken, the tree saplings in the wind tunnel may have desiccated partially, over the course of testing and instrumentation. This may have changed the structural response of the tree saplings.

The fine roots of the tree sapling root systems were pruned for the wind tunnel testing. As fine roots provide soil reinforcement [Reubens et al. 2007] and increase incremental plastic strains [Makarova et al. 1997], this may have altered the root system response but was not considered in this study for simplicity.

6.4 Recommendations for Future Work

- Winching tests need to be conducted on more mature field trees with strain gauges attached to both the trunk, branches and roots. The trees should be winched to uprooting failure. Ideally higher sampling rates should be used (>200 Hz). This would greatly help understand the load transfer in field conditions with static loads and free decay loading.

- Further dynamic analysis of tree saplings needs to be conducted for the first three modes of vibration to understand the complete change in tree dynamic response with increase in wind load. This would give the total changes in damping, which consequently will help explain tree stability.
- Tree saplings in clay need to be tested up to failure wind speeds; high range strain gauges and clay with lower strength (higher water content) need to be used to acquire the desired results. This will allow a clear comparison of cohesive and frictional soil base response and will also give data to estimate the sway and dynamic properties of tree saplings for clay up to failure wind speeds.
- While conducting the tree sapling windthrow tests in the wind tunnel, tracking of the soil surface around the stem base should be conducted. This would help better understand the soil anchorage mechanism in windthrow.
- A mature field tree should also be tested under varying wind conditions. The trend in damping ratio with increase in wind speed may give us the true nature of damping variation with increase in wind speed. The auto-correlation methodology could be a very useful methodology in windthrow research, to calculate the damping at various wind speeds and resonant frequencies, but further work needs to be conducted to fully test the damping at various resonant frequencies.
- Testing a group of trees in the wind tunnel would also help understand the change in damping and dynamic response due to changes in wind flow patterns and tree interaction.
- More tests need to be conducted with the wind tunnel experimental methodology and the analysis techniques used in this study with different size and species of tree, to further explore complex tree dynamic response and better establish scaling factors.
- In the wind tunnel, the effect of water in sands and some low percent cementation (better root plate shape), should be investigated to help understand the effect of soil-root anchorage and root plate development.
- Plants should be grown for wind tunnel testing in appropriate soil pots, this will enable more realistic rooting conditions to be investigated.

- Trenching tests need to be conducted with different soil media to further understand windthrow with trenching and change in soil conditions. Once the stability limitations with respect to soil shear strength are established, trenching recommendations can be made with more confidence.

6.5 Significance

The presented Winkler foundation model could be a possible way to examine the effect of soil on tree anchorage strength. Once the subgrade modulus for a given combination of root size and soil type is established, load-deflection behavior of roots under the given soil conditions can be established. Novel wind tunnel experimental techniques presented in this are versatile and manageable and can easily be extended to various wind, tree and soil conditions. Damping with increase in wind loading conditions was estimated for the time using the auto-correlation damping method. The root mechanical admittance estimates presented can provide an easy way to estimate the load transfer to the root system with increase in wind loading conditions. The dimensionless analysis presented can be used further to conduct sensitivity analysis and create more suitable experimental models to study windthrow. The Rainflow method used to analyze dynamic loading and response gave detailed information. Testing the tree stability with increase in trenching in the wind tunnel is a novel technique and gave clear experimental data with change in soil and wind conditions. The statistical analysis presented to estimate the tree factor of safety could be a simple tool and can be used with limited data.

6.6 References

Baker, C. J. (1995). The Development of a Theoretical Model for the Windthrow of Plants. *Journal of Theoretical Biology*, *175*, 355–372. https://doi.org/10.1006/jtbi.1995.0147

Crook, M. J., and Ennos, A. R. (1996). The anchorage mechanics of deep rooted larch, Larix europea x L-japonica. *Journal of Experimental Botany*, 47(303), 1509–1517. http://doi.org/10.1093/jxb/47.10.1509

Fourcaud, T., Ji, J. N., Zhang, Z. Q., & Stokes, A. (2008). Understanding the impact of root morphology on overturning mechanisms: A modelling approach. *Annals of Botany*, 101(8), 1267–1280. http://doi.org/10.1093/aob/mcm245

Gardiner, B. A. 1995. The interaction of wind and tree movement in forest canopies. In M. P. Coutts and J. Grace [eds.], *Wind and trees*, 41–59, Cambridge University Press, Cambridge, UK.

Ghani, M. A., Stokes, A., & Fourcaud, T. (2009). The effect of root architecture and root loss through trenching on the anchorage of tropical urban trees (Eugenia grandis Wight). *Trees - Structure and Function*, 23(2), 197–209. http://doi.org/10.1007/s00468-008-0269-9

Hassinen, A., Lemettinen, M., Peltola, H., & Gardiner, B. (1998). A prism-based system for monitoring the swaying of trees under wind loading, *Agricultural & Forest Meteorology* 90: 187–194.

Holbo, H. R., Corbett, T. C., & Horton, P. J. (1980). Aeromechanical behavior of selected Douglas-fir. *Agricultural Meteorology*, 21(2), 81–91. http://doi.org/10.1016/0002-1571(80)90056-4

Jonsson, M. J., Foetzki, a., Kalberer, M., Lundström, T., Ammann, W., & Stöckli, V. (2007). Natural frequencies and damping ratios of Norway spruce (Picea abies (L.) Karst) growing on subalpine forested slopes. *Trees - Structure and Function*, 21(5), 541–548. http://doi.org/10.1007/s00468-007-0147-x

Makarova, O. V., Cofie, P., & Koolen, A. J. (1998). Axial stress-strain relationships of fine roots of Beech and Larch in loading to failure and in cyclic loading. *Soil and Tillage Research*, *45*, 175–187. https://doi.org/10.1016/S0933-3630(97)00017-2.

Mattheck , C., and Breloer, H. (1994) *The body language of trees, a handbook for failure analysis*. London, England

Milne, R. (1991). Dynamics of swaying of Picea sitchensis. *Tree Physiology*, 9(11976), 383–99. Retrieved from http://www.ncbi.nlm.nih.gov/pubmed/14972849

Niklas, K. J. (2000). Computing factors of safety against wind-induced tree stem damage. *Journal of Experimental Botany*, 51(345), 797–806. http://doi.org/10.1093/jexbot/51.345.797

O'Sullivan, M. F., & Ritchie, R. M. (1993). Tree stability in relation to cyclic loading. *Forestry*, 66(1), 69–82. http://doi.org/10.1093/forestry/66.1.69

Reubens B., Poesen J., Danjon F., Geudens G., and Muys B. (2007) The role of fine and coarse roots in shallow slope stability and soil erosion control with a focus on root system architecture: a review. Trees 21 (4):385-402. doi:10.1007/s00468-007-0132-4.

Smiley, E. T., Holmes, L., & Fraedrich, B. R. (2014). Pruning of buttress roots and stability changes of red maple (Acer rubrum) Pruning of Buttress Roots and Stability Changes of Red Maple (Acer rubrum). *Arboriculture & Urban Forestry*, 40(4), 230–236.

Stokes, A. (1999). Strain distribution during anchorage failure of Pinus pinaster Ait. at different ages and tree growth response to wind-induced root movement. *Plant and Soil*, 217, 17–27. http://doi.org/10.1023/A:1004613126353

Appendix A: Damping Methods

Logarithmic decrement method

The logarithmic decrement method is the most useful and an easiest method to estimate the damping from free vibration decay [Clough and Penzien 1993] in the time domain. In this method, the rate at which the amplitude of a damped vibration decreases is measured over one or n number of cycles. If u_1 and u_{n+1} are the amplitudes of vibration of the first cycle and after n number of cycles respectively [Figure A- 1], the damping ratio (ξ) is given by:

$$\xi = \frac{\delta}{\sqrt{(2\pi)^2 + \delta^2}}$$

Where $\delta = \frac{1}{n}\ln\left(\frac{u_1}{u_{1+n}}\right)$

Half power band width method

The half power band width method was used to estimate the damping of a system in the frequency domain. From the frequency response function, the maximum amplitude (X_{max}) is obtained at the chosen natural frequency (f_n). The two frequencies f_1 and f_2 corresponding to the half power band, i.e. at $\frac{X_{max}}{\sqrt{2}}$ are used to obtain the damping. The ratio of the frequency range between two frequencies at the half power point and twice the natural frequency is given by:

$$\xi = \frac{f_2 - f_1}{f_1 + f_2} = \frac{f_2 - f_1}{2f_n} = \frac{\beta_2 - \beta_1}{2}$$

This method of evaluating the damping ratio is also illustrated in with the typical frequency response curve [Figure A-2]. A horizontal line is drawn across the curve at 1/√2 times the resonant-response value; the difference between the frequencies at which this line intersects the response curve is equal to twice the damping ratio.

Even though this method can be used to estimate the damping at all excited modes, one of the disadvantages of this power spectrum method is that for lightly damped systems the half power bandwidth is small and needs to be measured carefully.

Hilbert transformation method

The Hilbert transformation method used in this study is described in Jonsson et al. [2007]. The response data is transformed to the frequency domain using Fourier transformation. At the anticipated mode of vibration, the data is filtered using a Butterworth filter and is transformed to the time domain using the Hilbert transformation. The obtained data is plotted as a function of time [Figure A- 3]. The slope of the envelope divided by the natural frequency at the selected mode of vibration is the damping for that mode of vibration. One problem with this method is that it is usually only applied to free vibration damping.

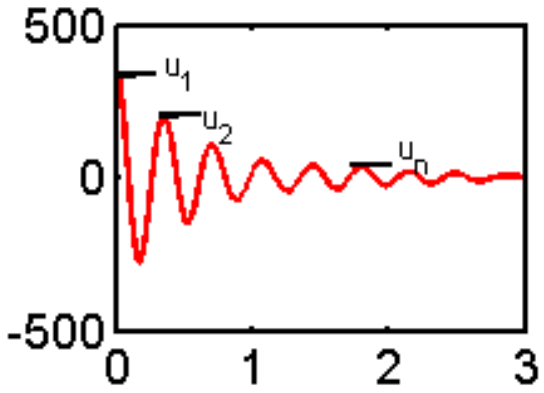

Figure A- 1 Logarithmic decrement method

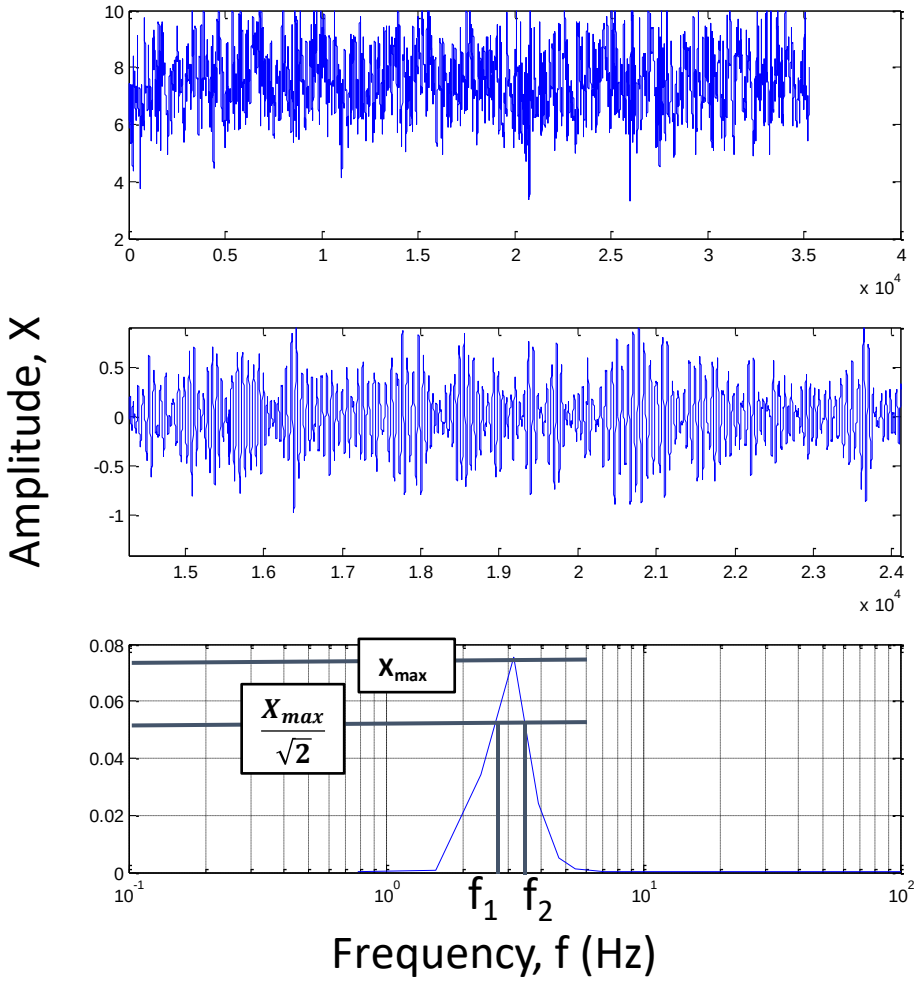

Figure A-2: Half power band width method

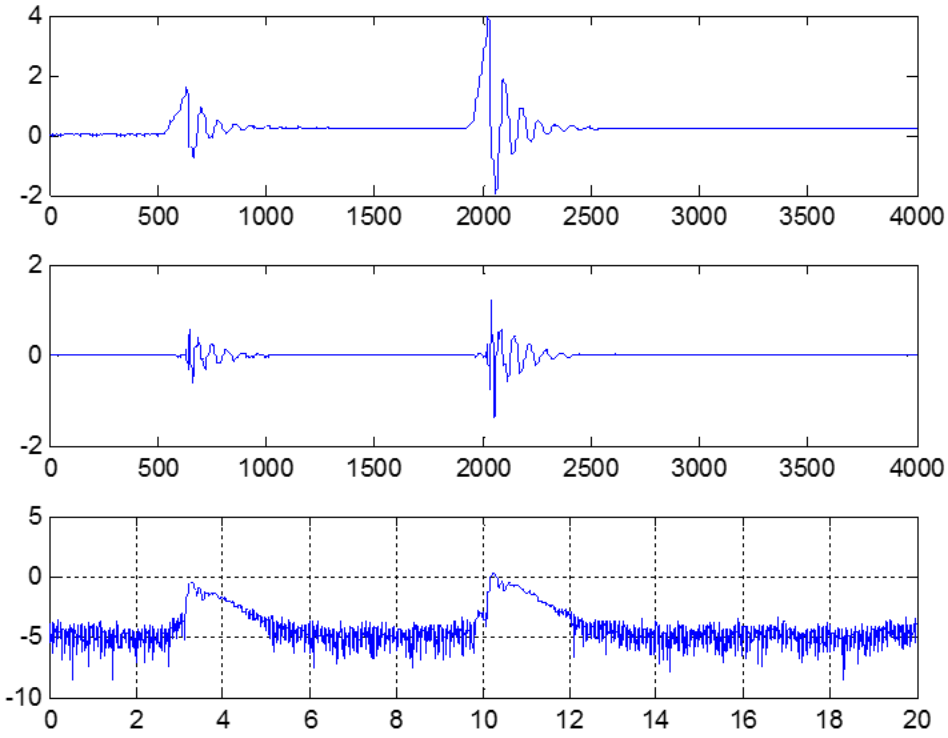

Figure A- 3 Hilbert transformation method

Appendix B: Rainflow Counting (ASTM E1049-85)

Rainflow algorithms were originally developed by Matsuishi and Endo [1968], it is a popular cycle counting technique. In this study, cycle counting is conducted using the rainflow counting algorithm of MATLAB software. This algorithm code was developed by Adam [2010] according to ASTM E1049-85 standards. Detailed cycle counting methodology is explained below:

Procedure

Rules for this method are as follows: let X denote range under consideration; Y, previous range adjacent to X; and S, starting point in the history.

(1) Read next peak or valley. If out of data, go to Step 6.

(2) If there are less than three points, go to Step 1. Form ranges X and Y using the three most recent peaks and valleys that have not been discarded.

(3) Compare the absolute values of ranges X and Y.

(a) If $X < Y$, go to Step 1.

(b) If $X \geq Y$, go to Step 4.

(4) If range Y contains the starting point S, go to Step 5; otherwise, count range Y as one cycle; discard the peak and valley of Y; and go to Step 2.

(5) Count range Y as one-half cycle; discard the first point (peak or valley) in range Y; move the starting point to the second point in range Y; and go to Step 2.

(6) Count each range that has not been previously counted as one-half cycle.

Illustration

The load history is plotted as Figure B-1(a) and is used to illustrate the process. Details of the cycle counting are as follows:

(1) S = A; Y = |A-B |; X = |B-C|; X > Y. Y contains S, that is, point A. Count |A-B| as one-half cycle and discard point A; S = B. (See Figure B-1(b).)

(2) Y = |*B-C*|; *X* = |*C-D*|; *X* > *Y. Y* contains *S*, that is, point *B*. Count| *B-C*| as one-half cycle and discard point *B*; *S* = *C.* (See Figure B-1(*c*).)

(3) Y = |*C-D*|; *X* = |*D-E*|; *X* < *Y*.

(4) Y = |*D-E*|; *X* = |*E-F*|; *X* < *Y*.

(5) Y = |*E-F*|; *X* = |*F-G*|; *X* > *Y*. Count |*E-F*| as one cycle and discard points *E* and *F*. (See Figure B-1(*d*). Note that a cycle is formed by pairing range *E-F* and a portion of range *F-G*.)

(6) Y = |*C-D*|; *X* = |*D-G*|; *X* > *Y*; *Y* contains *S*, that is, point *C*. Count |*C-D*| as one-half cycle and discard point *C*. *S* = *D.*(See Figure B-1(*e*).)

(7) Y = |*D-G*|; *X* = |*G-H*|; *X* < *Y*.

(8) Y = |*G-H*|; *X* = |*H-I*|; *X* < *Y*. End of data.

(9) Count |*D-G*| as one-half cycle, |*G-H*| as one-half cycle, and| *H-I*| as one-half cycle. (See Figure B-1(*f*).)

(10) End of counting. See the table in Figure B-1 for a summary of the cycles counted in this example.

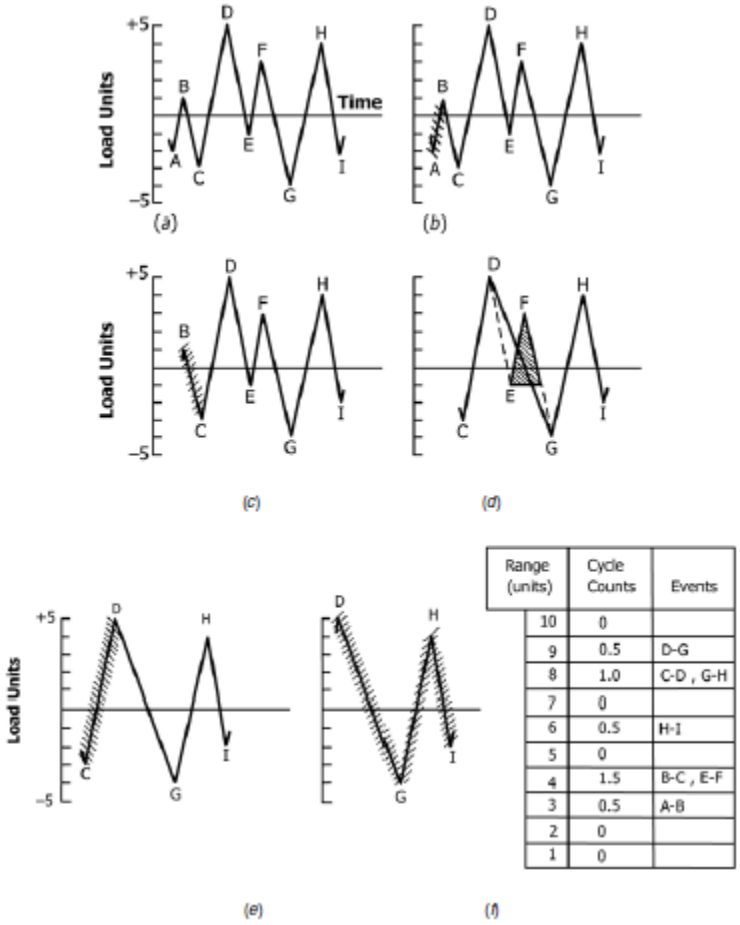

Range (units)	Cycle Counts	Events
10	0	
9	0.5	D-G
8	1.0	C-D , G-H
7	0	
6	0.5	H-I
5	0	
4	1.5	B-C , E-F
3	0.5	A-B
2	0	
1	0	

Figure B-1: Rainflow counting example

Curriculum Vitae

Name: Padmavathi V. Sagi

Post-secondary Education and Degrees:

Osmania University College of Engineering
Hyderabad, Andhra Pradesh, India
2000-2004 B.E.

Indian Institute of Technology Bombay (IITB)
Mumbai, Maharashtra, India
2004-2006 M.Tech.

The University of Western Ontario
London, Ontario, Canada
2008-2016 Ph.D.

Honors and Awards:

Western Graduate Research Scholarship (WGRS),
University of Western Ontario, Canada.
2008-2012

Ministry of Human Resource Development (MHRD) scholarship,
Indian Institute of Technology Bombay (IITB), India.
2004-2006

Related Work Experience

Teaching Assistant
The University of Western Ontario, Canada.
2008-2012

Research Assistant
The University of Western Ontario, Canada.
2008-2012

Research Assistant

Indian Institute of Technology Bombay, India.

2004-2006

Conference papers:

Sagi P., Newson T., Mitchell, S., and Miller C. (2012) "The effect of trenching and root loss on the cyclic stability of trees" *3rd International Conference on Soil Bio and Eco Engineering, the use of vegetation to improve slope stability*, UBC Vancouver, Canada, July 2012.

Padmavathi S., Newson T., Mitchell, S., Gatey D. A., and Miller C. (2012) "Scaled tree root system behavior in a sand substrate under wind loading" *6th IUFRO International conference on wind and trees*, University of Georgia, USA, July 2011.

Newson T., Padmavathi S., Craig Miller and Mitchell, S. (2009) "Application of yield surfaces in three-dimensional load space to the stability of trees under wind loading" *2nd International Conference on Wind Effects on Trees*, University of Freiburg, Germany, 2009.

Dewaikar, D. M. and Padmavathi, S.V. (2008) "Ultimate lateral load of a pile in soft clay under cyclic loading." *International Association for Computer Methods and Advances in Geomechanics (IACMAG)*, 2008, 12th International Conference, October 2008, Goa, India. PP. 3498-3507.

Padmavathi, S.V. and Dewaikar, D.M. (2006) "Response of pile in soft clay under one-way cyclic lateral loading." *DFI 2006 Annual Conference on Deep Foundations*, October 2006, Washington.

Dewaikar, D. M. and Padmavathi, S.V. (2006) "A new degradation model for one-way cyclic lateral loading of piles in soft clay." *2nd International Congress on Computational Mechanics and Simulations (ICCMS-06)*, December 2006, IIT Guwahati.

Katti, R.K. and Padmavathi, S.V. (2005) "Precast densified stone columns for soft soil ground improvement." *Indian Geotechnical Conference*, Vol. 2, PP. 1100-1104.